JCAP
JOINT CENTER FOR ARTIFICIAL PHOTOSYNTHESIS

Joint Center for Artificial Photosynthesis

FINAL SCIENCE REPORT

OCTOBER 2010 TO SEPTEMBER 2021

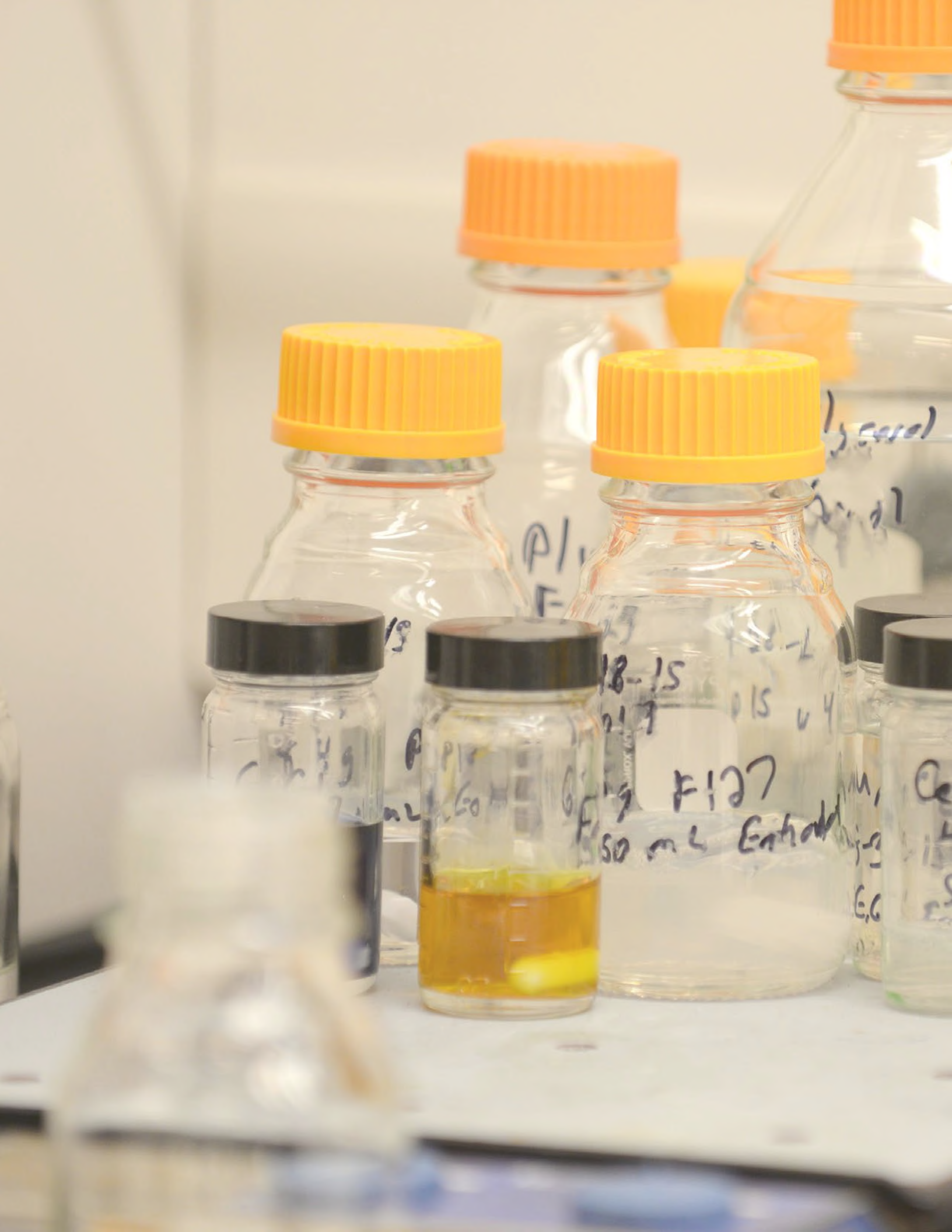

Final Science Report of the Joint Center for Artificial Photosynthesis (JCAP)

DOE Award DE-SC0004993 for Lead Institution
California Institute of Technology

The Joint Center for Artificial Photosynthesis (JCAP) was designated as the U.S. Department of Energy (DOE) Fuels from Sunlight Energy Innovation Hub on July 22, 2010, and began operations according to a cooperative agreement between the DOE and the California Institute of Technology on September 30, 2010. The cooperative agreement was renewed on September 30, 2015. This final science report outlines JCAP activities for the period ending September 30, 2021.

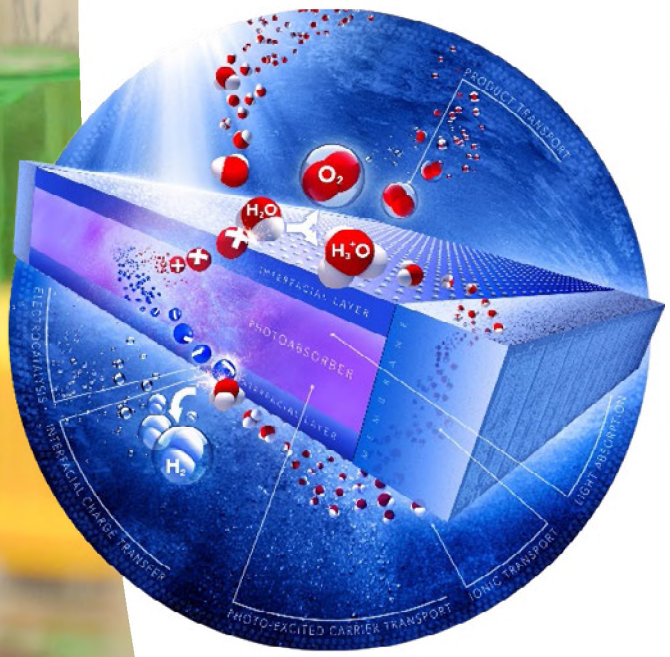

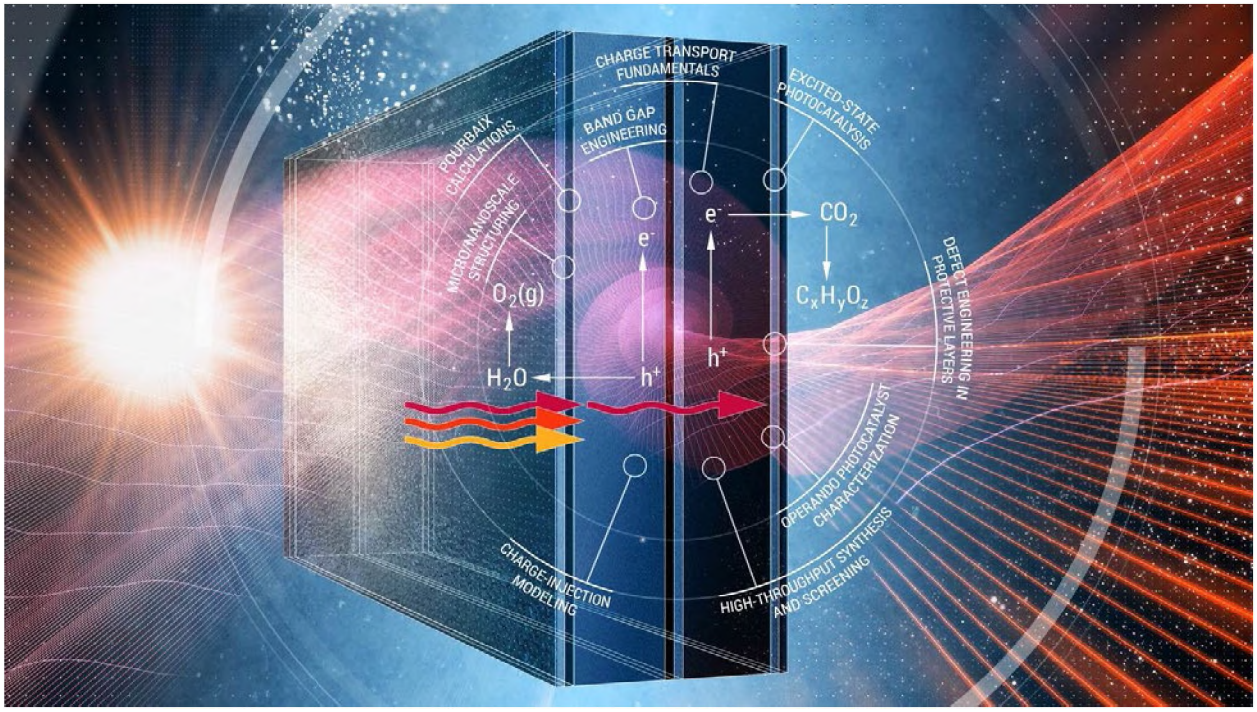

Drafting Authors:
Xenia Amashukeli (California Institute of Technology), Harry A. Atwater (California Institute of Technology), Joel A. Haber (California Institute of Technology), Frances Houle (Lawrence Berkeley National Laboratory)

JCAP Contributing Authors and Principal Investigators:
Frank Abild-Pedersen (SLAC), Theodor Agapie (Caltech), Joel W. Ager III (LBNL), Paul Alivisatos (LBNL), Harry A. Atwater (Caltech), Nitash Balsara (LBNL), Alexis T. Bell (LBNL), Marco Bernardi (Caltech), Bruce Brunschwig (Caltech), Christopher Chang (LBNL), Michael Crommie (LBNL), Jason K. Cooper (LBNL), David Dornfeld (LBNL), Walter Drisdell (LBNL), Heinz Frei (LBNL), Giulia Galli (LBNL), Phillip Geissler (LBNL), William A. Goddard III (Caltech), Harry B. Gray (Caltech), John Gregoire (Caltech), Robert Howard Grubbs (Caltech), Joel A. Haber (Caltech), Martin P. Head-Gordon (LBNL), John C. Hemminger (UC-Irvine), Michael R. Hoffmann (Caltech), Frances A. Houle (LBNL), Thomas Jaramillo (SLAC), Ali Javey (LBNL), Jian Jin (LBNL), Christian Kisielowski (LBNL), Carl A. Koval (Caltech), Clifford P. Kubiak (UC-San Diego), Nathan S. Lewis (Caltech), Jeffrey Long (LBNL), Eric MacFarland (UCSB), Philip Marcus (LBNL), Daniel J. Miller (LBNL), Thomas Francis Miller III (Caltech), Jeffrey B. Neaton (LBNL), John Newman (LBNL), Anders Nilsson (SLAC), Jens Norskov (SLAC), Kristin A. Persson (LBNL), Jonas C. Peters (Caltech), Rachel A. Segalman (LBNL), Ian D. Sharp (LBNL), Omar Savas (LBNL), T. Don Tilley (LBNL), Francesca Maria Toma (LBNL), F. Dean Toste (LBNL), Lin-Wang Wang (LBNL), Adam Z. Weber (LBNL), Will West (Caltech), Chengiang Xiang (Caltech), Vittal Yachandra (LBNL), Peidong Yang (LBNL), Junko Yano (LBNL), Tarek Zohdi (LBNL).

Table of Contents

Executive Summary

The Joint Center for Artificial Photosynthesis (JCAP) was established in October 2010 and completed operation after a no-cost extension in September 2021. At its inception, JCAP was a bold experiment in research organization by the US Department of Energy (DOE). Ambitious in objective and scale, the Fuels from Sunlight Hub was tasked with envisioning a new industry for which only basic science had previously been conducted, identifying the critical technical and basic knowledge gaps that needed to be bridged to achieve that vision, and focusing research activity to meet those critical needs. Led by the California Institute of Technology (Caltech), JCAP quickly brought together a diverse team of over 100 physical scientists and engineers, working in temporary and existing research space at several world-leading research institutions for the first two years, while new buildings were constructed with dedicated facilities and instrumentation for solar fuels research at Caltech and leading partner Lawrence Berkeley National Laboratory. In its decade of activity, JCAP made transformative progress in solving the scientific and engineering challenges to creating solar-fuels systems that surpass natural photosynthetic systems in efficiency and rival them in selectivity, the ability to generate desired products. This progress has been reported in over 775 peer-reviewed publications. Additionally, JCAP played a leading role in developing the nation's solar fuels workforce by providing training to some 250 graduate students, postdoctoral fellows, and staff, many of whom moved on to leadership roles in academia and industry. Over 45 JCAP researchers moved to tenure-track faculty positions, leading their own research teams, and hundreds have moved to industry, including to leading firms such as 3M, Dow, Intel, Lam, LG, and Applied Materials.

In natural photosynthesis, plants store the energy in sunlight by utilizing that energy to transform water and carbon dioxide (CO_2) into sugars and other biomass. Plants' efficiency at storing the energy in sunlight as fuel (biomass) is 1% or less, and plant photosynthetic systems operate for only 10 to 20 minutes before requiring repair. However, plants have elaborate processes for such repair, while manmade repair systems are very primitive, in comparison. Additionally, vegetation is self-propagating, and utilizes low atmospheric concentrations of CO_2. Given the inability to self-repair or self-replicate, to be feasible, non-biological systems must be both durable and achieve at least 10% efficiency, while directly producing useful fuels instead of bulky biomass.

Solar-fuels systems must operate for years outdoors: their active components must be both long-lasting and able to withstand daily temperature cycling and seasonal weather. This requires preventing corrosion at the liquid-solid interface caused by acidic or basic conditions inherent in the electrolyte or generated by reaction at the electrode, or by potential-dependent corrosion of the catalyst or light absorber. Two catalysts are required for the water-splitting process: one for oxygen evolution, which generates O_2 molecules and protons, and one for hydrogen evolution, which assembles H_2 molecules from the protons. Oxygen evolution typically occurs in either a very acidic or a very basic environment due to system-level requirements, but oxygen-evolution catalysts are unstable in very acidic environments, except for those based on the extremely rare precious metals iridium and ruthenium.

Solar-fuels systems combine photoexcitation, chemical transformation, and transport processes to produce fuel. A typical system includes light absorbers, oxidation and reduction catalysts integrated with them, membrane separators, and water-based electrolyte. Each component of the system must be designed so that the resulting combination uses the energy in sunlight to react water and carbon dioxide (CO_2) to produce fuel as efficiently as possible. The two primary types of solar-fuels systems are those designed to generate hydrogen (H_2) as the fuel, and those designed to reduce CO_2 to hydrocarbons or oxygenated hydrocarbons (e.g., ethanol) as the fuel. Although they share many common elements, these two types of solar fuel systems have distinct advantages and challenges. Specifically, the H_2-generating system consumes only water and produces only one fuel (H_2), but requires the use of corrosive electrolytes to achieve high efficiency, and

produces a gaseous fuel with low volumetric energy density. There are associated challenges for storage and distribution of H_2, which must be rigorously separated from the by-product oxygen (O_2) gas or risk forming an explosive mixture. The CO_2-consuming generators can operate using less corrosive electrolytes and can produce fuel similar to existing fossil fuels (natural gas or petroleum) enabling existing energy storage, distribution, and utilization infrastructure to be leveraged. However, the reaction of CO_2 produces a mixture of many different products and has low energy conversion efficiency due to low reactant concentrations and the complexity of the reaction mechanisms. The fundamental technical challenges are to achieve high solar-to-hydrogen (STH) efficiency with multi-year durability or to achieve high product selectivity using CO_2 (i.e., predominantly make the desired product) along with multi-year durability and high solar-to-fuel energy conversion efficiency.

Before JCAP, work in artificial photosynthesis was limited and focused on individual components, and little was understood about how to combine the components into artificial photosynthesis systems. Achieving higher efficiency and selectivity had not been demonstrated in complete, inherently safe systems with product separation, and universal standards and benchmarking did not exist.

The primary focus of JCAP's first phase (2010 to 2015) was water splitting to make H_2. To split water efficiently, light absorbers that utilize as much of the solar spectrum as possible, provide high voltage and high current, and are stable in a harsh environment are needed. JCAP made substantial progress in how to find effective light absorbers during this phase. Additional work included designing protective coatings and water oxidation catalysts, studying systems while they operated, developing component performance benchmarks, performance modeling, and designing and developing solar-fuels prototypes. In the second phase (2015 to 2021), the focus shifted to CO_2 reduction, with a research program to develop new materials and system-level designs to improve product selectivity and energy conversion efficiency.

Through its work, JCAP advanced mechanistic aspects of catalyst activity and selectivity, light absorption and carrier transport, operando measurement, materials discovery for catalysis and light absorbers, and multiphysics modeling and experimental prototyping of solar-fuels systems. JCAP demonstrated solar-fuels prototypes that exhibited performance characteristics and levels of integration inconceivable in 2010. An overview of these achievements and the phases is shown in **Figure ES.1**.

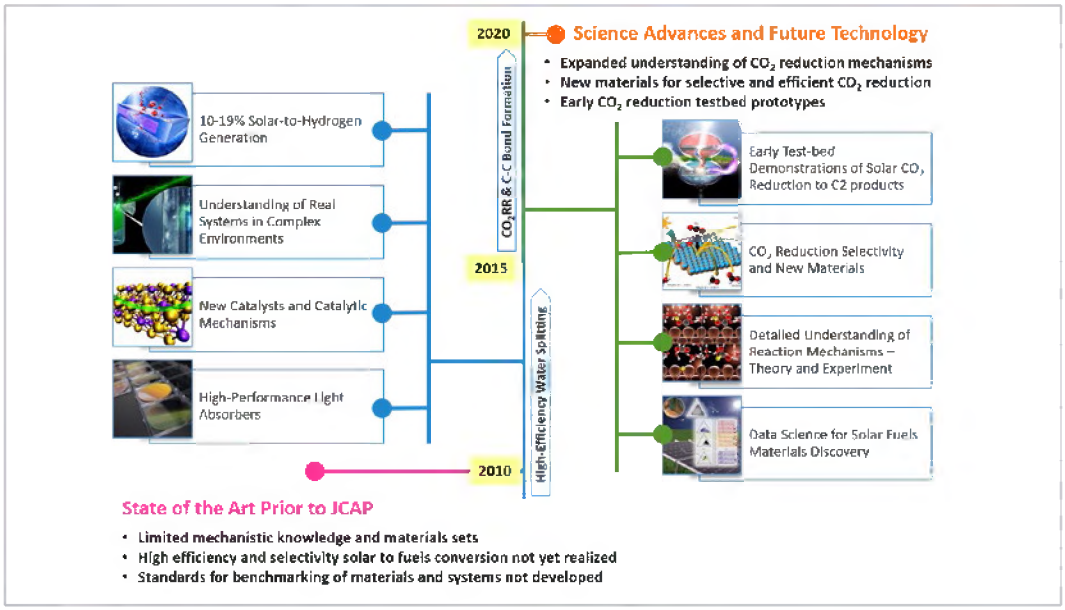

Figure ES.1. JCAP's record of accomplishment.

These accomplishments were made possible through JCAP's active, multidisciplinary, multi-institutional partnerships. JCAP enabled development of unique capabilities for solar fuels, both at member institution laboratories and in partnership with DOE user facilities. Through close and ongoing collaboration between theorists and experimentalists, JCAP has left a legacy of team-oriented science as a highly effective vehicle for accelerating fundamental advances in methods, materials, and mechanistic understanding of solar-fuels systems.

Mechanisms

Benchmarking and Testing Techniques

To help advance the field, JCAP developed standardized measurement protocols for solar-fuel generation reactions. The JCAP benchmarking project developed a new procedure for evaluating the activity, stability, and electrochemically active surface area of electrodeposited catalysts for the oxygen-evolution reaction (OER), which is required to balance the fuel-forming reaction. This procedure was initially used to compare the performance of 10 such catalysts, and the resulting manuscript was featured as a *Science* magazine Editors' Choice. The benchmarking protocol was later used to evaluate the performance of hydrogen evolution and additional oxygen-evolution catalysts. These standardized measurement protocols have been adopted by the solar fuels community, and performance measurements following these protocols are now routinely required for publication of solar fuel electrocatalyst discoveries.

JCAP developed a suite of microscopy and spectroscopy capabilities for versatile, in-depth characterization of catalysts and electrodes for electrochemical and photoelectrochemical (PEC) reactions important for artificial photosynthesis. The three levels of characterization are ex situ, in situ, and operando, where ex situ is "out of natural location" and in situ is "in natural location," but with no temporal discrimination; operando is defined as working, and the characterization is of an operating catalyst. Tremendous insight into the dynamic behavior of catalysts as a function of potential was obtained via the sequential implementation of multiple operando methods.

JCAP developed partnerships with DOE user facilities at Lawrence Berkeley National Laboratory and SLAC National Accelerator Laboratory that provide some of the world's most advanced technologies for synthesis and characterization of artificial photosynthesis materials. JCAP contributed to the development of new capabilities at these facilities enabling characterization of materials and systems under operating conditions.

Insights into Catalytic Mechanisms

JCAP investigated combinations of materials, catalytic environments, electrolytes, and operating conditions that improve efficiency and the ability to produce desired products while avoiding reactions that deactivate catalysts. While water splitting occurs most efficiently in extremely acidic or basic electrolyte environments, reducing CO_2 using copper requires neutral to basic electrolytes. JCAP has investigated how the concentration and kinds of cations and anions present in a solution strongly influence the efficiency of CO_2 reduction. Water plays a role not only as a source of hydrogen, but also through its interactions with interfacial intermediates. JCAP researchers utilized molecular additives in the electrolyte, as well as polymeric overcoats on copper surfaces, to tune the reaction microenvironment and improve the ability to produce desired products.

Materials

Discovery, Characterization, and Understanding of Catalysts

JCAP made progress in finding acid-stable oxygen-evolution catalysts made from inexpensive, abundant elements and in finding better-functioning catalysts for use in basic environments. JCAP also discovered new

hydrogen evolution catalysts composed of inexpensive, abundant elements, and improved the catalysts used to convert CO_2 into reduced molecules suitable for fuel.

Copper remains the most active electrocatalyst for reducing CO_2 to hydrocarbons and oxygenates. JCAP studied how to use surface structure, alloy composition and spatial distribution, and electrode functionalization to direct selectivity on copper and copper alloys. JCAP also studied development of non-copper-based materials, but concluded that copper and its alloys are the only materials able to function efficiently enough for this process. The researchers learned that the surface structure of the copper catalyst and which metals it is alloyed with are important to generating the desired products. For the CO_2 conversion process, JCAP also explored using two different catalysts sequentially, one to reduce CO_2 to CO and then CO to the desired products, rather than relying on a single catalyst for the full process.

High-Throughput Experimentation Facility for Light Absorber and Electrocatalyst Materials Discovery

JCAP established a high-throughput facility to discover new light absorbers, photocatalysts, and electrocatalysts using advanced automated experimental techniques and large-scale data analytic methods. These new high-throughput experimental capabilities were combined with high-throughput computational and theoretical prediction of materials via the Materials Project to identify functional solar-fuels materials. Rapid characterization using high-performance scanning instruments, such as the scanning droplet cell and online mass spectrometry, allowed materials and interfaces with desired properties to be identified and then synthesized on a larger scale for in-depth study. An extensive, searchable Materials Experiment and Analysis Database (MEAD) and associated big-data science techniques resulted from the work and are available to the materials community.

JCAP's high-throughput team developed several new technologies for screening (photo)electrocatalysts for the CO_2 reduction reaction. Through the development of small electrochemical reactors and their coupling to analytical chemistry tools, the team demonstrated experiment throughput approximately 10 to 100 times that of traditional methods with only moderate compromises in the quality of product detection.

Component Integration

Test-Bed Development

Understanding that components behave differently in a system than in isolation, JCAP developed multicomponent, multifunctional test beds focusing on understanding the science behind component integration. To understand, explore, and develop next-generation architectures, JCAP used multiphysics modeling combined with detailed studies. The modeling and experimental studies demonstrate the importance of the local environment in achieving both performance and selectivity.

Integration efforts expanded the portfolio and operating range of metal oxide protective coatings for photoanodes, and improved understanding of interfacial charge-transfer dynamics and efficiency. Integration at the test-bed scale can introduce significant variation in the reported activity, selectivity, and durability, even for well-studied catalysts such as copper. Mass-transfer effects and the local environment can lead to changes in the product distribution that could be incorrectly attributed to catalyst deactivation, as opposed to being caused by the cell geometry. JCAP developed standardized cells and analytical methods to quantify CO_2 reduction products. The cell designs and methods have been published for use by the scientific community.

Protective Coatings

JCAP reported strategies for stabilizing systems for hours and days, including day-night cycling, while ensuring >10% STH conversion efficiency with full product separation for safety. These strategies include the

use of protection layers and hybrid composite coatings to prevent corrosion in very acidic or basic electrolyte environments, including materials with the ability to generate their own protective surface layer. Alternatively, high-performance protection layers can be deposited to prevent corrosion while facilitating charge transport within the layer and at its interface with the electrolyte.

Membrane Permeability

Polyelectrolyte membranes separate the two regions of electrochemical devices, the anode and the cathode. For solar-fuels systems to be efficient, these membranes must minimize crossover of electrochemical products by not being overly permeable to them. However, the membranes must be permeable to conduct ions between the regions to prevent a build-up of charge that would divert much of the generated energy away from fuel formation. JCAP focused on three areas of this problem. First, JCAP studied anion-conducting membranes with polymers that are stable when operated in a basic environment. Second, researchers studied the correlation between polymer composition and permeability by synthesizing a series of related polymers and measuring their permeability and conductivity properties. Third, permeation through membranes at steady state had been well studied, and it was known that organics and CO_2 can interact with polymers and affect their permeability in use, but very little was known about the exact mechanisms of this transport. JCAP developed a multiscale modeling framework that enabled macroscopic observables, such as extent of permeation as a function of time, to be simulated while retaining a molecular description of the system. Daily and seasonal variability in solar intensity mean real systems will not operate at steady state. By studying time-dependent permeability, JCAP researchers learned membranes will behave differently when operating under real world conditions.

Solar-Fuels Prototypes and Associated Processes

JCAP demonstrated a portfolio of solar fuels test-bed systems exceeding 10% stand-alone solar-to-fuel energy conversion efficiency. These demonstration systems evaluated the full range of device configurations and electrolyte conditions. Both photoanode- and photocathode-based systems were demonstrated to be efficient. Efficient systems using strong acid, strong base, and near-neutral pH electrolytes were demonstrated utilizing acid exchange membranes, anion exchange membranes, and bipolar membranes, respectively. Efficient systems using liquid, vapor, or gas feed of reactant water and CO_2 were demonstrated in a combination of planar and high-porosity gas diffusion electrode configurations. Unassisted, highly selective plasmonic photocatalyst reduction of CO_2 was also demonstrated. The diversity of configurations that were characterized form a strong basis on which to improve durability without compromising efficiency going forward.

JCAP produced the world-record holder for unassisted photoelectrochemical water-splitting devices with an STH efficiency of 19%, approaching the theoretical maximum of 23% for a tandem junction device, using two light absorbers to efficiently utilize the solar spectrum. JCAP also demonstrated a 19% efficient unassisted solar-driven CO_2 reduction photovoltaic/electrolysis device using a gas-diffusion electrode directly coupled to a triple junction photovoltaic device.

Outlook Summary

In its more than 10 years of operation, JCAP moved the field forward dramatically in ways unimaginable in 2010. In addition to discovering new materials and protection strategies, deploying accelerated materials discovery and scale-up methods, developing new designs and computational models for solar-fuel generating systems, and demonstrating record-breaking system-level performance, JCAP built a solid foundation for the future success of the field by constructing and equipping dedicated research buildings, co-developing new techniques and facilities at DOE user facilities, developing and disseminating standard protocols and benchmarks for testing performance of solar materials, and developing a world-wide solar fuels workforce. However, a number of challenges related to durability, cost, and product selectivity remain to be solved before conversion of CO_2 into energy-dense liquid fuels through artificial photosynthesis becomes a viable method of meeting a portion of humanity's energy needs.

Achievements

Efficiency

JCAP increased solar-to-hydrogen (STH) energy conversion efficiency in unassisted water splitting to a record 19.3%, approaching the theoretical limit of 24% for this design. JCAP also increased solar-to-fuel energy conversion efficiency in unassisted CO_2 reduction to 19% by utilizing gas diffusion electrodes to overcome inherent solubility limits of CO_2 in electrolyte-only designs.

System design

JCAP demonstrated a portfolio of test-bed prototypes with solar-to-fuel conversion efficiencies exceeding 10%. This portfolio of test-bed designs enabled a thorough investigation of a full range of individual components and overall systems to maximize prerfomance.

Component Development

JCAP created a pipeline to accelerate materials discovery and scale-up for use as solar-fuels systems components. New catalysts for both the reduction and oxidation reactions were developed. A rich mechanistic understanding of these catalysts was developed through an integrated and iterative partnership of theory and experiment, which required the development of new methods and experimental facilities. Through an extensive search for new CO_2 reduction catalysts, JCAP confirmed that copper and its alloys are the best-performing materials as electrocatalysts for CO_2

ACHIEVEMENT HIGHLIGHTS

- Increased solar-to-fuel energy conversion efficiency in both unassisted water splitting and unassisted CO_2 reduction to >19%.
- Demonstrated a portfolio of test-bed prototypes with efficiencies exceeding 10%.
- Studied systems through test beds to maximize individual component and overall system performance.
- Confirmed copper and its alloys are the only materials that function efficiently enough to be electrocatalysts for CO_2 reduction to products beyond CO.
- Demonstrated tuning of the product selectivity of CO_2 reduction with copper catalysts via organic additives and tuning the composition of the electrolyte.
- Developed new catalysts for reduction and oxidation reactions and characterized their mechanisms using theory and experiment.
- Created a pipeline to accelerate materials discovery for solar-fuels systems' components.
- Established benchmarking and standard methods to allow systems to be compared.
- Developed partnerships with DOE user facilities that advanced research.
- Trained a world-wide solar fuels workforce.

reduction. JCAP also demonstrated tuning of the selectivity and reactivity of copper and its alloys through tailoring of the microenvironment via organic coatings on the electrocatalyst and by tuning the composition of the electrolyte.

Advanced the Solar Fuels Discipline

JCAP helped to place solar fuels on a firm footing as a scientific discipline by developing standard methods for measuring electrocatalyst performance and establishing benchmarks for performance and stability. These methods allow components to be compared, and have been adopted by the research community. JCAP also partnered with DOE user facilities to develop new experimental methods that greatly advance the study of electrocatalytic systems under operating conditions, and are available to the community.

JCAP developed a world-wide solar fuels workforce by training a cadre of graduate students, postdoctoral fellows, and staff who have gone on to leadership positions in academia, national labs, and industry around the world.

Continuing Challenges

Durability

JCAP researchers made significant advances in designing active components that are long-lasting and able to withstand daily temperature cycling and seasonal weather. However, new work is needed to design, discover, and develop high-performing components that are durable for many years.

High-Performing Systems and Components

Fundamental research is needed to provide a deeper mechanistic understanding of how systems of individual components and processes interact. This will allow better design of both components and prototypes for high performance.

Fuel Generation

An understanding of how to improve the efficiency of two chemical reactions that are essential parts of the artificial photosynthesis process, CO_2 reduction and water splitting, needs to be developed for future solar-fuels systems.

Using Sunlight Effectively

Current systems separate the process of light absorption from the catalytic reactions that generate fuels. Overall system efficiency could be improved by directly coupling diverse light-driven phenomena and chemical processes.

Development of Standards

Establishing common standards for measurements and cell designs for the field would provide a way to confirm claims made about solar-fuels systems prototypes.

Methods and Tools

Improvements in methods and tools used to characterize solar-fuels systems are needed to advance the field.

Introduction

JCAP was established in October 2010 and completed operation in September 2021. In JCAP's first phase, the goal was to address scientific and technological gaps in solar-driven water-splitting and CO_2 reduction catalysis. JCAP's first **five-year goal** was *"discovery of robust, Earth-abundant light absorbers, catalysts, linkers, and membranes and development of the scale-up science required to assemble the components into a complete artificial photosynthetic system."* JCAP made substantial progress in addressing all aspects of the scientific and engineering challenges, including discovery of new catalysts and photoabsorbers, assembly of components into a device, and scalability and sustainability analysis. JCAP also accomplished its goal of demonstrating operation of an integrated solar-driven water-splitting device 10 times more efficient than natural photosynthesis.

In its second phase, JCAP's **five-year goal** was to *"create the scientific foundation for a scalable technology to convert CO_2, water, and sunlight into renewable transportation fuels."* JCAP's approach was to master the use of selective heterogeneous electrocatalysis and photocatalysis to direct product formation from carbon dioxide reduction under mild conditions of temperature and pressure, with high selectivity and with efficiency exceeding that of natural photosynthesis. Doing this required accelerated discovery of new catalytic mechanisms and materials, as well as development of robust components suitable for integration into a solar-fuels generator. Three areas of research focus were defined to guide development of the scientific foundations for scalable CO_2 reduction to fuels:

1. Discovery and understanding of highly selective catalytic mechanisms for CO_2 reduction and oxygen evolution under mild conditions of temperature and pressure, and with input partial pressures of CO_2 in air between ambient atmospheric levels of 400 ppm and 1 atm.
2. Discovery of electrocatalytic and photoelectrocatalytic materials and useful light-absorber photoelectrodes, followed by integration.
3. Demonstration, in JCAP test-bed prototypes, of artificial photosynthetic carbon dioxide reduction components and oxygen-evolution components that exceed natural photosynthesis in efficiency and rival it in selectivity.

In JCAP, a major effort was made to discover and understand new mechanisms and new materials proficient for catalyzing CO_2 reduction. Despite systematic testing of new catalyst materials, Cu remains the most active electrocatalyst for reducing CO_2 to hydrocarbons and oxygenates, albeit with low selectivity. Consequently, a predominant focus was to understand deeply the mechanisms of CO_2 reduction on Cu surfaces and to gain control of these pathways to impart selectivity via the influence of nanostructuring, alloying, sequential catalysis, electrolyte effects, application of organic coatings, and electrochemical conditions. To elucidate electrocatalysis mechanisms, JCAP developed new experimental capabilities to probe the atomic-scale surface and composition of catalysts under operando electrochemical conditions. These experimental techniques were complemented by first-principles theory focused on the role of the catalytic environment, including the solvent, overlayers, and supports, in determining the activation energy landscape for CO_2 reduction. Understanding mechanisms of CO_2 reduction at photocatalysts involved the development and use of advanced computational techniques, as well as the use of ultrafast absorption spectroscopy and modeling of experimental product distributions to understand how excited states can alter CO_2 reduction selectivity and activity.

JCAP's materials discovery effort produced new electrocatalysts for selective CO_2 reduction and water oxidation, light absorbers for photoanodes and photocathodes, photoelectrocatalysts, and protection layers. CO_2 reduction electrocatalyst materials discovery activities can be classified into understanding how to use surface structure, alloy composition and spatial distribution, and electrode functionalization to direct selectivity on copper and copper alloys, including nanoparticle and oxide-derived (OD) Cu; development

of non-copper-based materials (e.g., Al-doped metal-organic frameworks [MOFs]); and development of plasmonic photocathode materials. The materials discovery effort deployed both directed discovery and a combined theory and experimental high-throughput discovery pipeline for photocathodes and photoanodes to screen candidate nanostructured metal alloy, metal chalcogenide, and metal oxide structures with optimal bandgaps and band edges that also satisfy stability criteria at the working pH conditions.

JCAP integration efforts expanded the portfolio and operating range of metal oxide protective coatings for photoanodes and improved understanding of interfacial charge-transfer dynamics and efficiency. High-throughput and directed discovery and characterization of integrated material assemblies yielded new integrated photoanodes and photocathodes with improved performance. Guided by JCAP's multiphysics device modeling, the performance of widely varying test-bed prototype configurations has been advanced, including both dark and light-driven gas-diffusion electrode (GDE) architectures and related membrane-electrode assemblies, as well as traditional planar bulk aqueous electrolyte cells. Both aqueous and vapor-fed test-bed systems achieved targets for selectivity and efficiency.

The pages that follow contain a narrative summary of JCAP research that describes key scientific and technical accomplishments, including discovery of novel materials and demonstration of water-splitting and CO_2 reduction test beds that exhibit performance characteristics and levels of integration that were inconceivable just 10 years ago. The narrative illustrates the breadth of JCAP's R&D programs spanning basic research to use-inspired and applied research. The narrative also describes several unique capabilities and partnerships that JCAP developed and its role in accelerating materials discovery research and breakthroughs in fundamental science.

Discovery and Understanding of Mechanisms

Electrocatalysis

Standardized Measurement of Oxygen-Evolution Reaction and Hydrogen-Evolution Reaction Electrocatalysts

The ability to quantitatively compare oxygen-evolution reaction (OER) and hydrogen-evolution reaction (HER) electrocatalyst materials was crucial for the development of new materials for water-splitting and CO_2RR.[1-9] When JCAP began, the literature contained hundreds of electrocatalytic systems with numerous elemental compositions and microstructures prepared in a multitude of ways. However, reliable methods for measuring and reporting the performance of these materials under identical conditions had never been uniformly applied, complicating meaningful comparisons of the catalytic activity and stability of these systems. There was an unmet need for standardization of catalytic performance to evaluate the utility of existing catalysts, provide experimental evidence to aid or corroborate theoretical models, and highlight existing technological gaps to help inform the development of new catalyst materials.

The JCAP benchmarking project developed a new procedure for evaluating the activity, stability, and electrochemically active surface area of electrodeposited catalysts for the OER. A comprehensive plot containing information regarding catalyst activity, stability, and specific activity was also designed. The primary figure of merit for the benchmarking measurements is the overpotential necessary to achieve 10 mA cm^{-2} current density: the approximate current density expected at the electrodes of a 10% efficient integrated STH prototype under 1 sun illumination.[9-11] In general, the best catalysts are expected to achieve 10 mA cm^{-2} current densities at low overpotential, maintain constant activity over time, and have low-surface roughness (i.e., high specific activity). This procedure was initially used to compare the performance of 10 OER catalysts,[12] and the resulting manuscript was featured as a *Science* magazine Editors' Choice.[13]

Subsequently, the benchmarking protocol was used to evaluate the performance of HER and OER catalysts comprised of Earth-abundant materials in 1 M NaOH and 1 M H_2SO_4.[14] These measurements are summarized in graphical form (**Figure 1**) for easy comparison of catalytic data. In the case of OER, most catalysts investigated were oxidatively unstable in acidic conditions. This suggests that the utility of a solar water-splitting prototype operating in acidic solution may be limited by the lack of non-noble metal catalysts that are oxidatively stable in acidic solution. In 1 M NaOH, most OER catalysts investigated showed roughly similar activity, achieving 10 mA cm^{-2} current densities at overpotentials between $0.3\ V \leq \eta \leq 0.5\ V$. This observation is qualitatively consistent with theoretical studies that suggest a limiting "thermodynamic overpotential" for OER at planar electrodes due to the existence of a common OER intermediate.[15] Several known HER catalysts show good activity and stability in acidic and basic electrolytes. JCAP extended its methods to benchmarking of nanoparticulate metal oxide electrocatalysts for water oxidation reaction under alkaline conditions.[16]

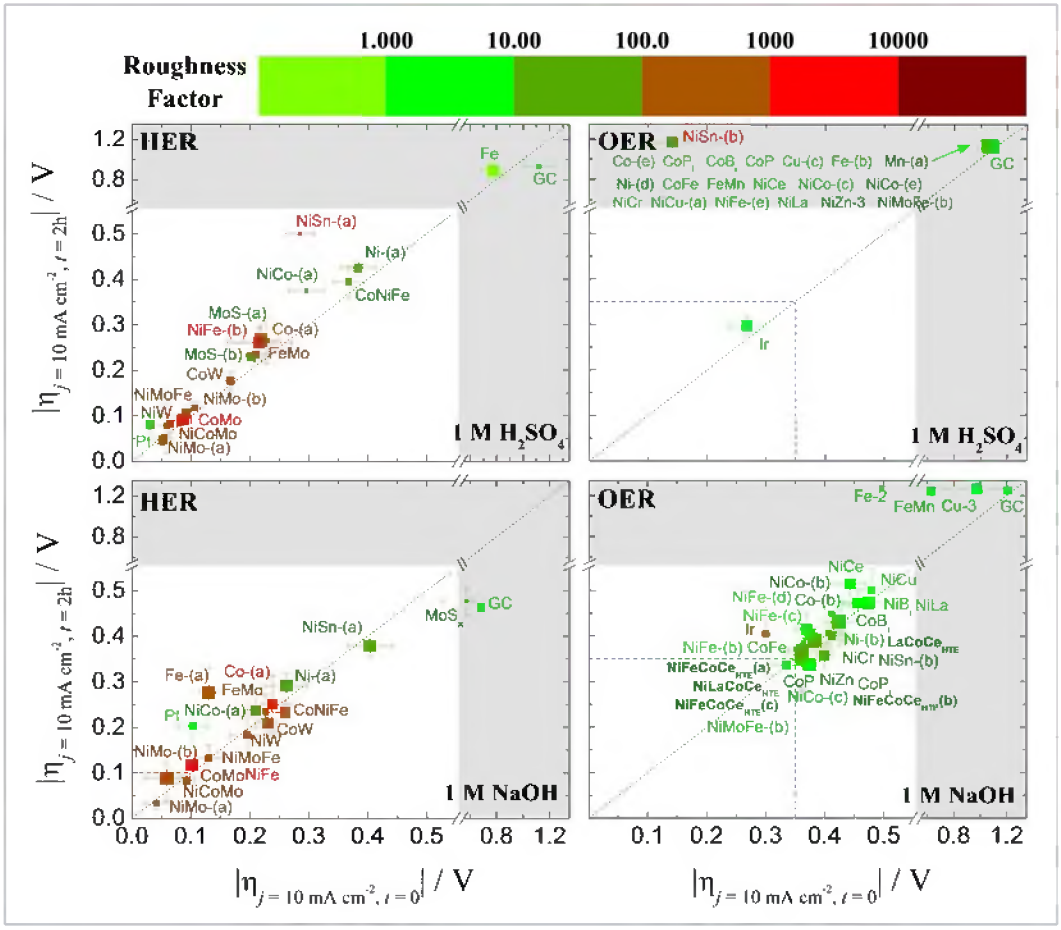

Figure 1. Plots of catalytic activity, stability, and electrochemically active surface area for HER (left) and OER (right) electrocatalysts in acidic (top) and alkaline (bottom) solutions. The x-axis is the overpotential required to achieve 10 mA cm^{-2} per geometric area at time t = 0. The y-axis is the overpotential required to achieve 10 mA cm^{-2} per geometric area at time t = 2 h. The diagonal dashed line is the expected response for a stable catalyst that does not change in activity during 2 h constant polarization. The color of each point represents the roughness factor of the catalyst with a bin size of one order of magnitude with light green representing RF = 1 and dark red representing RF > 10^4.

Advances in Methods for Mechanisms

JCAP developed a suite of capabilities for versatile, in-depth characterization of catalysts and electrodes for electrochemical and PEC reactions important for artificial photosynthesis. The techniques can be categorized as either microscopy or spectroscopy. The three levels of surface interrogation are ex situ, in situ, and operando, where ex situ is "out of natural location" and in situ is "in natural location," but with no temporal discrimination. Operando is defined as working, and the characterization is of an operating catalyst (**Figure 2**).

The electrochemical surface science laboratory at JCAP[17] established capabilities in catalyst characterization, surface structure-composition-function correlations, reaction pathways (thermodynamic selectivity), and reaction mechanisms (kinetic selectivity), and developed synergy between experimental and theoretical model studies. JCAP developed a laboratory-based combination of surface analytical methods encompassing ex situ, emersion, in situ, and operando surface techniques[18] and a sequential implementation of at least five operando methods:[19-20] electrochemistry, scanning tunneling microscopy (STM), polarization-modulation

infrared spectroscopy (PMIRS), electrochemical quartz crystal nanobalance (EQCN), and differential electrochemical mass spectrometry (DEMS). The combination of methods makes possible the identification of the unique structural constitution of the electrode surface that is responsible for performance, e.g., selective catalysis.[21]

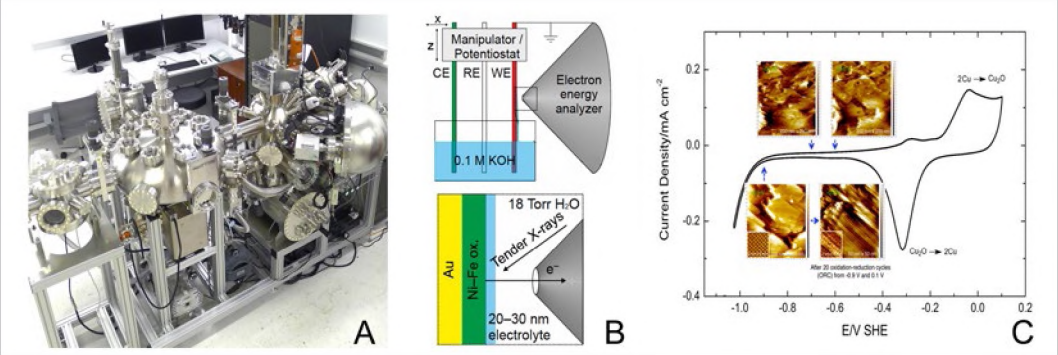

Figure 2. (a) Ex situ electrochemistry-surface science apparatus. (b) In situ near ambient pressure-XPS. (c) Operando EC-STM simultaneous with cyclic voltammetry.

The DOE user facilities at Berkeley Lab and SLAC house many of the most advanced X-ray, electron scattering, computational, and nanoscience capabilities in the world. Use of them for synthesis and characterization of artificial photosynthesis materials was crucial to JCAP's scientific success, because they offered the ability to fabricate complex nanoscale assemblies, connect materials composition to function at the scale of atoms, fully characterize the crystal and electronic structure of new semiconductors and catalysts, and investigate electrochemical processes under realistic conditions.

JCAP took full advantage of the DOE user facilities and contributed to the development of new capabilities as part of formal partnerships at the Advanced Light Source (ALS) and Stanford Synchrotron Radiation Lightsource (SSRL), and received large allocations of time from the National Energy Research Scientific Computing Center (NERSC). JCAP contributed new instrumentation for high-throughput SAXS-WAXS measurements, a liquid cell for studying in situ liquid-solid interfaces, and development of beamline capabilities at the ALS and SSRL for operando studies of catalysis. The significant allocations of facility time formed a core resource that was supplemented by single user proposal access as individual research projects evolved. The science made possible by the broad and flexible user facility access spanned JCAP's research portfolio, and was essential to the rapid progress made toward its mission and goals. Operando synchrotron-based X-ray characterization methods were developed by JCAP, including ambient pressure X-ray photoelectron spectroscopy (AP-XPS)[22] and operando PEC and GDE cells for X-ray spectroscopy and scattering at synchrotron end stations (**Figure 3**).[23-24] These methods were initially demonstrated with Pd-based catalysts to gain insight into the nature of hydrogen intercalation processes across a wide range of potentials.[25] Structural characteristics were also

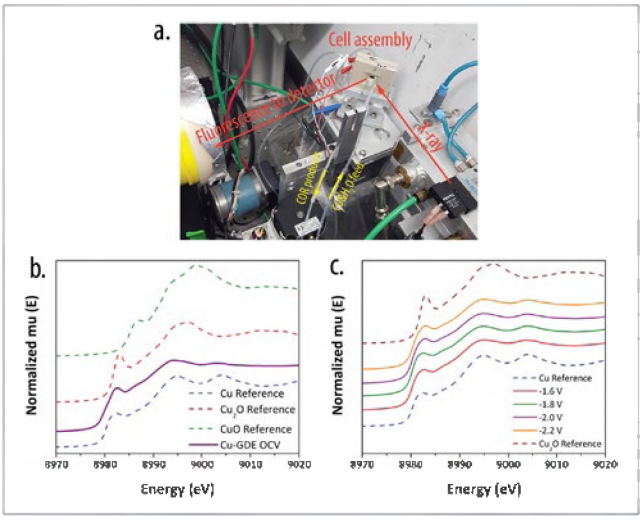

Figure 3: (a) Experimental setup for operando XAS at SSRL. (b) Operando XANES measurements at OCV and (c) under various applied potentials.

investigated for other catalyst families, including Cu under CO_2R conditions.[24, 26] X-ray absorption near edge structure (XANES) and extended X-ray absorption fine structure (EXAFS) were used to elucidate the electronic and structural changes of manganese oxide (MnOx) catalyst under electrocatalytic conditions.[27] Distinct Mn oxide structural phases were identified at oxygen reduction reaction (ORR) and OER relevant potentials. X-ray absorption spectroscopy (XAS) and electrochemical characterization of catalyst films revealed a highly porous structure. An X-ray emission spectrometer (XES) was developed, enabling the first study of the synergistic role of two metals, i.e., Ni in a mixed Mn-Ni oxide catalyst for water oxidation. The XES with multi-metal detection capability opened a new level of insight into synergistic effects (electronic, coordination) of one metal on another and the resulting influence on catalytic efficiency.[28]

The ALS and SSRL made possible characterization of semiconductor band structure,[29-35] in situ and operando catalysis mechanisms for the oxidation reactions,[27-28, 36-46] operando electrochemical interface characteristics,[47-48] characterization of heterogenized catalysts and anti-corrosion layers,[33, 46, 49-53] and the internal structure of polymeric membranes under ex situ and in situ conditions.[54-63] The High Throughput Experimentation project and the Critical Materials Institute worked together to develop high-throughput X-ray diffraction and composition measurement capabilities for materials libraries.[64]

The Molecular Foundry's Nanofabrication Facility and Inorganic Nanostructures Facility were essential to fabrication of thin films with controlled interfacial structure for creation and study of advanced electrode materials for solar-fuels devices. These include semiconductor and oxide thin films[50-51, 65-69] and nanostructured assemblies.[33, 36, 59, 70-74] The sub-Angstrom resolution capabilities at the Molecular Foundry's NCEM Facility were vital for imaging reactive and fragile specimens at the atomic level,[75-80] and both the NCEM and Imaging and Manipulation of Nanostructures Facility were used to examine the internal structure of materials assemblies to understand aspects of structure-function correlations.[32, 51, 56, 58, 81-86] Work at the Theory of Nanostructured Materials Facility of the Molecular Foundry using NERSC resources focused on the electronic structure of linker interfaces and tethered catalysts.[35, 50, 87-89] Additional studies at NERSC focused on molecular intermediates involved in reduction[90-91] and water oxidation catalysis[39, 43, 80, 92-94] and electronic band structures of semiconducting perovskites, oxides, and nitrides.[29-32, 50, 95-105] NERSC time was also used to simulate amorphous structures and corrosion protection layers[51, 105-108] and hot carrier generation.[109]

JCAP advanced both theoretical formulations and experimental capabilities for understanding the heterogeneous electrocatalytic and photocatalytic mechanisms of CO_2 reduction. The limitations of widely used continuum solvation models were considered,[110] including treating ions using a linearized Poisson–Boltzmann (LPB) model, which was shown to typically place charge unphysically close to the surface and adsorbates. JCAP scientists led the development of more sophisticated treatments, including use of explicit solvent and consideration of non-adiabaticity in electrochemical reactions.[111] The grand canonical potential kinetics (GCP-K) formulation was developed to provide a fundamental basis for understanding heterogeneous electrochemical reactions.[112] The importance of grand canonical quantum mechanical (QM) methods to describe the effect of electrode potential on the stability of intermediates involved in both CO_2R and the HER was demonstrated.[113] The methodology was developed to extract vibrational spectra from QM molecular dynamics (MD) trajectories in full solvent, and the spectra were related to experimental measurements.[114] Quantum embedding methods, including wavefunction (WF)-in-density-functional theory (DFT) embedding and embedded mean-field theory (EMFT), were applied to understand CO_2 reactivity pathways on a metal surface. WF-in-DFT embedding was applied with the path-based orbital partitioning approach to CO adsorption on a copper surface.[115] WF-in-DFT was reviewed for application to systems of interest to JCAP.[116]

Catalytic Mechanisms

JCAP's computational theory effort was strongly coupled to the experimental discovery science program and helped to elucidate how the composition and structure of molecular and heterogeneous catalysts affect their activity for HER, OER, and CO_2RR. Quantum chemical calculations of the energetics of the elementary steps via which these reactions occur were performed in order to identify the steps that limit catalyst activity and, in the case of the CO_2RR, the product selectivity. Related calculations were needed to interpret the results of spectroscopic and X-ray scattering and absorption experiments so that changes in catalyst structure occurring as a consequence of catalyst interaction with the electrolyte and the effects of applied potential could be properly described.

Hydrogen-Evolution Reaction

JCAP used an electrochemical cell and an ambient pressure X-ray photoelectron spectroscopy (XPS) system to probe the changes in the composition of molybdenum sulfide nanoparticles (MoSx) during HER.[117] The XPS spectra reveal that, as the system is humidified and taken to operating HER conditions, there is an irreversible change in the catalyst composition, with the growth of a lower binding energy (BE) feature at 162.0 eV. With enough applied voltage, the cell reaches current density regimes of the same order of magnitude as those required for solar-fuels prototypes. The electrochemical data showed that humidification plays an essential role by controlling the cell currents, with the transition from 1 to 5 Torr of water resulting in more than a doubling of the cell current, even with a lower applied voltage. This is attributed to the condensation of a water monolayer entirely covering the surface as the relative humidity reaches 30%. These experiments demonstrated that under operating conditions, MoS_3 sites gradually convert to MoS_2, and the electrolytic current densities are proportional to the extent of the transformation. The mechanism underlying MoS_2 activity was not known in detail.[118] To address this gap, JCAP developed a theoretical approach based on a cluster model, where the microscopically infinite Mo-edges of the MoS_2 crystals were modeled in a finite cluster. The rate-determining step on MoS_2 was found to be a reaction between the metal hydride and the hydronium water cluster (**Figure 4**). The result indicates that the sulfur hydrogen bond energy is not the relevant descriptor for HER activities. Similar work was also performed on $MoSe_2$, WS_2, and WSe_2, showing that the substitution of S with Se lowers the metal-hydride energies, while the substitution of Mo with W lowers the hydrogen chalcogen energies. Both substitutions might alter the reactions of these materials from those observed on pure MoS_2.[118] These insights and further theoretical studies led to identification of nanoclustered dichalcogenides as particularly active motifs.[119]

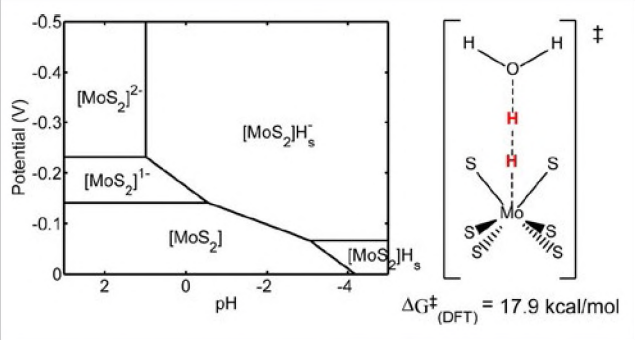

Figure 4. Calculated Pourbaix diagram for the surface states of the Mo-edge cluster.

Surface science techniques were also used to investigate Ni-Mo, which is among the most active hydrogen-evolution catalysts reported. The reason for its improved activity compared with that of pure Ni was not well understood. JCAP explored this issue by combined XPS and low-energy ion scattering spectroscopy (LEISS) measurements. It is clear that, whereas the XPS and energy-dispersive x-ray spectroscopy (EDS) results are identical and track the ideal 1:1 line, the LEISS data indicate a pronounced enrichment of molybdenum at the outermost layer.[17]

Oxygen-Evolution Reaction

Significant improvements in solar-fuels device efficiency require catalysts for the oxidation of water that exhibit overpotentials of less than 250 mV at a superficial current density of 10 mA/cm^2. JCAP focused on understanding the OER mechanism on selected catalysts in order to identify factors that affect activity, and potentially find ways to lower the overpotential, which is a direct means of increasing efficiency.

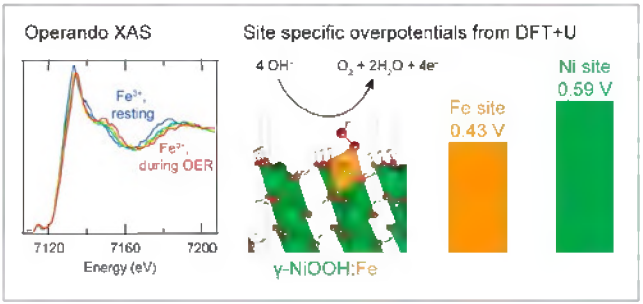

Figure 5. Operando XAS and high-energy resolution fluorescence detection (HERFD) reveal that Fe^{3+} in $Ni_{1-x}Fe_xOOH$ occupies octahedral sites with unusually short Fe–O bond distances, induced by edge-sharing with surrounding [NiO_6] octahedra. Using computational methods, it was established that this structural motif results in near optimal adsorption energies of OER intermediates and low overpotentials at Fe sites. By contrast, Ni sites in $Ni_{1-x}Fe_xOOH$ are not active sites for the oxidation of water.

The Fe-Ni system, which has one of the lowest overpotentials for the electrochemical oxidation of water in basic electrolytes, was of particular interest. Highly active $FeNiO_x$ catalysts were investigated in situ in order to identify the composition and local environment of the active sites.[120-121] $FeNiO_x$ films (2–70 nm) were electrodeposited on roughened Au electrodes and tested for OER activity; maximum activity was achieved for Fe/Ni ≈ 1.0. In situ Raman spectroscopy revealed that the catalyst was a mixture of γ-NiOOH and γ-FeOOH. The oxidation state and local coordination of Fe and Ni cations in working catalysts were probed by in situ XAS and in situ atmospheric XPS. XAS during OER showed that the oxidation state of bulk Ni cations exceeded 3+, whereas the oxidation state of bulk Fe cations remained 3+, independent of the proportions of Fe and Ni. The average Ni-O bond distance in FexNi1-xOOH was found to be higher than that in γ-NiOOH, and the average Fe-O bond distance was lower than that in γ-FeOOH. With increasing Fe addition, the applied potential at which Ni^{2+} was oxidized to Ni^{3+} increased, in good accord with in situ Raman and electrochemical measurements. Theoretical studies based on DFT support both of these findings and suggest that the high activity of $FeNiO_x$ is attributable to Fe^{3+} cations present in strained configurations within γ-NiOOH. Further studies[43] demonstrated that the presence of Fe in $Ni_{1-x}Fe_xOOH$ octahedral sites results in optimal adsorption energies for OER intermediates and low overpotentials (**Figure 5**).

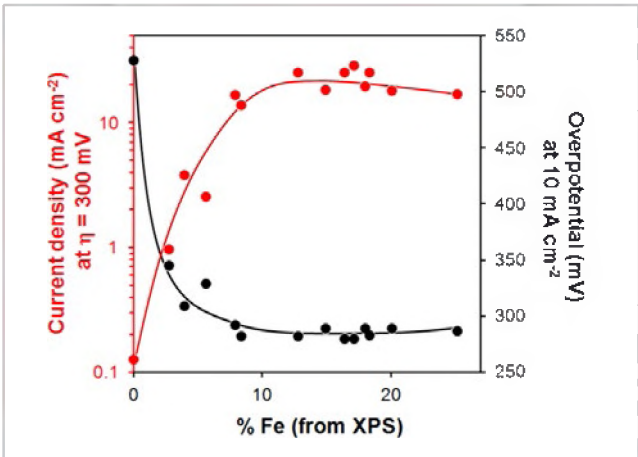

Figure 6. Oxygen evolution activity of electrodeposited NiOOH films deposited on Au RDEs at 300 mV overpotential and 10 mA cm-2 geometric current density in 1 M KOH as a function of Fe content. Curves are included to guide the eye.

To complement this work, JCAP performed a series of studies that deepened understanding of processes involved in $N_{il-x}Fe_xOOH$ catalyst evolution during electrochemical reactions, and the influence of catalyst preparation on activity. Incorporation of trace Fe impurities from commonly used KOH electrolytes significantly improved OER activity over NiOOH electrocatalysts.[122] It was found that Ni films aged in unpurified electrolyte can incorporate ≥ 20% Fe after five weeks of aging, and the maximum catalyst activity is comparable to that reported for optimized $N_{il-x}Fe_xOOH$ catalysts (**Figure 6**). Above ~11% Fe content, a separate, Fe-rich phase forms, providing direct evidence that a Ni-Fe layered double (oxy)hydroxide (LDH) phase

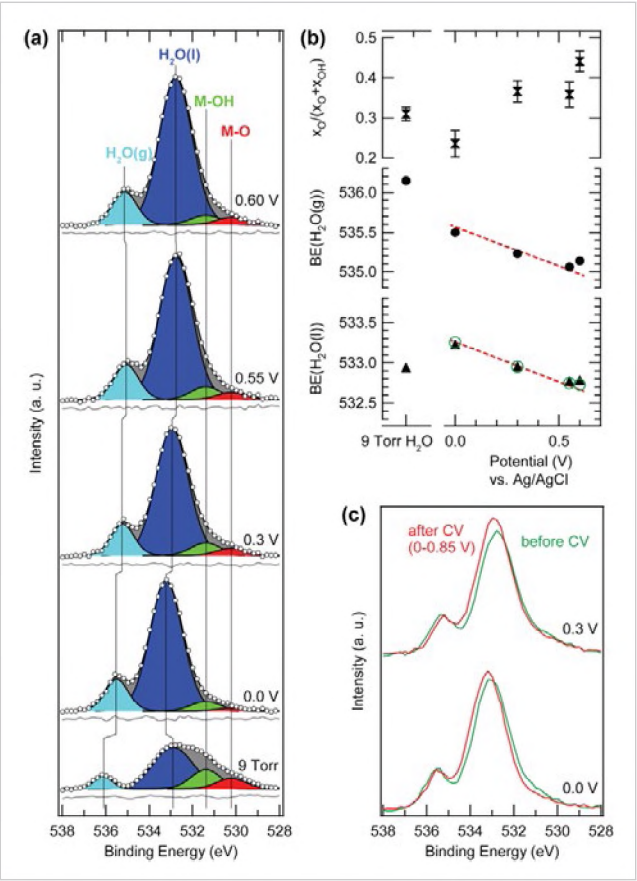

Figure 7. (a) Normalized and background-subtracted O1s XP spectra of Ni–Fe (7 nm) electrocatalyst, excited with 4020 eV X-ray photons. Bottom to top: as-prepared catalyst exposed to 9 Torr H_2O pressure, and operando measurements, taken after extended electrochemical conditioning (6 cycles, 0-0.65 V, and 6 cycles, 0-0.85 V) under a ~30 nm thick 0.1 M KOH liquid film at the indicated applied potentials (vs. Ag/AgCl). The measured spectra (circles) are fitted with four components (black lines, residuals: gray lines) representing H_2O in the gas and liquid phase, and OH and O in the catalyst. (b) Fit results for spectra in (a) relative intensity of the M–O component in the $MO_x(OH)_y$ catalyst, and measured H_2O peak positions (black symbols) at 9 Torr, and in liquid electrolyte as a function of applied potential. The expected 1:1 relationship between peak shift and applied potential is indicated with red dashes, and theoretically modeled peak positions considering potential losses in the thin electrolyte layer are shown with green circles. (c) Comparison of XPS measurements taken at identical applied potentials before (green) and after (red) the second electrochemical conditioning (0–0.85 V).

is critical for high OER activity. Interestingly, Fe cations present as impurities in 1 M KOH have even been found to bind to the surface of oxidized Au and exhibit enhanced OER activity.[123] The OER overpotential over Au decreases from ~0.85 to ~0.5 V with the presence of surface Fe sites at low current densities (j = 0.1 mA cm^{-2}), in close agreement with the decrease in the OER overpotential determined from DFT calculations for pure Au_2O_3 vs Fe chemically bound to Au_2O_3. This decrease in the OER overpotential was attributed to the more optimal adsorption energy of intermediates involved in the OER.

Electrochemical impedance and activation energy measurements were used to gain insight into the evolution of $Fe_xNi_{1-x}OOH$ catalysts with composition.[124] The results showed that as Fe is incorporated in a NiOOH lattice, the Faradaic resistances associated with the OER decrease and charge relaxation becomes more favorable. While Fe sites in NiOOH lattices have similar energetics regardless of film composition, the overall OER activity is also controlled by structural considerations. This characteristic was a focus in a comparison of the structure and OER activity of sputter-deposited and electrodeposited $Ni_{1-x}Fe_xOOH$ thin films.[125] Electrochemical cycling to convert sputtered metallic $Ni_{1-x}Fe_x$ films to metal oxides/(oxy)hydroxides was found to lower the Fe:Ni ratio, while the electrodeposited films exhibited similar Fe:Ni ratios before and after electrochemical cycling and characterization. Structurally, Fe was found to incorporate within the $Ni(OH)_2$/NiOOH lattice for films formed through both sputter-deposition and electrodeposition. Layered films were also compared to co-deposited 1:1 Fe:Ni films. It was found that for layered films, an Fe top layer inhibited the electrochemical conversion of metallic Ni to $Ni(OH)_2$/NiOOH, while migration of metals within Ni-on-top films occurred readily during electrochemical cycling. Electrochemical cycling was examined directly using "Tender" X-ray AP-XPS. A thin film of Ni-Fe oxyhydroxide was electrodeposited on Au as the working electrode at different applied potentials in 0.1 M KOH.[126] The as-prepared 7 nm thick Ni-Fe (50% Fe) film contained Fe and Ni in both their metallic and oxidized states, and underwent further oxidation to Fe^{3+} and $Ni^{2+/3+}$ when the sample was subjected to electrochemical oxidation-reduction cycles (**Figure 7**).

While a number of suitable OER catalysts that function in base were identified, that was not the case for OER in acid. The standardized evaluation of OER catalysts described above revealed that at the start of JCAP, only

IrO_2 was a suitable catalyst under acidic conditions. Understanding the fundamental reaction mechanism in acid informed work to develop catalysts with low Ir loading and/or find a replacement for Ir. The correlation between surface species and applied electrochemical potential on an iridium oxide electrocatalyst under OER conditions was probed in situ through AP-XPS using a customized electrochemical cell.[37] It was demonstrated that, under OER conditions, iridium undergoes a change in oxidation state from Ir(IV) to Ir(V) that takes place predominantly at the surface of the catalyst. In addition, DFT was used to identify new catalyst motifs capable of achieving targeted activity at low overpotential.[127-128]

CO_2RR Electrocatalysis

Cu-Based Electrocatalysis, Experiment and Theory

Mechanistic complexity. A significant effort across JCAP aimed to understand mechanistic pathways for the CO_2 reduction reaction (CO_2RR). There remains much to understand about this reaction, and the insights gained from mechanistic work are essential to provide the guiding principles needed to develop improved catalysts. Much progress was made in understanding mechanistic aspects of C-C coupling and key electrolyte factors that can tune activity and selectivity, in order to identify control points for the reaction. A variety of factors are known to impact CO_2R activity and selectivity, including the catalyst surface structure, morphology, and composition, the choice of electrolyte ions and pH, and factors involving the reactor design (e.g., mass transport, electrode area, etc.). Toward the end of the project, JCAP researchers comprehensively reviewed and analyzed these factors and their complex interplay in CO_2R catalysis on Cu to critically evaluate progress in understanding the complex reaction networks for CO_2R on Cu, based on substantial research efforts both inside and outside of JCAP (**Figure 8**).[129] The complexity of **Figure 8** and the variety of proposed mechanisms reveals the need for further research to understand CO_2R pathways to improve selectivity and activity. This will be particularly important to develop CO_2R into an energetically sustainable technology that minimizes chemical separations.[130]

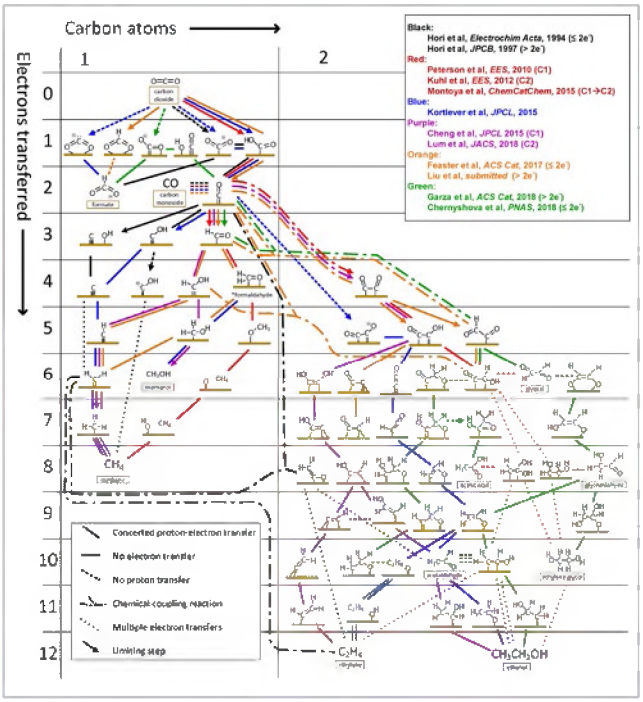

Figure 8. Possible mechanistic pathways of CO_2 reduction to C1 and C2 products on polycrystalline copper, grouped into different colored reaction schemes taken from the works in the top-right legend. The bottom-left legend states the meaning of the texture of the lines connecting intermediates.

Operando and in situ characterization. JCAP identified active sites and key reaction intermediates for the CO_2RR in order to provide the insights needed to develop improved catalysts. It is critical to probe the catalyst surface as well as surface-adsorbed species in situ to understand the atomic and molecular-scale phenomena that are occurring during the CO_2RR.

JCAP's early investigations of chemical and structural changes at Cu surfaces laid the foundation for subsequent mechanistic insights. Operando EC-STM was used to understand surface changes to Cu electrodes under reaction conditions. As-prepared Cu(100) was cathodically reduced to a clean and ordered Cu(100) surface under reaction conditions, while a polycrystalline Cu electrode was found to behave electrochemically similar to Cu(100) electrodes, because

it undergoes stepwise surface reconstruction, first to Cu(111) and then to Cu(100) under reaction conditions (**Figure 9**).[131] JCAP demonstrated that single crystals of Cu(100) and Cu(111) do not reconstruct, but Cu(110) undergoes a three-stage transformation, first to disordered Cu(110), then to disordered Cu(111), and finally to an ordered Cu(100).[132]

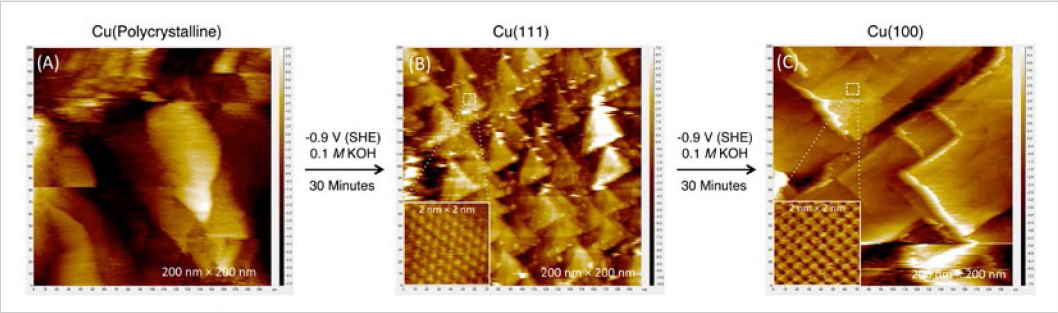

Figure 9. Operando EC-STM reveals the surface reconstruction of a Cu(poly) electrode under CO_2RR conditions.

The significance of the crystallographic surfaces of Cu (and other metals as well) for determining the product specificity of CO_2RR was demonstrated by investigation of several specific orientations of epitaxial and single-crystal Cu. Seriatim ECSTM-DEMS enabled the direct correlation between electrocatalyst surface structure and product selectivity or activity under reaction (operando) conditions. Cu-catalyzed reduction of CO can be regulated by an atomic-level control of the surface structure to yield only one product; for example, C_2H_5OH is produced in 0.1 M KOH at -1.0 V (SHE) from a stepped Cu(511) surface.[133] JCAP also utilized epitaxially grown large-format Cu thin films (ca. 6 cm^2) to fully probe product selectivity.[134] In situ EC-STM studies on Cu(100), (111), and (751) thin films revealed that Cu(100) and (111) are identical to the bulk structure, but that Cu(751) has a heterogeneous kinked surface with (110) terraces. Electrochemical CO_2R testing showed that while both Cu(100) and (751) thin films are more active and selective for C-C coupling than Cu(111), Cu(751) is the most selective for > 2e oxygenate formation at low overpotentials.[134] Similarly, the selectivity of nanoparticle catalysts was tuned via facet-specific functionalization of copper nanocrystals with passivating films of ALD-deposited Al_2O_3 increasing the Faradaic efficiency for ethylene synthesis.[135]

Application of STM and operando PMIRS uncovered that, at potentials higher than -0.85 V, no CO adsorption occurs. On Cu(100), the coverage θ_{CO} leveled off at 0.50 in a Cu(100)-c(2×2)-CO adlattice with the CO molecules located at alternate atop sites in vertical orientations; such coverage and mode of binding are as expected from the coordination of CO with zero valent Cu, a d^{10} transition metal.[136] Operando electrochemical STM further enabled visualization of the step edges of unreconstructed Cu(100), with and without CO dissolved in 0.1 M KOH, at the early onset-potential region for CO_2R, which revealed that the step-edge direction changes dramatically upon the adsorption–desorption of CO at potentials of –1.0 to –0.8 V.[137] In another seriatim permutation, operando EQCN was combined with STM and DEMS as a prelude to the acquisition of θ_{CO} as a continuous function of concentration and potential.[138] It is equally critical to know the adsorbate packing arrangement at the onset of the reaction because, if "CO dimers" were indeed the precursors to C_2 products, reduction can be initiated only when the adlayer consisted of closely packed, not loosely arrayed, CO molecules. The results show that the electrocatalytic reaction (i) lags the adsorption process and (ii) does not transpire until maximum CO adsorption is attained (**Figure 10**).

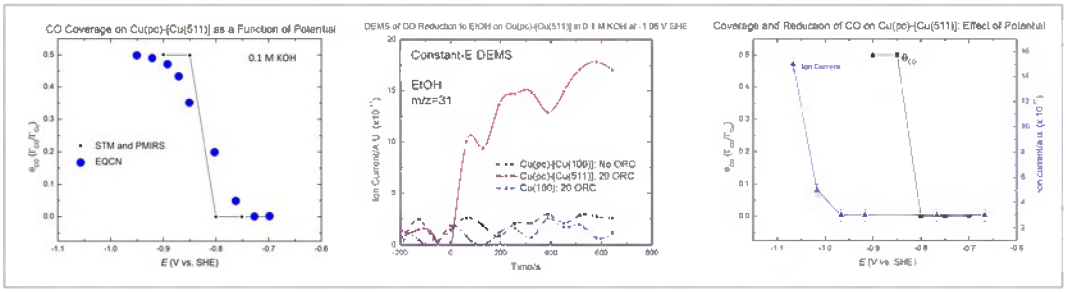

Figure 10. Near-perfect agreement between operando modes of STM, DEMS, and PMIRS. Onset of reduction of adsorbed CO to ethanol occurs at lowest potential in 0.1 M KOH on Cu(511), but only after maximum coverage of chemisorbed CO is attained.

Oxygen in Cu catalysts. The proposed effect of residual or subsurface oxygen on the activity and selectivity of Cu and oxide-derived (OD) Cu electrocatalysts has stimulated much scientific discussion. Studies of heterogeneous electrocatalysts for CO_2RR were performed in stringently controlled environments. The interfacial structures and compositions of Cu(100), Cu(110), and Cu(111), before and after exposure to gaseous oxygen and emersion in mildly alkaline media (pH 8 and 10), were characterized by a combination of electrochemistry, LEED, and AES.[139] The affinity of the low-index copper planes for oxygen gas was found to decrease in the order Cu(110) > Cu(100) > Cu(111). The initial stages of the anodic oxidation of copper, prior to formation of bulk oxides, span a wide potential window that is pH-sensitive; within this precursory region, sub-monolayer coverages of oxygen tended to form surface domains with long-range order. At potentials far below the anodic-oxidation region (E < -0.90V), the surface compositions and structures of Cu(hkl) are expected to mimic those of zero valent copper. These results bear significant implications in the generation and identification of surface-bound intermediates that define the electrocatalytic selectivity of copper.

Differences in product distributions observed between Cu-oxide and pure Cu electrodes during electrochemical CO_2 reduction were also investigated. In these studies, the stability of subsurface oxygen from thermodynamic and kinetic perspectives was considered. It was shown that under reducing potentials, subsurface oxygen alone should have negligible effects on the activity of crystalline Cu.[140] Using DFT, the stability and diffusion of subsurface oxygen in single crystals of copper exposing (111) and (100) facets was investigated. Oxygen was found to be at least 1.5 eV more stable on the surface than beneath it for both crystal orientations; interstitial sites are too small to accommodate oxygen, and diffusion is fast from one layer below the surface to the top layer. While oxygen can survive longer in deeper layers, it does not promote CO_2 adsorption there. Using the constant electrode potential model[141-142] and a nonlocal correlation functional, it was found that subsurface oxygen is unnecessary for CO_2 adsorption on copper, leading to the conclusion that subsurface oxygen is unlikely to be present near the surface during the reaction, and that it is not crucial in determining the ability of copper to reduce carbon dioxide.[142]

JCAP investigated the role of oxygen in Cu, Ag, and Cu/Ag alloy surfaces upon exposure to CO_2 or CO_2/H_2O using AP-XPS interpreted with QM simulations. In the Cu study, a thin suboxide structure below the copper surface may be essential to bind the CO_2 in the physisorbed configuration at 298 K and promote chemisorbed CO formation.[143] The stability of residual oxides was investigated by synthesizing ^{18}O enriched OD Cu catalysts and testing them for CO_2R (**Figure 11**). These catalysts maintain a high selectivity toward C_2/C_3 products (~60%), with secondary ion mass spectrometry (SIMS) measurements revealing that only a small fraction (<1%) of the original ^{18}O content remains; residual oxides are not present in significant amounts during CO_2R. OD Cu reoxidizes rapidly in the absence of a reducing potential, which could compromise the accuracy of ex situ methods for determining the true oxygen content.[144] The structural evolution of the near-surface region (probe depth of 2.6 nm) of polycrystalline Cu electrodes under in situ conditions was

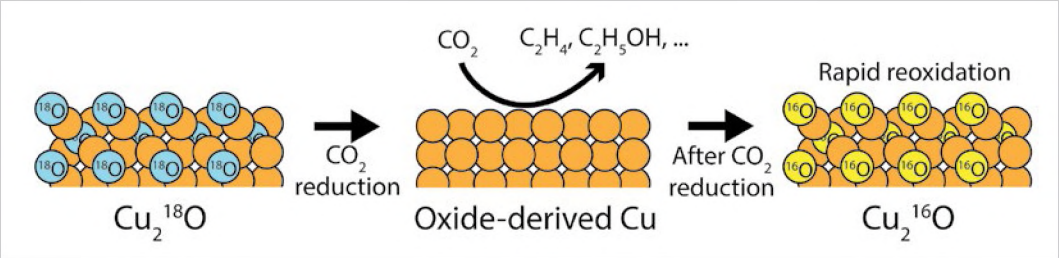

Figure 11. Cu_2O labelled with the ^{18}O isotope was synthesized. When employed under CO_2R conditions (~1 V vs. RHE in aqueous solution), the oxide converts to Cu metal. The Cu rapidly reoxidizes after the reducing potential is removed.

examined through a combination of grazing-incidence X-ray absorption spectroscopy (GIXAS) and GIXRD. These studies revealed that the surface oxide layer is fully reduced to metallic Cu before the onset potential for CO_2RR, and the catalyst maintains the metallic state across the potentials relevant to the CO_2RR. Additionally, a preferential surface reconstruction of the polycrystalline Cu surface toward (100) facets is observed in the presence of CO_2, consistent with the STM measurements,[131] confirming that the Cu surface is dynamic during the CO_2RR.[26]

The role of subsurface oxygen on production of C_2 products from CO_2 reduction over Cu electrocatalysts was elucidated using the newly developed grand canonical potential-kinetics DFT method, which predicts that the rate of C_2 production on pure Cu with no O is ~500 times slower than H_2 evolution. In contrast, starting with Cu_2O the rate of C_2 production is > 5,000 times faster than pure Cu(111) and comparable to H_2 production. Experimental validation combined time-dependent product detection (**Figure 12**) with multiple characterization techniques to show that ethylene production decreases substantially with time and that a sufficiently prolonged reaction time (e.g., 20 hours) leads to only H_2 evolution with ethylene production ~1,000 times slower, in agreement with theory. This result indicates that substantial subsurface oxygen is essential for long-term C_2 production with Cu catalysts.[145]

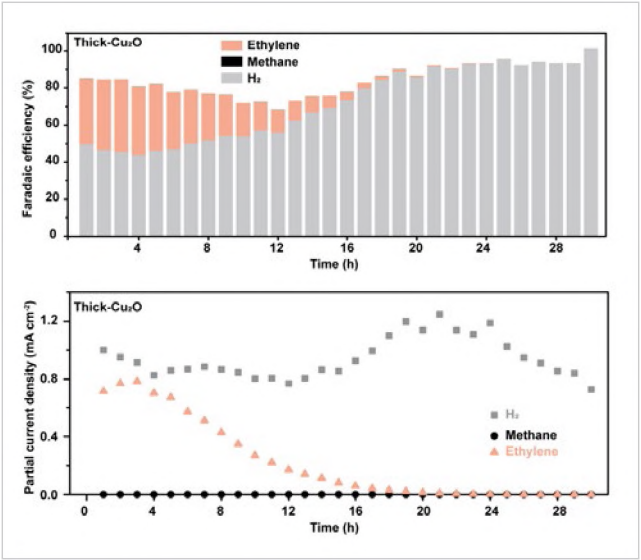

Figure 12. Long-term CO_2RR measurements on thick-Cu_2O indicate that depletion of oxygen leads to reduced C_2H_4 production.

Additional isotopic labeling studies identified whether all products are generated from the same types of active sites on OD Cu or if product-specific active sites are responsible for making certain products.[146] By reducing mixtures of ^{13}CO and $^{12}CO_2$, it was demonstrated that OD Cu catalysts have three different types of active sites for C-C coupled products, one for ethanol/acetate, another for ethylene, and yet another for 1-propanol. In contrast, the researchers did not find evidence of product-specific sites on polycrystalline Cu and oriented Cu (100) and (111). Analysis of the isotopic composition of the products leads to the prediction that the adsorption energy of *COOH, the product of the first step of CO_2 reduction, may be a descriptor for the product selectivity of a given active site.

CO reduction. Investigating electrochemical CO reduction (COR) can give valuable mechanistic insights on the CO_2RR, since CO is a key reaction intermediate to further reduced C-C bond-containing products. JCAP investigated how the applied potential, partial pressure of CO, and electrolyte pH can be controlled to guide selectivity toward fuels and chemicals on polycrystalline Cu (pc-Cu) electrocatalysts.[147] By comparing CO and CO_2 reduction data in similar reactors using the same Cu foils,[148] it was demonstrated that alkaline electrolytes can increase the energy efficiency toward C_{2+} products (**Figure 13a**). Common trends in selectivity for COR and CO_2R indicate that lower applied potentials will promote higher ratios for oxygenates/hydrocarbons (**Figure 13b**), with selectivity trends that are similar to state-of-the-art high surface area Cu catalysts (**Figure 13c**).[147-151] These design principles were applied to a high surface area nanostructured Cu catalyst (Cu-flowers) that exhibited a total Faradaic efficiency (FE) of nearly 100% for COR to C_{2+} oxygenates in alkaline electrolytes. A kinetic model for COR toward C_{2+} on stepped Cu was developed, based on activation energies determined from an explicit solvent model (**Figure 13**). This model elucidated the critical effect of pH on C_2 to C1 selectivity via differences in reaction pathways. Furthermore, the model suggested that C_{2+} product selectivity can be improved through increased CO pressure, since the coupling step is second order in CO coverage. They also found Cu(100) and stepped Cu(211) to be more favorable for C-C coupling than Cu(111). This investigation rationalized in part the improved activity of Cu nanocube catalysts toward C_2 products from CO_2, which preferentially expose steps and likely more defect and step sites.[152-153]

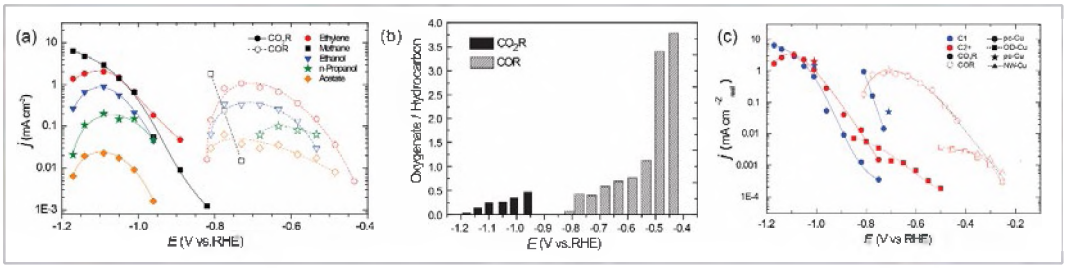

Figure 13. (a) Partial current densities for the indicated products from pc-Cu: (solid) CO_2 reduction and (dashed) CO reduction. (b) Oxygenate/hydrocarbon ratios as a function of the applied potential. (c) Normalized partial current densities for CO_2R and COR on different Cu electrode morphologies. All of the current densities have been normalized based on the reported roughness factor of the corresponding electrodes.

While numerous studies had examined the electroreduction of CO to oxygenates such as ethanol, none considered the possibility that oxygen in the product might arise from water rather than from CO. This assumption was tested by reducing $C^{16}O$ in $H_2{}^{18}O$ electrolyte.[154] Surprisingly, the team found that 60–70% of the ethanol has ^{18}O, which must have originated from the solvent (**Figure 14**). Prior all-solvent DFT metadynamics calculations were extended to consider the possibility of incorporating water, and found a potential new mechanism involving a Grotthuss chain of six H_2Os in a concerted reaction with the *C-CH intermediate to form *CH-CH(^{18}OH), subsequently leading to ^{18}O ethanol. This competes with the formation of ethylene that also arises from *C-CH. JCAP researchers also considered an alternative explanation for the incorporation of oxygen derived from solvent water into the oxygenated products of COR over Cu,[155] by attributing it to isotopic scrambling of carbonyl-containing intermediate reaction products that are reduced further to oxygenated products.

Understanding mechanisms through computation. JCAP employed a multifaceted approach to investigate the CO_2 reduction reaction (CO_2RR) using first-principles-based theoretical methods, a diverse effort involving numerous research groups. JCAP theorists focused on developing a detailed understanding of CO_2R energetics and mechanisms, using explicit solvent methods. The first steps toward a comprehensive microkinetic model for CO_2 reduction to C_2 products on stepped Cu were taken, based on reaction and

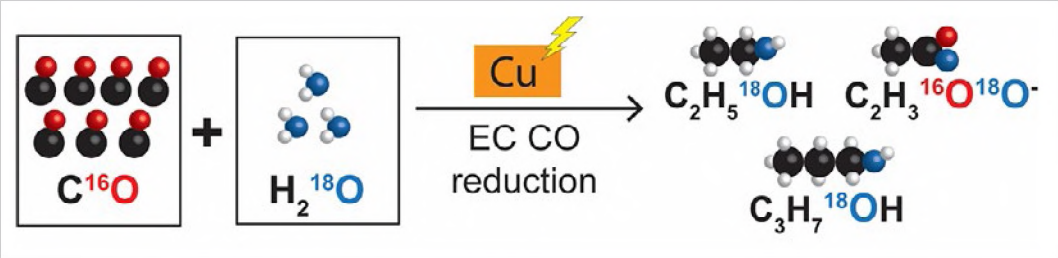

Figure 14. $C^{16}O$ reduction on Cu(100) in $H_2{}^{18}O$ electrolyte produces acetate, propanol, and ethanol which are enriched in ^{18}O. The enrichment is independent of potential suggesting that a chemical step involving an intermediate which does not contain any O atoms is responsible.

activation energies using an explicit solvent approximation. The observed differences in the multi-step mechanisms for C_1 and C_2 products (**Figure 15**) result from different dependences on pH as well as applied potential. These studies suggest that alkaline conditions generally favor the formation of C_2 products over C_1 for either CO_2 reduction or COR. At high overpotentials, however, CO is more readily hydrogenated to C_1 products, leading to lower CO coverage; because C-C coupling has a second-order dependence on CO coverage, reaction rates for C_2 products also decrease at higher overpotentials.[156]

JCAP theorists developed a detailed understanding of reaction mechanisms, including descriptors for C1 selectivity across the range of electrode materials,[157] C_2 mechanisms (identifying important reaction intermediates, descriptors, and comparison with experiment),[158] C_2 selectivity (hydrocarbons vs oxy-hydrocarbons), theoretical screening of new catalysts for CO_2R,[157] and the mechanisms for C3 formation on Cu electrodes. JCAP calculations support experimental observations showing that high activity and selectivity to C_{2+} products can be achieved by controlling atomic-scale spacings between two facets of different Cu particles.[159] Spacings of 5–6 Å allow a current density exceeding that of unmodified CuOx nanoparticles, by more than a factor of 10, with an FE of ≈80% to C_{2+}. The calculations show that such spacings maximize the binding energies of CO_2 reduction intermediates and promote C–C coupling reactions. A reaction network for the electrochemical reduction of CO/CO_2 on Cu was proposed that explains the formation of C_{2+} products and the observed selectivity for ethene versus ethanol formation.[142] This work forms the basis for developing ideas about how C3 products are formed. The researchers hypothesize that the third C atom originates from *CO addition to the C_2 intermediates.

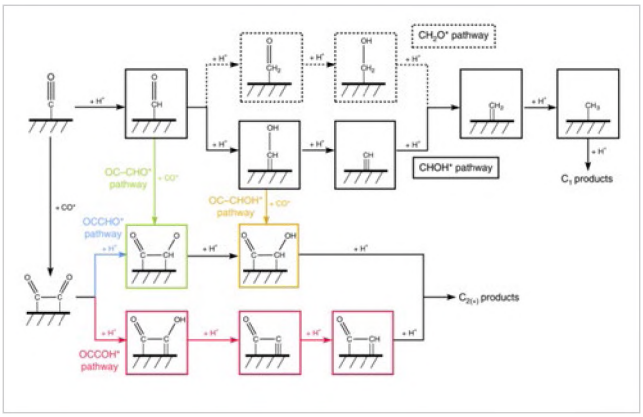

Figure 15. Reaction schemes of major pathways considered for CO reduction toward C_1 and C_{2+} products. The green path denotes C_2 production through coupling of OC–CHO; the blue and red path represents C_2 production through protonation of OCCO to form OCCHO and OCCOH, respectively; the yellow path represents C2 production via OC–CHOH coupling. The black path denotes C_1 production via CHOH and the dashed CH_2O.

Defects were investigated by JCAP theorists as possible active sites in star decahedron Cu nanoparticle catalysts, demonstrating that they are highly selective for ethylene production.[160] The calculations showed that the surface stacking faults and twin defects in the nanoparticles directly led to the enhanced CO_2R performance. Machine learning methods were combined with DFT to understand the nature of active sites on Cu nanoparticles grown on carbon nanotube supports. Since these nanoparticles involve ~200,000 or more atoms, the machine learning approaches are essential to bridge with QM methods.

The researchers used this to identify the most active sites, which turned out to be a twin boundary next to a 111 facet.[112] They further report that copper nanowires with rich surface steps exhibit a remarkably high FE for C_2H_4 that can be maintained for over 200 hours. Computational studies reveal that these steps are thermodynamically favored compared with the Cu(100) surface under the operating conditions, and the stepped surface favors C_2 products by suppressing the C1 pathway and hydrogen production.[161]

Au/Ag/Cu Alloys, Experiment and Theory

The noble metals, Au, Ag, and Cu, all reduce CO_2, but only Cu makes C-C bonds. JCAP worked extensively to understand the differences between these metals in order to refine understanding of product formation on Cu. Structure-activity relationships were investigated by electrochemically reducing CO_2 to CO over Ag thin films with (111), (100), and (110) orientations prepared via epitaxial growth on single-crystal Si wafers with the same crystallographic orientations.[162] The Ag(110) thin films exhibited superior activity to the Ag(111) and Ag(100) thin films, consistent with previous single-crystal studies. DFT calculations suggest that CO_2 reduction to CO is strongly facet dependent, and that steps are more active than highly coordinated terraces. These findings result from both a higher BE of the key intermediate COOH as well as an enhanced double-layer electric-field stabilization over undercoordinated surface atoms located at step edge defects.[162-163] As a consequence, step edge defects likely dominate the CO_2 reduction activity observed over the Ag(111) and Ag(100) thin films. The higher activity observed over the Ag(110) thin film is then related to the larger density of undercoordinated sites compared with the Ag(111) and Ag(100) thin films.[162] JCAP utilized a multiscale framework for ab initio simulation of the electrochemical reduction of CO_2 over a Ag(110) surface. A continuum model for species transport was combined with a microkinetic model for the cathode reaction dynamics. Free energies of activation for all elementary reactions were determined from DFT calculations. Examination of three alternative mechanisms for CO_2 reduction, which differed in the nature of the hydrogen donor—*H, **H_2O, and free H_2O—for producing CO via **COOH in the rate-limiting step, demonstrated that only free H_2O as the hydrogen donor matched the experimental data.[164]

The rate of electron transfer to CO_2 at the Au(211)-water interface during adsorption in an electrochemical environment under negative potentials was studied.[165] Based on results of several levels of theory, electron transfer to adsorbed *CO_2 was found to be very facile and it is, therefore, unlikely that electron transfer is rate limiting for this reaction. Surface charging is important for electrochemical kinetics and mass transport when examining CO_2 reduction experiments on Au at neutral to acidic pH values.[166] Finally, the researchers have investigated transition metal surface energies under lattice strain and CO environments.[167] Using AP-XPS,[22] Cu, Ag, and Cu/Ag alloy surfaces were studied when exposed to CO_2 or CO_2/H_2O. In coordination with theory, the researchers found that CO_2 surface adsorption on Ag surfaces is quite different from that on Cu surfaces.[143] On Ag, an adsorption mechanism involving the $O{=}CO_2^{\delta-}$ was observed, in comparison to that involving b-CO_2 on Cu. Each metal surface modifies both the chemical speciation and the respective adsorption energies, thus providing a new basis for tuning CO_2 adsorption behavior to facilitate selective product formation.[168] The researchers also studied Ag/Cu alloys and found that the metal stoichiometry at alloy surfaces, which may differ from that of the bulk, plays an important role in the interaction of surface metals and adsorbed species. These findings will stimulate new thinking about the CO_2 reduction reactions on metal surfaces, suggesting that stabilization of various surface adsorption configurations can be controlled through additives or alloying along with externally applied potentials to control the reaction processes (**Figure 16**).[169] The initial atomic-level events for CO_2 electroreduction on the metal catalysts were investigated with AP-XPS in combination with QM DFT.[143, 168-170] Oxygen plays an essential role in inducing reactions involving CO_2 and H_2O on both Ag and Cu surfaces, but the consequences for each metal are dramatically different. The most energetically favorable reduction reaction pathway to hydrogenate CO_2 to HOCO* involves the $O{=}CO_2^{\delta-}$ configuration present only on the Ag surface.

The distribution of products produced over stable CuAg bimetallic electrodes indicates that CO is primarily produced on the surface of the Ag domains, whereas COR occurs exclusively on the surface of the Cu

domains. However, the distribution of products observed over the Cu domains is altered compared with pure Cu, with H_2 production being suppressed by ~75%. While the suppression of HER does not inhibit the ability of the Cu domains to produce products derived from CO, the distribution of products shifts to favor carbonyl-containing products at the expense of hydrocarbons. The mechanism of surface promotion is compressive strain induced by the formation of a Cu+Ag surface alloy, which induces a shift in the valence band density of states of Cu to deeper levels. This electronic structure modification reduces the binding energies of H and O relative to CO, leading to an enhanced selectivity for the production of products derived from CO due to the selective suppression of HER. These strain effects also result in an enhanced selectivity to multi-carbon carbonyl-containing products at the expense of ethene due to the reduced coverage of adsorbed H and the reduced oxophilicity of the compressively strained Cu.[171]

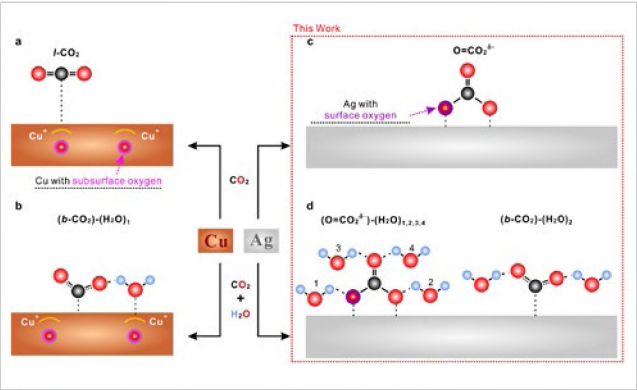

Figure 16. A schematic of the differences of CO_2 adsorption on Ag and Cu. Sublayer O stabilized both the *l*-CO_2 and *b*-CO_2 in the Cu system. Sublayer O goes to surface O without an energy barrier on Ag, and interacts with *g*-CO_2 to form a chemisorbed $O{=}CO_2\delta$- species.

Cu- and Pd-based catalysts were investigated under operando conditions by utilizing a grazing-incidence (GI) electrochemical cell for synchrotron-based X-ray characterization, where the top ~2–4 nm of a flat electrode can be probed at reaction rates where the performance of a catalyst is typically evaluated. The researchers performed experiments observing thin (1–2 nm) oxide layers on the surface of Cu thin-film catalysts and tracking changes in these oxides as a function of applied potential.[25] Additionally, the team ran both lab and synchrotron tests of the Cu catalyst during the HER, showing improved mass transport and high signal to noise in both GIXAS and GIXRD while operating in excess of -120 mA/cm^2. This makes the method ideal for examining catalytic reactions such as CO_2 reduction, where limited CO_2 concentration and competing HER chemistry necessitate sufficient mass transport of CO_2 to the surface. This system was used to examine Cu catalysts during COR chemistry, finding that initial surface oxide was reduced quickly once potential was applied, leaving no detectable oxide in the surface during catalysis, and some indications that the metallic Cu surface restructured toward the (100) surface under potential.[172]

Effect of Environment (Electrolytes, Additives, Coatings)

Solid-liquid interface design can optimize the activity and product selectivity of the electrochemical reduction of CO_2. Experimental and computational studies were carried out to understand the role of the concentration and identity of electrolyte anions and cations on the selectivity of CO_2 reduction at Cu surfaces.[173] The composition and concentration of electrolyte anions had relatively little effect on the formation of CO and H_2, but had a significant effect on the formation of CH_4, HCOO-, C_2H_4, and CH_3CH_2OH. Changes in the pH near the electrode surface were insufficient to explain the differences in activity and selectivity observed with changes in anion buffering capacity, assessed using continuum modeling, influencing the formation of H_2 and CH_4. Therefore, the effects of anion composition were ascribed to the ability of buffering anions to donate hydrogen directly to the electrode surface in competition with water.

The critical factor through which cations affect electrochemical CO_2 reduction is the hydrated cation size and how it impacts the interfacial electric field. Larger, less solvated cations better stabilize adsorbed species with large dipole moments; the formation of C_2H_4 and C_2H_5OH can be enhanced significantly by large cations, such as Cs^+.[163, 174-175] A multiscale modeling approach that combines size-modified Poisson-Boltzmann theory

with ab initio simulations of field effects on critical reaction intermediates was developed. The model showed unprecedented quantitative agreement with experimental trends of cation effects on CO production on Ag, C_2 production on Cu, and CO vibrational signatures on Pt, as well as Au(111) single-crystal experimental double-layer capacitances.[176-177]

The product distribution at the cathode of an electrochemical cell used for the reduction of CO_2 can differ significantly from that in the bulk electrolyte because of secondary reactions.[178] To probe the distribution of products as they form, a DEMS that enables product sampling directly from the cathode was designed, as shown in **Figure 17**. A notable finding from experiments using this instrument was that the abundance of aldehydes relative to alcohols near the Cu cathode surface is much higher than that observed in the bulk electrolyte. These findings suggest that acetaldehyde is a precursor to ethanol and that propionaldehyde is a precursor to n-propanol.

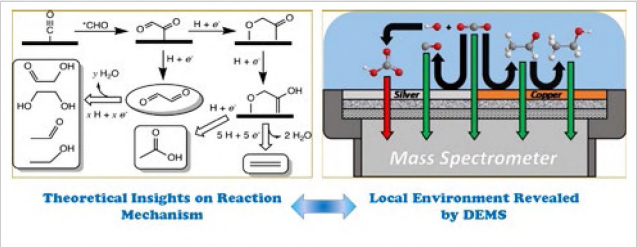

Figure 17. Interactive studies on electrochemical CO_2R by combining theoretical mechanism prediction with operando experimental approaches.

JCAP also developed a molecular tuning strategy—the functionalization of the surface of electrocatalysts with organic molecules—that stabilizes intermediates for more selective CO_2 reduction to C_2H_4.[179-181] Using electrochemical, operando/in situ spectroscopic and computational studies, the influence of a library of molecules, derived by electro-dimerization of arylpyridiniums and phenanthrolinium adsorbed on copper, was investigated. The additive and the resulting organic film influence local surface morphology, playing an important role both before and during catalysis (**Figure 18**). The organic film improves the stabilization of an "atop-bound" CO intermediate (that is, an intermediate bound to a single copper atom), thereby favoring further reduction to C_2H_4. As a result, the CO_2RR to C_2H_4 with an FE as high as 72% at a partial current density of 230 mA cm^{-2} in a liquid-electrolyte flow cell in a neutral medium was obtained. Stable C_2H_4 electrosynthesis was observed for 190 hours in a system based on a membrane-electrode assembly (MEA) that provided a full-cell energy efficiency of 20 per cent.[179]

Mechanistic studies to understand how N-substituted pyridinium films alter the CO_2RR selectivity profile with metallic electrodes[181-182] are complicated by the rich product profile of CO_2RR on copper electrodes.[148] In contrast, metallic silver surfaces catalyze primarily the CO_2-to-CO conversion in aqueous electrolytes, with concomitant production of H_2 and a small amount of HCOOH, depending on the potential applied.[183-184] Certain *N*-substituted pyridinium additives on Ag foils produce CO with extremely high selectivity by inhibiting proton (HER) but not CO_2 reduction. The data from electrokinetic studies suggest that hydrogen production was selectively inhibited by the growth of a hydrophobic organic layer on the silver surface that limits proton but not CO_2 transport. The data also point to a proton-transfer as the rate-determining step of the catalysis, instead of the commonly observed electron-transfer step for the case of planar Ag electrodes.[185] Similarly, the selectivity of Ag for CO_2 reduction to CO is dramatically enhanced by forming coatings with dihexadecyldimethylammonium bromide and other quaternary ammonium cations with long alkyl chains.[186]

Additional organic modifiers on Cu surfaces alter CO_2R selectivity between CO, formic acid, and H_2.[187] Polymeric and molecular modifiers featuring a wide variety of functional groups (aryl, amine, amide, and ether groups, for example) and diverse structural features (neutral or cationic, protic or aprotic) were screened to improve selectivity toward CO, formic acid, or H_2, with selectivities of up to 76% CO or 62% formic acid, and tuning the H_2 selectivity from 97% down to 2% (**Figure 19**). Among these aprotic species, cationic hydrophobic modifiers enhanced selectivity for CO, while hydrophilic modifiers enhanced selectivity

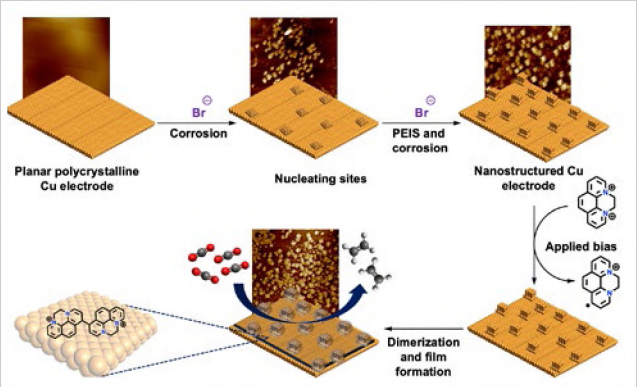

Figure 18. Pictorial representation of the model for nano-structuring of a polycrystalline copper electrode and film electrodeposition.

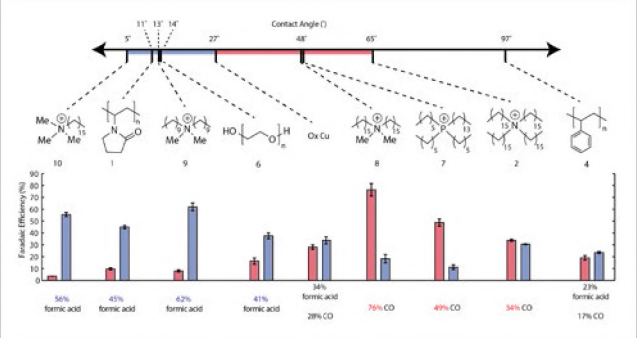

Figure 19. Relationship between hydrophilicity/phobicity and product selectivity. The contact angle was determined for Cu surfaces modified with the organic species shown. Surfaces that are more hydrophilic than OD Cu were more selective for formic acid (highlighted in blue), and those that are cationic and more hydrophobic were more selective for CO.

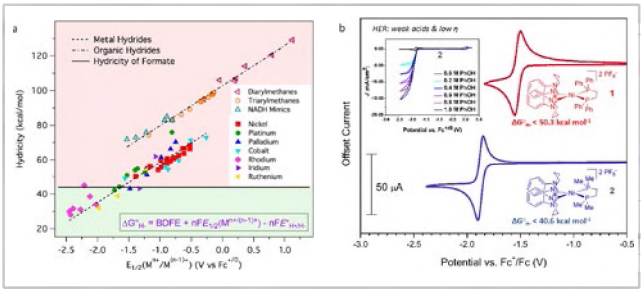

Figure 20. (a) Plot of known hydricities in acetonitrile as a function of $E_{1/2}(M^{n+/(n-1)+})$. Predicted hydricities of 1 and 2 are denoted by red and blue stars, respectively. (b) Cyclic voltammograms of 1 mM 1 and 2 in acetonitrile. Conditions: 0.1 M tetrabutylammonium hexafluorophosphate supporting electrolyte, glassy carbon working electrode, platinum counter electrode, Ag/AgCl reference electrode, 100 mV s^{-1} scan rate. Inset: Electrocatalytic hydrogen evolution with 2 and phenol used for experimental benchmarking of hydricity.

for formic acid. Simulations based on ReaxFF reactive molecular dynamics indicate that the hydrophilic/hydrophobic modifiers influence the formation of surface hydrides, which yield formic acid or H_2.

JCAP researchers utilized N-heterocyclic carbenes (NHCs) to direct CO_2RR selectivity at heterogeneous Au, Ag, and Cu electrode surfaces via the formation of NHC-CO_2 zwitterionic adducts.[188-189] Infrared spectroelectrochemical (IR-SEC) experiments indicate product formation dependent upon the donating character of the NHC substituents. Electrocatalytic reduction of CO_2 to formate and hydrogen evolution (HER) typically proceed via a metal-hydride intermediate. A robust thermodynamic scaling relationship between hydride donor ability, or hydricity ($\Delta G°_{H^-}$), and the first reduction potential of the parent metal complex ($E_{1/2}(M^{n+/(n-1)+})$) was elucidated.[190] This relationship provided a platform for rationally tuning hydride intermediates for reactivity toward CO_2 and proton sources (**Figure 20**).[191] Conditions can be rationally selected to switch HER on or off, and the most reducing of these systems have hydricities that are also thermodynamically capable of hydride transfer to CO_2 (ΔG_H < 44 kcal mol^{-1} in acetonitrile).[192] This work illustrated the kinetic challenges associated with hydride transfer to CO_2 even under thermodynamically optimized conditions.[193]

Photocatalysis

Hot Carriers

Immediately after photoexcitation, charge carriers (electrons and holes) can be sufficiently energetic to drive interfacial electrochemical reactions that are inaccessible when these carriers are thermalized. A significant theoretical and experimental effort in Phase 2 of JCAP focused on elucidating the mechanism for hot carrier generation, relaxation, and transport at solid-liquid interfaces.[194] This effort informed the design of PEC processes in which the kinetics and resulting products from CO_2 reduction exploiting hot carrier phenomena are significantly different from those obtained from conventional photoelectrochemistry with thermalized carriers.

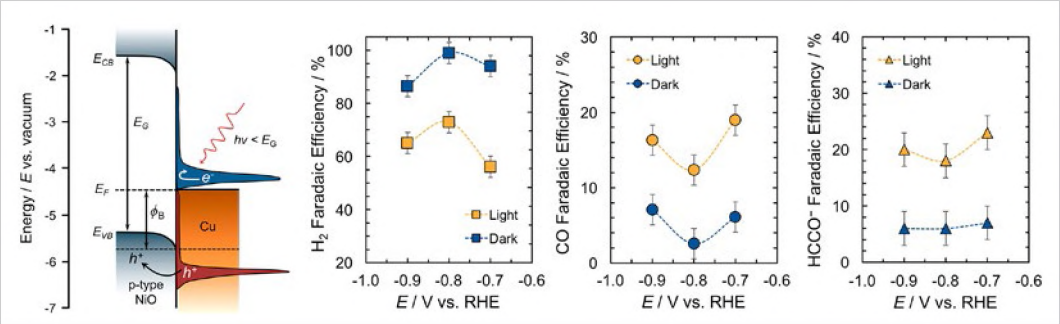

Figure 21. Hot hole injection in Cu/p-NiO and its impact on product distribution in CO_2RR, demonstrating that optical excitation can act as a mechanism to confer selectivity in CO_2 reduction.

In particular, the work began with development of theoretical predictions for the hot carrier distributions resulting from plasmon decay in Ag, Au, Cu, and Al by direct[195] and indirect phonon-mediated processes,[196] and for nonlinear plasmon processes at high intensities.[197] Spatiotemporal evolution of hot carrier distribution during transport was modeled using a Boltzmann equation approach informed by first-principles parameters.[198] First-principles models for electron-electron interactions and electron-phonon interaction were developed, representing a significant step beyond conventional two-temperature models for prediction of hot carrier temperature in materials.[199] These predictions for electronic relaxation by electron-electron interactions and electron-phonon coupling were tested experimentally using Au nanoparticles probed by ultrafast transient absorption (TA) spectroscopy, and the first-principles model was found to exhibit quantitative agreement with the experimentally observed carrier densities and temperatures.[200] Next, optoelectronic hot carrier photoconductivity and internal quantum efficiency measurements at Au/GaN Schottky junctions were used to elucidate the contributions to hot carrier transport from intraband plasmon generation and optical interband transitions. The comparison of the measured spectral variation of internal quantum efficiency with theory strongly supports the hypothesis that in plasmonic nanostructures with characteristic dimensions <10 nm, a high fraction (approaching 100%) of the generated hot carriers can ballistically impinge on the Schottky barrier interface, an important prerequisite for efficient hot carrier transport.[201] A significant experimental step forward was the observation in 2018 of hot hole collection in Au/p-type GaN heterostructures.[202] This important and highly cited finding demonstrated that visible photogeneration results in hot hole injection that can occur across heterojunction barriers of >1 eV barrier height, enabling hot carrier charge separation that results in electrons being localized on the metal nanoparticle photocathode, where they are available to perform reduction reactions. For both Au/p-type GaN[202] and Cu/p-type NiO heterostructures,[203] the product distribution under PEC carbon dioxide reduction conditions is significantly altered by hot carrier-mediated processes (**Figure 21**). Notably, the CO_2 reduction product Faradaic yield is significantly enhanced with respect to hydrogen evolution as compared with dark electrocatalysis under similar applied potential conditions. Further experiments have revealed the contribution of plasmon and interband excitation processes to hot carrier transport at both p-type and n-type Cu/GaN interfaces and indicate that the internal quantum efficiency varies with energy in proportion to the joint electronic densities of states for electron and hole states in Cu.[204] By combining visible and mid-infrared ultrafast TA spectroscopy, JCAP was able to show that hot hole injection directly influences hot electron relaxation.[205] These dual-wavelength TA experiments also indicated high (>90%) efficiency for hot hole injection across Au/GaN interfaces.

Another foundational demonstration of light-induced modulation of product distribution was observed with Ag thin-film electrodes. Product distributions during (photo)electrochemical CO_2 reduction were characterized using a cell design the team developed that allowed front illumination of electrodes and precise temperature control.[206] The thermal control afforded by this cell is unique and notable because solar-simulated illumination can substantially heat the electrolyte, causing large differences in reactant solubilities between light and dark conditions, thereby disallowing comparison between the two if cell temperature is

not properly controlled. Illumination of the electrode near its plasmon resonance (365 nm light) suppressed H_2 production and selectively promoted the formation of CO_2 reduction products, most notably methanol, which was only formed under illumination. The results demonstrate that plasmonics provide a promising approach to promote selectivity and efficiency for CO_2 reduction as well as other complex, multi-electron reactions. One hypothesis regarding the large product selectivity changes observed between light and dark conditions is that the surface plasmon impacts the adsorbate concentration at the electrode surface during electrolysis and therefore changes the probability of ground state electrochemical charge transfer to different reaction intermediates. Such experimental systems were combined with theory techniques to establish mechanisms by which excited electrons may affect CO_2 reduction. The model system examined was photoexcited charge injection from gold nanoparticles into CO_2 where catalytic enhancement could be due to thermalization of the electron-hole distribution or electric-field effects. This project elucidated methodological issues associated with the challenging excited state calculations of these and related systems, prompting continued effort in developing quantum embedding methods.[207]

Theoretical understanding of hot carrier injection from Au nanoparticles to GaN substrate per experiments was also pursued. Such hot carriers can be generated with a plasmon excitation. Nonadiabatic molecular dynamics (NAMD) was used to directly simulate the carrier cooling. It was found that the initial carrier can be injected into the GaN very quickly before it is cooled down, but part of the carrier population will return to the Au nanoparticle due to the band alignment, in agreement with the experiments.[208]

Carrier Dynamics Theory

JCAP developed carrier dynamics techniques from first principles that address plasmon phenomena as well as charge transport in semiconductors. The algorithms accurately treat long-range electron-phonon interactions, temperature-dependent lattice vibrations in materials with structural phase transition, and strong spin-orbital coupling. These approaches are implemented and integrated into a highly efficient computational code, which is well optimized and parallelized to achieve nearly linear scaling up to 10,000 cores. The temperature-dependent charge transport in $SrTiO^3$, a prototypical perovskite oxide, was investigated using the newly developed ab initio approach. The approach employs renormalized phonons to compute the temperature-dependent electron-phonon coupling for all phonon modes, including the soft modes associated with ferroelectricity and phase transitions. Electron transport in cubic $SrTiO_3$ is controlled by scattering with longitudinal optical phonons at room temperature and with ferroelectric soft phonons below 200 K.[209] The electron mobility computed using the Boltzmann transport equation (BTE) is significantly overestimated compared with experiments. Charge transport in $SrTiO_3$ was reinvestigated in the presence of polarons using the newly developed *ab initio* cumulant approach, which includes polaron effects. The revised calculations accurately predict the experimental electron mobility around room temperature and elucidate the long-sought microscopic origin of charge transport in cubic $SrTiO_3$:[210] a transition of the transport mechanism from band-like conduction at low temperature to an incoherent transport regime beyond the quasiparticle scattering paradigm near room temperature.

The piezoelectric (PE) electron-phonon interaction due to dynamical quadrupoles was derived and computed, and the interaction's contribution to charge transport in PE materials, such as GaN and $PbTiO_3$, investigated.[211-212] The quadrupole contribution is essential to correctly compute electron-phonon coupling and charge transport in these PE materials. By combining the dynamical quadrupole approach with previously developed approaches for polar phonons and soft phonon modes, transport properties in a wide range of semiconductors and oxides were quantitatively computed and investigated from first principles. All these approaches were implemented in the software package PERTURBO.[213]

Materials Discovery

Discovered and Characterized Electrocatalysts for the Oxygen-Evolution Reaction, Hydrogen-Evolution Reaction, and CO_2RR

Each half-reaction in artificial photosynthesis requires discovery of electrocatalysts that promote the oxidation of water (OER) and either the reduction of water (HER) or of carbon dioxide (CO_2RR) at low overpotentials. Prior to JCAP, the most effective heterogenous electrocatalysts for OER and HER were rare metals and metal oxides, i.e., Pt for HER, and RuO_2 and IrO_2 for OER. The challenge was to identify Earth-abundant catalysts for the HER and OER reactions that offer comparable or superior activity. For Cu, the most widely studied CO_2RR electrocatalyst, the overpotential for reduction of CO_2 to methane and other hydrocarbons is unacceptably high.[214] Therefore JCAP investigated new CO_2RR catalyst concepts. Both heterogeneous and homogeneous catalysts were investigated. The value of discovery of homogeneous catalysts lies in identification of catalytic center and ligand motifs that confer selectivity and activity, and inform heterogeneous catalyst design.

Established High-Throughput Experimentation Solar-Fuels Facility

Materials discovery was at the core of JCAP's mission. In addition to traditional directed discovery approaches, high-throughput experimentation (HTE) is a powerful approach for searching high-order composition spaces for new functional materials. Prior to JCAP's HTE project, basic research efforts utilizing high-throughput materials experimentation primarily resided in single-PI laboratories.[215-218] At the intersection of combinatorial materials science and solar-fuels research, several groups reported relevant experiments, demonstrating synthesis and/or screening of composition libraries,[215-216, 219] but the reported work was typically limited to demonstrations of a series of separated techniques. Concurrently, rapid advances in computational materials science, bolstered by evolving first-principles techniques[220] and the establishment of the Materials Genome Initiative, began to enable material properties to be predicted faster than they could be measured experimentally. The HTE project developed synthesis and screening techniques geared toward the discovery of both dark and photoelectrocatalysts. Furthermore, a workflow that balances data quality and throughput was developed, resulting in the first high-throughput pipeline for solar-fuels materials discovery, which included strong linkages to computational materials science to leverage the rapid material prediction of computational screening.

Established methodologies for high-throughput materials discovery in a mission-driven research effort: High-throughput experiments are most successful when conducted in close collaboration with scientists conducting directed research. Guided by these daily interactions, the HTE team designed and developed new instrumentation for synthesizing materials of interest, performing experiments under operational conditions, and reporting performance metrics directly comparable to those obtained using standard techniques.[221] Substantial development in library synthesis was required to obtain material quality commensurate with the desired performance. New screening technologies included parallel techniques such as the bubble,[221] stability[222] and colorimetry instruments,[223] and serial techniques such as the on-the-fly spectrometer,[224] quantum yield instrument,[225] and scanning drop cell.[209, 226]

Constructed and demonstrated a synthesis and screening pipeline with unprecedented daily throughput: With development of these new instruments and techniques, HTE deployed a synthesis and screening pipeline for light absorbers and electrocatalysts, complete with decision trees based on hard-won knowledge of process compatibilities and best practices. To increase throughput, the pipeline was designed to use a tiered screening strategy, in which substantial sample down-selection occurs between successive

measurements. Data obtained from running the pipeline at a throughput of over 104 samples per day were used to generate new algorithms for performing data-driven down-selection, increasing sample throughput and accelerating discovery.[227]

Hydrogen-Evolution Reaction

On metals, the HER proceeds by either of two mechanisms, Volmer-Heyrovsky and Volmer-Tafel, that are differentiated by whether the hydrogen-generation step involves reaction between two surface hydrogens or via an adsorbed hydrogen and a solution-borne proton. For other types of catalysts, such as synthetic compounds that mimic hydrogenase enzymes, the process would involve regenerative redox reactions of the transition metals at the active site.

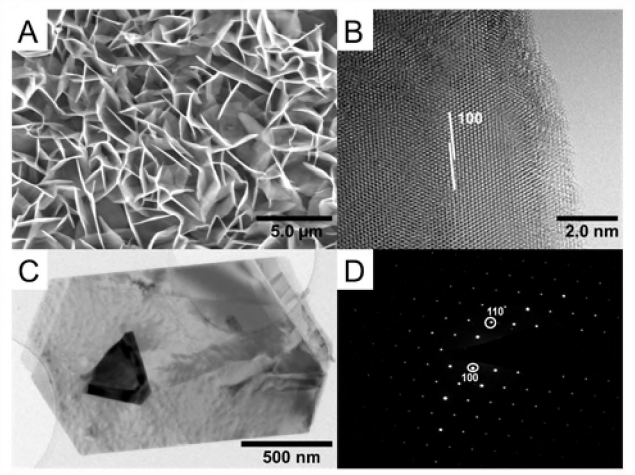

Figure 22. Electron microscopy of WSe_2.

The transition metal chalcogenides have been established to be good catalysts for industrial hydrodesulfurization (HDS) reactions and, because of the similarities of the HDS and HER mechanisms, the materials were investigated as potential HER catalysts (**Figure 22**). Well-defined WSe_2 was synthesized via the chemical vapor transport deposition method; catalytic activity was not exceptional, but the material was found to be stable in acid solutions.[228] Molybdenum diselenide was prepared operando by a wet chemical-synthesis procedure.[229] Both had overpotentials in the range of 200–350mV at 10 mA cm^{-2} and were stable in acidic environments. Cobalt selenide films, deposited electrochemically, were stable and exhibited improved overpotentials of 140 mV for 10 mA cm^{-2}; based on Raman and XPS data, the films were determined to be CoSe embedded in a matrix of amorphous selenium.[230] A computational study, based on DFT, has indicated that the HER mechanism on these chalcogenides follows the Volmer-Heyrovksy pathway (reaction between two surface-adsorbed H).[118] Molecular mimics of the heterogeneous catalyst have been prepared that incorporate the edge site structure.[231]

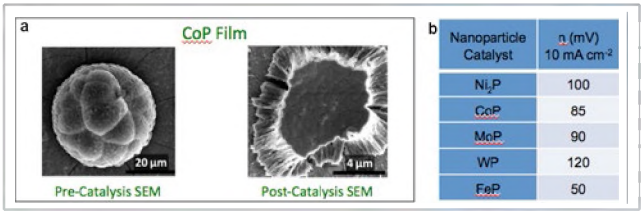

Figure 23. (a) Scanning-electron micrograph (SEM) images of CoP before and after HER. (B) Activities, in terms of overvoltage (η), of nanoparticle catalysts of selected transition-metal phosphides.

The role of the catalytic environment has been of particular interest, and redox non-innocence has been described for several Co-based molecular catalysts for proton reduction.[232-235] Heterogenized di-Fe hydrogenase-based complexes have also been examined and found to be quite robust.[236]

Superior activity was shown with transition metal phosphides. Thin films of cobalt phosphide were deposited electrochemically and excess cobalt metal was removed via anodic stripping, leaving only cobalt phosphide (Co:P ratio of 1:1) upon reduction at HER potentials. CoP exhibited an overpotential of only 85 mV at the benchmark current density of 10 mA cm^{-2}, and showed good stability for over 24 hours.[237] Operando XAS showed that, under catalytic conditions, CoP was the active material, without the presence of metal oxides or high-valent phosphorus.[237] Nanoparticles of other phosphides were also studied;[238-241] iron phosphide, FeP, showed the best activity in terms of lowest overpotential (**Figure 23**).

Oxygen-Evolution Reaction

Using JCAP's unique HTE capabilities, approximately 100,000 OER catalysts were screened with exciting results for lanthanide-rich compositions, particularly in the (Ni-Fe-Co-Ce)O_x[225] and (Ni-La-Co-Ce)O_x[242] composition spaces. In the (Ni-Fe-Co-Ce)O_x composition space, (**Figure 24**) HTE transitioned from initial discovery to test-bed demonstration of the new Ce-rich composition in only a few weeks.[225] The composition dependence of three engineering and four fundamental electrochemical parameters were then measured to reveal the unique attributes of the Ce-rich catalyst relative to the well-known transition metal oxides.[243] A related Ce-rich electrocatalyst (Ni-La-Co-Ce)O_x was discovered by expanding the composition search space.[225] For OER catalysis in basic electrolytes, these new materials exhibit activity that is comparable to the best electrocatalysts discovered previously, including RuO_2 and IrO_2.

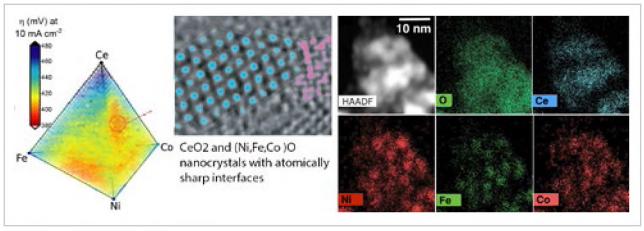

Figure 24. The OER overpotential for 10 mA cm^{-2} is shown for the entire quaternary composition (Ni-Fe-Co-Ce)O_x space. The discovered Ce-rich catalysts have a novel 2-phase nanostructure where ceria grains form sharp interfaces with alloyed transition metal oxides.

The unique activity of the new Earth-abundant mixed-metal oxide catalysts motivated detailed characterization that revealed a novel two-phase nanostructure composed of small particles that may appear "X-ray amorphous." Atomic resolution imaging of the catalysts was an essential aspect of their structural characterization and investigation of the structural integrity under electrocatalytic use. The application of electron in-line holography with variable voltages and dose rates removes sample-altering electron beam-sample interactions and enables the study of intact crystalline and amorphous structures at atomic resolution with single atom sensitivity.[244] TEM of printed catalyst at high and at low magnification (**Figure 24**) and EDS maps with high spatial resolution < 0.5 nm reveal that Fe, Ni, and Co are distributed similarly while the Ce precipitates in different locations. The microscopy and spectroscopy data is consistent with a microstructure where the transition metal oxides form miscible agglomerates of nanocrystals to create a matrix that encloses isolated CeO_2 precipitates. This novel two-phase nanostructure was believed to enable OER catalysis at low overpotential via a tandem catalysis or other cooperative mechanism; subsequent in situ, ambient pressure XPS and XAS analysis demonstrates that the CeO_2 nanoparticles reduce the oxidation potential of the transition metal oxide nanoparticles to decrease their onset potential.[245]

Motivated by sensitivity analysis of water-splitting prototypes, HTE developed a combined electrochemical and optical screening tool to characterize the darkening of metal oxide catalysts during operation and identified the compositions with both high catalytic activity and high transparency (**Figure 25**).[246]

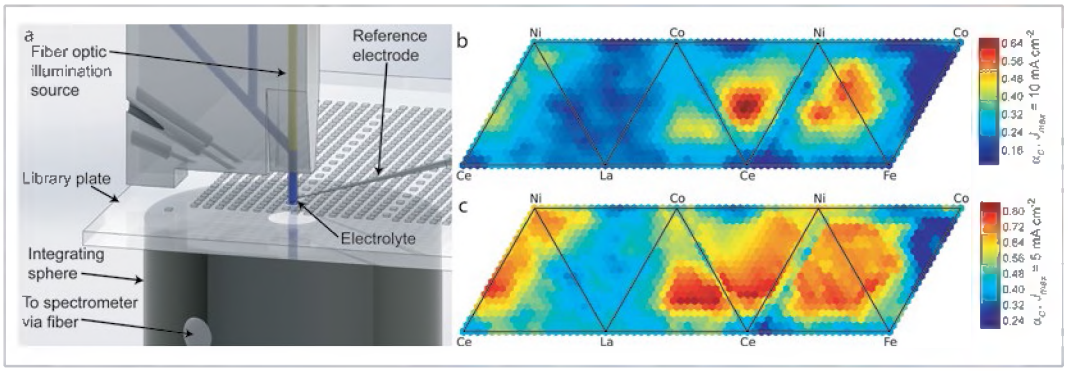

Figure 25. OER catalyst efficiency of metal oxides determined from catalytic activity and in situ measurement of AM1.5 transmission using the custom high-throughput instrument.

The research effort in materials discovery for OER electrocatalysts for coupling to CO_2RR focused on lowering overpotentials and increasing stability. This latter consideration was demonstrated to be of utmost importance by the observation that cation corrosion from the OER catalyst followed by crossover and plating on the cathode compromises stability in CO_2RR product distributions over time. Using HTE, two avenues of inquiry were followed. First, a pipeline to rapidly explore 15 pseudo-quaternary oxide libraries synthesized on a single plate with compositional characterization as-deposited and after two hours of OER operation, using multiple electrolytes from pH 1 to 13, provided crucial information on operational stability and activity. Successful operation of the pipeline yielded a wealth of data for which visualization and interpretation algorithms were developed to facilitate human comprehension, and revealed a new class of Co-rich OER catalysts that can be compositionally tailored to a specified pH and perform on par with state-of-the-art acid OER catalysts.[247] Second, a concerted effort was made to stabilize known active species such as Mn^{+3} in acidic conditions. The greatest success has been with rutile alloys of the form $Mn_{1-x}Sb_xO_{2+\delta}$, where high-throughput catalyst screening was combined with a computational materials investigation and synchrotron characterization. Systematic control of Mn^{+3} concentration in this alloy oxide identified compositions with excellent Pourbaix stability and operational stability in strong acid (**Figure 26**), demonstrating a very promising precious-metal-free OER catalyst.[248]

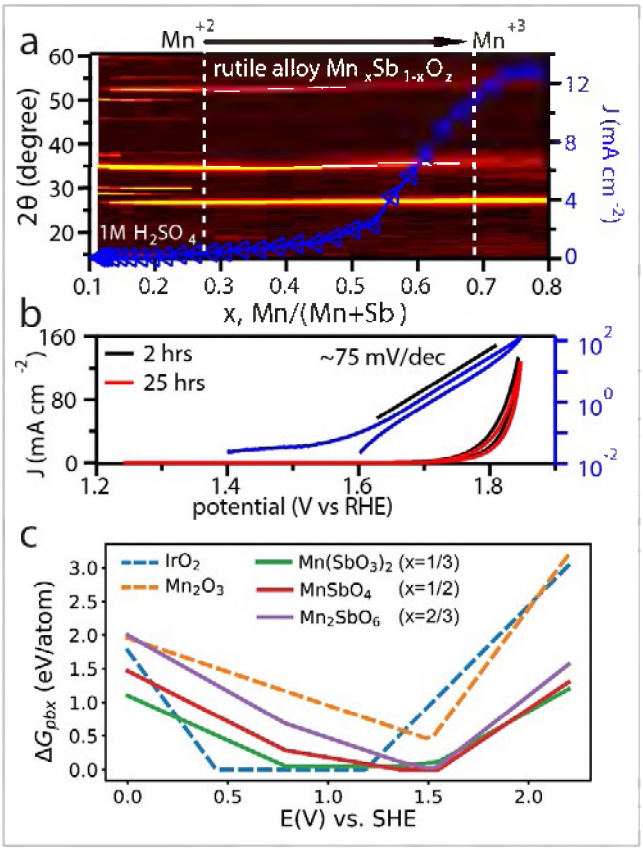

Figure 26. Increasing Mn^{+3} concentration in $Mn_{1-x}Sb_xO_{2+\delta}$ rutile alloys increases OER activity in 1 M H_2SO_4, and due to thermodynamic stabilization of the active sites, excellent activity is retained over 25 hours of testing.

Computational methods provided guidance for new catalyst compositions. The mechanism for OER on Fe-doped gamma NiOOH was established and used to calculate an onset potential of 0.42 V using high-level DFT (experiment: ~0.37 V) with a Tafel slope of 24 mV/dec (experiment: 30 mV/dec).[249] Using these approaches, high-throughput in silico screening suggested that replacing Fe with Co, Rh, or Ir would have significantly lower onset potential for OER.[250]

Directed discovery of OER catalyst materials focused on the birnessites, a heterogeneous analog for the OER complex in natural photosynthesis, where the influence of redox-inactive cations on the structure and electrochemical reactivity was studied. Birnessite is a natural mineral of manganese characterized by stacked sheets of edge-sharing octahedral MnO_6 units.[251] The structural similarity of birnessite to the oxygen-evolving center (OEC) in Photosystem II stems from the abundance of mono-μ-oxo and di-μ-oxo bridges in the edge-sharing octahedra of birnessite. The same connectivity is present between three $Mn^{3+/4+}$ ions and one Ca^{2+} in the Mn_4CaO_5 cluster of the OEC.[252] Electrochemical protocols were developed for the facile potentiostatic deposition of birnessite films, supported on Au substrates, to serve as a structural motif for OER electrocatalysts.[253] The rapid synthesis of near-isostructural members of the birnessite family was invaluable in the isolation of compositional effects from the closely intertwined structural effects in the rational design of electrocatalysts. Intercalated cations Na^+, Ca^{2+},

Sr^{2+}, Y^{3+}, and Zn^{2+} generally preserved the electroneutrality of the sheets in birnessite. The potential needed to sustain a current density of 10 mA cm^{-2} in 0.1 *M* NaOH increased according to the sequence $Na^{+} < Ca^{2+} < Sr^{2+} < Y^{3+} < Zn^{2+}$, which encompasses a 170-mV potential range. Unlike the case of the homogeneous cluster catalysts, the electrochemical reactivity of birnessite does not vary linearly with the pK_a of the redox-inactive cations. The results offer the prospect of property modulation via the use of cations that are classically labeled as spectator-supporting ions in electrochemistry.

Carbon Dioxide Reduction Reaction

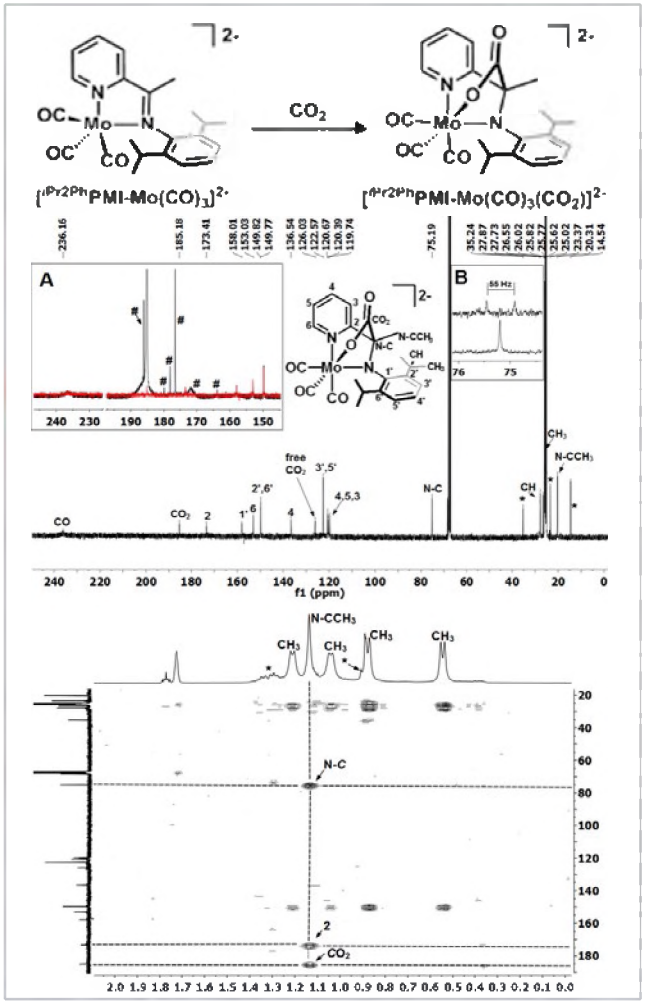

Figure 27. Proposed reaction path for the reaction of the dianion with CO_2 and a nuclear magnetic resonance (NMR) spectroscopic characterization of the product of the reaction with CO_2.

In JCAP, theory and experiment operated in synergy to accelerate the discovery of materials for the CO_2RR. Screening different catalyst formulations for CO_2 reduction activity and selectivity was a focus. The activity and product selectivity of electrochemically polished Cu was compared to those of various rough Cu surfaces. Differences in product current densities, the ratio of current densities for HER to CO_2RR, and the ratio of current densities for C_{2+} to C_1 product formation depend on the surface roughness. Cu derived from electrochemical reduction of Cu_3N exhibited activity and selectivity similar to Cu obtained from Cu_2O. Analysis of simulated Cu surfaces revealed that relative to an electropolished surface, a roughened surface exhibits a higher fraction of undercoordinated Cu sites. These sites bind CO preferentially relative to more fully coordinated sites and contain square sites similar to those on a Cu(100) surface, but with neighboring step sites, which adsorb OC-COH, a precursor to C_{2+} products.[254-255]

JCAP's molecular catalysis team investigated a number of homogeneous systems for CO_2RR and achieved some notable results. Electrocatalytic reduction of CO_2 to CO can be achieved with high current efficiencies in wet acetonitrile solvent with a cobalt molecular catalyst, $[Co^{III}N_4H(Br)_2]^{+}$ (N_4H=2,12-dimethyl-3,7,11,17-tetraazabicyclo-[11.3.1]-heptadeca-1(7),2,11,13,15-pentaene). JCAP demonstrated that Co-based homogeneous catalysts display remarkable selectivity for CO_2RR in the presence of water and other proton donor solvents.[256-257] The study includes the isolation and characterization of several reduced compounds that are relevant to both HER and CO_2RR catalysis. In situ FT-IR measurements and DFT calculations indicate that reducing equivalents are stored on the ligand, implicating redox non-innocence in the ligands for CO_2 reduction electrocatalysis.

The team also focused on new ligand systems, which were based on design principles that came from the JCAP theory group and previous experimental work. Pyridine monoimine (PMI) complexes of Re and Mo

were investigated toward electrocatalytic CO_2 reduction because of their close relation to the well-studied bipyridine system, their fairly positive first reduction potentials, and the fact that this ligand system can be easily functionalized (**Figure 27**). Carbon-carbon bond formation between the CO_2 molecule and the reduced PMI ligand was found to present an unexpected pathway for CO_2 reduction by these complexes.[258] In related work, a set of PMI Rhenium (I) tricarbonyl chlorido complexes with substituents of different steric and electronic properties were synthesized and fully characterized. Rhodium diphosphine with P_2N_2 pendant base-containing ligands, was prepared, and thermochemical studies were conducted to determine hydricities. With typical measured hydricity values on the order of 30 kcal/mol, these are some of the most hydridic d8 metal hydrides known. These complexes were also determined to be excellent catalysts for CO_2 hydrogenation to formic acid.[259] The hydricity of the Fe-H species and its catalytic activity in CO_2RR were also investigated.[260]

JCAP researchers also investigated NHCs as co-catalysts to pre-activate CO_2 for reduction. Notable success was achieved in the use of this pre-activator/co-catalyst in conjunction with a nickel cyclam ($Ni(cyclam)^{2+}$) catalyst to convert CO_2 to methane with 93% FE. The source of carbon in the produced CH_4 is shown to arise from CO_2 through labeling experiments in which $^{13}CO_2$ is first converted to NHC-$^{13}CO_2$, and then electrochemically reduced to $^{13}CH_4$. Likewise, deuterium-labeling experiments of the proton source show that the source of deuterium in the produced $^{13}CD_4$ comes exclusively from CF_3CH_2OD. The results demonstrate the viability of a pre-activation strategy toward the selective, electrochemical conversion of CO_2 by 8e-.[261]

Tandem and Cascade Catalysts (Cu/Ag or Au)

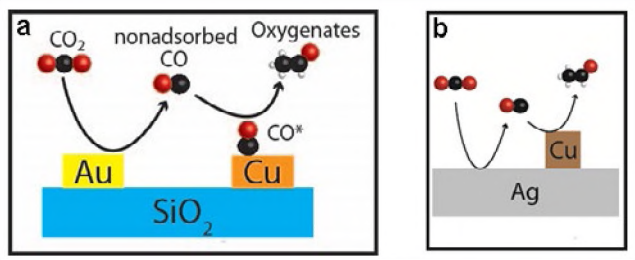

Figure 28. (a) Independently addressable and (b) coupled (right) bimetallic arrays are used for two-step cascade conversion of CO_2. Increasing the activity of CO near Cu in the second step of the cascade increases selectivity to C_{2+} oxygenate products.

Nanostructured dual-phase catalysts were investigated for controlling the flow of CO_2R intermediates during electrocatalysis, taking advantage of proximate reaction centers to control chemical selectivity. Inspired by the multi-step enzymatic pathways found in the Calvin cycle,[262] a tandem cascade electrocatalysis pathway using CO as an intermediate species was demonstrated.[263] The higher areal density of active sites on metals as compared to enzymes allows diffusional transport of intermediates over micron-length scales, opening the door to fabrication of bimetallic sequential catalysis devices with standard photolithographic techniques (**Figure 28**). The sequential catalysis pathway dramatically increased the yield of oxygenated products when Cu was used as the second catalyst in the sequence. The bimetallic design is essentially modular, allowing for individual components to be optimized before integration. The tandem cascade conversion of CO_2 on cathodes was further demonstrated by deposition of Ag and Cu on different <111>-oriented facets of Si, yielding higher current densities and much lower faradic efficiencies (FE) for CO than the single metal controls.[264]

Cu sulfides were used as templates for bimetallic Ag/Cu sulfide catalysts with well-controlled Ag/Cu mass ratios using Ag^+ cation-exchange as both nanoparticles and foil electrodes. For nanosheets, the Ag/Cu ratio can reach 25 with the nanosheet structure remaining, while it is difficult to produce a Ag-rich surface beginning with sulfides on Cu foil. Formate was the only product detected at low overpotentials (–0.2 V vs. reversible hydrogen electrode [RHE]). With the introduction of moderate Ag loadings, nanosheet catalysts showed increased C_{2+} product generation for CO_2 reduction. The product profiles appear to be influenced by CO availability controlled by Ag concentration, suggesting a tandem catalytic mechanism. Both the nanosheets and copper foil catalyst morphology changed during the CO_2 reduction, which may explain why

the product distributions change as the CO_2 reduction proceeds. The reconstruction of the catalyst during CO_2 reduction increased the production of multi-carbon products.[265]

An electrocatalyst composed of gold nanoparticles on a polycrystalline copper foil (Au/Cu) is highly active for CO_2 reduction to alcohols.[266] At low overpotentials, the Au/Cu electrocatalyst is over 100 times more selective for the formation of products containing C–C bonds versus methane or methanol, largely favoring the generation of alcohols over hydrocarbons. A combination of electrochemical testing and transport modeling supports the hypothesis that CO_2 reduction on gold generates a high CO concentration on nearby copper, where CO is further reduced to alcohols such as ethanol and n-propanol under locally alkaline conditions.

Under alkaline conditions, planar CuAg electrodes can reduce CO to acetaldehyde with over 50% FE and over 90% selectivity on a carbon basis at a modest electrode potential of –0.536 V vs. the reversible hydrogen electrode.[267] This study emphasized how deliberate modification to the catalyst surface and reaction conditions can greatly improve product selectivity, providing design principles that can be extended to other catalysts and related electrocatalytic reactions.

High-Throughput Alloy Discovery

JCAP's high-throughput team developed several new technologies for screening (photo)electrocatalysts for the CO_2RR with a focus on mapping composition-structure-property relationships to facilitate the down-selection of materials for detailed computational and experimental exploration. Through the development of small electrochemical reactors and their coupling to analytical chemistry tools, the team demonstrated experiment throughput approximately 10–100 times that of traditional methods with moderate compromises to the quality of product detection. The two new screening systems are (i) high-throughput analytical electrochemistry (HT-ANEC), which uses electrolyte recirculation to rapidly concentrate products for accelerated gas chromatography (GC) and high-performance liquid chromatography (HPLC) product detection,[268] and (ii) high-throughput electrochemistry and mass spectroscopy (HT-ECMS) (**Figure 29**), which performs quasi-real-time product detection of H_2 and CH_4.[269] Both systems have been deployed for screening Cu-alloy and non-Cu catalyst libraries, as demonstrated by seminal work revealing the sensitivity of Cu-alloy catalysts to various alloying elements (**Figure 30**).[270]

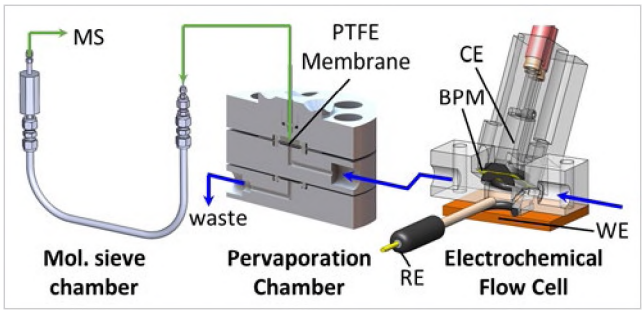

Figure 29. The HT-ECMS system combines real-time measurement with mass transport models to estimate the full FE profiles of H_2, and CH_4 during 10 mV/s CVs.

Cu-based bimetallic catalysts. The electrocatalytic properties of Cu bimetallics were investigated using a combination of experiment and theory to evaluate whether improved selectivity could be obtained. Bimetallic Zn-rich Zn-Cu was prepared by a facile galvanic procedure. The Zn-Cu catalyst exhibited dramatically improved selectivity and activity for CO formation compared with pristine Zn and Cu electrocatalysts and, remarkably, also showed higher intrinsic activity than a planar Ag catalyst within the operating potential window from –0.8 to –1.0 V versus RHE. This enhanced intrinsic activity for CO formation on Zn-Cu catalysts was attributed to the electronic effect originating from the Cu adatoms on the Zn surface. DFT calculations suggest that the incorporation of Cu onto the Zn surface lowers the reaction energy (from 0.44 to 0.15 eV) of the potential-determining step (PDS) to form COOH*, which improves CO production rates, while suppressing the HER due to a higher coverage of CO that impedes H adsorption. The changes in these relative energies rationalize the enhanced CO production activity and selectivity of Zn catalysts with Cu modification.[271]

Cu-Free Catalysts

JCAP discovered electrocatalytic systems for CO_2R that do not contain Cu, Pd, Ag, or other metals that were explored in early studies of electrocatalytic CO_2R.[184] Ni–Ga films operated in contact with aqueous electrolytes reduce CO_2 to methane, ethylene, and ethane,[272] and MoS_2 crystals reduce CO_2 to 1-propanol (among other products).[273] Bimetallic near-surface alloys were investigated, with a monolayer of Au on W yielding selectivity toward CH_3OH.[274]

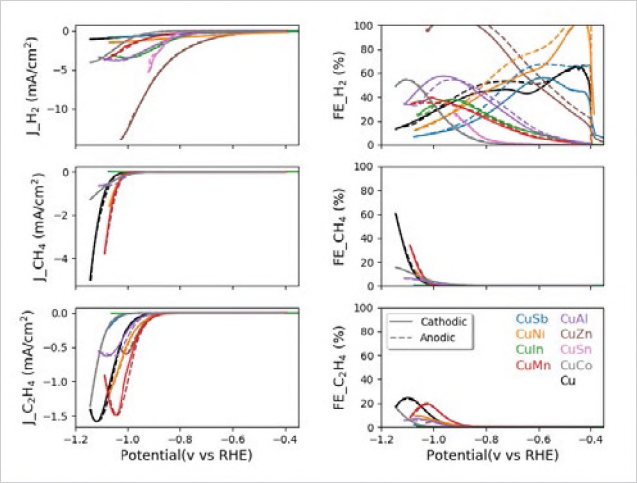

Figure 30. The HT-ECMS system combines real-time measurement with mass transport models to estimate the full FE profiles of H_2, CH_4, and C_2H_4 during 10 mV/s CVs. The results shown here compare pure Cu (black) with a series of Cu alloys with a bulk concentration of 5% of the alloying element, revealing that Mn and Zn improve hydrocarbon formation while suppressing the HER.

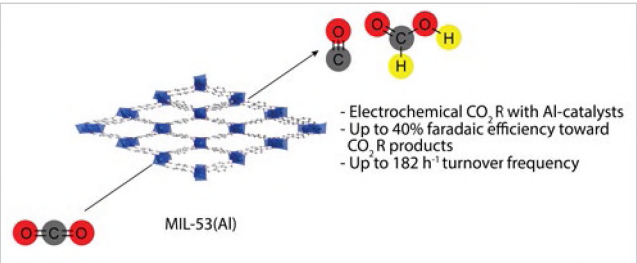

Figure 31. Electrochemical CO_2 reduction mediated by MIL-53 (Al) to HCOOH and CO.

The JCAP materials discovery effort extended to other classes of non-Cu materials for CO_2R, including single-site catalysts, in hopes of identifying other materials capable of making highly reduced carbon products. A number of active catalysts were discovered whose products were primarily CO and formate. For example, an aluminum MOF derivative is active under electrochemical CO_2R conditions and able to produce the important carbon-based products,[275] carbon monoxide (CO) and formic acid (**Figure 31**). Notably, while Al metal foil is active only for HER,[276-278] it was found that confining Al in MOFs, such as MIL-53(Al), provides an active construct for CO_2R, with FEs reaching up to 21% for CO production and 19% for formic acid production. At potential -1.1 V vs RHE, the turnover frequency (TOF) reaches 174 h^{-1}, comparable to the TOF of one of the best performing cobalt porphyrin covalent organic frameworks (COFs).[279]

Metal- and nitrogen-doped carbon materials derived from the cheap and non-toxic carbonization of polyacrylonitrile (PACN) are an exciting class of materials that are promising candidates for heterogeneous catalysis applications due to the chemical tunability of their hypothesized nitrogen-coordinated MN_x active sites. Ni, N-doped carbon (Ni-N-C), has impressive activity and selectivity for electrochemical reduction of CO_2 to CO (CO_2R).[280] Explicit proof of the existence of the hypothesized NiN_x sites, a description of the nitrogen ligand environment, and correlation of these sites to CO_2R activity were obtained by combining scanning transmission electron microscopy (STEM), single atom electron energy loss spectroscopy (EELS), and time-of-flight secondary ion mass spectrometry (ToF-SIMS).[281] Collectively, these probes of the Ni-N-C catalysts indicate that molecular-like NiN_4 sites are responsible for selective CO_2 to CO conversion. The atomically dispersed Ni sites yield selective CO_2 to CO catalysis under both electrochemical and thermal driving force, raising the prospect for improved performance under combined electrothermal conditions.[282] JCAP researchers also demonstrated that water-sensitive Re, Ir, or Co molecular electrocatalysts for CO_2 reduction can be used in aqueous solution when dispersed in a polymer ion gel coating the electrode.[283]

Photoanode Materials

High-Throughput Discovery

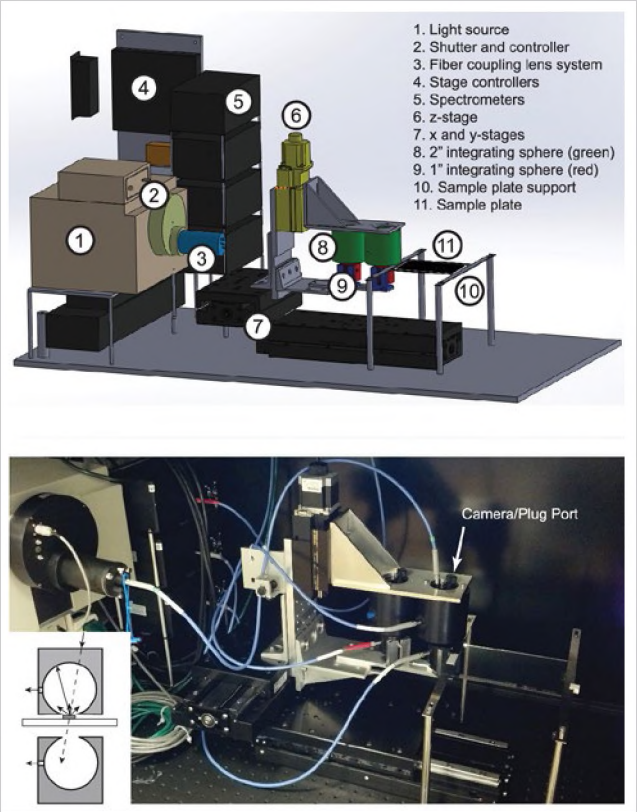

Figure 32. Automated optical screening instrument (design and photograph), a critical component of the HTE pipeline for light absorber discovery.

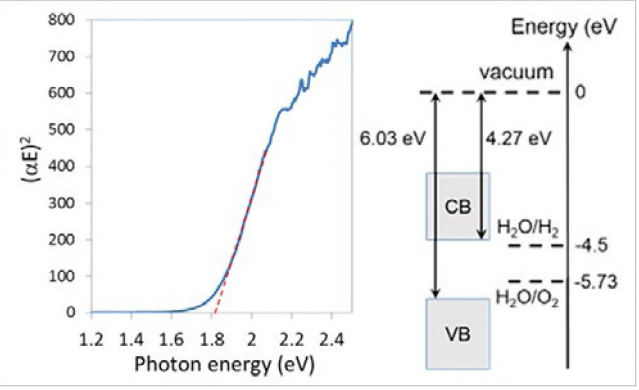

Figure 33. Experimental band gap measurement and calculated band alignment of $Mn_2V_2O_7$, a light absorber discovered through computation-guided operation of the HTE pipeline.

Following the initial focus on discovery of OER electrocatalysts, photoanode discovery became the focus, with development of infrastructure for discovery. Optical property mapping was enabled by an on-the-fly spectrometer (**Figure 32**), which measures optical absorption with throughput on the order of one second per sample.[224] Combined with PEC measurements using the scanning drop cell, the framework for rapid investigation of light absorbers was completed and validated, prompting the deployment of a light-absorber discovery campaign based on combined computation-experiment screening, as described below.

The HTE team established close cooperation with JCAP theorists via the Materials Project to identify promising composition spaces to investigate and to enable rapid understanding of newly discovered materials.[35, 89] To guide the composition search spaces for the experimental pipeline, the team performed data mining on the Materials Project database and developed specific testable hypotheses from first-principles calculations. Theory interactions are equally important on the back end of the experimental pipeline by providing another layer of screening through computation of material properties that cannot be readily measured. An initial discovery from the combined theory-experiment screening was the $Mn_2V_2O_7$ compound[89] with near-optimal band alignment to the standard potentials for water oxidation and reduction (**Figure 33**). This ternary metal vanadate has a unique combination of stability, bandgap energy, and valence band position. The accelerated discovery of photoanodes proceeded with three primary lines of inquiry, where high-throughput experiments and detailed electronic structure characterizations were combined to discover and understand photoanodes. These were (i) a framework for evaluating composition-structure-property relationships in high-dimensional alloying spaces demonstrating that alloy-based tuning of the

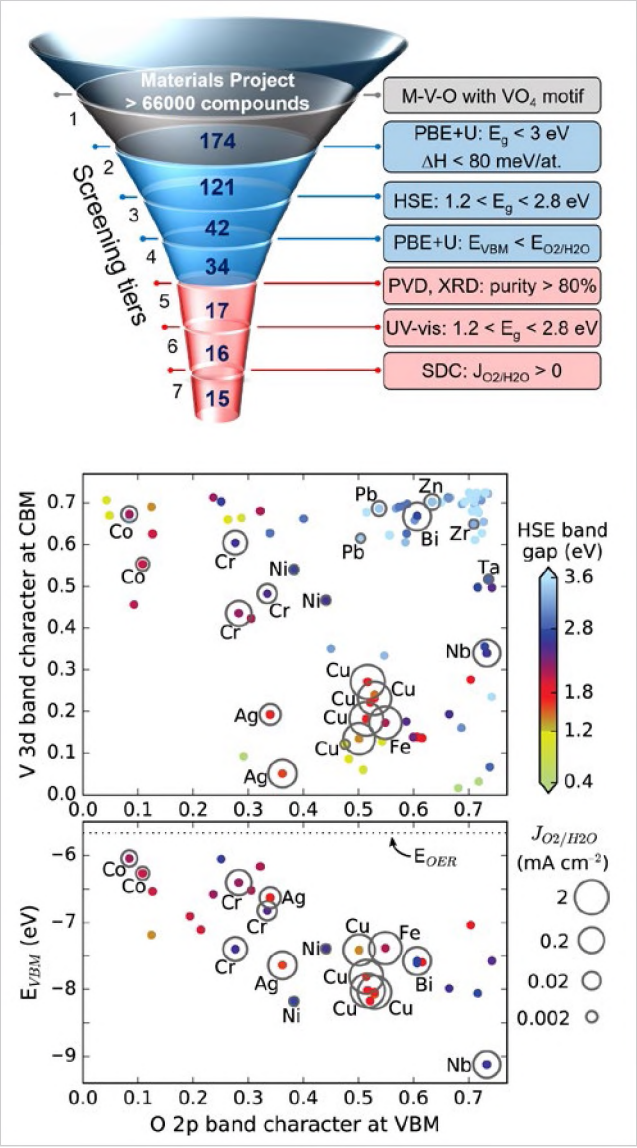

Figure 34. The integrated theory-experiment screening pipeline for photoanode discovery is shown with the number of compounds (bold) and screening criteria based on database mining (gray), high-throughput computational screening (blue), and high-throughput experimental screening (red). Computational and experimental data are combined in a summary plot of band gap and band edge tuning along within with circles denoting OER photoanodes in pH 9 (borate buffer) solution.

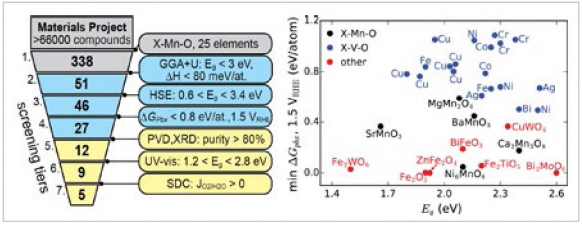

Figure 35. The integrated theory-experiment screening pipeline for discovery of operationally stable photoaonodes is shown with the number of compounds (bold) and screening criteria. This pipeline revealed the first five ternary metal manganate photoanodes, plotted in black on the right plot, which summarizes the map of all known OER photoanodes (within the plotted band gap range, as of summer 2017), including 15 phases from the literature and 17 phases identified in JCAP.

monoclinic distortion in $BiVO_4$ can improve carrier transport,[284] (ii) advancement of the integrated computation-experiment screening workflows for rapid identification of metal oxide photoanodes (**Figure 34**),[285-286] which included seminal incoproration of screening based on Pourbaix energetics (**Figure 35**),[287-289] and (iii) many metal oxide photoanodes exhibit a small photovoltage compared to their band gap, making photovoltage screening a focus of continued exploration of 3-cation oxide libraries with additional variation in materials processing. These efforts led to identification of Bi_2O_3-coated $FeWO_4$, which can only be synthesized as an n-type semiconductor in specific, non-equilibrium conditions (**Figure 36**). The 2 eV bandgap photoanode exhibits excellent stability and, perhaps most notably, an illuminated open circuit voltage below 0.4 V vs RHE, corresponding to the best photovoltage for any metal oxide with a band gap below that of $BiVO_4$.[290] The importance of exploring processing conditions is demonstrated by the observation that previous research on iron tungstate photoanodes, both directed and combinatorial materials discovery,[291-293] failed to identify this promising material. Given the quantity of photoanode data that has been compiled in the JCAP database (**Figure 37**), data science techniques were developed and applied to establish new understanding. A machine learning model for optical properties of metal oxides has provided a foundational example of generative models in materials science.[294] Further investigating systematic composition-property trends in discovered families of photoanodes, XPS and Kelvin probe measurements for 11 ternary vanadate photoanodes were used to characterize the relation between band edge energetics, cation selection, and crystal structure. Across compounds with seven different cation structures with the VO_4 structural motif, the range of band edge

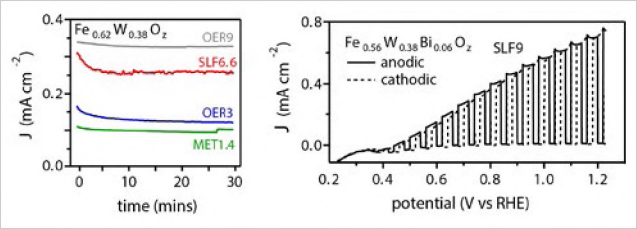

Figure 36. Due to self-passivation in acid and base, stable operation of $FeWO_4$-based photoanodes is obtained over a wide pH range, and including 5% Bi in the $FeWO_4$ film provides excellent photovoltage.

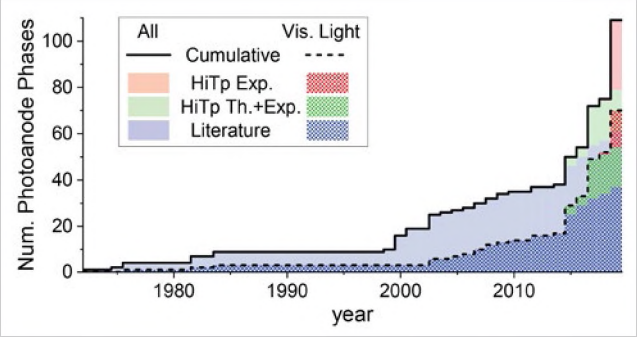

Figure 37. Discovery of metal oxide photoanodes by JCAP high-throughput efforts (red and green) compared with the rest of the field (blue), demonstrating markedly accelerated discovery.

positions was lower than that predicted theoretically, but provides the largest band edge tuning demonstrated to date for any analogous class of metal oxide semiconductors.[295] The combined efforts on dark and photo-electrocatalysis of the OER comprised the majority of experiments that were included in JCAP's release of the largest database of materials experiments and associated analyses. This database features tracking of data lineage, which is a key requirement for data management in the age of advanced data science.[296]

Photocathode Materials

In accordance with the goal to identify CO_2RR photocathodes that contribute to the controlled selectivity in CO_2RR, as opposed to optimization of known p-type semiconductors that drive CO_2RR via a buried photovoltaic (PV) junction, the materials discovery efforts comprised two primary themes. The first aimed to enact photonic and plasmonic processes through nanostructuring of known semiconductors and metals, and the second adopted directed and high-throughput methodologies to identify photocathodes with appropriate energetics and stability for photoelectrocatalysis of CO_2RR in the presence of water.

Photonic Structures

JCAP developed photocathodes with photonic structures that enable use of opaque CO_2RR catalysts in a photocathode illuminated device configuration. Arrays of mesophotonic dielectric cone structures serve as tapered waveguides to guide incident light through apertures in an opaque catalyst into the underlying light absorber. This transparency enabled simultaneous achievement of high photoelectrode current density and high catalytic activity, and represents a versatile strategy for rendering optically opaque (e.g., metallic) catalysts to be optically transparent. Experimental progress on optical measurements matched well with the simulated results using full wave electromagnetic simulations. Less than 10% reflection (>90% transmission) is achieved experimentally for Cu metal coverage as high as 70% with incorporation of nanostructured TiO_2 dielectric cones (**Figure 38**).

Semiconductor Photocatalysts

Exploration of reductively stable photocathodes employed high-throughput methods, with JCAP reporting the largest photocathodes screening search to date.[297] Starting with 68,860 candidate materials (orders of magnitude larger than previous reports), the team identified 43 new (and rediscovered 9 reported) photocatalytic materials which can be easily synthesized, are robust in the highly reducing conditions needed for CO_2 reduction, can harvest visible light, and present a wide range of electronic properties (**Figure 39**). The identified materials include arsenides, tellurides, selenides, and oxides presenting a wide range of chemistries suited for extracting different reduction products. These materials were identified via a systematic

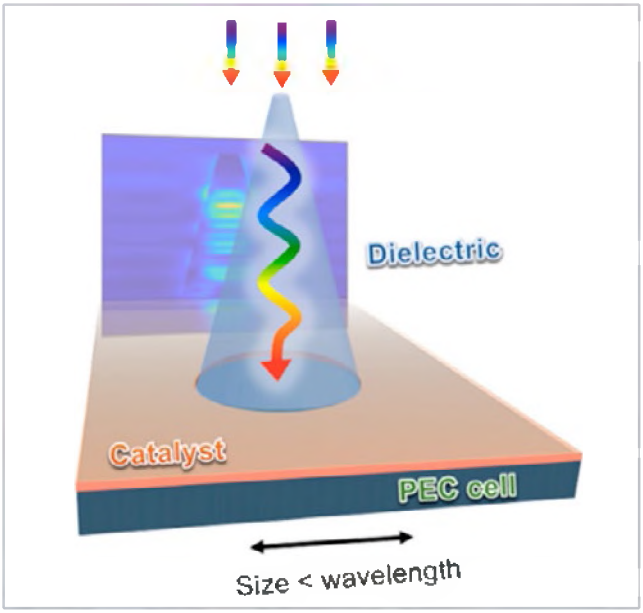

Figure 38. Schematic illustration of light management with dielectric nanocones on top of a semiconductor photo-electrochemical cell.

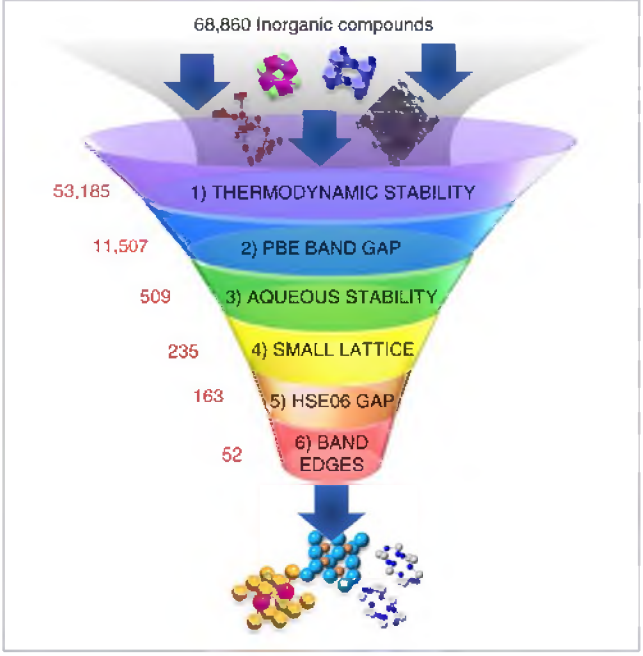

Figure 39. The first-principles-based computational screening pipeline for reductively stable photocathodes identifying 52 candidate materials predicted to be stable in water under reducing conditions, have band gaps in the visible light region, and have surfaces with suitable band-alignments for CO_2RR.

search based on first-principles simulations of intrinsic properties of candidate materials. The screening strategy identified semiconductors not only fulfilling metrics for synthesizability and corrosion-resistance, but also bandgaps and band-edge energies suited for efficient solar-energy conversion.

The effect of semiconductor conduction-band edge position on electrochemical CO_2 reduction yield and selectivity were assessed using MoS_2, $MoSe_2$, and $Mo(S_xSe_{1-x})_2$ alloy transition metal dichalcogenide (TMDC) semiconductor catalysts. Alloying Se into MoS_2 produces an increase in valence band-edge position. The resulting upward shift of the band edges relative to the electrochemical reduction potentials for CO_2 reduction suggests their promise as (photo)-electrocatalysts for the CO_2R.[298]

Spin-coating and sputtering recipes have been developed that enable synthesis of large area (<l0x10 cm^2) and homogeneous photocathode thin films with accurate and reproducible control of component stoichiometry, deployed for study of the Cu-Bi,[299] and Cu-Fe,[300] oxide systems. For $CuBi_2O_4$, copper-rich films demonstrated improved incident photon to current efficiency (IPCE), which optical and XPS analysis showed resulted from CuO segregated to the fluorine-doped tin oxide (FTO) interface acting as a hole-selective contact. The electronic structure of $CuFeO_2$ was elucidated through a combination of optical, X-ray spectroscopic techniques, and first-principles computational methods. The visible absorption edges of $CuFeO_2$ correspond to Cu to Fe metal-to-metal charge transfer, and the ultrafast (<1 ps) decay of the photoexcited state is related to the formation of polarons.

Component Integration

JCAP developed multicomponent, multifunctional test beds for water splitting and CO_2 reduction, focusing on understanding the science behind component integration, from interface formation at the component level up to test-bed devices. This knowledge is key, since synergistic interactions are prevalent within these complex assemblies, and there is a need to exploit emergent properties to realize systems that are more selective and higher performing than natural photosynthesis.

Protective Coatings for Photoelectrodes

Photocathodes for the Hydrogen-Evolution Reaction

Atomic layer deposition (ALD) -grown TiO_2 layers were shown to be effective at protecting photocathodes, such as textured amorphous Si n-i-p structures. This material corrodes rapidly under HER conditions in the absence of a protective layer. An onset potential of over 900 mV for the amorphous Si structure was achieved with a photocurrent in excess of 10 mA cm^{-2}. Even very thick layers of ALD-grown TiO_2 (up to 40 nm) do not significantly reduce the current density or fill factor, suggesting that this approach might be generally applicable to high surface-area photocathodes. The concept was also used to optimize electron extraction from p-InP using electron-selective TiO_2, producing the highest onset potential, >800 mV vs. RHE, for H_2 generation using this light-absorbing material.[301-302]

Photoanodes

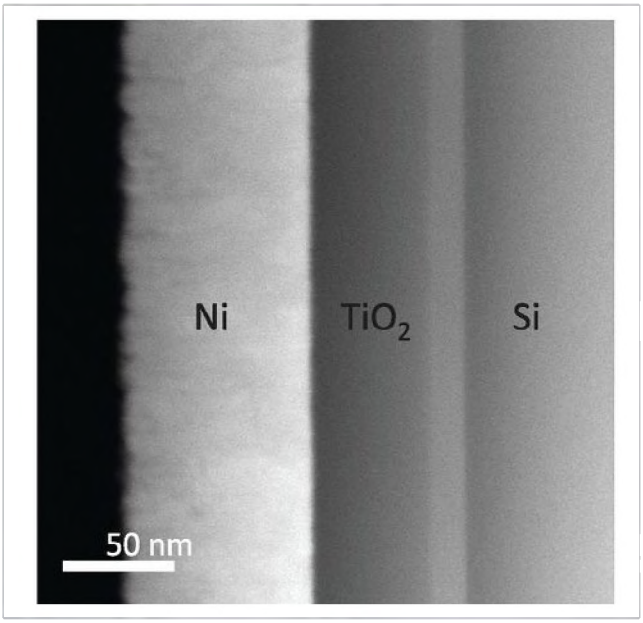

Figure 40. Structural and chemical characterization of the Si/TiO_2/Ni interface. Both Ni and TiO_2 films in this study were continuous, with thicknesses of 100 nm and 68 nm, respectively. Shown is an elemental contrast image of the Si/TiO_2/Ni interface by scanning TEM.

Life cycle assessments performed by JCAP researchers and others have made it clear that operational lifetimes for solar water-splitting devices must be on the order of at least 5–10 years to ensure a positive return on energy, which is a fundamental requirement for any sustainable energy conversion strategy.[303-305] This requirement contrasts with the demonstrated experimental lifetimes of spontaneous solar water-splitting devices, which are at most on the order of one month and more generally less than a day.[306] Operational stability of water-splitting devices presents a fundamental materials challenge, especially for photoanodes, which perform the needed water oxidation reaction. Notably, only a few materials, such as TiO_2 and related metal oxides, are relatively stable under photo-driven water oxidation conditions.[96]

(≤ 2 eV) were not stable in acidic or basic aqueous electrolytes. To address this critical materials gap, JCAP employed parallel strategies, i.e., protection of otherwise unstable known semiconductors and discovery of intrinsically stable semiconductors. Research on semiconductor discovery was described above and protection strategies are discussed here. Previous work involving protective layers on semiconductor photoanodes typically employed TiO_2 as a tunnel

barrier, significantly limiting the useful range of thicknesses, and thus durability, of the coatings. Leveraging that knowledge, JCAP developed a remarkably versatile approach to stabilizing known semiconductors that involves combining a physical barrier layer with a catalytic coating. Photoanodes were protected against oxidative corrosion during extended operation in 1 M KOH by ALD of optically transparent TiO_2, with modified electronic properties to allow the facile transport of holes. Ni is deposited onto the "leaky" TiO_2 to catalyze water oxidation (**Figure 40**). This method was first demonstrated on Si, GaAs, and GaP, with Si photoanodes operated in 1 M KOH electrolyte solutions at photocurrent densities > 30 mA cm^{-2} for > 100 h.[307] In subsequent publications, JCAP demonstrated that a Group II-V semiconductor, n-CdTe, can also be stabilized against corrosion for > 100 h of operation at pH 14, while producing 435 mV of photovoltage and 21 mA cm^{-2} of photocurrent.[308] An ultrathin dual-layer TiO_2/Ni coating deposited on polycrystalline $BiVO_4$ photoanodes improved stability in pH 13 from minutes for bare electrodes to hours for coated electrodes.[309] This work showed that protection of photoanodes by "leaky" TiO_2 coatings is generalizable to many technologically important semiconductors with band gaps of interest for solar-fuels generation. In addition, thin layers of ALD TiO_2 can be used to tune and increase the activity of IrO_2, RuO_2, and F-doped SnO_2 (FTO) electrocatalysts by altering the surface charge density.[310]

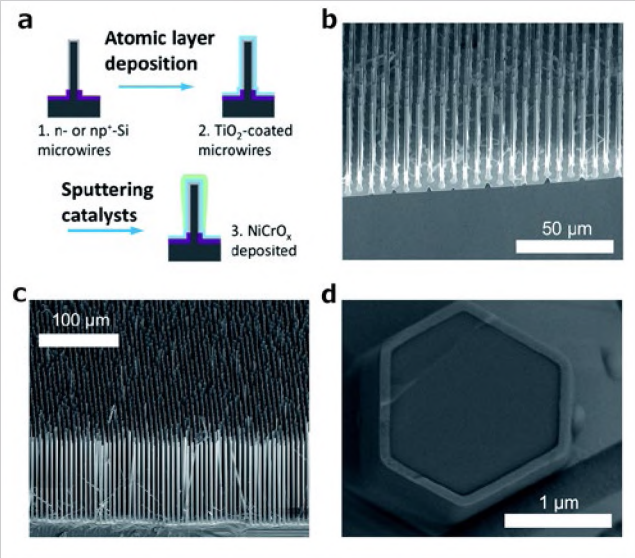

Figure 41. (a) Schematic of a structure that consists of an np^+-Si microwire-array conformally coated with a protective, transparent, and hole-conducting TiO_2 layer, with the TiO_2 layer subsequently coated with a $NiCrO_x$ oxygen-evolution catalyst. (b) SEM images of an np^+-Si microwire-array prior to further processing. (c) SEM image of a fully processed microwire array. (d) SEM cross-section near the base of a single microwire, showing the conformality of the TiO_2 coating with a thickness of 94 nm.

JCAP further investigated the mechanism of anodic conduction across heterojunctions between Si and electronically "leaky" amorphous TiO_2 protective coatings, [17, 307] with Mg, In, Ti, Ni, Au, Ir, Pt, and Pd contacts. Anodic conduction occurs via Ti^{3+} defect-mediated charge-carrier hopping through an energy band 0.83 eV in width and centered 1.47 eV below the conduction-band maximum.[311] The results show that interfaces between TiO_2 and metals having work functions less than that of TiO_2 generally provide higher conductivities than interfaces between TiO_2 and higher-work-function metals. These results elucidate the mechanism underlying anodic conduction through TiO_2 films despite the ~2 eV barrier to conduction expected for such junctions, and inform the design of protective coatings for semiconductor electrodes. To understand the differences in conduction between Ni, Ir, and Au contacts, resonant photoemission spectroscopy (resPES) and resonant inelastic X-ray scattering (RiXS) measurements at the Ti 2p edge were used to investigate the *a*-TiO_2 gap state at buried *a*-TiO_2/metal interfaces. The three characteristics of a highly conductive interface between *a*-TiO_2 and a metal contact are (1) a "reductive" layer that does not oxidize the "leaky" *a*-TiO_2; (2) upward band bending that pushes holes toward the surface but does not push the Fermi level below the defect band in *a*-TiO_2; and (3) an increase in the *a*-TiO_2 density of states to provide a quasi-metallic interface with the metal.[312] JCAP also developed a method to deposit a catalytically active, transparent, conductive oxide, NiO_x, on Si photoanodes. JCAP demonstrated the stabilization of Si, III-V, and II-VI photoanodes for > 1200 h of continuous light-driven evolution of O_2(g) in 1.0 M KOH(aq).[313]

JCAP demonstrated that the protection method based on "leaky" TiO_2 coatings could be extended to structured photoanodes. Si microwire-array photoanodes, protected by a combination of a "leaky" TiO_2

layer and a sputter-deposited $NiCrO_x$ oxygen-evolution catalyst, operated for > 1700 h of continuous, stable photoanodic water oxidation in 1.0 M KOH(aq) (**Figure 41**).[314] Multiple corrosion pathways for TiO_2-protected Si microwire arrays in a polymer membrane either attached to a substrate or free-standing were identified. Top-down corrosion was observed through defects in the TiO_2 coating, while bottom-up corrosion was observed through the substrate and up the adjacent wires and, in the free-standing samples, uniform bottom-up corrosion was observed through the membrane.[315] Additionally, arrays of vertical GaAs nanowires were grown on photoactive planar Si substrates and then protected with the *a*-TiO_2/NiO_x coating. These microwire photoanodes exhibited continuous solar-driven water oxidation in 1.0 M KOH(aq) for >600 h without substantial photocurrent decay.316 Investigation of the failure modes of *a*-TiO_2 protection layers on GaAs anodes indicated that extrinsic pinhole defects formed during deposition and testing control the short-term protective performance of the *a*-TiO_2 film for GaAs anodes evolving O_2 from water; however, additional intrinsic mechanisms are implicated in longer duration failure.[317]

JCAP also demonstrated that SnO_x is a versatile protective coating for n-Si photoanodes that provides efficient and stable light-driven water oxidation when coupled to a variety of known catalysts for the OER in aqueous electrolytes across a wide range (0–14) of pH.[318] The n-Si/SiO_x/SnO_x heterojunction photoanodes provide a photovoltage of 620 mV under 100 mW cm^{-2} simulated solar illumination. The SnO_x protective coating provides low-resistance ohmic contacts to known catalysts (Ni, Ir, and Pt oxides) for the OER. In acidic electrolytes, the stability of the photoanodes was limited by corrosion of the Ir or Pt catalyst films. Unlike other protective coatings for photoanodes, such as electronically "leaky" TiO_2,[307] conduction through the SnOx coating does not depend on the catalyst, and thus the coating allows independent selection of the catalyst and therefore a more modular approach to photoanode design. The SnO_x coating was deposited conformally on high aspect-ratio three-dimensional structures, such as Si microcone arrays, and was combined with amorphous TiO_2 to form a protective SnO_x/TiO_2 bilayer that exhibits the beneficial properties of both materials. Photoanodes coated with SnO_x/TiO_2 exhibited a similar photovoltage to that of SnO_x-coated photoanodes, and showed >480 h of stable photocurrent for planar photoelectrodes and >140 h of stable photocurrent for n-Si microcone arrays under continuous simulated solar illumination in alkaline electrolytes.[319] The stability of the protective coating across a wide range of pH values will allow stable operation for oxygen evolution in contact with the neutral electrolytes used for CO_2 reduction cells even as the pH decreases locally as protons are liberated at the photoanode.[320]

In another approach, JCAP developed a multifunctional water-splitting catalyst that was specifically engineered to be interfaced with semiconductor light absorbers without the need for an interfacial corrosion protection layer. The major impact of this work was to highlight the importance of tailoring new catalysts to effectively balance chemical, optical, and electrical properties in integrated assemblies. This was accomplished using plasma-enhanced ALD (PE-ALD) to create a biphasic cobalt oxide catalyst coating.[321] An ~4 nm thick conformal nanocrystalline Co_3O_4 spinel provided a stable interface with the chemically sensitive light absorber, and was combined with a chemically labile and disordered $Co(OH)_2$ surface layer providing high catalytic activity. By applying this coating to p^+n-Si junctions, the highest performance for crystalline Si photoanodes performing OER reported to that time was achieved. Nanotextured interfaces were found to promote deposition of amorphous, rather than nanocrystalline, cobalt oxide, allowing more efficient protection.[51]

JCAP researchers co-authored a comprehensive review article on protection layers for photoelectrodes used for solar-fuel generation.[322] Focusing on the photoanode, which is an n-type semiconductor, one can imagine three regimes for charge transfer of minority holes to the surface (**Figure 42**). In the first case (**42(a)**), the valence band of the protection layer is lower than that of the absorber, and holes are transported by tunneling. In the second case (**42(b)**), the protection layer possesses a valence band below that of the absorber but allows hole transport through a defect band. In the third case, the valence band of the protection layer is above that of the absorber, such that holes can reach the surface via band conduction (**42(c)**).

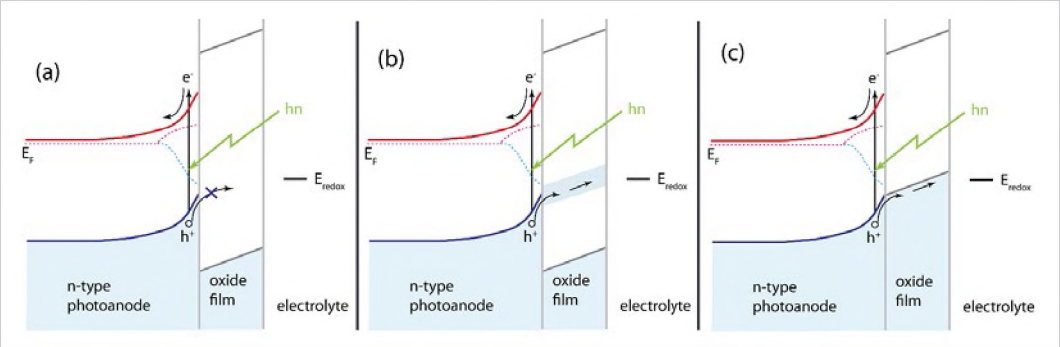

Figure 42. Schematic band diagram of hole transport through a protective oxide layer deposited on an n-type photoanode. Conduction and valence band edges are red and blue lines, respectively, and quasi-Fermi levels are indicated by dotted lines. Three mechanisms for hole transport are depicted: (a) tunneling, (b) defect band conduction, and (c) valence band transport.

This third case was experimentally demonstrated using $NiCo_2O_4$, which is a p-type transparent oxide, as a protective coating on n-type Si.[323] Measurements of the work function of the $NiCo_2O_4$ by XPS confirmed that the band alignment depicted in **Figure 42(c)** was achieved. Due to the transparency of the protective layer and also its efficient hole collection properties **(Figure 43)** a limiting current density of over 30 mA cm^{-2} with 25 mA cm^{-2} at 1.23 vs. RHE was achieved with an np^+-Si/$NiCo_2O_4$/Ni-Fe device stack in which the Ni-Fe serves as a water oxidation catalyst. Stable operation was confirmed by observing a constant current density over 72 hours and by sensitive measurements of corrosion products in the electrolyte. Extrapolation of the corrosion rate predicts an operational lifetime of several years for this approach. The generality of using p-type transparent conductors as protection layers was demonstrated by multihour, stable water oxidation with an n-InP/p-$NiCo_2O_4$ heterojunction photoanode.

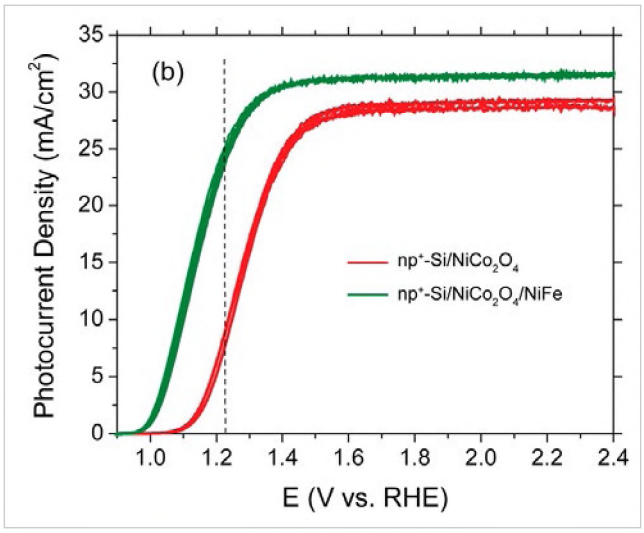

Figure 43. CV scans of $NiCo_2O_4$ coated np^+ Si with (dark green) and without (red) a 2 nm Ni–Fe (50/50) coating serving as an oxygen evolving catalyst. For this film, the onset potential for OER is 0.95 V vs RHE and the current density at the reversible potential for oxygen evolution is 26 mA cm^{-2}. The vertical dashed line is at 1.23 V vs. RHE.

JCAP also conducted an in-depth investigation of hybrid organic-inorganic halide perovskites, where the team developed a novel process for synthesis of halide perovskite-based PV devices exhibiting high internal quantum yields and ~19% power conversion efficiency, which is among the highest reported for this emerging solar-energy harvesting material.[68-69] This synthesis process has been extended to allow the fabrication of materials with tunable bandgaps, from 1.6 to 2.3 eV, thus making them well suited for integration in tandem device configurations.[69] Using this process, photovoltages in excess of 1.1 V have been generated from single junction devices. In addition, it was demonstrated that thin-film crystallographic texture (i.e., preferential grain orientation) can have a significant impact on PV performance.[68] By probing the PV properties at the nanoscale, the team found that facet-dependent defect concentrations exist that lead to significant photovoltage inhomogeneity within individual grains. This research points to new ways to engineer interfaces and halide perovskite

synthesis conditions to obtain higher efficiency. In addition to understanding basic factors that contribute to photocarrier recombination within and on the perovskite, JCAP investigated the role of electron-selective contacts in defining device performance. Deep level hole traps were introduced into contacting TiO_2 layers and contributed to a high photoconductive gain and reduced photocatalytic activity. The high photoconductivity of the TiO_2 electron transport led to improved efficiency for the fabricated planar protective coatings. In addition, the reduced photocatalytic activity of the TiO_2 layer led to enhanced long-term stability for the planar protective coatings. Under continuous operation near the maximum power point, a power conversion efficiency of over 15.4% was demonstrated for 100 h for the first time with perovskite materials.

The local structure effects of different A site cations (e.g., methylammonium, formamidinium, cesium) on hybrid organo-lead halide perovskite materials was investigated using high-energy resolution fluorescence detected (HERFD) XAS and first principles DFT. The unique spectral signatures for cesium cations arise from coupling between the Cs d orbitals and the Pb-halide d-d coupling.[324] New insights into light-induced halide segregation mechanisms were uncovered using in situ methods.[325-326] Theoretical investigation of transport in halide hybrid perovskite found that large polarons reduce carrier mobility by a factor of two.[327] The optimization of compositions is aided by computation, including elucidation of the mechanism for photoinduced HER on the methyl amine PbI3 organic-inorganic hybrid perovskites[328] and rapid in silico QM optimization of organic-inorganic hybrid perovskites photocathodes.[328]

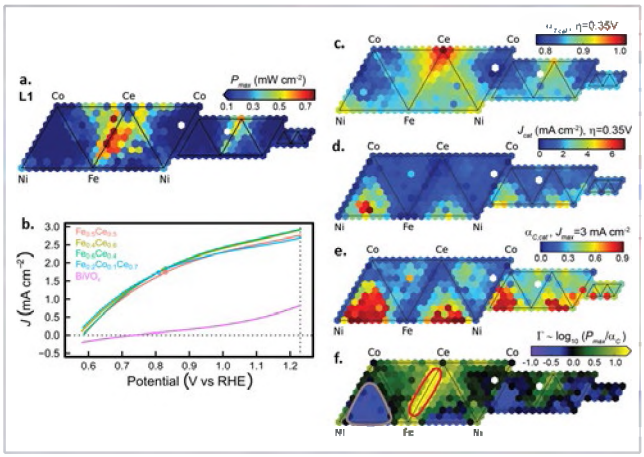

Figure 44. Combinatorial integration of (Ni-Fe-Co-Ce)O_x onto $BiVO_4$. (a) Composition maps of PEC P_{max}, plotted with a common color scale using the flattened pseudo-ternary triangle scheme. (b) Representative photocurrent density signals from three of the best photoanodes are shown along with the photocurrent density signal from bare $BiVO_4$. Composition maps of (c) optical transmission efficiency ($\alpha_{T,cat}$), (d) catalytic current density (J_{cat}), and the ensuing (e) combined figure of merit ($\alpha_{C,cat}$). The parameter Γ compares photoanode performance (P_{max}) (a) to that predicted by $\alpha_{C,cat}$, and the corresponding composition map is shown in (f).

Integration of semiconductor light absorbers and functional coatings (e.g., electrocatalysts) requires simultaneously balancing catalysis, corrosion protection, light trapping, carrier transport, and mitigation of photocarrier recombination at interfaces.[329] JCAP introduced a high-throughput, combinatorial methodology for discovering emergent properties at interfaces between light absorbers and catalysts to address this challenge. Uniform BiVO4 thin films were coated with pseudo-quaternary composition spaces — (Ni-La-Co-Ce)O_x and (Ni-Fe-Co-Ce)O_x — with three different loadings.[330-332] Each integrated photoanode was photoelectrochemically and optically characterized and compared with the isolated metal oxides. Data-driven discovery was used to identify composition regions that form high-performance interfaces (**Figure 44**). In both cases, the optimal catalyst compositions, when integrated with $BiVO_4$, are substantially different than the optimal electrocatalysts on FTO, revealing that consideration of the isolated properties of semiconductors and catalysts is insufficient for predicting functional characteristics of integrated PEC assemblies. A subset of integrated assemblies exhibited performance characteristics that were significantly better than anticipated, indicating that material interactions can lead to emergent properties. To provide insight into function and stability, a photoanodic deposition approach was established to access promising multicomponent oxides over larger areas.[333] The high-throughput evaluation of integrated catalyst/light-absorber combinations[330-332] was extended to investigate pH-dependent

behavior in photoanodes.[334] Duplicate $(Fe\text{-}Ce)O_x$ composition-loading gradient films were sputtered onto 100 cm^2, high-performing, undoped, compact, spin-coated $BiVO_4$ films to create *photoanode assemblies*, which were photoelectrochemically evaluated in pH 13 NaOH and pH 9 borate buffer. The PEC performance is much more sensitive to composition in pH 9 than in pH 13 (**Figure 45**), with pronounced photocurrent transients in pH 9, except at the optimal composition and loading.

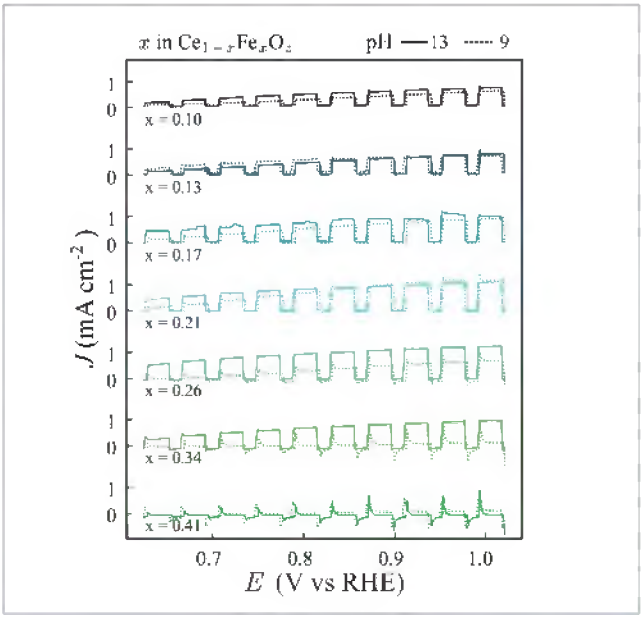

Figure 45. Overlay of anodic sweep toggled-illumination CV data collected using pH 9 and pH 13 electrolyte at similar loading (0.9 nmol mm^{-2}) and compositions in the $Ce_{1-x}Fe_xO_z$ coating on $BiVO_4$. The current transients are more pronounced in pH 9 than in pH 13 at all but the optimal and poor Fe-rich compositions (21% and 41% Fe).

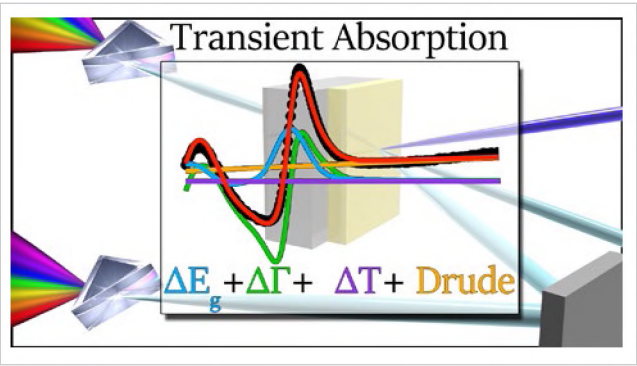

Figure 46. The transient absorption spectrum of solid-state systems, such as the model system bismuth vanadate ($BiVO_4$), is found to be related to free-carrier induced modifications to the band gap (ΔE_g), the band broadening ($\Delta\Gamma$), laser induced heating (ΔT), and free-carrier absorption (Drude). Using ground state optical properties, we were able to model the transient spectral components from fs – ps.

Photocathode assemblies were developed by evaluation of 2,574 different metal oxide layers (in composition spaces $(Ce\text{-}Y\text{-}Zr\text{-}Cu)O_x$, $(Ga\text{-}Sn\text{-}Gd\text{-}Cu)O_x$, and $(La\text{-}Y\text{-}Ti\text{-}Cu)O_x$)) deposited using inkjet printing onto 100 cm^2 sputtered copper bismuth oxide films,[335] which identified a $(Cu\text{-}Ti)O_x$ coating that enhanced both photocurrent and stability in pH 7 bicarbonate buffer with a sodium persulfate electron acceptor. The optimized overlayer ($Cu_{1.5}TiO_z$) improves the onset potential by 110 mV, the photocurrent by 2.8×, and the absorbed photon-to-current efficiency by 15.5%. These enhancements result from passivation of surface defect states and improved carrier extraction efficiency through Fermi-level engineering.[335]

Component and Interface Characterization

Within JCAP, a suite of ex situ and in situ characterization techniques and multimodal approaches allowed a robust picture of interfacial processes to be developed. TA spectroscopy is uniquely suited for understanding kinetic processes initiated by light over vast time scales, but requires careful interpretation. In the transient spectra of a monoclinic $BiVO_4$ thin-film sample, heating from the optical pumping, which begins at ~10 ps and plateaus by ~200 ps, dominates the overall spectral response at longer times (**Figure 46**). However, by using the Drude optical model of free carriers, the transient response related to free hole density was also identified. This comprehensive approach to analyzing and modeling the TA spectra offers a generalizable basis for understanding the complex pump-probe data, reveals thermal heating artifacts that are frequently erroneously assigned to long-lived photocarriers, and offers a path to eliminating ambiguity in analysis of photocarrier dynamics in solid state systems.[336] Application of these methods of comprehensive spectroscopic and

first-principles characterization to $CuBi_2O_4$ thin films led to a description of their fundamental electronic structure and optical properties and exposed a limited electron diffusion length of 45 nm attributed to electron small polaron transport.[337]

Complementary to charge-carrier dynamics in light absorbers, the operando quantification of surface and bulk losses is key to developing strategies for optimizing photoelectrodes and realizing high-efficiency PEC solar-energy conversion systems. The spatial collection efficiency (SCE), which is defined as the fraction of photogenerated charge carriers at each point below the surface that contributes to the measured current, was introduced as a novel technique to identify performance bottlenecks arising from lossy charge transport properties or slow reaction kinetics at semiconductor/electrolyte interfaces under operating conditions.[338-339] Researchers applied this approach to the understanding of different phases of copper vanadate.[340] Specifically, copper-rich phases were shown to have a collection length larger than anticipated, but with a performance limited by low charge carrier photogeneration yield.

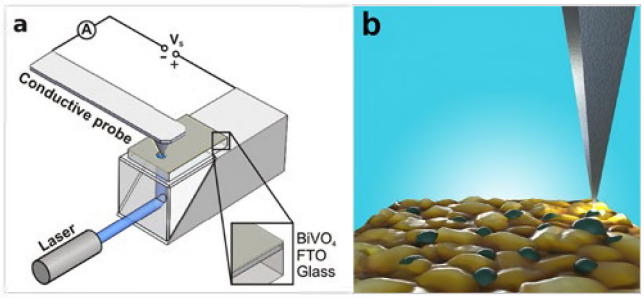

Figure 47. (a) Schematic of photoconductive probe AFM instrument. (b) AFM technique for investigating the interfacial charge transfer mechanism.

Understanding and optimizing semiconductor/catalyst and catalyst/electrolyte interfaces remain key challenges to realization of efficient PEC solar-fuel generators. Using complementary macroscopic PEC measurements and nanoscale atomic force microscopy (AFM) techniques, the interfacial charge transfer and collection mechanisms of light-absorber/catalyst interfaces were interrogated to simultaneously optimize the passivating and catalytic functions. Multicomponent $(Ni\text{-}Fe\text{-}Co\text{-}Ce)O_x$ overlayers on $BiVO_4$ photoanodes were assembled and analyzed. $(Ni\text{-}Fe)O_x$ was identified as the surface catalytic component and $(Co\text{-}Fe\text{-}Ce)O_x$ as the charge capture/collection component. A bilayer $(Co\text{-}Fe\text{-}Ce/Ni\text{-}Fe)O_x$ overlayer was rationally engineered to yield $BiVO_4$ photoanodes with almost 100% efficiency for the OER. The effective charge transfer through the $(Co\text{-}Fe\text{-}Ce)O_x$ hole collector and $(Ni\text{-}Fe)O_x$ catalyst interfaces was verified by mapping current distributions with photoconductive AFM measurements (**Figure 47**). [333, 341]

Picosecond time-resolved X-ray photoemission spectroscopy (TRXPS) was utilized to investigate photoinduced electron transfer in a model plasmonic system composed of 20 nm gold nanoparticles attached to a nanoporous film of TiO_2.[342] The results of TRXPS provide an absolute measure of the charge injected from the gold nanoparticles (AuNPs) into the semiconductor substrate. This study provides the first reference-free, quantitative, microscopic, real-time insight into the efficiency and temporal evolution of charge-transfer dynamics in a standard nanoplasmonic heterostructure. It demonstrates that currently available benchmark values for the first steps of photon-to-charge conversion in AuNP-sensitized TiO_2 need to be re-evaluated based on newly available data and corresponding theoretical estimates.

Spatially resolved X-ray absorption spectra obtained by scanning transmission X-ray microscopy (STXM) provide information about changes in the chemical composition and electronic structure, combined with the corresponding Mo:$BiVO_4$ film morphology obtained by AFM.[343] Using STXM as a spectromicroscopic technique, the different X-ray absorption spectra corresponding to grain centers and grain boundaries compositions of the Mo:$BiVO_4$ films were disentangled. The absorption spectrum at grain centers corresponds to Mo:$BiVO_4$, whereas the spectrum at grain boundaries indicates the presence of V_2O_5. Many-body DFT calculations of the O K-edge absorption spectra for Mo:$BiVO_4$ and V_2O_5 provided further understanding of the chemical composition in heterogeneous regions within the thin film. STXM analysis of Mo:$BiVO_4$ films degraded by PEC operation provided insight into the impact of material heterogeneities on the degradation

mechanism and material stability. The same approach was used to investigate the impact of nanoscale heterogeneities and composition–reactivity relationships in copper vanadate photoanodes with varying Cu/(Cu + V) ratios around the ideal stoichiometry of stoiberite $Cu_5V_2O_{10}$. Nanoscale segregation of Cu in films with different stoichiometries showed that the average macroscale film composition is insufficient for defining structure-function relationships in complex ternary compounds. Correlating microscopic variations in chemical composition to macroscopic PEC performance provides insights into photocatalytic activity and stability that are not apparent from purely macroscopic characterization.[344]

Membrane Materials for Solar-Fuels Applications

A fully integrated solar-fuels prototype requires separating gaseous products for both safety and efficiency, while maintaining sufficient ion conduction between the reduction and oxidation chambers in order to maintain charge neutrality and avoid undesirable pH gradients. Prior to JCAP, appropriate membranes existed for related technologies, such as fuel cells and water electrolyzers, but the optimal properties for membrane separators in solar-fuels prototypes were unknown, as were strategies for synthesizing the appropriate materials.

JCAP's initial investigations were of relevant aspects of membranes and membrane composites derived from material systems used widely by the fuel-cell community, such as perfluorosulfonic acid ionomers (e.g, Nafion). These included utilization of small-angle X-ray scattering to determine sub-second morphological changes in Nafion during water uptake[345] by utilization of in situ GI small-angle X-ray scattering techniques. The measurements demonstrated that the wetting interaction in thin-film interfaces can drastically affect the internal morphology of ionomers and in turn modify its transport properties,[346] and that confinement of Nafion in thin films induced thickness-dependent proton conductivity.[347] These results deepened understanding of the properties of Nafion and revealed options for controlling its properties in a solar-fuels device. A key modeling study by JCAP revealed the impacts of the tradeoff between gas-blocking characteristics and conductivity in Nafion for a solar H_2-generating device, and led to JCAP's definition of unique membrane requirements for solar-fuel generators, i.e., a successful membrane must have better product blocking characteristics than Nafion but does not require its high conductivity.[348] New acid- and base-stable membrane materials would be required to meet these criteria.

JCAP's research on new membrane material discovery focused on developing polymer platforms having balanced and tunable ion and gas transport properties. Two different strategies were pursued: block copolymers (BCPs), which are highly customizable, and randomly crosslinked polymers synthesized by reactive blending. Additionally, methods for control of membrane properties during synthesis and processing were evaluated.

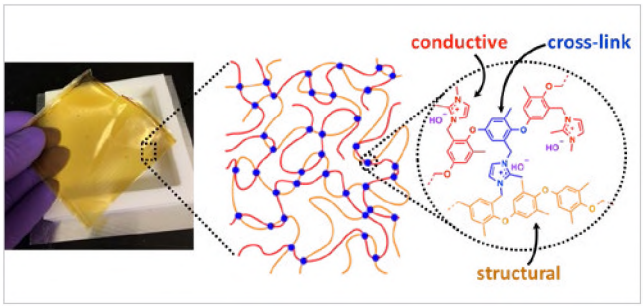

Figure 48. Reactive blending of functionalized poly(2,6-dimethyl phenylene oxide) is used to prepare membranes with tunable mechanical and conductive properties.

BCPs offer the ability to select both the hydrophobic and the hydrophilic blocks and tune their domain sizes to have controlled water uptake and good conductivity. Work by JCAP researchers focused on polymer designs to optimize those specific characteristics. Several novel classes were reported. All have low water uptake compared to Nafion, indicating a potentially reduced gas crossover relative to it. BCP membranes with polystyrene (PS) as the structural, hydrophobic block and polymerized ionic liquids (PIL) containing imidazolium as the hydrophilic block

were prepared[54, 58, 63, 349-351] and demonstrated to have conductivities around 0.3 mS/cm,[60] in the range of about 1 mS/cm predicted as optimum.60 In an alternative approach, block copolyelectrolytes using PS and cyclopropenium ions as the hydrophilic block have been demonstrated to have conductivities in the range of 4 mS/cm.[352] A specific focus was placed on finding new BCP anion-exchange membrane (AEMs) materials for operation in basic electrolytes, since the number of available materials (commercial and in the literature) is quite small.[353] Membranes prepared with imidazolium and phosphonium blocks may not be sufficiently stable in base for use in high-performance solar-fuels devices; however, improved stability has been demonstrated with new membrane BCPs containing PS and polydimethyl ammonium.

Amorphous, randomly crosslinked polymers (**Figure 48**) offer a completely different approach to membrane design. A novel reactive blending process yielded a highly adaptable platform demonstrated for base-stable anion-conducting membranes. A series of membranes were prepared and evaluated for their stability under electrolysis conditions, as well as their conductivity, water uptake, and product crossover properties. They were found to have very promising performance relative to the commercial membrane Selemion, including a diffusive permeability to methanol reduced by more than a factor of 10, indicating they may be useful for CO_2 reduction systems.

In addition to discovery of new membrane materials, JCAP evaluated techniques for modification of membrane properties through process control and developed a scientific understanding of their performance. These techniques include thermal processing to control slow transport through hydrophobic regions of the membrane, demonstrated for Nafion,[60] preparation of BCP films using partly soluble blends to create artificial free volume and hence controlled transport properties,[62] and development of a new simplified model for control of polymer synthesis kinetics through monomer reactivity ratios, which facilitates design of synthetic strategies.[354]

A critical issue for the operation of CO_2R devices is the isolation of reactants and products, thereby ensuring safe and efficient operation as well as high selectivity. This is of even more importance for the GDE and MEA systems since reactants at higher concentrations may exist at the membrane interface. Furthermore, the ion-conducting membranes are critical for efficient water delivery and regulation in those architectures, and require hydration for sufficient conduction. These needs drove the exploration of membranes, which for JCAP are ion-exchange membranes that ideally transport only the ions of choice (e.g., OH^-) and not the product fuels.[355]

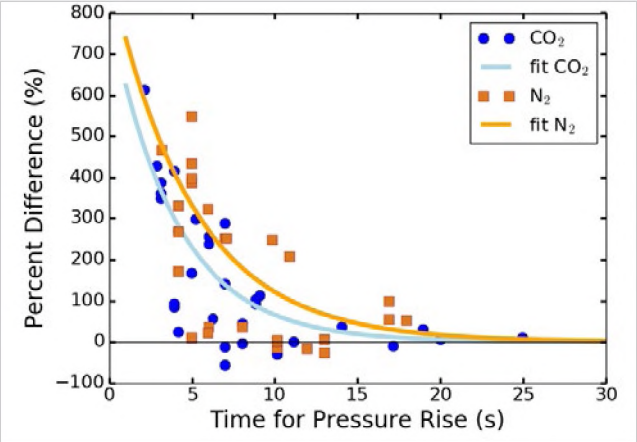

Figure 49. Percentage difference between the time obtained in the simulations for the pressure-dependent (Henry's Law) concentration of N_2 or CO_2 in PPO to reach a maximum, and the pressure rise time upstream (from the membrane) in the experimental apparatus.

Permeation through membranes at steady state is well studied,[356-357] and it is known that organics and CO_2 can interact with polymers and affect their permeability in use.[358] However, very little is known about the exact mechanisms of this transport and how transient operation (e.g., due to diurnal fluctuations) impacts the transport processes. JCAP researchers developed a multiscale modeling framework that enables macroscopic observables, such as extent of permeation as a function of time, to be simulated while retaining a fundamentally molecular description of the system. Stochastic simulation methods lend themselves well to this type of modeling, particularly for membrane systems where permeation is accompanied by volume and internal environment changes. In an initial study,

a basic framework was developed for permeation of small gaseous molecules through rubbery polymers.[359] The time-dependent maximum concentration of the solute, determined by Henry's law, varied instantly with external pressure changes, suggesting that the polymer is not an inert host. Time-dependent permeation of weakly and strongly interacting solutes through a model glassy polymer, poly(dimethylphenylene oxide) (PPO) and through Nafion was also studied.[360] Detailed studies of N_2 and CO_2 permeation through PPO have shown that external pressure variations lead to similar behavior as rubbers, but the polymer response is sluggish (**Figure 49**).[361] The solution diffusion model accurately describes permeation in glasses, and yields the same results as a more complex dual model involving migration through dynamic and static voids.[362] As found in the rubbery polymer case, PPO is not an inert host: the free energy profiles calculated for the solutes show that sorbed gases are at lower energy than in the gas phase. The agreement between the simulations and time-dependent data shows that interactions between N_2 and CO_2 and the polymer dynamically influence the solute diffusivity. Polymer relaxations have been identified by MD studies, but on a much shorter timescale than that found in this work. This suggests that additional, longer term physical mechanisms are involved, pointing to gaps in our understanding of polymer stability in use.

Ion-exchange membranes play dual roles in PEC carbon dioxide reduction devices: they promote the transport of electrolyte ions so that current can flow in the device and minimize the crossover of redox products. To assess the connection between membrane composition, structure, and function in co-transport environments, JCAP developed a new technique featuring a standard diffusion cell with temperature control and using an in situ Fourier transform infrared spectroscopy (FTIR) probe. The in situ FTIR probe of the solution was demonstrated to be valid for co-solutes and neutral species transport, by measuring the transport of methanol, formate, and acetate through Nafion 117 membranes. The diffusive permeabilities of formate and acetate were suppressed when co-permeated with methanol. The approach was used to quantify the permeability of individual and mixed alcohols (methanol, ethanol, and n-propanol) through Selemion AMV.[363] Experimental measurements and multiscale simulation of methanol transport in Nafion was used to develop and validate a multiscale model describing solute permeation through a hydrated membrane as a series of physical mechanistic steps: reversible adsorption from solution at the membrane interface, diffusion driven by a concentration gradient within the membrane, and reversible desorption into solution at the opposite membrane interface. The validated model was used to predict methanol transport across a solar-driven CO_2 reduction device and to assess the impact of polymer changes on the measured value. The approach of combining experimental data, computational fluid dynamics, and the mechanistic multiscale model will provide more accurate analysis of membrane permeation data in cases with polymer swelling or unusual device geometries, among others.[364]

To understand the fundamental membrane properties governing the transport of electrolyte ions and CO_2 reduction products, two families of AEMs with tunable properties were synthesized. One family of membranes consisted of imidazolium-functionalized poly(phenylene oxide),[365] and the other was comprised of photo-crosslinked vinyl(imidazolium) materials.[366] The degree of functionalization in both families was varied to control ion-exchange capacity and membrane water content. The ionic conductivity and permeability to CO_2 reduction products, such as low molecular weight alcohols,[363, 367] was measured as a function of ion-exchange capacity and water content. In both poly(phenylene oxide) and poly(vinyl imidazolium) membranes, ionic conductivity and CO_2 reduction product (e.g., alcohol) crossover scaled with membrane water content.[365-366] In crosslinked poly(vinyl imidazolium) materials, ionic conductivity and alcohol permeability were reduced by increasing crosslink density.[366] This was the first experimental demonstration of the fundamental tradeoff challenging the development of membranes for artificial photosynthesis devices. Membranes with water contents greater than and less than legacy ion-exchange materials (e.g., Selemion, Nafion) were synthesized.[365-366] In CO_2 reduction devices, the crossover of charged products (e.g., acetate, formate) due to the application of an electric field was found to exceed the crossover due to concentration-driven diffusion.[368]

Multiscale Modeling of Solar-Fuel Device Architectures

Multiphysics modeling of complete solar-fuels prototypes is critical for guiding materials development, defining operational conditions and constraints for various cell designs, providing detailed geometric parameters for prototypes, and evaluating the viability of novel cell designs. Prior to JCAP, the modeling of solar-fuel cells was primarily focused on materials properties of individual components and simplified 0-dimensional or 1-dimensional system analysis without a detailed cell construct.[369-370]

Architectures for H_2 Generation

JCAP developed a robust multiphysics, multidimensional modeling/simulation platform that accounts for the performance of the photoabsorbers and electrocatalysts, the transport properties of electrolytes, and the requirements for membrane separators.[371-374] The modular modeling platform, in which individual processes are coupled with the preceding and subsequent processes by interactive boundary conditions, allowed for study of the overall cell performance of planar systems,[371] as well as of more advanced designs involving components with micro- or meso-scale structures.[106, 375-376] Coupled with the electron/hole transport in the semiconductor and multi-ion transport in the solution electrolyte, the detailed reaction rates at the catalytic sites in three-dimensional photoelectrodes were modeled and simulated for the first time.[371-372] Leveraging the whole cell model, JCAP identified several sufficiently specific, yet generic cell constructs, including a "louvered" design, a "side-by-side" design, etc., in which fully integrated, efficient, and scalable solar-hydrogen generators could be fabricated with proper materials assemblies. JCAP also established a comprehensive relation between the overall STH conversion efficiency and the physical dimensions of the electrode width, electrode height, and the film thickness of the membrane separators in specific designs.

In addition, JCAP investigated the trade-offs between the illumination intensity and temperature-dependence of the photocurrent and photovoltage. JCAP also investigated losses associated with factors that include ohmic resistance, concentration overpotentials, kinetic overpotentials, and mass transport.[372] The target materials properties of the photoabsorber, the electrolyte solution, and the membrane separator were provided by the whole cell model to achieve optimal STH conversion efficiencies, and the optimal bandgap combinations of tandem photoabsorber structures were revealed.[377] The trade-offs between the permeability and conductivity of the next-generation membrane separator were investigated to reveal the target material properties needed to achieve efficient ion conduction and product separation for solar-fuel devices.[348] The performance limits and associated potential losses in near-neutral pH operation were also simulated and experimentally validated.[378] The large voltage penalty associated with local pH gradients at the surface of the electrodes in near-neutral pH operation significantly limited the cell efficiency in a membrane-based device.[378] Additional JCAP modeling showed that a device architecture that externally recirculates the electrolyte through the system was beneficial at near-neutral pH because it substantially reduced the potential loss associated with pH gradients at the surface of the electrodes, and minimized electrodialysis of the bulk electrolytes.[379] JCAP performed sensitivity analyses on a variety of generic solar-fuels generator designs comparing the relative importance of electrocatalyst overpotential reduction, improvements in light-absorber properties, and parameter optimization.[380] One strategy for reducing the optical obscuration from metal electrocatalysts is to use a low geometric filling fraction of the catalyst on the surface of the light absorbers.[381] In addition, JCAP studied the design criteria of novel cell designs: an integrated PEC cell coupled with a solar concentrator with low solar concentration,[373] an integrated vapor-fed PEC device,[374] and a membrane-encapsulated device.[382] Annual thermal and efficiency aspects of solar concentration have revealed the importance of siting and temperature management.[383] JCAP researchers published a comprehensive review on the modeling of solar-fuel devices, which encapsulated the best practices, as well as pitfalls, in the modeling of different device architectures.[384]

Architectures for CO_2 Reduction

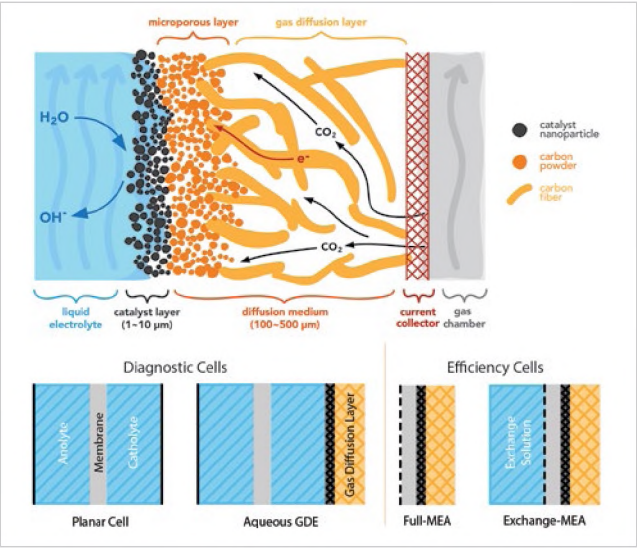

Figure 50. Schematic of a GDE and schematics of different GDE and membrane-electrode-assembly (MEA) cell designs.

The architecture of the solar-fuels generator directly impacts the product selectivity and activity for CO_2R catalysis. Integration at the test-bed scale can introduce significant variation in the reported activity, selectivity, and durability, even for well-studied catalysts such as copper. Mass-transfer effects and the local environment can lead to changes in the product distribution that could be incorrectly attributed to catalyst deactivation, a common concern in such studies, as opposed to being caused by the cell design.[385-387] To understand, explore, and develop next-generation architectures, JCAP used multiphysics modeling combined with detailed studies. The modeling and experimental studies demonstrated the importance of the local environment, including overpotential, and how the aqueous CO_2 concentration is limiting in terms of mass transport and performance.[387] The latter is especially true because the CO_2 concentration limits the operation window due to acid/base reactions, which result in non-Fickian diffusion profiles and lack of local equilibrium.[388] This is one reason that vapor-fed systems were explored.[389]

Multiphysics simulations using continuum equations allowed for virtual evaluation of different test-bed designs, as well as providing feedback on optimal material properties and limiting phenomena. The voltage efficiency of a solar-driven electrochemical cell depends on the physical properties of its components (catalysts, electrolyte, and membrane); operating conditions (carbon dioxide flow rate and pressure, current density); and the physical dimensions of the cell.[390] A multiphysics, multidimensional model for electrochemical CO_2 reduction cells with a focus on GDEs and MEAs was developed. The models account for electrocatalysis for CO_2RR and OER, ionic transport, and chemical acid/base homogeneous reactions in any liquid or ion-conducting polymer electrolyte.[389]

GDE and MEA architectures (**Figure 50**) overcome the inherent ohmic losses associated with liquid layers (with a typical drop of 1 V/cm). Cells with liquid between the electrodes are labeled diagnostic as they allow one to explore specific physical phenomena. However, to reach higher current densities and explore other benefits of vapor feed (e.g., low water concentrations, different possible mechanisms, use of CO feeds, etc.),[389] one should use the high-efficiency cells. The cell design for the simple case of CO_2 reduction to CO on Ag was explored numerically, and high current densities are possible at relatively low total cell potentials (**Figure 51**). It is also clear that hydration of the membrane becomes important, and thus liquid and even ion-containing exchange solutions can help lower cell voltage, although there is a precipitation limit due to carbonate crossover. In fact, this model was one of the first to explicitly evaluate CO_2 utilization, where it is very low in the exchange solutions due to carbon dioxide pumping across the anion-conducting membrane. Due to some of these concerns, cell performance and CO_2 utilization efficiency was modeled in cells with different separators (AEM, cation-exchange membrane, and bipolar membrane). The AEM led to only 14.4% CO_2 utilization for 6-electron reactions, and the optimum membrane was the bipolar membrane with a CO_2 utilization efficiency of 66% with higher utilization possible with membranes designed to inhibit CO_2 transport.[391]

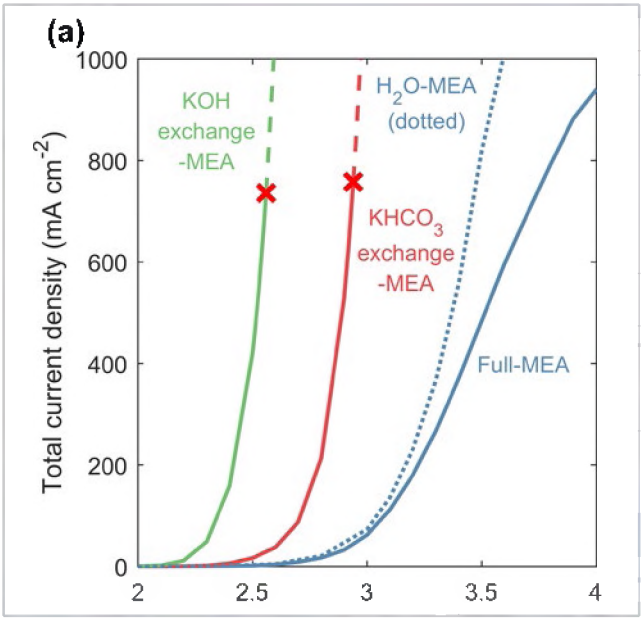

Figure 51. Total current density for a full-MEA, $KHCO_3$-MEA, and KOH-MEA. The red crosses indicate the current densities at which precipitation occurs in the MEA cell.

A one-dimensional, steady-state model for MEA designs operated with a Cu catalyst was developed.[392] The model demonstrated that the product selectivity depends on such parameters as catalyst-layer thickness and humidity or liquid anode feed due to the intricacies of water and thermal management within the cell and its impact on ionic conductivity. In addition, changing the feed from vapor to an exchange solution on the anode side demonstrated much higher current densities with similar selectivity and product distributions, as well as full catalyst utilization.

Integrated Artificial Photosynthetic Test Beds

Test Beds for H_2 Generation

JCAP's initial goal was to build fully integrated solar-fuels generators that utilize Earth-abundant semiconductors and catalysts for the efficient conversion of water to H_2 and provide for full product separation using membranes. Criteria for success were efficiencies exceeding 10% STH, with stability and durability for days to weeks and longer. As discussed in a JCAP review article,[306] at the time these were leading-edge criteria for the technology. JCAP achieved this goal in several demonstrations and pursued further improvements, such as design and fabrication of more efficient light absorbers using custom made (e.g., energy gap selection) tandems for water photolysis and further electronic optimization of the various interfaces in the structure to produce larger currents at the water-splitting potential.

JCAP prototypes were designed to enable separation of products, and therefore require membranes and complex interfaces between various material components that will function under realistic operating conditions. Most solar-fuels devices described in the literature represent only portions of a complete system, or are miniaturized combinations of PVs and electrolyzers.[306] Here we summarize results demonstrating that JCAP made substantial progress in addressing the scientific and engineering challenges associated with designing, building, testing, and analyzing fully integrated H_2 solar generators.

>19% device operating in acidic media: Advanced prototypes combined photonic design, transparent catalyst synthesis, and heterostructure band alignment of protective coatings, catalysts, and semiconductor tandem photoelectrodes to achieve record PEC STH efficiency. A still-standing world record for STH efficiency was achieved in 2018 by an integrated PEC solar-fuels generator functioning as a monolithic photocathode (**Figure 52**).[393] This test-bed prototype architecture exhibited significantly reduced surface reflectivity, minimizing parasitic light absorption and reflection losses. A tailored multifunctional crystalline titania interphase layer acted as a corrosion protection layer, with favorable band alignment between the semiconductor conduction band and the energy level for water reduction, facilitating electron transport at the cathode–electrolyte interface. It also provided a favorable substrate for adhesion of high-activity Rh catalyst nanoparticles. Under simulated AM 1.5G irradiation, STH efficiencies of 19.3 and 18.5% were obtained in acidic and neutral electrolytes, respectively. The system reached a value of 0.85 of the theoretical limit for PEC water splitting for the energy gap combination employed in the tandem-junction photoelectrode structure.

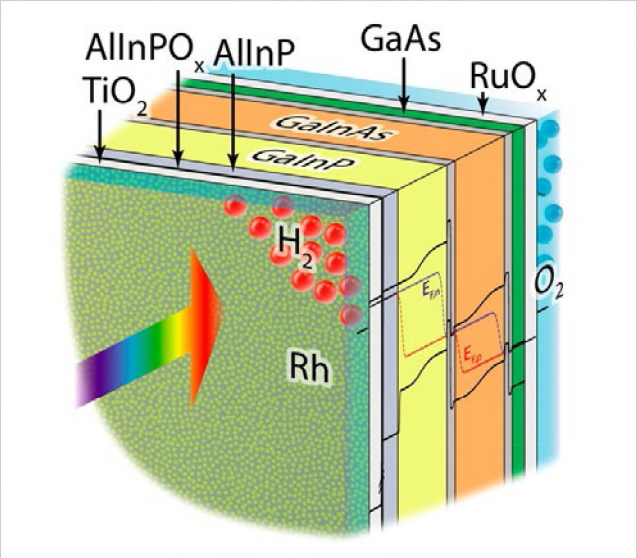

Figure 52. Schematic of a solar-fuels generator for photo-electrochemical water splitting with a > 19% solar-to-fuel efficiency.

>10% device operating in alkaline media: JCAP built an integrated device that exhibited an STH conversion efficiency, η_{STH}, of 10.5% in a 2-electrode cell configuration under 1 sun illumination, with stable performance for > 40 h of continuous operation (**Figure 53b**).[394] The tandem photoabsorbers were designed using a 1-D numerical simulator and were custom grown for efficient operation under AM 1.5 solar spectrum. The fully integrated prototype includes a tandem-junction GaAs/InGaP photoanode coated by an amorphous TiO_2 stabilization layer, Ni-based, earth-abundant active electrocatalysts for the hydrogen-evolution and OERs, and an AEM for product-gas separations (**Figure 53a**). The unassisted solar-driven water-splitting performance under 1 sun illumination was measured to be 8.6% in 1.0 M KOH(aq) without any external voltage bias. The prototype exhibited an average hydrogen and oxygen production rate of 0.81 μL s^{-1} and 0.41 μL s^{-1} (**Figure 53c**). The gas evolved from the cathode chamber and from the anode chamber showed minimal (<0.5%) product-gas crossover.

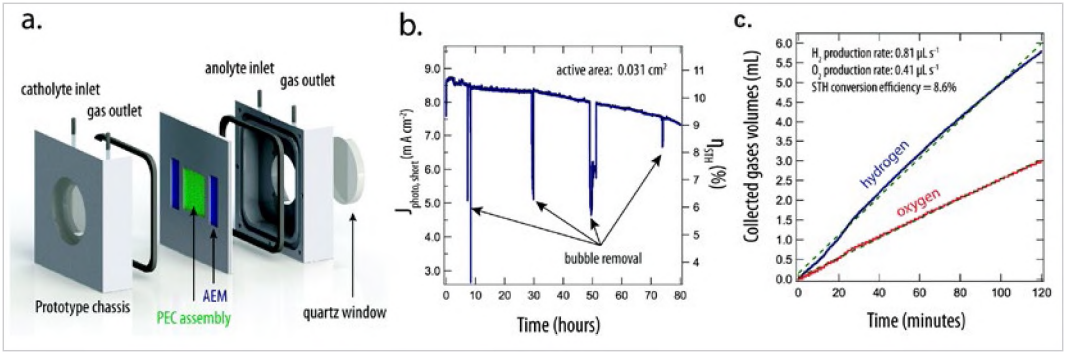

Figure 53. (a) Schematic illustration of a fully monolithically integrated intrinsically safe, solar-hydrogen system prototype. (b) The short-circuit photocurrent density, $J_{photo,\ short}$, and the corresponding STH conversion efficiency, η_{STH}, as a function of time in a two-electrode configuration (active area = 0.031 cm^2) under 1 sun illumination in 1.0 M KOH(aq). (c) Collected hydrogen and oxygen as a function of time for the integrated prototype (active area = 1.0 cm^2) under 1 sun illumination in 1.0 M KOH(aq).

>10% device with bipolar membrane: JCAP demonstrated unassisted solar-driven water splitting with an STH conversion efficiency of >10% in a 2-electrode integrated photoelectrosynthetic cell that incorporates a bipolar membrane.[395] A relatively large photoactive area of > 1 cm^2 was stabilized under 1 sun illumination for >100 hours of efficient (10%) and continuous operation with minimal decrease in the device efficiency. The bipolar membrane cell configuration enabled successful integration of a JCAP HER electrocatalyst that operates in 1.0 M H_2SO_4 (aq.) with a III-V photoanode-catalyst combination at near-neutral pH to provide an alternative approach to ensuring stable performance. The unassisted solar-driven water-splitting performance of the bipolar membrane-containing cell (CoP/H_2SO_4 (pH=0)/BPM/KBi (pH=9.3)/Ni/TiO_2/InGaP/GaAs) (**Figure 54**) Relative to a Nafion membrane, the bipolar membrane exhibited reduced

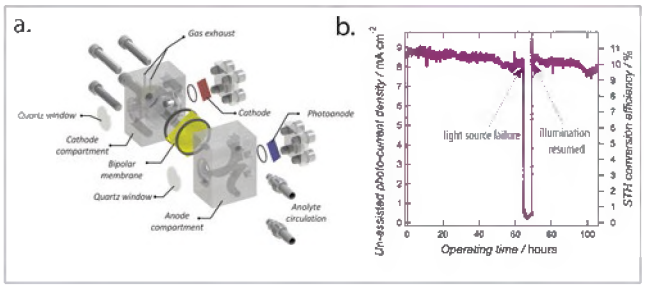

Figure 54. (a) A schematic illustration of the flow cell. (b) The photocurrent density and corresponding STH conversion efficiency, η_{STH}, observed during unassisted water splitting using a BPM-containing GaAs/InGaP/TiO_2/Ni cell in a two-electrode configuration incorporating a CoP/Ti mesh cathode and under 1 sun of simulated solar illumination from a halogen lamp. The light source failed after ~70 h of operation and illumination was resumed ~5 h later.

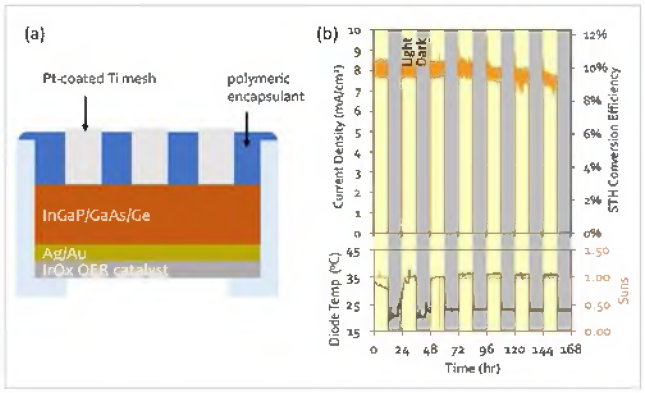

Figure 55. (a) Schematic of high efficiency photocathode device for solar water splitting. The Pt coated grid serves as an HER catalyst and is embedded in a transparent epoxy encapsulation coating with mechanical contact to the semiconductor; (b) Efficiency of device under diurnal cycling of the solar simulator illumination, 1 sun, AM 1.5G. The device area was 1 cm^2, in 1 M H_2SO_4 electrolyte, using a Nafion membrane for H_2 and O_2 product separation. The efficiency loss at the end of the week was due to loss of Pt catalyst.

permeability for both O_2(g) and H_2(g). At the relatively low operational current density of the membrane, ~ 4 mA cm^{-2}, a near-unity transference number for the H^+ and OH^- was observed in the bipolar membrane, and the pH gradient between the catholyte and anolyte was maintained for weeks under continuous operation.

>10% polymer-encapsulant device: JCAP designed a new device architecture that decouples fabrication of the catalyst layer from fabrication of the semiconductor electrode, and offers significant flexibility in selection of materials.[396] A typical device (**Figure 55a**) achieves efficiencies in the range of >10% using a laboratory solar simulator and membrane separator to ensure pure H_2 and O_2 product streams, and has demonstrated significantly higher efficiency in preliminary testing in natural sunlight. The current proof-of-concept device utilizes a commercial substrate and a Pt-coated mesh that is encapsulated in transparent epoxy coating. The epoxy coating is stable in 1 M base as well as 1 M acid electrolyte, and performs with similar efficiency under steady illumination and diurnal solar simulator cycling (**Figure 55b**).

Monolithic vapor-fed device: A fully monolithic PEC device architecture incorporating a III-V PV embedded in an ion-exchange membrane provides stable PEC hydrogen generation in multiple configurations. AM 1.5G solar illumination of this device in a vapor cathode/liquid anode format, where the anolyte is neutral-pH water, has an STH efficiency ranging from 12.6% to ca. 7% over a four-day period. The device design is significant as it allows incorporation of conventional, dark catalyst materials and supports an integrated PEC device. Incorporation of a shunt path between the PV and the cathode catalyst with potentiostat in series enables the direct measurement of real-time Faradaic yields. Using this device in a vapor cathode/vapor anode, where the anode vapor is from neutral-pH water, JCAP demonstrated integrated PEC devices displaying record stabilities and efficiencies (> 1,000 hours for H_2 evolution at 14% STH efficiency under 1 sun).[397-398]

Louvered prototype: The louvered design provides a robust platform for the further implementation of various types of improved PEC assemblies and can lead to an efficient, scalable, stable, and intrinsically safe solar-driven water-splitting system. JCAP demonstrated this device by constructing a fully integrated, acid-stable solar-driven water-splitting system comprised of WO_3/FTO/p^+n Si as the photoanode, Pt/TiO_2/Ti/n^+p Si as the photocathode, and Nafion as the membrane separator. It was designed, assembled, operated

in 1.0 M $HClO_4$, and evaluated for performance and safety characteristics under dual side illumination.[399] A hydrogen production rate of 0.17 mL hr^{-1} was observed in a full-cell configuration for > 20 h with minimal product crossover.

Microwire devices: One of JCAP's unique accomplishments was the development of n-p^+-Si/n-WO_3 and n-p^+-Si/n-TiO_2 core-shell microwire devices for solar water splitting in acidic and basic electrolytes.[376] Preparation of these complex structures required optimization and control of a series of processing techniques and tools. JCAP demonstrated an Si microwire-based tandem-junction device capable of unassisted solar water splitting under 1 sun illumination. In addition, the team tested the stability of the device for 24 h, showing *ca.* 10% degradation in 1 M KOH. With JCAP's newly developed protection methods, stable microwire devices provide a viable platform for development of more robust and efficient solar-fuels components.[314, 400-401] Unlike planar electrodes, bubble-producing microwire-array photocathodes can function without external convection, regardless of the orientation of the electrode.[402] Microwires can be tapered, demonstrating superior light-trapping properties with < 1% angular averaged reflection, and absorption reaching the $4n^2$ light-trapping limit due to enhanced coupling of incident light into waveguide modes.[403]

Recirculating device and pH gradient effect on operation: Controlled recirculating electrolyte streams between compartments were used to demonstrate self-regulating and pure solar-hydrogen generation from near-neutral pH electrolytes with solar-fuel efficiencies above 6.2%.[404] Stable operations for over 12 h were achieved without significant concentration differences between compartments or noticeable overpotential build-up. JCAP also built a fully integrated membrane-free solar-driven water-splitting system with an STH conversion efficiency of 3.2% at near-neutral pH.[378] The integrated system contained a triple-junction *a*-Si:H light absorber, Pt and Co-Pi electrocatalysts, and a 1.0 M boric acid buffer (pH 9.2). Analysis of the gas composition in the cathode and anode compartments showed high product-gas crossover, with 10% O_2(g) found in the cathode chamber and up to 40% H_2(g) measured in the anode chamber. Hence this system was not intrinsically safe, and constituted a significant explosion hazard during operation, producing flammable mixtures of H_2(g). Even though the bulk electrolyte was buffered, the local pH values near the electrodes were driven significantly toward alkaline or acidic conditions at steady state. This work served to establish the need for extreme pH to achieve high efficiency in a safe device.

Solar-hydrogen plant: JCAP developed a detailed physical description of a hypothetical 1 GW hydrogen plant (220,000 metric tons H_2/year) using a wired JCAP prototype design.[304] Materials requirements, initial primary energy requirements, and annual net energy balance for the full plant were built upon the initial device study[303] and estimated using lifecycle assessment methodologies. The focus was on the balance of system, which included structural supports, electrolyte, piping, storage, drying and compression, water transport and purification, land and road improvements, maintenance, panel replacement, and end-of-life decommissioning. Uncertainties were estimated for all key parameters and used to drive a Monte Carlo simulation to obtain sensitivities and ranges of the energy returned on energy invested (EROEI), net energy balance, and energy payback time. Key uncertainties were found to be the STH efficiency and panel lifetime. In the base case, the team found an EROEI of 1.7 and an energy payback time of approximately eight years. By moving to alternative structural designs and a thin-film device requiring simpler manufacturing methods, substantial reductions in energy invested were estimated,[305] resulting in an EROEI of 2.5 and an energy payback time of 3.9 years. These studies all point to the importance of ensuring high efficiency and a long lifetime for sustainable PEC hydrogen production.

Test Beds for CO_2 Reduction

The modeling and experimental studies demonstrated the importance of the local environment, including overpotential and how aqueous CO_2 is limiting in terms of mass transport and performance.[387] The latter is especially true, as it limits the operating window due to its acid/base reactions, which results in non-

Fickian diffusion profiles and lack of local equilibrium.[388] JCAP used test beds coupled to these models to explore the traditional aqueous planar cells, including mechanism and kinetic discovery. JCAP integrated materials discoveries into optimized aqueous test-bed prototypes to perform solar powered CO_2 conversion to hydrocarbons and oxygenates.

Photocathode-based planar aqueous unassisted CO_2 reduction device: A device based on JCAP-developed bimetallic catalysts[405] (Ag/Cu, Au/Cu) integrated with a photoabsorber was demonstrated to form a CO_2 reduction photocathode with over 60% FE to hydrocarbon and oxygenate products (mainly ethylene, ethanol, and propanol) for several days under diurnal simulated conditions.[406-407] In addition, a tandem, self-powered CO_2 reduction device was formed by coupling a Si photocathode with two series-connected semitransparent $CH_3NH_3PbI_3$ perovskite solar cells,[408] achieving a conversion efficiency of sunlight to hydrocarbons and oxygenates of 1.5% (3.5% for all products).[406]

Membraneless laminar-flow device: JCAP used multiscale models to evaluate and design a membraneless laminar-flow device.[409] Computational modeling showed that near-unity separation efficiencies were possible at achievable current densities via optimization of the spacing between the electrodes and the electrolyte flow rate. Laminar-flow reactor prototypes were fabricated with a range of channel widths by 3D printing and using CO_2 reduction to formic acid on Sn electrodes. Trends in product separation efficiency with channel width and flow rate qualitatively agreed with the model, but the separation efficiency was lower, with a maximum value of 90% achieved.

GDEs for CO_2 and COR: Beyond modeling, GDE test beds were fabricated for evaluation under both CO and CO_2 reduction. Current densities up to ~130 mA/cm^2 and total carbon product selectivity of up to ~75% using Cu as an electrocatalyst for COR was demonstrated.[410] This configuration was also used for operando XAS measurements.[23] Humidity had minimal impact on COR products. X-ray diffraction (XRD) patterns of deposited Cu-GDEs showed small amounts of Cu_2O while operando XANES measurements indicated Cu with a mixed oxidation state at open circuit voltage conditions. During bulk electrolysis, ethylene Faradaic yields decreased over time and corresponded to the reduction of the initial Cu-oxide phases to metallic Cu.

>19% unassisted solar-driven GDE CO_2 reduction device: JCAP reported an over 19% efficient unassisted solar-driven CO_2 reduction device using a GDE directly powered by a PV heterostructure. A GaInP/GaInAs/Ge triple-junction photoelectrode was used to power a reverse-assembled GDE employing an Ag nanoparticle catalyst layer. The prototype solar-fuels generator had a solar-to-CO energy conversion efficiency of 19.1% under simulated AM 1.5G illumination at 1 Sun.[411] The use of a reverse-assembled GDE prevented transition from a wetted to a flooded catalyst bed and allowed the device to operate stably for >150 h with no loss in efficiency. Outdoor measurements performed under ambient solar illumination in Pasadena, California, produced a peak solar-to-CO efficiency of 18.7% with a CO production rate of 47 mg-cm^{-2} per day and a diurnal-averaged solar-to-fuel conversion efficiency of 5.8%.

10% solar-to-formate CO_2 reduction device with a bipolar membrane: JCAP investigated in-depth the effects of the buffer capability of the solution on the local pH and CO_2 concentrations at the electrode surface under operating conditions and revealed that the total polarization loss and system efficiency is highly dependent on these local parameters. For example, such local values were simulated to explain the operational losses of a system using a bipolar membrane for solar-driven CO_2RR.[386] This solar-driven CO_2 device exhibited a solar-to-formate (STF) conversion efficiency of 10% under 1.0 sun illumination, which was the highest reported conversion efficiency for CO_2 reduction reported at that time. A tandem InGaP/GaAs/TiO_2/Ni photoanode operated in 1.0 M KOH for OER, while a Pd/C nanoparticles-coated Ti mesh cathode operated in 2.8 M $KHCO_3$ (aq., pH=8.0) for CO_2RR. The effective coupling between the two electrolytes with different pHs for CO_2R reaction and OER provided a new cell design space for efficient solar-fuel generation.

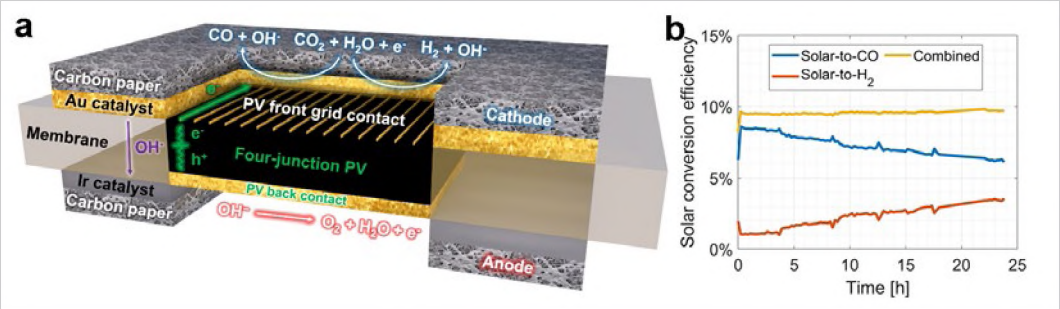

Figure 56. (a) Cross-section view of the device's active components, such as PV-integrated membrane and catalyst-coated carbon papers. (b) 24-hour durability test showing no overall efficiency degradation.

Monolithic PEC CO_2 reduction producing syngas at 10% efficiency: A 4 cm^2 monolithic, PEC device (**Figure 56**) exceeding 10% solar-to-fuel efficiency was demonstrated, representing a doubling in the reported peak efficiency for such devices.[412] The best performance was found through a systematic analysis of the operating conditions. Straightforward scale-up from 1 to 4 cm^2 was demonstrated. No overall efficiency degradation occurred during a 24-hour durability test. The changing product distribution over time was analyzed and solutions to stabilize the distribution were provided.

Direct capture and reduction of CO_2 from sea water: A direct coupled, proof-of-concept electrochemical system was demonstrated that used a bipolar membrane electrodialysis (BPMED) cell and a vapor-fed CO_2 reduction (CO_2R) cell to capture and convert CO_2 from oceanwater.[413] The BPMED cell replaced the commonly used water-splitting reaction with one-electron, reversible redox couples at the electrodes and demonstrated the ability to capture CO_2 at an electrochemical energy consumption of 0.98 kWh kg^{-1} of CO_2 and a CO_2 capture efficiency of 71%. The direct coupled, vapor-fed CO_2R cell yields a total FE of up to 95% for electrochemical CO_2 reduction to CO. The proof-of-concept system provides a unique technological pathway for CO_2 capture and conversion from oceanwater with only electrochemical processes.

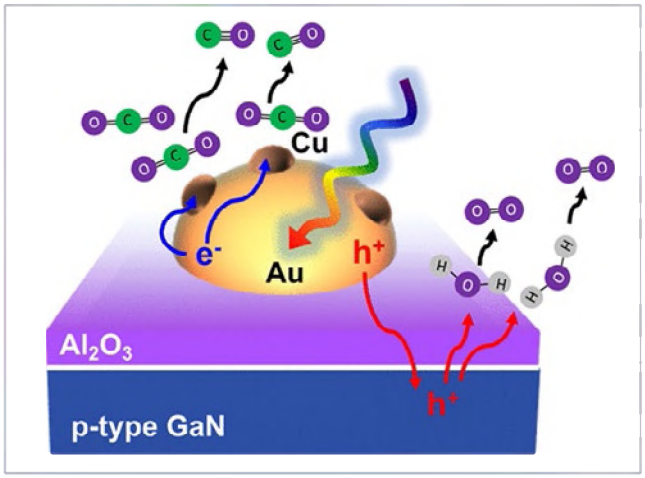

Figure 57. Schematic diagram of highly selective, unassisted CO_2 to CO reduction on plasmonic Au particles.

Unassisted highly selective gas-phase CO_2 reduction with a plasmonic Au/p-GaN photocatalyst: JCAP reported the first example of gas-phase photocatalytic CO_2 reduction to CO on plasmonic-metal/p-type semiconductor heterostructures (**Figure 57**) without applied bias or the presence of a sacrificial electron donor.[414] An interfacial layer of aluminum oxide (Al_2O_3) deposited between the plasmonic metal and the underlying p-type semiconductor significantly improved the interfacial separation of hot holes across the Au/p-GaN heterojunction, and further decorating Cu nanoparticles onto the Au surface accelerated the rate of CO_2 reduction. Overall, these plasmonic Au/p-GaN and Au–Cu/Al_2O_3/p-GaN heterostructures are capable of performing selective, unassisted, gas-phase photocatalytic CO_2 reduction to produce CO as the only detectable reduction product, balanced by water oxidation to yield O_2. The plasmonic metal (Au or Au–Cu) was identified as the locus of CO_2 reduction and the underlying p-GaN as the locus of water oxidation.

Table of Abbreviations

ALD	atomic layer deposition
ALS	Advanced Light Source
AP-XPS	ambient pressure X-ray photoelectron spectroscopy
AuNP	gold nanoparticle
BCP	block copolymers
BE	binding energy
BPMED	bipolar membrane electrodialysis
BTE	Boltzmann transport equation
COR	CO reduction
DEMS	differential electrochemical mass spectrometer
DFT	density-functional theory
DOE	Department of Energy
EDS	energy dispersive x-ray spectroscopy
EELS	electron energy loss spectroscopy
EMFT	embedded mean-field theory
EQCN	electrochemical quartz crystal nanobalance
EROEI	energy returned on energy invested
EXAFS	extended X-ray absorption fine structure
FE	Faradaic efficiency
FTIR	Fourier transform infrared spectroscopy
FTO	fluorine-doped tin oxide (F:SnO2)
GC	gas chromatography
GDE	gas-diffusion electrode
GI	grazing-incidence
GIXAS	grazing-incidence X-ray absorption spectroscopy
GIXRD	grazing-incidence X-ray diffraction
HDS	hydrodesulfurization
HER	hydrogen-evolution reaction
HPLC	high-performance liquid chromatography
HTE	high-throughput experimentation
IPCE	incident photon to current efficiency
JCAP	Joint Center for Artificial Photosynthesis
LDH	layered double (oxy)hydroxide
LEISS	low energy ion scattering spectroscopy
LPB	linearized Poisson–Boltzmann
MEA	membrane-electrode assembly
MOF	metal-organic framework
NAMD	nonadiabatic molecular dynamics
NCEM	National Center for Electron Microscopy
NERSC	National Energy Research Scientific Computing Center
NHC	N-heterocyclic carbenes
NMR	nuclear magnetic resonance
OD	oxide-derived
OEC	oxygen-evolving center
OER	oxygen-evolution reaction
ORR	oxygen reduction reaction
PACN	polyacrylonitrile
PDS	potential-determining step
PE	piezoelectric
PEC	photoelectrochemical
PIL	polymerized ionic liquids
PMI	pyridine monoimine
PMIRS	polarization-modulation infrared spectroscopy
PPO	poly(dimethylphenylene oxide)
PS	polystyrene
PV	photovoltaic
QM	quantum mechanical
RHE	reversible hydrogen electrode
RiXS	resonant inelastic X-ray scattering
SCE	spatial collection efficiency
SIMS	secondary ion mass spectrometry
SLAC	Stanford Linear Accelerator
SSRL	Stanford Synchrotron Radiation Lightsource
STEM	scanning transmission electron microscopy
STF	solar-to-formate
STH	solar-to-hydrogen
STM	scanning tunneling microscopy
STXM	scanning transmission X-ray microscopy
TA	transient absorption
THF	tetrahydrofuran
TMDC	transition metal dichalcogenide
TOF	turnover frequency
TRXPS	time-resolved X-ray photoemission spectroscopy
XANES	X-ray absorption near edge structure
XAS	X-ray absorption spectroscopy
XES	X-ray emission spectrometer
XPS	X-ray photoelectron spectroscopy
XRD	X-ray diffraction

Figure Credits

Title Page Image (circle). Image is reprinted with permission from *Angewandte Chemie Int. Edition*, Xiang et al., **2016**, 55, 12974–12988.

Credits Page Image. Photodriven generation of fuels. Credit: Reprinted with permission from Caltech/JCAP

Figure ES.1. JCAP's record of accomplishments. Credits: Clockwise from the bottom left, individual images credited to: CR Reprinted with permission from Caltech/JCAP; Image adapted from *Physical Chemistry Chemical Physics*, Hansen et al., **2016**, *18*, 9194–9201; CR Reprinted with permission from Caltech/JCAP; adapted from *Angewandte Chemie Int. Edition*, Xiang et al., **2016**, *55*, 12974–12988; adapted with permission from *ACS Energy Letters*, Zhou et al., **2016**, *1*, 764–770, Copyright 2021 American Chemical Society; adapted from Singh *Nat Commun* 10, 443 (2019); CR Reprinted with permission from Caltech/JCAP; adapted from *ACS Combinatorial Science*, Suram et al., **2017**, *19*, 37–46, Open access.

Figure 1. Reprinted with permission from *J. Am. Chem. Soc.* **2015**, *137*, 4347–4357. Copyright 2015 American Chemical Society.

Figure 2. Credits: (a) Caltech/JCAP original image. (b) Reprinted with permission from *J. Phys. Chem. C* 2016, 120, 4, 2247–2253. Copyright 2016 American Chemical Society. (c) Reprinted with permission from *J. Electrochem. Soc.* **165** J3350.

Figure 3. Reprinted with permission from *ACS Sustainable Chem. Eng.* **2019**, 7, 16964–16970. Copyright 2019 American Chemical Society.

Figure 4. Reprinted with permission from *J. Am. Chem. Soc.* **2015**, *137*, 6692–6698. Copyright 2015 American Chemical Society. This is an unofficial adaptation of an article that appeared in an ACS publication. ACS has not endorsed the content of this adaptation or the context of its use.

Figure 5. Reprinted with permission from *J. Am. Chem. Soc.* **2015**, *137*, 1305–1313. Copyright 2015 American Chemical Society.

Figure 6. Reprinted with permission from *J. Phys. Chem. C* **2015**, *119*, 7243–7254. Copyright 2015 American Chemical Society.

Figure 7. Reprinted with permission from *J. Phys. Chem. C* 2016, 120, 4, 2247–2253. Copyright 2016 American Chemical Society.

Figure 8. Reprinted with permission from *Chem Rev* **2019**, *119*, 7610–7672. Copyright 2019 American Chemical Society. This is an unofficial adaptation of an article that appeared in an ACS publication. ACS has not endorsed the content of this adaptation or the context of its use.

Figure 9. Reprinted with permission from *Langmuir* **2014**, *30*, 15053–15056. Copyright 2014 American Chemical Society.

Figure 10. Reprinted from *J. Electrochem. Soc.* **165** J3350.

Figure 11. Reprinted from *Angewandte Chemie International Edition* **2018**, *57*, 551–554.

Figure 12. Reprinted from *PNAS* **2021**, *118*, e2012649118.

Figure 13. Reprinted with permission from *ACS Catal.* **2018**, *8*, 7445–7454. Copyright 2018 American Chemical Society.

Figure 14. Reprinted with permission from *ACS Catal.* **2018**, *8*, 7445–7454. Copyright 2018 American Chemical Society.

Figure 15. Reprinted from *Nat Commun* **2019**, *10*, 32. https://doi.org/10.1038/s41467-018-07970-9.

Figure 16. Reprinted from *Nat Commun* **2019**, *10*, 1875. https://doi.org/10.1038/s41467-019-09846-y.

Figure 17. (a) Reprinted with permission from *ACS Catal.* **2018**, *8*, 1490–1499. Copyright 2018 American Chemical Society. (b) Reprinted with permission from *J. Am. Chem. Soc.* **2018**, *140*, 7012–7020. Copyright 2018 American Chemical Society.

Figure 18. Adapted from *Angew. Chem. Int. Ed.* **2019**, *58*, 16952.

Figure 19. Reprinted with permission from *J. Am. Chem. Soc.* **2019**, *141*, 7355–7364. Copyright 2019 American Chemical Society.

Figure 20. (a) Adapted with permission from *ACS Catal.* **2018**, *8*, 9596–9603. Copyright 2018 American Chemical Society. Adapted with permission from *ACS Catal.* **2018**, *8*, 1313–1324. Copyright 2018 American Chemical Society. (b) Reprinted with permission from *Chem. Mater.* **2019**, *31*, 1908–1919. Copyright 2019 American Chemical Society.

Figure 21. Reprinted with permission from *Nano Letters.* **2020**, *141*, 7355–7364. Copyright 2020 American Chemical Society.

Figure 22. Reprinted with permission from *J. Electroanal. Chem.* **2014**, *716*, 45–48.

Figure 23. Left: Reprinted with permission from *J. Phys. Chem. C* **2014**, *118*, *50*, 29294–29300. Copyright 2014 American Chemical Society.

Figure 24. Reproduced from *Energy Environ. Sci.*, **2014**, *7*, 682–688 with permission from the Royal Society of Chemistry and adapted from *Adv. Energy Mater.*, **2015**, *5*: 1402307. doi: 10.1002/aenm.201402307.

Figure 25. Figure is reprinted with permission from *Journal of Materials Research*, Shinde et al., 2015, 30, 442–450.

Figure 26. Reprinted with permission from *ACS Catal.* **2018,** *8*, 10938–10948. Copyright 2018 American Chemical Society.

Figure 27. Reprinted with permission from *Chem. Eur. J.*, **2015**, *21*: 8497–8503.

Figure 28. Left: Original art by Lum Yanwe Lum JCAP/LBNL. Right: Reproduced from *Energy Environ. Sci.*, **2018,** 11, 2935 with permission from the Royal Society of Chemistry.

Figure 29. Reproduced from *J. Mater. Chem. A* **2019**, *7*, 26785–26790 with permission from the Royal Society of Chemistry.

Figure 30. Reproduced from *J. Mater. Chem. A* **2019**, *7*, 26785–26790 with permission from the Royal Society of Chemistry.

Figure 31. Reprinted with permission from *ACS Appl. Energy Mater.* **2020**, *3*, 1286–1291. Copyright 2020 American Chemical Society.

Figure 32. Reproduced from *Rev. Sci. Inst.* **2015**, *86*, 013904, with permission of AIP Publishing.

Figure 33. Adapted with permission from *Adv. Energy Mater.* **2015**, *5*, 1401840.

Figure 34. Reprinted from *PNAS* **2017**, *114*, 3040–3043.

Figure 35. Reprinted with permission from *ACS Energy Lett.* **2017**, *2*, 2307–2312. Copyright 2017 American Chemical Society.

Figure 36. Reprinted with permission from *ACS Energy Lett.* **2018**, *3*, 2769–2774. Copyright 2018 American Chemical Society.

Figure 37. Reprinted with permission from *ACS Energy Lett.* **2020**, *5*, 1413–1421. Copyright 2020 American Chemical Society.

Figure 38. Reprinted with permission from *Nano Lett.* **2020**, *20*, 502–508. Copyright 2020 American Chemical Society.

Figure 39. Reproduced from *Nat Commun* **2019**, *10*, 443. https://doi.org/10.1038/s41467-019-08356-1.

Figure 40. Figure from *Science*, **2014**, *344 (6187)*, 1005–1009. Reprinted with permission from AAAS.

Figure 41. Figure from *Energy Environ. Sci.* **2015**, *8*, 203–207. Reprinted with permission from Royal Society of Chemistry.

Figure 42. Figures adapted with permission from *J. Am. Chem. Soc.* **2015**, *137*, 9595–9603. Copyright 2015 American Chemical Society.

Figure 43. Figure adapted with permission from *J. Am. Chem. Soc.* **2015**, *137*, 9595–9603. Copyright 2015 American Chemical Society.

Figure 44. Figure adapted with permission from Shinde et al., *ACS Appl. Mater. Interfaces* **2016**, *8*, 23696–23705. Copyright 2016 American Chemical Society.

Figure 45. Figure adapted with permission from Zhou et al., *ACS Appl. Energy Mater.* **2018**, *1*, 5766–5771. Copyright 2018 American Chemical Society.

Figure 46. Figure adapted with permission from *J. Phys. Chem. C* **2018**, *122*, 20642–20652. Copyright 2018 American Chemical Society.

Figure 47. (a) Figure adapted from Eichhorn, J., Kastl, C., Cooper, J.K. et al. *Nat Commun* 9, 2597 (**2018**). https://doi.org/10.1038/s41467-018-04856-8, via creative commons license http://creativecommons.org/licenses/by/4.0/. (b) Reproduced from *Sustainable Energy Fuels*, **2019**, *3*, 127–135 with permission from the Royal Society of Chemistry.

Figure 48. Credit: Used with permission from LBNL/JCAP by Nathaniel Lynd.

Figure 49. Adapted with permission from Soniat et al., *J Polym Sci* **2020**, *58*, 1207–1228.

Figure 50. Adapted with permission from Weng et al., *Energy Environ. Sci.* **2019**, *12*, 1950–1968 and Weng et al., *Phys.Chem.Chem.Phys.* **2018**, *20*, 16973.

Figure 51. Adapted with permission from Weng et al., *Energy Environ. Sci.* **2019**, *12*, 1950–1968.

Figure 52. *ACS Energy Lett.* **2018**, *3*, 1795–1800. Copyright 2018 American Chemical Society.

Figure 53. Adapted from *Energy & Environmental Science* **2015**, *8* (11), 3166–3172.

Figure 54. (a) Credit: Caltech/JCAP. (b) Adapted from *Adv. Energy Mater.* **2016**, 6: 1600379. doi: 10.1002/aenm.201600379.

Figure 55. Adapted from *Adv. Energy Mater.* **2017**, I DOI:10.1002/aenm.201602791.

Figure 56. Adapted from *Adv. Energy Mater.* **2021**, *11*, 2100070. https://doi.org/10.1002/aenm.202100070.

Figure 57. Reprinted with permission from *ACS Energy Lett.* **2021**, *6*, 1849–1856. Copyright 2021 American Chemical Society.

References

1. Grätzel, M., Artificial photosynthesis: water cleavage into hydrogen and oxygen by visible light. *Accounts of Chemical Research* **1981,** *14* (12), 376–384.

2. Bard, A. J.; Fox, M. A., Artificial Photosynthesis: Solar Splitting of Water to Hydrogen and Oxygen. *Accounts of Chemical Research* **1995,** *28* (3), 141–145.

3. Turner, J. A., Sustainable Hydrogen Production. *Science* **2004,** *305* (5686), 972–974.

4. Lewis, N. S.; Nocera, D. G., Powering the planet: Chemical challenges in solar energy utilization. *Proceedings of the National Academy of Sciences* **2006,** *103* (43), 15729–15735.

5. Lewis, N. S., Toward Cost-Effective Solar Energy Use. *Science* **2007,** *315* (5813), 798–801.

6. Crabtree, G. W.; Dresselhaus, M. S., The Hydrogen Fuel Alternative. *Materials Research Society Bulletin* **2008,** *33*, 421–428.

7. Gray, H. B., Powering the planet with solar fuel. *Nature Chemistry* **2009,** *1*, 7.

8. Cook, T. R.; Dogutan, D. K.; Reece, S. Y.; Surendranath, Y.; Teets, T. S.; Nocera, D. G., Solar Energy Supply and Storage for the Legacy and Nonlegacy Worlds. *Chemical Reviews* **2010,** *110* (11), 6474–6502.

9. Walter, M. G.; Warren, E. L.; McKone, J. R.; Boettcher, S. W.; Mi, Q.; Santori, E. A.; Lewis, N. S., Solar Water Splitting Cells. *Chemical Reviews* **2010,** *110* (11), 6446–6473.

10. Weber, M. F.; Dignam, M. J., Efficiency of Splitting Water with Semiconducting Photoelectrodes. *Journal of the Electrochemical Society* **1984,** *131* (6), 1258–1265.

11. Gorlin, Y.; Jaramillo, T. F., A Bifunctional Nonprecious Metal Catalyst for Oxygen Reduction and Water Oxidation. *Journal of the American Chemical Society* **2010,** *132* (39), 13612–13614.

12. McCrory, C. C. L.; Jung, S. H.; Peters, J. C.; Jaramillo, T. F., Benchmarking Heterogeneous Electrocatalysts for the Oxygen Evolution Reaction. *Journal of the American Chemical Society* **2013,** *135* (45), 16977–16987.

13. Yeston, J., Water-Splitting Standards. *Science* **2013,** *342* (6161), 911.

14. McCrory, C. C. L.; Jung, S.; Ferrer, I. M.; Chatman, S. M.; Peters, J. C.; Jaramillo, T. F., Benchmarking Hydrogen Evolving Reaction and Oxygen Evolving Reaction Electrocatalysts for Solar Water Splitting Devices. *Journal of the American Chemical Society* **2015,** *137* (13), 4347–4357.

15. Koper, M. T. M., Thermodynamic theory of multi-electron transfer reactions: Implications for electrocatalysis. *Journal of Electroanalytical Chemistry* **2011,** *660* (2), 254–260.

16. Jung, S.; McCrory, C. C. L.; Ferrer, I. M.; Peters, J. C.; Jaramillo, T. F., Benchmarking nanoparticulate metal oxide electrocatalysts for the alkaline water oxidation reaction. *Journal of Materials Chemistry A* **2015.**

17. Soriaga, M. P.; Baricuatro, J. H.; Cummins, K. D.; Kim, Y. G.; Saadi, F. H.; Sun, G. F.; McCrory, C. C. L.; McKone, J. R.; Velazquez, J. M.; Ferrer, I. M.; Carim, A. I.; Javier, A.; Chmielowiec, B.; Lacy, D. C.; Gregoire, J. M.; Sanabria-Chinchilla, J.; Amashukeli, X.; Royea, W. J.; Brunschwig, B. S.; Hemminger, J. C.; Lewis, N. S.; Stickney, J. L., Electrochemical surface science twenty years later: Expeditions into the electrocatalysis of reactions at the core of artificial photosynthesis. *Surface Science* **2015,** *631*, 285–294.

18. Soriaga, M. P.; Baricuatro, J. H.; Javier, A. C.; Kim, Y. G.; Cummins, K. D.; Tsang, C. F.; Hemminger, J. C.; Bui, N. N.; Stickney, J. L., Electrochemical Surface Science of CO_2 Reduction at Well-Defined Cu Electrodes: Surface Characterization by Emersion, Ex Situ, In Situ, and Operando Methods. In *Encyclopedia of Interfacial Chemistry*, Wandelt, K., Ed. Elsevier: Oxford, 2018; pp 562–576.

19. Tsang, C. F.; Javier, A. C.; Kim, Y.-G.; Baricuatro, J. H.; Cummins, K. D.; Kim, J.; Jerkiewicz, G.; Hemminger, J. C.; Soriaga, M. P., Potential-Dependent Adsorption of CO and Its Low-Overpotential Reduction to CH_3CH_2OH on Cu(511) Surface Reconstructed from Cu(pc): Operando Studies by Seriatim STM-EQCN-DEMS. *Journal of The Electrochemical Society* **2018,** *165* (15), J3350–J3354.

20. Baricuatro, J. H.; Kim, Y.-G.; Korzeniewski, C. L.; Soriaga, M. P., Seriatim ECSTM-ECPMIRS of the adsorption of carbon monoxide on Cu(100) in alkaline solution at CO_2-reduction potentials. *Electrochemistry Communications* **2018,** *91*, 1–4.

21. Javier, A.; Chmielowiec, B.; Sanabria-Chinchilla, J.; Kim, Y. G.; Baricuatro, J. H.; Soriaga, M. P., A DEMS Study of the Reduction of CO_2, CO, and HCHO Pre-Adsorbed on Cu Electrodes: Empirical Inferences on the CO_2RR Mechanism. *Electrocatalysis* **2015,** *6* (2), 127–131.

22. Favaro, M.; Jeong, B.; Ross, P. N.; Yano, J.; Hussain, Z.; Liu, Z.; Crumlin, E. J., Unravelling the electrochemical double layer by direct probing of the solid/liquid interface. *Nature Communications* **2016,** *7* (1), 12695.

23. Sullivan, I.; Han, L.; Lee, S. H.; Lin, M.; Larson, D. M.; Drisdell, W. S.; Xiang, C., A Hybrid Catalyst-Bonded Membrane Device for Electrochemical Carbon Monoxide Reduction at Different Relative Humidities. *ACS Sustainable Chemistry & Engineering* **2019,** *7* (20), 16964–16970.

24. Lee, S. H.; Sullivan, I.; Larson, D. M.; Liu, G.; Toma, F. M.; Xiang, C.; Drisdell, W. S., Correlating Oxidation State and Surface Area to Activity from Operando Studies of Copper CO Electroreduction Catalysts in a Gas-Fed Device. *ACS Catalysis* **2020,** *10* (14), 8000–8011.

25. Farmand, M.; Landers, A. T.; Lin, J. C.; Feaster, J. T.; Beeman, J. W.; Ye, Y.; Clark, E. L.; Higgins, D.; Yano, J.; Davis, R. C.; Mehta, A.; Jaramillo, T. F.; Hahn, C.; Drisdell, W. S., Electrochemical flow cell enabling operando probing of electrocatalyst surfaces by X-ray spectroscopy and diffraction. *Physical Chemistry Chemical Physics* **2019,** *21* (10), 5402–5408.

26. Lee, S. H.; Lin, J. C.; Farmand, M.; Landers, A. T.; Feaster, J. T.; Avilés Acosta, J. E.; Beeman, J. W.; Ye, Y.; Yano, J.; Mehta, A.; Davis, R. C.; Jaramillo, T. F.; Hahn, C.; Drisdell, W. S., Oxidation State and Surface Reconstruction of Cu under CO_2 Reduction Conditions from In Situ X-ray Characterization. *Journal of the American Chemical Society* **2021,** *143* (2), 588–592.

27. Gorlin, Y.; Lassalle-Kaiser, B.; Benck, J. D.; Gul, S.; Webb, S. M.; Yachandra, V. K.; Yano, J.; Jaramillo, T. F., In Situ X-ray Absorption Spectroscopy Investigation of a Bifunctional Manganese Oxide Catalyst with High Activity for Electrochemical Water Oxidation and Oxygen Reduction. *Journal of the American Chemical Society* **2013,** *135* (23), 8525–8534.

28. Gul, S.; Ng, J. W. D.; Alonso-Mori, R.; Kern, J.; Sokaras, D.; Anzenberg, E.; Lassalle-Kaiser, B.; Gorlin, Y.; Weng, T. C.; Zwart, P. H.; Zhang, J. Z.; Bergmann, U.; Yachandra, V. K.; Jaramillo, T. F.; Yano, J., Simultaneous detection of electronic structure changes from two elements of a bifunctional catalyst using wavelength-dispersive X-ray emission spectroscopy and in situ electrochemistry. *Physical Chemistry Chemical Physics* **2015,** *17* (14), 8901–8912.

29. Chen, S. Y.; Narang, P.; Atwater, H. A.; Wang, L. W., Phase Stability and Defect Physics of a Ternary ZnSnN2 Semiconductor: First Principles Insights. *Advanced Materials* **2014,** *26* (2), 311–315.

30. Narang, P.; Chen, S. Y.; Coronel, N. C.; Gul, S.; Yano, J.; Wang, L. W.; Lewis, N. S.; Atwater, H. A., Bandgap Tunability in Zn(Sn,Ge)N_2 Semiconductor Alloys. *Advanced Materials* **2014,** *26* (8), 1235–1241.

31. Cooper, J. K. G., S.; Toma, F. M.; Chen, L.; Glans, P. –A.; Guo, J.; Ager, J. W.; Yano, J.; Sharp, I. D. , Electronic Structure of Monoclinic $BiVO_4$. *Chem Mater* **2014,** *26*, 5365–5373.

32. Loiudice, A.; Ma, J.; Drisdell, W. S.; Mattox, T. M.; Cooper, J. K.; Thao, T.; Giannini, C.; Yano, J.; Wang, L. W.; Sharp, I. D.; Buonsanti, R., Bandgap Tunability in Sb-Alloyed $BiVO_4$ Quaternary Oxides as Visible Light Absorbers for Solar Fuel Applications. *Advanced Materials* **2015,** *27* (42), 6733.

33. Niu, K. Y.; Lin, F.; Jung, S.; Fang, L.; Nordlund, D.; McCrory, C. C. L.; Weng, T. C.; Ercius, P.; Doeff, M. M.; Zheng, H. M., Tuning Complex Transition Metal Hydroxide Nanostructures as Active Catalysts for Water Oxidation by a Laser-Chemical Route. *Nano Letters* **2015,** *15* (4), 2498–2503.

34. Woods-Robinson, R.; Cooper, J. K.; Xu, X. J.; Schelhas, L. T.; Pool, V. L.; Faghaninia, A.; Lo, C. S.; Toney, M. F.; Sharp, I. D.; Ager, J. W., P-Type Transparent Cu-Alloyed ZnS Deposited at Room Temperature. *Advanced Electronic Materials* **2016,** *2* (6), 10.1002/aelm.201500396.

35. Zhou, L.; Yan, Q.; Shinde, A.; Guevarra, D.; Newhouse, P. F.; Becerra-Stasiewicz, N.; Chatman, S. M.; Haber, J. A.; Neaton, J. B.; Gregoire, J. M., High Throughput Discovery of Solar Fuels Photoanodes in the CuO-V_2O_5 System. *Advanced Energy Materials* **2015,** *5* (22), 1500968.

36. Alayoglu, S.; An, K. J.; Melaet, G.; Chen, S. Y.; Bernardi, F.; Wang, L. W.; Lindeman, A. E.; Musselwhite, N.; Guo, J. H.; Liu, Z.; Marcus, M. A.; Somorjai, G. A., Pt-Mediated Reversible Reduction and Expansion of CeO_2 in Pt Nanoparticle/Mesoporous CeO_2 Catalyst: In Situ X-ray Spectroscopy and Diffraction Studies under Redox (H_2 and O_2) Atmospheres. *Journal of Physical Chemistry C* **2013,** *117* (50), 26608–26616.

37. Casalongue, H. G. S.; Ng, M. L.; Kaya, S.; Friebel, D.; Ogasawara, H.; Nilsson, A., In Situ Observation of Surface Species on Iridium Oxide Nanoparticles during the Oxygen Evolution Reaction. *Angewandte Chemie-International Edition* **2014,** *53* (28), 7169–7172.

38. Friebel, D.; Bajdich, M.; Yeo, B. S.; Louie, M. W.; Miller, D. J.; Casalongue, H. S.; Mbuga, F.; Weng, T. C.; Nordlund, D.; Sokaras, D.; Alonso-Mori, R.; Bell, A. T.; Nilsson, A., On the chemical state of Co oxide electrocatalysts during alkaline water splitting. *Physical Chemistry Chemical Physics* **2013,** *15*, 17460–17467.

39. Friebel, D.; Bajdich, M.; Yeo, B. S.; Louie, M. W.; Miller, D. J.; Casalongue, H. S.; Mbuga, F.; Weng, T. C.; Nordlund, D.; Sokaras, D.; Alonso-Mori, R.; Bell, A. T.; Nilsson, A., On the chemical state of Co oxide electrocatalysts during alkaline water splitting. *Physical Chemistry Chemical Physics* **2013,** *15* (40), 17460–17467.

40. Miller, D.; Casalongue, H. S.; Bluhm, H.; Ogasawara, H.; Nilsson, A.; Kaya, S., Different Reactivity of the Various Platinum Oxides and Chemisorbed Oxygen in CO Oxidation on Pt(111). *Journal of the American Chemical Society* **2014,** *136* (17), 6340–6347.

41. Miller, D. J.; Oberg, H.; Kaya, S.; Casalongue, H. S.; Friebel, D.; Anniyev, T.; Ogasawara, H.; Bluhm, H.; Pettersson, L. G. M.; Nilsson, A., Oxidation of Pt(111) under Near-Ambient Conditions. *Phys Rev Lett* **2011,** *107* (19).

42. Ali-Loytty, H.; Louie, M. W.; Singh, M. R.; Li, L.; Casalongue, H. G. S.; Ogasawara, H.; Crumlin, E. J.; Liu, Z.; Bell, A. T.; Nilsson, A.; Friebel, D., Ambient-Pressure XPS Study of a Ni-Fe Electrocatalyst for the Oxygen Evolution Reaction. *Journal of Physical Chemistry C* **2016,** *120* (4), 2247–2253.

43. Friebel, D.; Louie, M. W.; Bajdich, M.; Sanwald, K. E.; Cai, Y.; Wise, A. M.; Cheng, M. J.; Sokaras, D.; Weng, T. C.; Alonso-Mori, R.; Davis, R. C.; Bargar, J. R.; Norskov, J. K.; Nilsson, A.; Bell, A. T., Identification of Highly Active Fe Sites in (Ni,Fe)OOH for Electrocatalytic Water Splitting. *Journal of the American Chemical Society* **2015,** *137* (3), 1305–1313.

44. Malacrida, P.; Casalongue, H. G. S.; Masini, F.; Kaya, S.; Hernandez-Fernandez, P.; Deiana, D.; Ogasawara, H.; Stephens, I. E. L.; Nilsson, A.; Chorkendorff, I., Direct observation of the dealloying process of a platinum-yttrium nanoparticle fuel cell cathode and its oxygenated species during the oxygen reduction reaction. *Physical Chemistry Chemical Physics* **2015,** *17* (42), 28121–28128.

45. Ogasawara, H.; Kaya, S.; Nilsson, A., Operando X-Ray Photoelectron Spectroscopy Studies of Aqueous Electrocatalytic Systems. *Topics in Catalysis* **2016,** *59* (5), 439–447.

46. Van Allsburg, K. M.; Anzenberg, E.; Drisdell, W. S.; Yano, J.; Tilley, T. D., Oxygen-Atom Transfer Chemistry and Thermolytic Properties of a Di-tert-Butylphosphate-Ligated Mn_4O_4 Cubane. *Chem-Eur J* **2015,** *21* (12), 4646–4654.

47. Lichterman, M. F.; Hu, S.; Richter, M. H.; Crumlin, E.; Axnanda, S.; Favaro, M.; Drisdell, W. S.; Hussain, Z.; Mayer, T.; Brunschwig, B. S.; Lewis, N.; Liu, Z.; Lewerenz, H.-J., Direct Observation of the Energetics at a Semiconductor/Liquid Junction by Operando X-ray Photoelectron Spectroscopy. *Energy & Environmental Science* **2015,** *8* (8), 2409–2416.

48. Hu, S.; Richter, M. H.; Lichterman, M. F.; Beardslee, J. A.; Mayer, T.; Brunschwig, B. S.; Lewis, N. S., Electrical, Photoelectrochemical, and Photoelectron Spectroscopic Investigation of the Interfacial Transport and Energetics of Amorphous TiO_2/Si Heterojunctions. *The Journal of Physical Chemistry C* **2016,** *120* (6), 3117–3129.

49. Krawicz, A.; Yang, J. H.; Anzenberg, E.; Yano, J.; Sharp, I. D.; Moore, G. F., Photofunctional Construct That Interfaces Molecular Cobalt-Based Catalysts for H_2 Production to a Visible-Light-Absorbing Semiconductor. *Journal of the American Chemical Society* **2013,** *135* (32), 11861–11868.

50. Rivest, J. B.; Li, G.; Sharp, I. D.; Neaton, J. B.; Milliron, D. J., Phosphonic Acid Adsorbates Tune the Surface Potential of TiO_2 in Gas and Liquid Environments. *Journal of Physical Chemistry Letters* **2014,** *5* (14), 2450–2454.

51. Yang, J. H.; Walczak, K.; Anzenberg, E.; Toma, F. M.; Yuan, G. B.; Beeman, J.; Schwartzberg, A.; Lin, Y. J.; Hettick, M.; Javey, A.; Ager, J. W.; Yano, J.; Frei, H.; Sharp, I. D., Efficient and Sustained Photoelectrochemical Water Oxidation by Cobalt Oxide/Silicon Photoanodes with Nanotextured Interfaces. *Journal of the American Chemical Society* **2014,** *136* (17), 6191–6194.

52. Suseno, S.; McCrory, C. C. L.; Tran, R.; Gul, S.; Yano, J.; Agapie, T., Molecular Mixed-Metal Manganese Oxido Cubanes as Precursors to Heterogeneous Oxygen Evolution Catalysts. *Chem-Eur J* **2015,** *21* (38), 13420–13430.

53. You, B.; Jiang, N.; Sheng, M. L.; Drisdell, W. S.; Yano, J.; Sun, Y. J., Bimetal-Organic Framework Self-Adjusted Synthesis of Support-Free Nonprecious Electrocatalysts for Efficient Oxygen Reduction. *Acs Catalysis* **2015,** *5* (12), 7068–7076.

54. Hoarfrost, M. L.; Segalman, R. A., Conductivity Scaling Relationships for Nanostructured Block Copolymer/Ionic Liquid Membranes. *Acs Macro Letters* **2012,** *1* (8), 937–943.

55. Kusoglu, A.; Modestino, M. A.; Hexemer, A.; Segalman, R. A.; Weber, A. Z., Subsecond Morphological Changes in Nafion during Water Uptake Detected by Small-Angle X-ray Scattering. *Acs Macro Letters* **2012,** *1* (1), 33–36.

56. Modestino, M. A.; Kusoglu, A.; Hexemer, A.; Weber, A. Z.; Segalman, R. A., Controlling Nafion Structure and Properties via Wetting Interactions. *Macromolecules* **2012,** *45* (11), 4681–4688.

57. Modestino, M. A.; Paul, D. K.; Dishari, S.; Petrina, S. A.; Allen, F. I.; Hickner, M. A.; Karan, K.; Segalman, R. A.; Weber, A. Z., Self-Assembly and Transport Limitations in Confined Nafion Films. *Macromolecules* **2013,** *46* (3), 867–873.

58. Schneider, Y.; Modestino, M. A.; McCulloch, B. L.; Hoarfrost, M. L.; Hess, R. W.; Segalman, R. A., Ionic Conduction in Nanostructured Membranes Based on Polymerized Protic Ionic Liquids. *Macromolecules* **2013,** *46* (4), 1543–1548.

59. Cho, E. S.; Evans, C. M.; Davidson, E. C.; Hoarfrost, M. L.; Modestino, M. A.; Segalman, R. A.; Urban, J. J., Enhanced Water Vapor Blocking in Transparent Hybrid Polymer-Nanocrystal Films. *Acs Macro Letters* **2015,** *4* (1), 70–74.

60. Evans, C. M.; Singh, M. R.; Lynd, N. A.; Segalman, R. A., Improving the Gas Barrier Properties of Nafion via Thermal Annealing: Evidence for Diffusion through Hydrophilic Channels and Matrix. *Macromolecules* **2015,** *48* (10), 3303–3309.

61. Jiang, Y. V.; Freyer, J. L.; Cotanda, P.; Brucks, S. D.; Killops, K. L.; Bandar, J. S.; Torsitano, C.; Balsara, N. P.; Lambert, T. H.; Campos, L. M., The evolution of cyclopropenium ions into functional polyelectrolytes. *Nature Communications* **2015,** *6*, 5950.

62. Petzetakis, N.; Doherty, C. M.; Thornton, A. W.; Chen, X. C.; Cotanda, P.; Hill, A. J.; Balsara, N. P., Membranes with artificial free-volume for biofuel production. *Nature Communications* **2015,** *6*.

63. Sanoja, G. E. P., B. C.; Beckingham, B. S.; Evans, C. M.; Lynd, N. A.; Segalman, R. A., Structure–Conductivity Relationships of Block Copolymer Membranes Based on Hydrated Protic Polymerized Ionic Liquids: Effect of Domain Spacing. *Macromolecules* **2016,** *49*, 2216–2223.

64. Gregoire, J. M.; Van Campen, D. G.; Miller, C. E.; Jones, R. J. R.; Suram, S. K.; Mehta, A., High-throughput synchrotron X-ray diffraction for combinatorial phase mapping. *J Synchrotron Radiat* **2014,** *21*, 1262–1268.

65. Battaglia, C.; Yin, X. T.; Zheng, M.; Sharp, I. D.; Chen, T.; McDonnell, S.; Azcatl, A.; Carraro, C.; Ma, B. W.; Maboudian, R.; Wallace, R. M.; Javey, A., Hole Selective MoO_x Contact for Silicon Solar Cells. *Nano Letters* **2014,** *14* (2), 967–971.

66. Bullock, J. H., M.; Geissbuhler, J.; Ong, A. J.; Allen, T.; Sutter-Fella, C.M.; Chen, T.; Ota, H.; Schaler, E.W.; DeWolf, S.; Ballif, C.; Cuevas, A.; Javey, A., Efficient silicon solar cells with dopant-free asymmetric heterocontacts. *Nature Energy* **2016,** *DOI: 10.1038/NENERGY.2015.31.*

67. Hettick, M.; Zheng, M.; Lin, Y. J.; Sutter-Fella, C. M.; Ager, J. W.; Javey, A., Nonepitaxial Thin-Film InP for Scalable and Efficient Photocathodes. *Journal of Physical Chemistry Letters* **2015,** *6* (12), 2177–2182.

68. Li, Y. B.; Cooper, J. K.; Buonsanti, R.; Giannini, C.; Liu, Y.; Toma, F. M.; Sharp, I. D., Fabrication of Planar Heterojunction Perovskite Solar Cells by Controlled Low-Pressure Vapor Annealing. *Journal of Physical Chemistry Letters* **2015,** *6* (3), 493–499.

69. Sutter-Fella, C. M.; Li, Y.; Amani, M.; Ager, J. W.; Toma, F. M.; Yablonovitch, E.; Sharp, I. D.; Javey, A., High Photoluminescence Quantum Yield in Band Gap Tunable Bromide Containing Mixed Halide Perovskites. *Nano Letters* **2016,** *16* (1), 800–6.

70. Williams, T. E.; Chang, C. M.; Rosen, E. L.; Garcia, G.; Runnerstrom, E. L.; Williams, B. L.; Koo, B.; Buonsanti, R.; Milliron, D. J.; Helms, B. A., NIR-Selective electrochromic heteromaterial frameworks: a platform to understand mesoscale transport phenomena in solid-state electrochemical devices. *Journal of Materials Chemistry C* **2014,** *2* (17), 3328–3335.

71. Cai, S. L.; Zhang, Y. B.; Pun, A. B.; He, B.; Yang, J. H.; Toma, F. M.; Sharp, I. D.; Yaghi, O. M.; Fan, J.; Zheng, S. R.; Zhang, W. G.; Liu, Y., Tunable electrical conductivity in oriented thin films of tetrathiafulvalene-based covalent organic framework. *Chem Sci* **2014,** *5* (12), 4693–4700.

72. Edri, E.; Frei, H., Charge Transport through Organic Molecular Wires Embedded in Ultrathin Insulating Inorganic Layer. *Journal of Physical Chemistry C* **2015,** *119* (51), 28326–28334.

73. Helms, B. A.; Williams, T. E.; Buonsanti, R.; Milliron, D. J., Colloidal Nanocrystal Frameworks. *Advanced Materials* **2015,** *27* (38), 5820–5829.

74. Kiriya, D.; Zhou, Y. Z.; Nelson, C.; Hettick, M.; Madhvapathy, S. R.; Chen, K.; Zhao, P. D.; Tosun, M.; Minor, A. M.; Chrzan, D. C.; Javey, A., Oriented Growth of Gold Nanowires on MoS_2. *Adv Funct Mater* **2015,** *25* (39), 6257–6264.

75. Kisielowski, C.; Wang, L. W.; Specht, P.; Calderon, H. A.; Barton, B.; Jiang, B.; Kang, J. H.; Cieslinski, R., Real-time sub-Angstrom imaging of reversible and irreversible conformations in rhodium catalysts and graphene. *Phys Rev B* **2013,** *88* (2).

76. Helveg, S.; Kisielowski, C. F.; Jinschek, J. R.; Specht, P.; Yuan, G.; Frei, H., Observing gas-catalyst dynamics at atomic resolution and single-atom sensitivity. *Micron* **2015,** *68*, 176–185.

77. Kisielowski, C.; Specht, P.; Gygax, S. M.; Barton, B.; Calderon, H. A.; Kang, J. H.; Cieslinski, R., Instrumental requirements for the detection of electron beam-induced object excitations at the single atom level in high-resolution transmission electron microscopy. *Micron* **2015,** *68*, 186–193.

78. Van Dyck, D.; Lobato, I.; Chen, F. R.; Kisielowski, C., Do you believe that atoms stay in place when you observe them in HREM? *Micron* **2015,** *68*, 158–163.

79. Zhu, Y. Y.; Ramasse, Q. M.; Brorson, M.; Moses, P. G.; Hansen, L. P.; Kisielowski, C. F.; Helveg, S., Visualizing the Stoichiometry of Industrial-Style Co-Mo-S Catalysts with Single-Atom Sensitivity. *Angewandte Chemie-International Edition* **2014,** *53* (40), 10723–10727.

80. Kisielowski, C.; Wang, L. W.; Specht, P.; Calderon, H. A.; Barton, B.; Jiang, B.; Kang, J. H.; Cieslinski, R., Real-time sub-Angstrom imaging of reversible and irreversible conformations in rhodium catalysts and graphene. *Physical Review B* **2013,** *88* (2), 12.

81. Cedeno, D.; Krawicz, A.; Doak, P.; Yu, M.; Neaton, J. B.; Moore, G. F., Using Molecular Design to Control the Performance of Hydrogen-Producing Polymer-Brush-Modified Photocathodes. *Journal of Physical Chemistry Letters* **2014,** *5* (18), 3222–3226.

82. Chen, L.; Yang, J. H.; Klaus, S.; Lee, L. J.; Woods-Robinson, R.; Ma, J.; Lum, Y.; Cooper, J. K.; Toma, F. M.; Wang, L. W.; Sharp, I. D.; Bell, A. T.; Ager, J. W., p-Type Transparent Conducting Oxide/n-Type Semiconductor Heterojunctions for Efficient and Stable Solar Water Oxidation. *Journal of the American Chemical Society* **2015,** *137* (30), 9595–9603.

83. Eaton, S. W.; Lai, M. L.; Gibson, N. A.; Wong, A. B.; Dou, L. T.; Ma, J.; Wang, L. W.; Leone, S. R.; Yang, P. D., Lasing in robust cesium lead halide perovskite nanowires. *P Natl Acad Sci USA* **2016,** *113* (8), 1993–1998.

84. Loiudice, A.; Cooper, J. K.; Hess, L. H.; Mattox, T. M.; Sharp, I. D.; Buonsanti, R., Assembly and Photocarrier Dynamics of Heterostructured Nanocomposite Photoanodes from Multicomponent Colloidal Nanocrystals. *Nano Letters* **2015,** *15* (11), 7347–7354.

85. Lynch, J.; Giannini, C.; Cooper, J. K.; Loiudice, A.; Sharp, I. D.; Buonsanti, R., Substitutional or Interstitial Site-Selective Nitrogen Doping in TiO_2 Nanostructures. *Journal of Physical Chemistry C* **2015,** *119* (13), 7443–7452.

86. Sun, J. W.; Cui, F.; Kisielowski, C.; Yu, Y.; Kornienko, N.; Yang, P. D., Low-Temperature Solution-Phase Growth of Silicon and Silicon Containing Alloy Nanowires. *Journal of Physical Chemistry C* **2016,** *120* (37), 20525–20529.

87. Ugeda, M. M.; Yu, M.; Bradley, A. J.; Doak, P.; Liu, W. J.; Moore, G. F.; Sharp, I. D.; Tilley, T. D.; Neaton, J. B.; Crommie, M. F., Adsorption and Stability of pi-Bonded Ethylene on GaP(110). *Journal of Physical Chemistry C* **2013,** *117* (49), 26091–26096.

88. Yu, M.; Doak, P.; Tamblyn, I.; Neaton, J. B., Theory of Covalent Adsorbate Frontier Orbital Energies on Functionalized Light-Absorbing Semiconductor Surfaces. *Journal of Physical Chemistry Letters* **2013,** *4* (10), 1701–1706.

89. Yan, Q. M.; Li, G.; Newhouse, P. F.; Yu, J.; Persson, K. A.; Gregoire, J. M.; Neaton, J. B., $Mn_2V_2O_7$: An Earth Abundant Light Absorber for Solar Water Splitting. *Advanced Energy Materials* **2015,** *5* (8), 6.

90. Baker, L. R.; Kennedy, G.; Van Spronsen, M.; Hervier, A.; Cai, X. J.; Chen, S. Y.; Wang, L. W.; Somorjai, G. A., Furfuraldehyde Hydrogenation on Titanium Oxide-Supported Platinum Nanoparticles Studied by Sum Frequency Generation Vibrational Spectroscopy: Acid-Base Catalysis Explains the Molecular Origin of Strong Metal-Support Interactions. *Journal of the American Chemical Society* **2012,** *134* (34), 14208–14216.

91. Xiao, H.; Cheng, T.; Goddard, W. A.; Sundararaman, R., Mechanistic Explanation of the pH Dependence and Onset Potentials for Hydrocarbon Products from Electrochemical Reduction of CO on Cu (111). *Journal of the American Chemical Society* **2016,** *138* (2), 483–486.

92. Bajdich, M.; Garcia-Mota, M.; Vojvodic, A.; Norskov, J. K.; Bell, A. T., Theoretical Investigation of the Activity of Cobalt Oxides for the Electrochemical Oxidation of Water. *Journal of the American Chemical Society* **2013,** *135* (36), 13521–13530.

93. Garcia-Mota, M.; Bajdich, M.; Viswanathan, V.; Vojvodic, A.; Bell, A. T.; Norskov, J. K., Importance of Correlation in Determining Electrocatalytic Oxygen Evolution Activity on Cobalt Oxides. *Journal of Physical Chemistry C* **2012,** *116* (39), 21077–21082.

94. Lucht, K. P.; Mendoza-Cortes, J. L., Birnessite: A Layered Manganese Oxide To Capture Sunlight for Water-Splitting Catalysis. *Journal of Physical Chemistry C* **2015,** *119* (40), 22838–22846.

95. Chen, S. Y.; Wang, L. W., Intrinsic defects and electronic conductivity of TaON: First-principles insights. *Appl Phys Lett* **2011,** *99* (22).

96. Chen, S. Y.; Wang, L. W., Thermodynamic Oxidation and Reduction Potentials of Photocatalytic Semiconductors in Aqueous Solution. *Chem Mater* **2012,** *24* (18), 3659–3666.

97. Wang, W. C.; Chen, S. Y.; Yang, J. H.; Lang, L.; Xiang, H. J.; Gong, X. G.; Walsh, A.; Wei, S. H., Design of I-2-II-IV-VI4 Semiconductors through Element Substitution: The Thermodynamic Stability Limit and Chemical Trend. *Chem Mater* **2014,** *26* (11), 3411–3417.

98. Wang, W. C.; Chen, S. Y.; Yang, P. X.; Duan, C. G.; Wang, L. W., Si:WO_3 heterostructure for Z-scheme water splitting: an ab initio study. *Journal of Materials Chemistry A* **2013,** *1* (4), 1078–1085.

99. Diamond, A. M.; Corbellini, L.; Balasubramaniam, K. R.; Chen, S. Y.; Wang, S. Z.; Matthews, T. S.; Wang, L. W.; Ramesh, R.; Ager, J. W., Copper-alloyed ZnS as a p-type transparent conducting material. *Phys. Status Solidi A-Appl. Mat.* **2012,** *209* (11), 2101–2107.

100. Fan, F. J.; Wu, L.; Gong, M.; Liu, G. Y.; Wang, Y. X.; Yu, S. H.; Chen, S. Y.; Wang, L. W.; Gong, X. G., Composition- and Band-Gap-Tunable Synthesis of Wurtzite-Derived $Cu_2ZnSn(S_{1-x}S_{ex})(4)$ Nanocrystals: Theoretical and Experimental Insights. *Acs Nano* **2013,** *7* (2), 1454–1463.

101. Chen, S. Y.; Wang, L. W.; Walsh, A.; Gong, X. G.; Wei, S. H., Abundance of Cu-Zn + Sn-Zn and 2Cu(Zn) + Sn-Zn defect clusters in kesterite solar cells. *Appl Phys Lett* **2012,** *101* (22).

102. Chen, S. Y.; Wang, L. W., Double-hole-induced oxygen dimerization in transition metal oxides. *Phys Rev B* **2014,** *89* (1).

103. Ma, J.; Wang, L. W., The role of the isolated 6s states in $BiVO_4$ on the electronic and atomic structures. *Appl Phys Lett* **2014,** *105* (17).

104. Ping, Y.; Sundararaman, R.; Goddard III, W. A., Solvation effects on the band edge positions of photocatalysts from first principles. *Physical Chemistry Chemical Physics* **2015,** *17*, 30499–30509.

105. Pham, H. H.; Wang, L. W., Oxygen vacancy and hole conduction in amorphous TiO_2. *Physical Chemistry Chemical Physics* **2015,** *17* (1), 541–550.

106. Hu, S.; Chi, C. Y.; Fountaine, K. T.; Yao, M. Q.; Atwater, H. A.; Dapkus, P. D.; Lewis, N. S.; Zhou, C. W., Optical, electrical, and solar energy-conversion properties of gallium arsenide nanowire-array photoanodes. *Energy & Environmental Science* **2013,** *6* (6), 1879–1890.

107. Pham, H. H.; Barkema, G. T.; Wang, L. W., DFT plus U studies of Cu doping and p-type compensation in crystalline and amorphous ZnS. *Physical Chemistry Chemical Physics* **2015,** *17* (39), 26270–26276.

108. Pham, H. H.; Wang, L. W., Electronic structures and current conductivities of B, C, N and F defects in amorphous titanium dioxide. *Physical Chemistry Chemical Physics* **2015,** *17* (17), 11908–11913.

109. Ma, J.; Wang, Z.; Wang, L. W., Interplay between plasmon and single-particle excitations in a metal nanocluster. *Nature Communications* **2015,** *6*, 10107.

110. Gauthier, J. A.; Ringe, S.; Dickens, C. F.; Garza, A. J.; Bell, A. T.; Head-Gordon, M.; Nørskov, J. K.; Chan, K., Challenges in Modeling Electrochemical Reaction Energetics with Polarizable Continuum Models. *ACS Catalysis* **2019,** *9* (2), 920–931.

111. Zheng, F.; Wang, L.-w., Exploring non-adiabaticity to CO reduction reaction through ab initio molecular dynamics simulation. *APL Materials* **2020,** *8* (4), 041115.

112. Huang, Y.; Chen, Y.; Cheng, T.; Wang, L.-W.; Goddard, W. A., Identification of the Selective Sites for Electrochemical Reduction of CO to C2+ Products on Copper Nanoparticles by Combining Reactive Force Fields, Density Functional Theory, and Machine Learning. *ACS Energy Letters* **2018,** *3* (12), 2983–2988.

113. Zhang, H.; Goddard, W. A.; Lu, Q.; Cheng, M.-J., The importance of grand-canonical quantum mechanical methods to describe the effect of electrode potential on the stability of intermediates involved in both electrochemical CO_2 reduction and hydrogen evolution. *Physical Chemistry Chemical Physics* **2018,** *20* (4), 2549–2557.

114. Baricuatro, J. H.; Kwon, S.; Kim, Y.-G.; Cummins, K. D.; Naserifar, S.; Goddard, W. A., Operando Electrochemical Spectroscopy for CO on Cu(100) at pH 1 to 13: Validation of Grand Canonical Potential Predictions. *ACS Catalysis* **2021,** *11* (5), 3173–3181.

115. Welborn, M.; Manby, F. R.; Miller, T. F., Even-handed subsystem selection in projection-based embedding. *The Journal of Chemical Physics* **2018,** *149* (14), 144101.

116. Lee, S. J. R.; Welborn, M.; Manby, F. R.; Miller, T. F., Projection-Based Wavefunction-in-DFT Embedding. *Accounts of Chemical Research* **2019,** *52* (5), 1359–1368.

117. Casalongue, H. G. S.; Benck, J. D.; Tsai, C.; Karlsson, R. K. B.; Kaya, S.; Ng, M. L.; Pettersson, L. G. M.; Abild-Pedersen, F.; Norskov, J. K.; Ogasawara, H.; Jaramillo, T. F.; Nilsson, A., Operando Characterization of an Amorphous Molybdenum Sulfide Nanoparticle Catalyst during the Hydrogen Evolution Reaction. *Journal of Physical Chemistry C* **2014,** *118* (50), 29252–29259.

118. Huang, Y.; Nielsen, R. J.; Goddard Iii, W. A.; Soriaga, M. P., The Reaction Mechanism with Free Energy Barriers for Electrochemical Dihydrogen Evolution on MoS_2. *Journal of the American Chemical Society* **2015.**

119. Li, Y. P.; Yu, Y. F.; Huang, Y. F.; Nielsen, R. A.; Goddard, W. A.; Li, Y.; Cao, L. Y., Engineering the Composition and Crystallinity of Molybdenum Sulfide for High-Performance Electrocatalytic Hydrogen Evolution. *Acs Catalysis* **2015,** *5* (1), 448–455.

120. Yeo, B. S.; Bell, A. T., In Situ Raman Study of Nickel Oxide and Gold-Supported Nickel Oxide Catalysts for the Electrochemical Evolution of Oxygen. *Journal of Physical Chemistry C* **2012,** *116*, 8394–8400.

121. Louie, M. W.; Bell, A. T., An Investigation of Thin-Film Ni-Fe Oxide Catalysts for the Electrochemical Evolution of Oxygen. *Journal of the American Chemical Society* **2013,** *135*, 12329–12337.

122. Klaus, S.; Cai, Y.; Louie, M. W.; Trotochaud, L.; Bell, A. T., Effects of Fe Electrolyte Impurities on Ni(OH)(2)/NiOOH Structure and Oxygen Evolution Activity. *Journal of Physical Chemistry C* **2015,** *119* (13), 7243–7254.

123. Klaus, S.; Trotochaud, L.; Cheng, M.-J.; Head-Gordon, M.; Bell, A. T., Experimental and Computational Evidence of Highly Active Fe Impurity Sites on the Surface of Oxidized Au for the Electrocatalytic Oxidation of Water in Basic Media. *ChemElectroChem* **2016,** *3* (1), 66–73.

124. Swierk, J. R.; Klaus, S.; Trotochaud, L.; Bell, A. T.; Tilley, T. D., An Electrochemical Study of the Energetics of the Oxygen Evolution Reaction at Nickel Iron (oxy)hydroxide Catalysts. *The Journal of Physical Chemistry C* **2015,** *119* (33), 19022–19029.

125. Klaus, S.; Louie, M. W.; Trotochaud, L.; Bell, A. T., Role of Catalyst Preparation on the Electrocatalytic Activity of $Ni_{1-x}F_{ex}OOH$ for the Oxygen Evolution Reaction. *The Journal of Physical Chemistry C* **2015,** *119* (32), 18303–18316.

126. Ali-Löytty, H.; Louie, M. W.; Singh, M. R.; Li, L.; Sanchez Casalongue, H. G.; Ogasawara, H.; Crumlin, E. J.; Liu, Z.; Bell, A. T.; Nilsson, A.; Friebel, D., Ambient-Pressure XPS Study of a Ni–Fe Electrocatalyst for the Oxygen Evolution Reaction. *The Journal of Physical Chemistry C* **2016,** *120* (4), 2247–2253.

127. Ping, Y.; Galli, G.; Goddard, W. A., Electronic Structure of IrO_2: The Role of the Metal d Orbitals. *Journal of Physical Chemistry C* **2015,** *119* (21), 11570–11577.

128. Ping, Y.; Goddard, W. A.; Galli, G. A., Energetics and Solvation Effects at the Photoanode/Catalyst Interface: Ohmic Contact versus Schottky Barrier. *Journal of the American Chemical Society* **2015,** *137* (16), 5264–5267.

129. Nitopi, S.; Bertheussen, E.; Scott, S. B.; Liu, X.; Engstfeld, A. K.; Horch, S.; Seger, B.; Stephens, I. E. L.; Chan, K.; Hahn, C.; Nørskov, J. K.; Jaramillo, T. F.; Chorkendorff, I., Progress and Perspectives of Electrochemical CO_2 Reduction on Copper in Aqueous Electrolyte. *Chemical Reviews* **2019,** *119* (12), 7610–7672.

130. Greenblatt, J. B.; Miller, D. J.; Ager, J. W.; Houle, F. A.; Sharp, I. D., The Technical and Energetic Challenges of Separating (Photo)Electrochemical Carbon Dioxide Reduction Products. *Joule* **2018,** *2* (3), 381–420.

131. Kim, Y.-G.; Baricuatro, J. H.; Javier, A.; Gregoire, J. M.; Soriaga, M. P., The Evolution of the Polycrystalline Copper Surface, First to Cu(111) and Then to Cu(100), at a Fixed CO_2RR Potential: A Study by Operando EC-STM. *Langmuir* **2014,** *30* (50), 15053–15056.

132. Kim, Y.-G.; Javier, A.; Baricuatro, J. H.; Torelli, D.; Cummins, K. D.; Tsang, C. F.; Hemminger, J. C.; Soriaga, M. P., Surface reconstruction of pure-Cu single-crystal electrodes under CO-reduction potentials in alkaline solutions: A study by seriatim ECSTM-DEMS. *Journal of Electroanalytical Chemistry* **2016,** *780*, 290–295.

133. Kim, Y.-G.; Javier, A.; Baricuatro, J. H.; Soriaga, M. P., Regulating the Product Distribution of CO Reduction by the Atomic-Level Structural Modification of the Cu Electrode Surface. *Electrocatalysis* **2016,** *7* (5), 391–399.

134. Hahn, C.; Hatsukade, T.; Kim, Y.-G.; Vailionis, A.; Baricuatro, J. H.; Higgins, D. C.; Nitopi, S. A.; Soriaga, M. P.; Jaramillo, T. F., Engineering Cu surfaces for the electrocatalytic conversion of CO_2: Controlling selectivity toward oxygenates and hydrocarbons. *Proceedings of the National Academy of Sciences* **2017,** *114* (23), 5918.

135. Li, H.; Yu, P.; Lei, R.; Yang, F.; Wen, P.; Ma, X.; Zeng, G.; Guo, J.; Toma, F. M.; Qiu, Y.; Geyer, S. M.; Wang, X.; Cheng, T.; Drisdell, W., Facet-selective deposition of ultrathin $A_{l2}O_3$ on copper nanocrystals for highly stable CO_2 electroreduction to ethylene. *Angewandte Chemie International Edition* **2021,** *n/a* (n/a).

136. Baricuatro, J. H.; Kim, Y.-G.; Tsang, C. F.; Javier, A. C.; Cummins, K. D.; Hemminger, J. C., Selective conversion of CO into ethanol on Cu(511) surface reconstructed from Cu(pc): Operando studies by electrochemical scanning tunneling microscopy, mass spectrometry, quartz crystal nanobalance, and infrared spectroscopy. *Journal of Electroanalytical Chemistry* **2020,** *857*, 113704.

137. Kwon, S.; Kim, Y.-G.; Baricuatro, J. H.; Goddard, W. A., Dramatic Change in the Step Edges of the Cu(100) Electrocatalyst upon Exposure to CO: Operando Observations by Electrochemical STM and Explanation Using Quantum Mechanical Calculations. *ACS Catalysis* **2021,** *11* (19), 12068–12074.

138. Baricuatro, J. H.; Kim, Y.-G.; Korzeniewski, C. L.; Soriaga, M. P., Tracking the prelude of the electroreduction of carbon monoxide via its interaction with Cu(100): Studies by operando scanning tunneling microscopy and infrared spectroscopy. *Catalysis Today* **2020,** *358*, 210–214.

139. Baricuatro, J. H.; Ehlers, C. B.; Cummins, K. D.; Soriaga, M. P.; Stickney, J. L.; Kim, Y. G., Structure and composition of Cu(hkl) surfaces exposed to O_2 and emersed from alkaline solutions: Prelude to UHV-EC studies of CO_2 reduction at well-defined copper catalysts. *Journal of Electroanalytical Chemistry* **2014,** *716*, 101–105.

140. Fields, M.; Hong, X.; Nørskov, J. K.; Chan, K., Role of Subsurface Oxygen on Cu Surfaces for CO_2 Electrochemical Reduction. *The Journal of Physical Chemistry C* **2018,** *122* (28), 16209–16215.

141. Goodpaster, J. D.; Bell, A. T.; Head-Gordon, M., Identification of Possible Pathways for C–C Bond Formation during Electrochemical Reduction of CO_2: New Theoretical Insights from an Improved Electrochemical Model. *The Journal of Physical Chemistry Letters* **2016,** *7* (8), 1471–1477.

142. Garza, A. J.; Bell, A. T.; Head-Gordon, M., Mechanism of CO_2 Reduction at Copper Surfaces: Pathways to C2 Products. *ACS Catalysis* **2018,** *8* (2), 1490–1499.

143. Favaro, M.; Xiao, H.; Cheng, T.; Goddard, W. A.; Yano, J.; Crumlin, E. J., Subsurface oxide plays a critical role in CO_2 activation by Cu(111) surfaces to form chemisorbed CO_2, the first step in reduction of CO<sub>2</sub&gt. *Proceedings of the National Academy of Sciences* **2017,** *114* (26), 6706.

144. Lum, Y.; Ager, J. W., Stability of Residual Oxides in Oxide-Derived Copper Catalysts for Electrochemical CO_2 Reduction Investigated with ^{18}O Labeling. *Angewandte Chemie International Edition* **2018,** *57* (2), 551–554.

145. Liu, G.; Lee, M.; Kwon, S.; Zeng, G.; Eichhorn, J.; Buckley, A. K.; Toste, F. D.; Goddard, W. A.; Toma, F. M., CO_2 reduction on pure Cu produces only H_2 after subsurface O is depleted: Theory and experiment. *Proceedings of the National Academy of Sciences* **2021,** *118* (23), e2012649118.

146. Lum, Y.; Ager, J. W., Evidence for product-specific active sites on oxide-derived Cu catalysts for electrochemical CO_2 reduction. *Nat Catal* **2019,** *2* (1), 86–93.

147. Wang, L.; Nitopi, S. A.; Bertheussen, E.; Orazov, M.; Morales-Guio, C. G.; Liu, X.; Higgins, D. C.; Chan, K.; Nørskov, J. K.; Hahn, C.; Jaramillo, T. F., Electrochemical Carbon Monoxide Reduction on Polycrystalline Copper: Effects of Potential, Pressure, and pH on Selectivity toward Multicarbon and Oxygenated Products. *ACS Catalysis* **2018,** *8* (8), 7445–7454.

148. Kuhl, K. P.; Cave, E. R.; Abram, D. N.; Jaramillo, T. F., New insights into the electrochemical reduction of carbon dioxide on metallic copper surfaces. *Energy & Environmental Science* **2012,** *5* (5), 7050–7059.

149. Hori, Y.; Takahashi, R.; Yoshinami, Y.; Murata, A., Electrochemical Reduction of CO at a Copper Electrode. *The Journal of Physical Chemistry B* **1997,** *101* (36), 7075–7081.

150. Li, C. W.; Ciston, J.; Kanan, M. W., Electroreduction of carbon monoxide to liquid fuel on oxide-derived nanocrystalline copper. *Nature* **2014,** *508* (7497), 504–507.

151. Raciti, D.; Cao, L.; Livi, K. J. T.; Rottmann, P. F.; Tang, X.; Li, C.; Hicks, Z.; Bowen, K. H.; Hemker, K. J.; Mueller, T.; Wang, C., Low-Overpotential Electroreduction of Carbon Monoxide Using Copper Nanowires. *ACS Catalysis* **2017,** *7* (7), 4467–4472.

152. Jiang, K.; Sandberg, R. B.; Akey, A. J.; Liu, X.; Bell, D. C.; Nørskov, J. K.; Chan, K.; Wang, H., Metal ion cycling of Cu foil for selective C–C coupling in electrochemical CO_2 reduction. *Nat Catal* **2018,** *1* (2), 111–119.

153. Loiudice, A.; Lobaccaro, P.; Kamali, E. A.; Thao, T.; Huang, B. H.; Ager, J. W.; Buonsanti, R., Tailoring Copper Nanocrystals towards C_2 Products in Electrochemical CO_2 Reduction. *Angewandte Chemie International Edition* **2016,** *55* (19), 5789–5792.

154. Lum, Y.; Cheng, T.; Goddard, W. A.; Ager, J. W., Electrochemical CO Reduction Builds Solvent Water into Oxygenate Products. *Journal of the American Chemical Society* **2018,** *140* (30), 9337–9340.

155. Clark, E. L.; Wong, J.; Garza, A. J.; Lin, Z.; Head-Gordon, M.; Bell, A. T., Explaining the Incorporation of Oxygen Derived from Solvent Water into the Oxygenated Products of CO Reduction over Cu. *Journal of the American Chemical Society* **2019,** *141* (10), 4191–4193.

156. Liu, X.; Schlexer, P.; Xiao, J.; Ji, Y.; Wang, L.; Sandberg, R. B.; Tang, M.; Brown, K. S.; Peng, H.; Ringe, S.; Hahn, C.; Jaramillo, T. F.; Nørskov, J. K.; Chan, K., pH effects on the electrochemical reduction of CO(2) towards C2 products on stepped copper. *Nature Communications* **2019**, *10* (1), 32.

157. Tang, M. T.; Peng, H.; Lamoureux, P. S.; Bajdich, M.; Abild-Pedersen, F., From electricity to fuels: Descriptors for C1 selectivity in electrochemical CO_2 reduction. *Applied Catalysis B: Environmental* **2020**, *279*, 119384.

158. Peng, H.; Tang, M.; Liu, X.; Schlexer Lamoureux, P.; Bajdich, M.; Abild-Pedersen, F., The Role of Atomic Carbon in Directing Electrochemical CO(2) Reduction to Multicarbon Products. *Energy Environ. Sci.*, **2021**, *14*, 473–482.

159. Jeong, H. M.; Kwon, Y.; Won, J. H.; Lum, Y.; Cheng, M.-J.; Kim, K. H.; Head-Gordon, M.; Kang, J. K., Atomic-Scale Spacing between Copper Facets for the Electrochemical Reduction of Carbon Dioxide. *Advanced Energy Materials* **2020**, *10* (10), 1903423.

160. Choi, C.; Cheng, T.; Flores Espinosa, M.; Fei, H.; Duan, X.; Goddard Iii, W. A.; Huang, Y., A Highly Active Star Decahedron Cu Nanocatalyst for Hydrocarbon Production at Low Overpotentials. *Advanced Materials* **2019**, *31* (6), 1805405.

161. Choi, C.; Kwon, S.; Cheng, T.; Xu, M.; Tieu, P.; Lee, C.; Cai, J.; Lee, H. M.; Pan, X.; Duan, X.; Goddard, W. A.; Huang, Y., Highly active and stable stepped Cu surface for enhanced electrochemical CO_2 reduction to C_2H_4. *Nat Catal* **2020**, *3* (10), 804–812.

162. Clark, E. L.; Ringe, S.; Tang, M.; Walton, A.; Hahn, C.; Jaramillo, T. F.; Chan, K.; Bell, A. T., Influence of Atomic Surface Structure on the Activity of Ag for the Electrochemical Reduction of CO_2 to CO. *ACS Catalysis* **2019**, *9* (5), 4006–4014.

163. Chen, L. D.; Urushihara, M.; Chan, K.; Nørskov, J. K., Electric Field Effects in Electrochemical CO_2 Reduction. *ACS Catalysis* **2016**, *6* (10), 7133–7139.

164. Singh, M. R.; Goodpaster, J. D.; Weber, A. Z.; Head-Gordon, M.; Bell, A. T., Mechanistic insights into electrochemical reduction of CO_2 over Ag using density functional theory and transport models. *Proceedings of the National Academy of Sciences* **2017**, *114* (42), E8812.

165. Gauthier, J. A.; Fields, M.; Bajdich, M.; Chen, L. D.; Sandberg, R. B.; Chan, K.; Nørskov, J. K., Facile Electron Transfer to CO_2 during Adsorption at the Metal|Solution Interface. *The Journal of Physical Chemistry C* **2019**, *123* (48), 29278–29283.

166. Ringe, S.; Morales-Guio, C. G.; Chen, L. D.; Fields, M.; Jaramillo, T. F.; Hahn, C.; Chan, K., Double layer charging driven carbon dioxide adsorption limits the rate of electrochemical carbon dioxide reduction on Gold. *Nature Communications* **2020**, *11* (1), 33.

167. Tang, M. T.; Ulissi, Z. W.; Chan, K., Theoretical Investigations of Transition Metal Surface Energies under Lattice Strain and CO Environment. *The Journal of Physical Chemistry C* **2018**, *122* (26), 14481–14487.

168. Ye, Y.; Yang, H.; Qian, J.; Su, H.; Lee, K.-J.; Cheng, T.; Xiao, H.; Yano, J.; Goddard, W. A.; Crumlin, E. J., Dramatic differences in carbon dioxide adsorption and initial steps of reduction between silver and copper. *Nature Communications* **2019**, *10* (1), 1875.

169. Ye, Y.; Qian, J.; Yang, H.; Su, H.; Lee, K.-J.; Etxebarria, A.; Cheng, T.; Xiao, H.; Yano, J.; Goddard, W. A.; Crumlin, E. J., Synergy between a Silver–Copper Surface Alloy Composition and Carbon Dioxide Adsorption and Activation. *ACS Applied Materials & Interfaces* **2020**, *12* (22), 25374–25382.

170. Qian, J.; Ye, Y.; Yang, H.; Yano, J.; Crumlin, E. J.; Goddard, W. A., Initial Steps in Forming the Electrode–Electrolyte Interface: H_2O Adsorption and Complex Formation on the Ag(111) Surface from Combining Quantum Mechanics Calculations and Ambient Pressure X-ray Photoelectron Spectroscopy. *Journal of the American Chemical Society* **2019**, *141* (17), 6946–6954.

171. Clark, E. L.; Hahn, C.; Jaramillo, T. F.; Bell, A. T., Electrochemical CO_2 Reduction over Compressively Strained CuAg Surface Alloys with Enhanced Multi-Carbon Oxygenate Selectivity. *Journal of the American Chemical Society* **2017**, *139* (44), 15848–15857.

172. Scott, S. B.; Hogg, T. V.; Landers, A. T.; Maagaard, T.; Bertheussen, E.; Lin, J. C.; Davis, R. C.; Beeman, J. W.; Higgins, D.; Drisdell, W. S.; Hahn, C.; Mehta, A.; Seger, B.; Jaramillo, T. F.; Chorkendorff, I., Absence of Oxidized Phases in Cu under CO Reduction Conditions. *ACS Energy Letters* **2019**, *4* (3), 803–804.

173. Resasco, J.; Lum, Y.; Clark, E.; Zeledon, J. Z.; Bell, A. T., Effects of Anion Identity and Concentration on Electrochemical Reduction of CO_2. *ChemElectroChem* **2018**, *5* (7), 1064–1072.

174. Singh, M. R.; Kwon, Y.; Lum, Y.; Ager, J. W.; Bell, A. T., Hydrolysis of Electrolyte Cations Enhances the Electrochemical Reduction of CO_2 over Ag and Cu. *Journal of the American Chemical Society* **2016**, *138* (39), 13006–13012.

175. Resasco, J.; Chen, L. D.; Clark, E.; Tsai, C.; Hahn, C.; Jaramillo, T. F.; Chan, K.; Bell, A. T., Promoter Effects of Alkali Metal Cations on the Electrochemical Reduction of Carbon Dioxide. *Journal of the American Chemical Society* **2017**, *139* (32), 11277–11287.

176. Ringe, S.; Clark, E. L.; Resasco, J.; Walton, A.; Seger, B.; Bell, A. T.; Chan, K., Understanding cation effects in electrochemical CO_2 reduction. *Energy & Environmental Science* **2019**, *12* (10), 3001–3014.

177. Gauthier, J. A.; Dickens, C. F.; Heenen, H. H.; Vijay, S.; Ringe, S.; Chan, K., Unified Approach to Implicit and Explicit Solvent Simulations of Electrochemical Reaction Energetics. *Journal of Chemical Theory and Computation* **2019**, *15* (12), 6895–6906.

178. Clark, E. L.; Bell, A. T., Direct Observation of the Local Reaction Environment during the Electrochemical Reduction of CO_2. *Journal of the American Chemical Society* **2018**, *140* (22), 7012–7020.

179. Li, F.; Thevenon, A.; Rosas-Hernández, A.; Wang, Z.; Li, Y.; Gabardo, C. M.; Ozden, A.; Dinh, C. T.; Li, J.; Wang, Y.; Edwards, J. P.; Xu, Y.; McCallum, C.; Tao, L.; Liang, Z.-Q.; Luo, M.; Wang, X.; Li, H.; O'Brien, C. P.; Tan, C.-S.; Nam, D.-H.; Quintero-Bermudez, R.; Zhuang, T.-T.; Li, Y. C.; Han, Z.; Britt, R. D.; Sinton, D.; Agapie, T.; Peters, J. C.; Sargent, E. H., Molecular tuning of CO_2-to-ethylene conversion. *Nature* **2020**, *577* (7791), 509–513.

180. Ozden, A.; Li, F.; García de Arquer, F. P.; Rosas-Hernández, A.; Thevenon, A.; Wang, Y.; Hung, S.-F.; Wang, X.; Chen, B.; Li, J.; Wicks, J.; Luo, M.; Wang, Z.; Agapie, T.; Peters, J. C.; Sargent, E. H.; Sinton, D., High-Rate and Efficient Ethylene Electrosynthesis Using a Catalyst/Promoter/Transport Layer. *ACS Energy Letters* **2020**, *5* (9), 2811–2818.

181. Thevenon, A.; Rosas-Hernández, A.; Peters, J. C.; Agapie, T., In-Situ Nanostructuring and Stabilization of Polycrystalline Copper by an Organic Salt Additive Promotes Electrocatalytic CO_2 Reduction to Ethylene. *Angewandte Chemie International Edition* **2019**, *58* (47), 16952–16958.

182. Han, Z.; Kortlever, R.; Chen, H.-Y.; Peters, J. C.; Agapie, T., CO_2 Reduction Selective for C≥2 Products on Polycrystalline Copper with N-Substituted Pyridinium Additives. *ACS Central Science* **2017**, *3* (8), 853–859.

183. Hatsukade, T.; Kuhl, K. P.; Cave, E. R.; Abram, D. N.; Jaramillo, T. F., Insights into the electrocatalytic reduction of CO_2 on metallic silver surfaces. *Physical Chemistry Chemical Physics* **2014,** *16* (27), 13814–13819.

184. Hori, Y., Electrochemical CO_2 Reduction on Metal Electrodes. In *Modern Aspects of Electrochemistry, No 42*, Vayenas, C. G.; White, R. E.; GamboaAldeco, M. E., Eds. Springer: New York, 2008; pp 89–189.

185. Thevenon, A.; Rosas-Hernández, A.; Fontani Herreros, A. M.; Agapie, T.; Peters, J. C., Dramatic HER Suppression on Ag Electrodes via Molecular Films for Highly Selective CO_2 to CO Reduction. *ACS Catalysis* **2021,** *11* (8), 4530–4537.

186. Buckley, A. K.; Cheng, T.; Oh, M. H.; Su, G. M.; Garrison, J.; Utan, S. W.; Zhu, C.; Toste, F. D.; Goddard, W. A.; Toma, F. M., Approaching 100% Selectivity at Low Potential on Ag for Electrochemical CO_2 Reduction to CO Using a Surface Additive. *ACS Catalysis* **2021,** *11* (15), 9034–9042.

187. Buckley, A. K.; Lee, M.; Cheng, T.; Kazantsev, R. V.; Larson, D. M.; Goddard Iii, W. A.; Toste, F. D.; Toma, F. M., Electrocatalysis at Organic–Metal Interfaces: Identification of Structure–Reactivity Relationships for CO_2 Reduction at Modified Cu Surfaces. *Journal of the American Chemical Society* **2019,** *141* (18), 7355–7364.

188. Van Ausdall, B. R.; Glass, J. L.; Wiggins, K. M.; Aarif, A. M.; Louie, J., A Systematic Investigation of Factors Influencing the Decarboxylation of Imidazolium Carboxylates. *The Journal of Organic Chemistry* **2009,** *74* (20), 7935–7942.

189. Waldie, K. M.; Brunner, F. M.; Kubiak, C. P., Transition Metal Hydride Catalysts for Sustainable Interconversion of CO_2 and Formate: Thermodynamic and Mechanistic Considerations. *ACS Sustainable Chemistry & Engineering* **2018,** *6* (5), 6841–6848.

190. Ostericher, A. L.; Waldie, K. M.; Kubiak, C. P., Utilization of Thermodynamic Scaling Relationships in Hydricity To Develop Nickel Hydrogen Evolution Reaction Electrocatalysts with Weak Acids and Low Overpotentials. *ACS Catalysis* **2018,** *8* (10), 9596–9603.

191. Waldie, K. M.; Ostericher, A. L.; Reineke, M. H.; Sasayama, A. F.; Kubiak, C. P., Hydricity of Transition-Metal Hydrides: Thermodynamic Considerations for CO_2 Reduction. *ACS Catalysis* **2018,** *8* (2), 1313–1324.

192. DuBois, D. L.; Berning, D. E., Hydricity of transition-metal hydrides and its role in CO_2 reduction. *Applied Organometallic Chemistry* **2000,** *14* (12), 860–862.

193. Ostericher, A. L.; Porter, T. M.; Reineke, M. H.; Kubiak, C. P., Thermodynamic targeting of electrocatalytic CO_2 reduction: advantages, limitations, and insights for catalyst design. *Dalton Transactions* **2019,** *48* (42), 15841–15848.

194. Prineha, N.; Ravishankar, S.; Harry, A. A., Plasmonic hot carrier dynamics in solid-state and chemical systems for energy conversion. *Nanophotonics* **2016,** *5* (1), 96–111.

195. Sundararaman, R.; Narang, P.; Jermyn, A. S.; Goddard Iii, W. A.; Atwater, H. A., Theoretical predictions for hot-carrier generation from surface plasmon decay. *Nature Communications* **2014,** *5* (1), 5788.

196. Brown, A. M.; Sundararaman, R.; Narang, P.; Goddard, W. A.; Atwater, H. A., Nonradiative Plasmon Decay and Hot Carrier Dynamics: Effects of Phonons, Surfaces, and Geometry. *ACS Nano* **2016,** *10* (1), 957–966.

197. Narang, P.; Sundararaman, R.; Jermyn, A. S.; Goddard, W. A.; Atwater, H. A., Cubic Nonlinearity Driven Up-Conversion in High-Field Plasmonic Hot Carrier Systems. *The Journal of Physical Chemistry C* **2016,** *120* (37), 21056–21062.

198. Jermyn, A. S.; Tagliabue, G.; Atwater, H. A.; Goddard, W. A.; Narang, P.; Sundararaman, R., Transport of hot carriers in plasmonic nanostructures. *Physical Review Materials* **2019**, *3* (7), 075201.

199. Brown, A. M.; Sundararaman, R.; Narang, P.; Goddard, W. A.; Atwater, H. A., Ab initio phonon coupling and optical response of hot electrons in plasmonic metals. *Phys Rev B* **2016**, *94* (7), 075120.

200. Brown, A. M.; Sundararaman, R.; Narang, P.; Schwartzberg, A. M.; Goddard, W. A.; Atwater, H. A., Experimental and Ab Initio Ultrafast Carrier Dynamics in Plasmonic Nanoparticles. *Phys Rev Lett* **2017**, *118* (8), 087401.

201. Tagliabue, G.; Jermyn, A. S.; Sundararaman, R.; Welch, A. J.; DuChene, J. S.; Pala, R.; Davoyan, A. R.; Narang, P.; Atwater, H. A., Quantifying the role of surface plasmon excitation and hot carrier transport in plasmonic devices. *Nature Communications* **2018**, *9* (1), 3394.

202. DuChene, J. S.; Tagliabue, G.; Welch, A. J.; Cheng, W.-H.; Atwater, H. A., Hot Hole Collection and Photoelectrochemical CO_2 Reduction with Plasmonic Au/p-GaN Photocathodes. *Nano Letters* **2018**, *18* (4), 2545–2550.

203. DuChene, J. S.; Tagliabue, G.; Welch, A. J.; Li, X.; Cheng, W.-H.; Atwater, H. A., Optical Excitation of a Nanoparticle Cu/p-NiO Photocathode Improves Reaction Selectivity for CO_2 Reduction in Aqueous Electrolytes. *Nano Letters* **2020**, *20* (4), 2348–2358.

204. Tagliabue, G.; DuChene, J. S.; Habib, A.; Sundararaman, R.; Atwater, H. A., Hot-Hole versus Hot-Electron Transport at Cu/GaN Heterojunction Interfaces. *ACS Nano* **2020**, *14* (5), 5788–5797.

205. Tagliabue, G.; DuChene, J. S.; Abdellah, M.; Habib, A.; Gosztola, D. J.; Hattori, Y.; Cheng, W.-H.; Zheng, K.; Canton, S. E.; Sundararaman, R.; Sá, J.; Atwater, H. A., Ultrafast hot-hole injection modifies hot-electron dynamics in Au/p-GaN heterostructures. *Nature Materials* **2020**, *19*, 1312–1318.

206. Corson, E. R.; Creel, E. B.; Kim, Y.; Urban, J. J.; Kostecki, R.; McCloskey, B. D., A temperature-controlled photoelectrochemical cell for quantitative product analysis. *Review of Scientific Instruments* **2018**, *89* (5), 055112.

207. Ding, F.; Tsuchiya, T.; Manby, F. R.; Miller, T. F., Linear-Response Time-Dependent Embedded Mean-Field Theory. *Journal of Chemical Theory and Computation* **2017**, *13* (9), 4216–4227.

208. Zheng, F.; Wang, L.-W., Ultrafast Hot Carrier Injection in Au/GaN: The Role of Band Bending and the Interface Band Structure. *The Journal of Physical Chemistry Letters* **2019**, *10* (20), 6174–6183.

209. Zhou, J.-J.; Hellman, O.; Bernardi, M., Electron-Phonon Scattering in the Presence of Soft Modes and Electron Mobility in $SrTiO_3$ Perovskite from First Principles. *Phys Rev Lett* **2018**, *121* (22), 226603.

210. Zhou, J.-J.; Bernardi, M., Predicting charge transport in the presence of polarons: The beyond-quasiparticle regime in $SrTiO_3$. *Physical Review Research* **2019**, *1* (3), 033138.

211. Jhalani, V. A.; Zhou, J.-J.; Park, J.; Dreyer, C. E.; Bernardi, M., Piezoelectric Electron-Phonon Interaction from Ab Initio Dynamical Quadrupoles: Impact on Charge Transport in Wurtzite GaN. Phys. Rev. Lett. **2020**, *125*, 136602.

212. Park, J.; Zhou, J.-J.; Jhalani, V. A.; Dreyer, C. E.; Bernardi, M., Long-range quadrupole electron-phonon interaction from first principles. *Phys. Rev. B*, **2020**, *102*, *125203*.

213. Zhou, J.-J.; Park, J.; Lu, I. T.; Maliyov, I.; Tong, X.; Bernardi, M., Perturbo: a software package for ab initio electron-phonon interactions, charge transport and ultrafast dynamics. *Computer Physics Communications* **2021**, 264, 107970.214. Peterson, A. A.; Abild-Pedersen, F.; Studt, F.; Rossmeisl, J.; Norskov, J. K., How copper catalyzes the electroreduction of carbon dioxide into hydrocarbon fuels. *Energy & Environmental Science* **2010**, *3* (9), 1311–1315.

215. Woodhouse, M.; Herman, G. S.; Parkinson, B. A., Combinatorial Approach to Identification of Catalysts for the Photoelectrolysis of Water. *Chem Mater* **2005**, *17* (17), 4318–4324.

216. Jaramillo, T. F.; Baeck, S. H.; Kleiman-Shwarsctein, A.; Choi, K. S.; Stucky, G. D.; McFarland, E. W., Automated electrochemical synthesis and photoelectrochemical characterization of $Zn_{1-x}Co_xO$ thin films for solar hydrogen production. *J Comb Chem* **2005**, *7* (2), 264–271.

217. Gregoire, J. M.; Tague, M. E.; Cahen, S.; Khan, S.; Abruña, H. c. D.; DiSalvo, F. J.; van Dover, R. B., Improved Fuel Cell Oxidation Catalysis in $Pt_{1-x}Ta_x$. *Chem Mater* **2009**, *22* (3), 1080–1087.

218. Green, M. L.; Takeuchi, I.; Hattrick-Simpers, J. R., Applications of high throughput (combinatorial) methodologies to electronic, magnetic, optical, and energy-related materials. *Journal of Applied Physics* **2013**, *113*, 231101.

219. Jang, J. S.; Lee, J.; Ye, H.; Fan, F. R. F.; Bard, A. J., Rapid Screening of Effective Dopants for Fe_2O_3 Photocatalysts with Scanning Electrochemical Microscopy and Investigation of Their Photoelectrochemical Properties. *Journal of Physical Chemistry C* **2009**, *113* (16), 6719–6724.

220. Curtarolo, S.; Hart, G. L. W.; Nardelli, M. B.; Mingo, N.; Sanvito, S.; Levy, O., The high-throughput highway to computational materials design. *Nature materials* **2013**, *12* (3), 191–201.

221. Gregoire, J. M.; Haber, J. A.; Mitrovic, S.; Xiang, C.; Suram, S.; Newhouse, P. F.; Soedarmadji, E.; Marcin, M.; Kan, K.; Guevarra, D.; Jones, R.; Becerra, N.; Cornell, E. W.; Jin, J., Enabling Solar Fuels Technology With High Throughput Experimentation. *Mater. Res. Soc. Symp. Proc.* **2014**, *1654*.

222. Jones, R. J. R.; Shinde, A.; Guevarra, D.; Xiang, C.; Haber, J. A.; Jin, J.; Gregoire, J. M., Parallel Electrochemical Treatment System and Application for Identifying Acid-Stable Oxygen Evolution Electrocatalysts. *ACS Combinatorial Science* **2015**, *17* (2), 71–75.

223. Mitrovic, S.; Soedarmadji, E.; Newhouse, P. F.; Suram, S. K.; Haber, J. A.; Jin, J.; Gregoire, J. M., Colorimetric Screening for High-Throughput Discovery of Light Absorbers. *ACS Combinatorial Science* **2015**, *17* (3), 176–181.

224. Mitrovic, S.; Cornell, E. W.; Marcin, M. R.; Jones, R. J. R.; Newhouse, P. F.; Suram, S. K.; Jin, J.; Gregoire, J. M., High-throughput on-the-fly scanning ultraviolet-visible dual-sphere spectrometer. *Review of Scientific Instruments* **2015**, *86* (1), 5.

225. Xiang, C.; Haber, J.; Marcin, M.; Mitrovic, S.; Jin, J.; Gregoire, J. M., Mapping Quantum Yield for $(Fe–Zn–Sn–Ti)O_x$ Photoabsorbers Using a High Throughput Photoelectrochemical Screening System. *ACS Comb. Sci.* **2014**, *16* (3), 120–127.

226. Gregoire, J. M.; Xiang, C. X.; Liu, X. N.; Marcin, M.; Jin, J., Scanning droplet cell for high throughput electrochemical and photoelectrochemical measurements. *Review of Scientific Instruments* **2013**, *84* (2), 6.

227. Suram, S. K.; Haber, J. A.; Jin, J.; Gregoire, J. M., Generating Information Rich High-Throughput Experimental Materials Genomes using Functional Clustering via Multi-Tree Genetic Programming and Information Theory. *ACS Combinatorial Science* **2015**, *17* (4), 224–33.

228. Velazquez, J. M.; Saadi, F. H.; Pieterick, A. P.; Spurgeon, J. M.; Soriaga, M. P.; Brunschwig, B. S.; Lewis, N. S., Synthesis and hydrogen-evolution activity of tungsten selenide thin films deposited on tungsten foils. *Journal of Electroanalytical Chemistry* **2014,** *716*, 45–48.

229. Saadi, F. H.; Carim, A. I.; Velazquez, J. M.; Baricuatro, J. H.; McCrory, C. C. L.; Soriaga, M. P.; Lewis, N. S., Operand Synthesis of Macroporous Molybdenum Diselenide Films for Electrocatalysis of the Hydrogen-Evolution Reaction. *Acs Catalysis* **2014,** *4* (9), 2866–2873.

230. Carim, A. I.; Saadi, F. H.; Soriaga, M. P.; Lewis, N. S., Electrocatalysis of the hydrogen-evolution reaction by electrodeposited amorphous cobalt selenide films. *Journal of Materials Chemistry* A **2014,** *2* (34), 13835–13839.

231. Karunadasa, H. I.; Montalvo, E.; Sun, Y. J.; Majda, M.; Long, J. R.; Chang, C. J., A Molecular MoS_2 Edge Site Mimic for Catalytic Hydrogen Generation. *Science* **2012,** *335* (6069), 698–702.

232. Letko, C. S.; Panetier, J. A.; Head-Gordon, M.; Tilley, T. D., Mechanism of the Electrocatalytic Reduction of Protons with Diaryldithiolene Cobalt Complexes. *Journal of the American Chemical Society* **2014,** *136* (26), 9364–9376.

233. Nippe, M.; Khnayzer, R. S.; Panetier, J. A.; Zee, D. Z.; Olaiya, B. S.; Head-Gordon, M.; Chang, C. J.; Castellano, F. N.; Long, J. R., Catalytic proton reduction with transition metal complexes of the redox-active ligand bpy2PYMe. *Chem Sci* **2013,** *4* (10), 3934–3945.

234. Panetier, J. A.; Letko, C. S.; Tilley, T. D.; Head-Gordon, M., Understanding the electronic structure of cobalt-dithiolene H_2 evolution catalysts. *Abstr Pap Am Chem S* **2014,** *248*.

235. Panetier, J. A.; Letko, C. S.; Tilley, T. D.; Head-Gordon, M., Computational Characterization of Redox Non-Innocence in Cobalt-Bis(Diaryldithiolene)-Catalyzed Proton Reduction. *Journal of Chemical Theory and Computation* **2016,** *12* (1), 223–230.

236. Baricuatro, J.; Kim, Y.-G.; Saadi, F.; McCrory, C. L.; Sanabria-Chinchilla, J.; Crouthers, D.; Darensbourg, M.; Soriaga, M., Heterogenization of a Water-Insoluble Molecular Complex for Catalysis of the Proton-Reduction Reaction in Highly Acidic Aqueous Solutions. *Electrocatalysis* **2014**, *5*, 226–228.

237. Saadi, F. H.; Carim, A. I.; Verlage, E.; Hemminger, J. C.; Lewis, N. S.; Soriaga, M. P., CoP as an Acid-Stable Active Electrocatalyst for the Hydrogen-Evolution Reaction: Electrochemical Synthesis, Interfacial Characterization and Performance Evaluation. *Journal of Physical Chemistry C* **2014,** *118* (50), 29294–29300.

238. McEnaney, J. M.; Crompton, J. C.; Callejas, J. F.; Popczun, E. J.; Biacchi, A. J.; Lewis, N. S.; Schaak, R. E., Amorphous Molybdenum Phosphide Nanoparticles for Electrocatalytic Hydrogen Evolution. *Chem Mater* **2014,** *26* (16), 4826–4831.

239. McEnaney, J. M.; Crompton, J. C.; Callejas, J. F.; Popczun, E. J.; Read, C. G.; Lewis, N. S.; Schaak, R. E., Electrocatalytic hydrogen evolution using amorphous tungsten phosphide nanoparticles. *Chemical Communications* **2014,** *50* (75), 11026–11028.

240. Callejas, J. F.; McEnaney, J. M.; Read, C. G.; Crompton, J. C.; Biacchi, A. J.; Popczun, E. J.; Gordon, T. R.; Lewis, N. S.; Schaak, R. E., Electrocatalytic and Photocatalytic Hydrogen Production from Acidic and Neutral-pH Aqueous Solutions Using Iron Phosphide Nanoparticles. *Acs Nano* **2014,** *8* (11), 11101–11107.

241. Popczun, E. J.; Roske, C. W.; Read, C. G.; Crompton, J. C.; McEnaney, J. M.; Callejas, J. F.; Lewis, N. S.; Schaak, R. E., Highly branched cobalt phosphide nanostructures for hydrogen-evolution electrocatalysis. *Journal of Materials Chemistry A* **2015,** *3* (10), 5420–5425.

242. Haber, J. A.; Guevarra, D.; Jung, S. H.; Jin, J.; Gregoire, J. M., Discovery of New Oxygen Evolution Reaction Electrocatalysts by Combinatorial Investigation of the Ni- La- Co- Ce Oxide Composition Space. *Chemelectrochem* **2014,** *1* (10), 1613–1617.

243. Haber, J. A.; Xiang, C. X.; Guevarra, D.; Jung, S. H.; Jin, J.; Gregoire, J. M., High-Throughput Mapping of the Electrochemical Properties of (Ni-Fe-Co-Ce)O_x Oxygen-Evolution Catalysts. *Chemelectrochem* **2014,** *1* (3), 524–528.

244. Haber, J. A.; Anzenburg, E.; Yano, J.; Kisielowski, C.; Gregoire, J. M., Multiphase Nanostructure of a Quinary Metal Oxide Electrocatalyst Reveals a New Direction for OER Electrocatalyst Design. *Advanced Energy Materials* **2015,** *5* (10), n/a--n/a. doi:10.1002/aenm.201402307

245. Favaro, M.; Drisdell, W. S.; Marcus, M. A.; Gregoire, J. M.; Crumlin, E. J.; Haber, J. A.; Yano, J., An Operando Investigation of (Ni–Fe–Co–Ce)O_x System as Highly Efficient Electrocatalyst for Oxygen Evolution Reaction. *ACS Catalysis* **2017,** *7* (2), 1248–1258.

246. Shinde, A.; Guevarra, D.; Haber, J. A.; Jin, J.; Gregoire, J. M., Identification of optimal solar fuel electrocatalysts via high throughput in situ optical measurements. *Journal of Materials Research* **2015,** *30* (3), 442–450.

247. Stein, H. S.; Guevarra, D.; Shinde, A.; Jones, R. J. R.; Gregoire, J. M.; Haber, J. A., Functional mapping reveals mechanistic clusters for OER catalysis across (Cu–Mn–Ta–Co–Sn–Fe)O_x composition and pH space. *Materials Horizons* **2019,** *6* (6), 1251–1258.

248. Zhou, L.; Shinde, A.; Montoya, J. H.; Singh, A.; Gul, S.; Yano, J.; Ye, Y.; Crumlin, E. J.; Richter, M. H.; Cooper, J. K.; Stein, H. S.; Haber, J. A.; Persson, K. A.; Gregoire, J. M., Rutile Alloys in the Mn–Sb–O System Stabilize Mn^{3+} To Enable Oxygen Evolution in Strong Acid. *ACS Catalysis* **2018**, 10938–10948.

249. Xiao, H.; Shin, H.; Goddard, W. A., Synergy between Fe and Ni in the optimal performance of (Ni,Fe) OOH catalysts for the oxygen evolution reaction. *Proceedings of the National Academy of Sciences* **2018,** *115* (23), 5872.

250. Shin, H.; Xiao, H.; Goddard, W. A., In Silico Discovery of New Dopants for Fe-Doped Ni Oxyhydroxide ($Ni_{1-x}F_{ex}OOH$) Catalysts for Oxygen Evolution Reaction. *Journal of the American Chemical Society* **2018,** *140* (22), 6745–6748.

251. Post, J. E.; Veblen, D. R., Crystal-Structure Determinations of Synthetic Sodium, Magnesium, and Potassium Birnessite Using Tem and the Rietveld Method. *Am Mineral* **1990,** *75* (5-6), 477–489.

252. Umena, Y.; Kawakami, K.; Shen, J. R.; Kamiya, N., Crystal structure of oxygen-evolving photosystem II at a resolution of 1.9 angstrom. *Nature* **2011,** *473* (7345), 55–U65.

253. Baricuatro, J. H.; Saadi, F. H.; Carim, A. I.; Velazquez, J. M.; Kim, Y.-G.; Soriaga, M. P., Influence of Redox-Inactive Cations on the Structure and Electrochemical Reactivity of Synthetic Birnessite, a Heterogeneous Analog for the Oxygen-Evolving Complex. *The Journal of Physical Chemistry C* **2015,** *120* (29), 15618–15631.

254. Ebaid, M.; Jiang, K.; Zhang, Z.; Drisdell, W. S.; Bell, A. T.; Cooper, J. K., Production of C2/C3 Oxygenates from Planar Copper Nitride-Derived Mesoporous Copper via Electrochemical Reduction of CO_2. *Chem Mater* **2020,** *32* (7), 3304–3311.

255. Jiang, K.; Huang, Y.; Zeng, G.; Toma, F. M.; Goddard, W. A.; Bell, A. T., Effects of Surface Roughness on the Electrochemical Reduction of CO_2 over Cu. *ACS Energy Letters* **2020,** *5* (4), 1206–1214.

256. Lacy, D. C.; McCrory, C. C. L.; Peters, J. C., Studies of Cobalt-Mediated Electrocatalytic CO_2 Reduction Using a Redox-Active Ligand. *Inorganic Chemistry* **2014,** *53* (10), 4980–4988.

257. Zhang, M.; El-Roz, M.; Frei, H.; Mendoza-Cortes, J. L.; Head-Gordon, M.; Lacy, D. C.; Peters, J. C., Visible Light Sensitized CO_2 Activation by the Tetraaza [(CoN4H)-N-II(MeCN)](2+) Complex Investigated by FT-IR Spectroscopy and DFT Calculations. *Journal of Physical Chemistry C* **2015,** *119* (9), 4645–4654.

258. Sieh, D.; Lacy, D. C.; Peters, J. C.; Kubiak, C. P., Reduction of CO_2 by Pyridine Monoimine Molybdenum Carbonyl Complexes: Cooperative Metal-Ligand Binding of CO_2. *Chemistry* **2015,** *21* (23), 8497–503.

259. Lilio, A. M.; Reineke, M. H.; Moore, C. E.; Rheingold, A. L.; Takase, M. K.; Kubiak, C. P., Incorporation of Pendant Bases into Rh(diphosphine)(2) Complexes: Synthesis, Thermodynamic Studies, And Catalytic CO_2 Hydrogenation Activity of Rh(P2N2)(2) (+) Complexes. *Journal of the American Chemical Society* **2015,** *137* (25), 8251–8260.

260. Fong, H.; Peters, J., Hydricity of an Fe–H Species and Catalytic CO_2 Hydrogenation. *Inorganic Chemistry* **2015,** I, 5124–5135.

261. Luca, O. R.; McCrory, C. C. L.; Dalleska, N. F.; Koval, C. A., The Selective Electrochemical Conversion of Preactivated CO_2 to Methane. *Journal of The Electrochemical Society* **2015,** *162* (7), H473–H476.

262. Shi, J.; Jiang, Y.; Jiang, Z.; Wang, X.; Wang, X.; Zhang, S.; Han, P.; Yang, C., Enzymatic conversion of carbon dioxide. *Chemical Society Reviews* **2015,** *44* (17), 5981–6000.

263. Lum, Y.; Ager, J. W., Sequential catalysis controls selectivity in electrochemical CO_2 reduction on Cu. *Energy & Environmental Science* **2018,** *11* (10), 2935–2944.

264. Liu, Y.; Qiu, H.; Li, J.; Guo, L.; Ager, J. W., Tandem Electrocatalytic CO_2 Reduction with Efficient Intermediate Conversion over Pyramid-Textured Cu–Ag Catalysts. *ACS Applied Materials & Interfaces* **2021,** *13* (34), 40513–40521.

265. Li, J.; Li, J.; Dun, C.; Chen, W.; Zhang, D.; Gu, J.; Urban, J. J.; Ager, J. W., Copper sulfide as the cation exchange template for synthesis of bimetallic catalysts for CO_2 electroreduction. *RSC Advances* **2021,** *11* (39), 23948–23959.

266. Morales-Guio, C. G.; Cave, E. R.; Nitopi, S. A.; Feaster, J. T.; Wang, L.; Kuhl, K. P.; Jackson, A.; Johnson, N. C.; Abram, D. N.; Hatsukade, T.; Hahn, C.; Jaramillo, T. F., Improved CO_2 reduction activity towards C2+ alcohols on a tandem gold on copper electrocatalyst. *Nat Catal* **2018,** *1* (10), 764–771.

267. Wang, L.; Higgins, D. C.; Ji, Y.; Morales-Guio, C. G.; Chan, K.; Hahn, C.; Jaramillo, T. F., Selective reduction of CO to acetaldehyde with CuAg electrocatalysts. *Proceedings of the National Academy of Sciences* **2020,** *117* (23), 12572.

268. Jones, R. J. R.; Wang, Y.; Lai, Y.; Shinde, A.; Gregoire, J. M., Reactor design and integration with product detection to accelerate screening of electrocatalysts for carbon dioxide reduction. *Review of Scientific Instruments* **2018,** *89* (12), 124102.

269. Lai, Y.; Jones, R. J. R.; Wang, Y.; Zhou, L.; Gregoire, J. M., Scanning Electrochemical Flow Cell with Online Mass Spectroscopy for Accelerated Screening of Carbon Dioxide Reduction Electrocatalysts. *ACS Combinatorial Science* **2019,** *21* (10), 692–704.

270. Lai, Y.; Jones, R. J. R.; Wang, Y.; Zhou, L.; Richter, M. H.; Gregoire, J., The sensitivity of Cu for electrochemical carbon dioxide reduction to hydrocarbons as revealed by high throughput experiments. *Journal of Materials Chemistry A* **2019,** *7* (47), 26785–26790.

271. Wang, L.; Peng, H.; Lamaison, S.; Qi, Z.; Koshy, D. M.; Stevens, M. B.; Wakerley, D.; Zamora Zeledón, J. A.; King, L. A.; Zhou, L.; Lai, Y.; Fontecave, M.; Gregoire, J.; Abild-Pedersen, F.; Jaramillo, T. F.; Hahn, C., Bimetallic effects on Zn-Cu electrocatalysts enhance activity and selectivity for the conversion of CO_2 to CO. *Chem Catalysis* **2021,** *1* (3), 663–680.

272. Torelli, D. A.; Francis, S. A.; Crompton, J. C.; Javier, A.; Thompson, J. R.; Brunschwig, B. S.; Soriaga, M. P.; Lewis, N. S., Nickel–gallium-catalyzed electrochemical reduction of CO_2 to highly reduced products at low overpotentials. *ACS Catalysis* **2016,** *6* (3), 2100–2104.

273. Francis, S. A.; Velazquez, J. M.; Ferrer, I. M.; Torelli, D. A.; Guevarra, D.; McDowell, M. T.; Sun, K.; Zhou, X.; Saadi, F. H.; John, J.; Richter, M. H.; Hyler, F. P.; Papadantonakis, K. M.; Brunschwig, B. S.; Lewis, N. S., Reduction of Aqueous CO_2 to 1-Propanol at MoS_2 Electrodes. *Chem Mater* **2018,** *30* (15), 4902–4908.

274. Javier, A.; Baricuatro, J. H.; Kim, Y.-G.; Soriaga, M. P., Overlayer Au-on-W Near-Surface Alloy for the Selective Electrochemical Reduction of CO_2 to Methanol: Empirical (DEMS) Corroboration of a Computational (DFT) Prediction. *Electrocatalysis* **2015,** *6* (6), 493–497.

275. Lee, M.; De Riccardis, A.; Kazantsev, R. V.; Cooper, J. K.; Buckley, A. K.; Burroughs, P. W. W.; Larson, D. M.; Mele, G.; Toma, F. M., Aluminum Metal–Organic Framework Triggers Carbon Dioxide Reduction Activity. *ACS Applied Energy Materials* **2020,** *3* (2), 1286–1291.

276. Hidetomo, N.; Shoichiro, I.; Yoshiyuki, O.; Kazumoto, I.; Masunobu, M.; Kaname, I., Electrochemical Reduction of Carbon Dioxide at Various Metal Electrodes in Aqueous Potassium Hydrogen Carbonate Solution. *Bulletin of the Chemical Society of Japan* **1990,** *63* (9), 2459–2462.

277. Azuma, M.; Hashimoto, K.; Hiramoto, M.; Watanabe, M.; Sakata, T., Electrochemical Reduction of Carbon Dioxide on Various Metal Electrodes in Low-Temperature Aqueous $KHCO_3$ Media. *Journal of The Electrochemical Society* **1990,** *137* (6), 1772–1778.

278. Hara, K.; Kudo, A.; Sakata, T., Electrochemical reduction of carbon dioxide under high pressure on various electrodes in an aqueous electrolyte. *Journal of Electroanalytical Chemistry* **1995,** *391* (1), 141–147.

279. Lin, S.; Diercks, C. S.; Zhang, Y.-B.; Kornienko, N.; Nichols, E. M.; Zhao, Y.; Paris, A. R.; Kim, D.; Yang, P.; Yaghi, O. M.; Chang, C. J., Covalent organic frameworks comprising cobalt porphyrins for catalytic CO₂ reduction in water. *Science* **2015,** *349* (6253), 1208–1213.

280. Koshy, D. M.; Chen, S.; Lee, D. U.; Stevens, M. B.; Abdellah, A. M.; Dull, S. M.; Chen, G.; Nordlund, D.; Gallo, A.; Hahn, C.; Higgins, D. C.; Bao, Z.; Jaramillo, T. F., Understanding the Origin of Highly Selective CO_2 Electroreduction to CO on Ni,N-doped Carbon Catalysts. *Angewandte Chemie International Edition* **2020,** *59* (10), 4043–4050.

281. Koshy, D. M.; Landers, A. T.; Cullen, D. A.; Ievlev, A. V.; Meyer III, H. M.; Hahn, C.; Bao, Z.; Jaramillo, T. F., Direct Characterization of Atomically Dispersed Catalysts: Nitrogen-Coordinated Ni Sites in Carbon-Based Materials for CO_2 Electroreduction. *Advanced Energy Materials* **2020,** *n/a* (n/a), 2001836.

282. Koshy, D. M.; Nathan, S. S.; Asundi, A. S.; Abdellah, A. M.; Dull, S. M.; Cullen, D. A.; Higgins, D.; Bao, Z.; Bent, S. F.; Jaramillo, T. F., Bridging Thermal Catalysis and Electrocatalysis: Catalyzing CO_2 Conversion with Carbon-Based Materials. *Angewandte Chemie International Edition* **2021,** *n/a* (n/a), 17472–17480.

283. Sato, S.; McNicholas, B. J.; Grubbs, R. H., Aqueous electrocatalytic CO_2 reduction using metal complexes dispersed in polymer ion gels. *Chemical Communications* **2020,** *56* (32), 4440–4443.

284. Newhouse, P. F.; Guevarra, D.; Umehara, M.; Reyes-Lillo, S. E.; Zhou, L.; Boyd, D. A.; Suram, S. K.; Cooper, J. K.; Haber, J. A.; Neaton, J. B.; Gregoire, J. M., Combinatorial alloying improves bismuth vanadate photoanodes via reduced monoclinic distortion. *Energy & Environmental Science* **2018,** *11* (9), 2444–2457.

285. Shinde, A.; Suram, S. K.; Yan, Q.; Zhou, L.; Singh, A. K.; Yu, J.; Persson, K. A.; Neaton, J. B.; Gregoire, J. M., Discovery of Manganese-Based Solar Fuel Photoanodes via Integration of Electronic Structure Calculations, Pourbaix Stability Modeling, and High-Throughput Experiments. *ACS Energy Letters* **2017,** 2307–2312.

286. Yan, Q.; Yu, J.; Suram, S. K.; Zhou, L.; Shinde, A.; Newhouse, P. F.; Chen, W.; Li, G.; Persson, K. A.; Gregoire, J. M.; Neaton, J. B., Solar fuels photoanode materials discovery by integrating high-throughput theory and experiment. *Proceedings of the National Academy of Sciences* **2017,** *114* (12), 3040–3043.

287. Suram, S. K.; Zhou, L.; Shinde, A.; Yan, Q.; Yu, J.; Umehara, M.; Stein, H. S.; Neaton, J. B.; Gregoire, J. M., Alkaline-stable nickel manganese oxides with ideal band gap for solar fuel photoanodes. *Chemical Communications* **2018,** *54* (36), 4625–4628.

288. Zhou, L.; Shinde, A.; Guevarra, D.; Richter, M. H.; Stein, H. S.; Wang, Y.; Newhouse, P. F.; Persson, K. A.; Gregoire, J. M., Combinatorial screening yields discovery of 29 metal oxide photoanodes for solar fuel generation. *Journal of Materials Chemistry A* **2020,** *8* (8), 4239–4243.

289. Zhou, L.; Shinde, A.; Guevarra, D.; Haber, J. A.; Persson, K. A.; Neaton, J. B.; Gregoire, J. M., Successes and Opportunities for Discovery of Metal Oxide Photoanodes for Solar Fuels Generators. *ACS Energy Letters* **2020,** *5* (5), 1413–1421.

290. Zhou, L.; Shinde, A.; Suram, S. K.; Stein, H. S.; Bauers, S. R.; Zakutayev, A.; DuChene, J. S.; Liu, G.; Peterson, E. A.; Neaton, J. B.; Gregoire, J. M., Bi-Containing n-$FeWO_4$ Thin Films Provide the Largest Photovoltage and Highest Stability for a Sub-2 eV Band Gap Photoanode. *ACS Energy Letters* **2018,** *3* (11), 2769–2774.

291. Meyer, R.; Sliozberg, K.; Khare, C.; Schuhmann, W.; Ludwig, A., High-Throughput Screening of Thin-Film Semiconductor Material Libraries II: Characterization of Fe-W-O Libraries. *ChemSusChem* **2015,** *8* (7), 1279–1285.

292. Abdi, F. F.; Chemseddine, A.; Berglund, S. P.; van de Krol, R., Assessing the Suitability of Iron Tungstate (Fe_2WO_6) as a Photoelectrode Material for Water Oxidation. *J. Phys. Chem. C* **2017,** *121* (1), 153–160.

293. Kollender, J. P.; Mardare, A. I.; Hassel, A. W., Localized Photoelectrochemistry on a Tungsten Oxide-Iron Oxide Thin Film Material Library. *ACS Comb. Sci.* **2013,** *15* (12), 601–608.

294. Stein, H. S.; Guevarra, D.; Newhouse, P. F.; Soedarmadji, E.; Gregoire, J. M., Machine learning of optical properties of materials – predicting spectra from images and images from spectra. *Chem Sci* **2019,** *10* (1), 47–55.

295. Richter, M. H.; Peterson, E. A.; Zhou, L.; Shinde, A. A.; Newhouse, P. F.; Yan, Q.; Fackler, S. W.; Yano, J.; Cooper, J. K.; Persson, K. A.; Neaton, J. B.; Gregoire, J. M., Band Edge Energy Tuning through Electronic Character Hybridization in Ternary Metal Vanadates. *Chem Mater* **2021,** *33* (18), 7242–7253.

296. Soedarmadji, E.; Stein, H. S.; Suram, S. K.; Guevarra, D.; Gregoire, J. M., Tracking materials science data lineage to manage millions of materials experiments and analyses. *npj Computational Materials* **2019,** *5* (1), 79.

297. Singh, A. K.; Montoya, J. H.; Gregoire, J. M.; Persson, K. A., Robust and synthesizable photocatalysts for CO_2 reduction: a data-driven materials discovery. *Nature Communications* **2019,** *10* (1), 443.

298. Lin, Y.-R.; Cheng, W.-H.; Richter, M. H.; DuChene, J. S.; Peterson, E. A.; Went, C. M.; Al Balushi, Z. Y.; Jariwala, D.; Neaton, J. B.; Chen, L.-C.; Atwater, H. A., Band Edge Tailoring in Few-layer Two-dimensional Molybdenum Sulfides/Selenides Alloys. *The Journal of Physical Chemistry C* **2020,** *124* (42), 22893–22902.

299. Zhang, Z.; Lindley, S. A.; Dhall, R.; Bustillo, K.; Han, W.; Xie, E.; Cooper, J. K., Beneficial CuO Phase Segregation in the Ternary p-Type Oxide Photocathode $CuBi_2O_4$. *ACS Applied Energy Materials* **2019,** *2* (6), 4111–4117.

300. Jiang, C.-M.; Reyes-Lillo, S. E.; Liang, Y.; Liu, Y.-S.; Liu, G.; Toma, F. M.; Prendergast, D.; Sharp, I. D.; Cooper, J. K., Electronic Structure and Performance Bottlenecks of $CuFeO_2$ Photocathodes. *Chem Mater* **2019,** *31* (7), 2524–2534.

301. Lin, Y. J.; Kapadia, R.; Yang, J. H.; Zheng, M.; Chen, K.; Hettick, M.; Yin, X. T.; Battaglia, C.; Sharp, I. D.; Ager, J. W.; Javey, A., Role of TiO_2 Surface Passivation on Improving the Performance of p-InP Photocathodes. *Journal of Physical Chemistry C* **2015,** *119* (5), 2308–2313.

302. Lee, M. H.; Takei, K.; Zhang, J.; Kapadia, R.; Zheng, M.; Chen, Y.-Z.; Nah, J.; Matthews, T. S.; Chueh, Y.-L.; Ager, J. W.; Javey, A., p-Type InP Nanopillar Photocathodes for Efficient Solar-Driven Hydrogen Production. *Angewandte Chemie International Edition* **2012,** *51* (43), 10760–10764.

303. Zhai, P.; Haussener, S.; Ager, J.; Sathre, R.; Walczak, K.; Greenblatt, J.; McKone, T., Net primary energy balance of a solar-driven photoelectrochemical water-splitting device. *Energy & Environmental Science* **2013,** *6* (8), 2380–2389.

304. Sathre, R.; Scown, C. D.; Morrow, W. R.; Stevens, J. C.; Sharp, I. D.; Ager, J. W.; Walczak, K.; Houle, F. A.; Greenblatt, J. B., Life-cycle net energy assessment of large-scale hydrogen production via photoelectrochemical water splitting. *Energy & Environmental Science* **2014,** *7* (10), 3264–3278.

305. Sathre, R.; Greenblatt, J. B.; Walczak, K.; Sharp, I. D.; Stevens, J. C.; Ager, J. W.; Houle, F. A., Opportunities to improve the net energy performance of photoelectrochemical water-splitting technology. *Energy & Environmental Science* **2016,** *9* (3), 803–819.

306. Ager Iii, J. W.; Shaner, M.; Walczak, K.; Sharp, I. D.; Ardo, S., Experimental Demonstrations of Spontaneous, Solar-Driven Photoelectrochemical Water Splitting. *Energy & Environmental Science* **2015,** *8* (10), 2811–2824.

307. Hu, S.; Shaner, M. R.; Beardslee, J. A.; Lichterman, M.; Brunschwig, B. S.; Lewis, N. S., Amorphous TiO_2 coatings stabilize Si, GaAs, and GaP photoanodes for efficient water oxidation. *Science* **2014,** *344* (6187), 1005–1009.

308. Lichterman, M. F.; Carim, A. I.; McDowell, M. T.; Hu, S.; Gray, H. B.; Brunschwig, B. S.; Lewis, N. S., Stabilization of n-cadmium telluride photoanodes for water oxidation to O_2(g) in aqueous alkaline electrolytes using amorphous TiO_2 films formed by atomic-layer deposition. *Energy & Environmental Science* **2014,** *7* (10), 3334–3337.

309. McDowell, M. T.; Lichterman, M. F.; Spurgeon, J. M.; Hu, S.; Sharp, I. D.; Brunschwig, B. S.; Lewis, N. S., Improved Stability of Polycrystalline Bismuth Vanadate Photoanodes by Use of Dual-Layer Thin TiO_2/Ni Coatings. *Journal of Physical Chemistry C* **2014,** *118* (34), 19618–19624.

310. Finke, C. E.; Omelchenko, S. T.; Jasper, J. T.; Lichterman, M. F.; Read, C. G.; Lewis, N. S.; Hoffmann, M. R., Enhancing the activity of oxygen-evolution and chlorine-evolution electrocatalysts by atomic layer deposition of TiO_2. *Energy & Environmental Science* **2019,** *12*, 358–365.

311. Nunez, P.; Richter, M. H.; Piercy, B. D.; Roske, C. W.; Cabán-Acevedo, M.; Losego, M. D.; Konezny, S. J.; Fermin, D. J.; Hu, S.; Brunschwig, B. S.; Lewis, N. S., Characterization of Electronic Transport through Amorphous TiO_2 Produced by Atomic Layer Deposition. *The Journal of Physical Chemistry C* **2019,** *123* (33), 20116–20129.

312. Richter, M. H.; Cheng, W.-H.; Crumlin, E. J.; Drisdell, W. S.; Atwater, H. A.; Schmeißer, D.; Lewis, N. S.; Brunschwig, B. S., X-ray Photoelectron Spectroscopy and Resonant X-ray Spectroscopy Investigations of Interactions between Thin Metal Catalyst Films and Amorphous Titanium Dioxide Photoelectrode Protection Layers. *Chem Mater* **2021,** *33* (4), 1265–1275.

313. Lichterman, M. F.; Sun, K.; Hu, S.; Zhou, X.; McDowell, M. T.; Shaner, M. R.; Richter, M. H.; Crumlin, E. J.; Carim, A. I.; Saadi, F. H.; Brunschwig, B. S.; Lewis, N. S., Protection of inorganic semiconductors for sustained, efficient photoelectrochemical water oxidation. *Catalysis Today* **2016,** *262*, 11–23.

314. Shaner, M. R.; Hu, S.; Sun, K.; Lewis, N. S., Stabilization of Si microwire arrays for solar-driven H_2O oxidation to O_2(g) in 1.0 M KOH(aq) using conformal coatings of amorphous TiO2. *Energy & Environmental Science* **2015,** *8* (1), 203–207.

315. Kennedy, K. M.; Kempler, P. A.; Cabán-Acevedo, M.; Papadantonakis, K. M.; Lewis, N. S., Primary Corrosion Processes for Polymer-Embedded Free-Standing or Substrate-Supported Silicon Microwire Arrays in Aqueous Alkaline Electrolytes. *Nano Letters* **2021,** *21* (2), 1056–1061.

316. Shen, X.; Yao, M.; Sun, K.; Zhao, T.; He, Y.; Chi, C.-Y.; Zhou, C.; Dapkus, P. D.; Lewis, N. S.; Hu, S., Defect-Tolerant TiO_2-Coated and Discretized Photoanodes for >600 h of Stable Photoelectrochemical Water Oxidation. *ACS Energy Letters* **2021,** *6* (1), 193–200.

317. Buabthong, P.; Ifkovits, Z. P.; Kempler, P. A.; Chen, Y.; Nunez, P. D.; Brunschwig, B. S.; Papadantonakis, K. M.; Lewis, N. S., Failure modes of protection layers produced by atomic layer deposition of amorphous TiO_2 on GaAs anodes. *Energy & Environmental Science* **2020,** *13* (11), 4269–4279.

318. Moreno-Hernandez, I. A.; Brunschwig, B. S.; Lewis, N. S., Tin Oxide as a Protective Heterojunction with Silicon for Efficient Photoelectrochemical Water Oxidation in Strongly Acidic or Alkaline Electrolytes. *Advanced Energy Materials* **2018**, 1801155.

319. Moreno-Hernandez, I. A.; Yalamanchili, S.; Fu, H. J.; Atwater, H. A.; Brunschwig, B. S.; Lewis, N. S., Conformal SnO_x heterojunction coatings for stabilized photoelectrochemical water oxidation using arrays of silicon microcones. *Journal of Materials Chemistry A* **2020,** *8* (18), 9292–9301.

320. Singh, M. R.; Papadantonakis, K. M.; Xiang, C. X.; Lewis, N. S., An electrochemical engineering assessment of the operational conditions and constraints for solar-driven water-splitting systems at near-neutral pH. *Energy & Environmental Science* **2015,** *8*, 2760–2767.

321. Yang, J.; Cooper, J. K.; Toma, F. M.; Walczak, Karl A.; Favaro, M.; Beeman, Jeffrey W.; Hess, Lucas H.; Wang, C.; Zhu, C.; Gul, S.; Yano, J.; Kisielowski, C.; Schwartzberg, A.; Sharp, Ian D., A multifunctional biphasic water splitting catalyst tailored for integration with high-performance semiconductor photoanodes. *Nature Materials* **2017,** *16* (3), 335–341.

322. Hu, S.; Lewis, N. S.; Ager, J. W.; Yang, J.; McKone, J. R.; Strandwitz, N. C., Thin-Film Materials for the Protection of Semiconducting Photoelectrodes in Solar-Fuel Generators. *The Journal of Physical Chemistry C* **2015,** *119* (43), 24201–24228.

323. Chen, L.; Yang, J.; Klaus, S.; Lee, L. J.; Woods-Robinson, R.; Ma, J.; Lum, Y.; Cooper, J. K.; Toma, F. M.; Wang, L.-W.; Sharp, I. D.; Bell, A. T.; Ager, J. W., P-type Transparent Conducting Oxide / n-type Semiconductor Heterojunctions for Efficient and Stable Solar Water Oxidation. *Journal of the American Chemical Society* **2015,** *137* (30), 9595–603.

324. Drisdell, W. S.; Leppert, L.; Sutter-Fella, C. M.; Liang, Y.; Li, Y.; Ngo, Q. P.; Gul, S.; Kroll, T.; Sokaras, D.; Javey, A.; Yano, J.; Neaton, J. B.; Toma, F. M.; Prendergast, D.; Sharp, I. D., Determining atomic-scale structure and composition of organo-lead halide perovskites by combining high-resolution X-ray absorption spectroscopy and first-principles calculations. *ACS Energy Letters* **2017,** *2* (5), 1183–1189.

325. Babbe, F.; Sutter-Fella, C. M., Optical Absorption-Based In Situ Characterization of Halide Perovskites. *Advanced Energy Materials* **2020,** *10* (26), 1903587.

326. Babbe, F.; Masquelier, E.; Zheng, Z.; Sutter-Fella, C., *Multi stage and illumination dependent segregation in MAPb(I,Br)3*. SPIE: 2020; Vol. 11474.

327. Zheng, F.; Wang, L.-w., Large polaron formation and its effect on electron transport in hybrid perovskites. *Energy & Environmental Science* **2019,** *12* (4), 1219–1230.

328. Wang, L.; Xiao, H.; Cheng, T.; Li, Y.; Goddard, W. A., Pb-Activated Amine-Assisted Photocatalytic Hydrogen Evolution Reaction on Organic–Inorganic Perovskites. *Journal of the American Chemical Society* **2018,** *140* (6), 1994–1997.

329. Smith, W. A.; Sharp, I. D.; Strandwitz, N. C.; Bisquert, J., Interfacial band-edge energetics for solar fuels production. *Energy & Environmental Science* **2015,** *8* (10), 2851–2862.

330. Guevarra, D.; Shinde, A.; Suram, S. K.; Sharp, I. D.; Toma, F. M.; Haber, J. A.; Gregoire, J. M., Development of solar fuels photoanodes through combinatorial integration of Ni-La-Co-Ce oxide catalysts on $BiVO_4$. *Energy & Environmental Science* **2016,** *9* (2), 565–580.

331. Shinde, A.; Guevarra, D.; Liu, G. J.; Sharp, I. D.; Toma, F. M.; Gregoire, J. M.; Haber, J. A., Discovery of Fe-Ce Oxide/$BiVO_4$ Photoanodes through Combinatorial Exploration of Ni-Fe-Co-Ce Oxide Coatings. *Acs Applied Materials & Interfaces* **2016,** *8* (36), 23696–23705.

332. Shinde, A.; Li, G.; Zhou, L.; Guevarra, D.; Suram, S. K.; Toma, F. M.; Yan, Q.; Haber, J. A.; Neaton, J. B.; Gregoire, J. M., The role of the CeO_2/$BiVO_4$ interface in optimized Fe-Ce oxide coatings for solar fuels photoanodes. *Journal of Materials Chemistry A* **2016,** *4* (37), 14356–14363.

333. Liu, G.; Eichhorn, J.; Jiang, C.-M.; Scott, M. C.; Hess, L. H.; Gregoire, J. M.; Haber, J. A.; Sharp, I. D.; Toma, F. M., Interface engineering for light-driven water oxidation: unravelling the passivating and catalytic mechanism in $BiVO_4$ overlayers. *Sustainable Energy & Fuels* **2019,** *3* (1), 127–135.

334. Zhou, L.; Shinde, A.; Guevarra, D.; Toma, F. M.; Stein, H. S.; Gregoire, J. M.; Haber, J. A., Balancing Surface Passivation and Catalysis with Integrated $BiVO_4$/$(Fe–Ce)O_x$ Photoanodes in pH 9 Borate Electrolyte. *ACS Applied Energy Materials* **2018,** *1* (10), 5766–5771.

335. Zhang, Z.; Lindley, S. A.; Guevarra, D.; Kan, K.; Shinde, A.; Gregoire, J. M.; Han, W.; Xie, E.; Haber, J. A.; Cooper, J. K., Fermi Level Engineering of Passivation and Electron Transport Materials for p-Type $CuBi_2O_4$ Employing a High-Throughput Methodology. *Adv Funct Mater* **2020,** *30* (24), 2000948.

336. Cooper, J. K.; Reyes-Lillo, S. E.; Hess, L.; Jiang, C.-M.; Neaton, J. B.; Sharp, I. D., Physical Origins of the Transient Absorption Spectra and Dynamics in Thin Film Semiconductors: The Case of $BiVO_4$. *Journal of Physical Chemistry C* **2018,** *122* (36), 20642–20652.

337. Cooper, J. K.; Zhang, Z.; Roychoudhury, S.; Jiang, C.-M.; Gul, S.; Liu, Y.-S.; Dhall, R.; Ceballos, A.; Yano, J.; Prendergast, D.; Reyes-Lillo, S. E., CuBi2O4: Electronic Structure, Optical Properties, and Photoelectrochemical Performance Limitations of the Photocathode. *Chem Mater* **2021,** *33* (3), 934–945.

338. Segev, G.; Dotan, H.; Ellis, D. S.; Piekner, Y.; Klotz, D.; Beeman, J. W.; Cooper, J. K.; Grave, D. A.; Sharp, I. D.; Rothschild, A., The Spatial Collection Efficiency of Charge Carriers in Photovoltaic and Photoelectrochemical Cells. *Joule* **2018,** *2* (2), 210–224.

339. Segev, G.; Jiang, C.-M.; Cooper, J. K.; Eichhorn, J.; Toma, F. M.; Sharp, I. D., Quantification of the loss mechanisms in emerging water splitting photoanodes through empirical extraction of the spatial charge collection efficiency. *Energy & Environmental Science* **2018,** *11* (4), 904–913.

340. Jiang, C.-M.; Segev, G.; Hess, L. H.; Liu, G.; Zaborski, G.; Toma, F. M.; Cooper, J. K.; Sharp, I. D., Composition-Dependent Functionality of Copper Vanadate Photoanodes. *ACS Applied Materials & Interfaces* **2018,** *10* (13), 10627–10633.

341. Eichhorn, J.; Kastl, C.; Cooper, J. K.; Ziegler, D.; Schwartzberg, A. M.; Sharp, I. D.; Toma, F. M., Nanoscale imaging of charge carrier transport in water splitting photoanodes. *Nature Communications* **2018,** *9* (1), 2597.

342. Borgwardt, M.; Mahl, J.; Roth, F.; Wenthaus, L.; Braußе, F.; Blum, M.; Schwarzburg, K.; Liu, G.; Toma, F. M.; Gessner, O., Photoinduced Charge Carrier Dynamics and Electron Injection Efficiencies in Au Nanoparticle-Sensitized TiO_2 Determined with Picosecond Time-Resolved X-ray Photoelectron Spectroscopy. *The Journal of Physical Chemistry Letters* **2020,** *11* (14), 5476–5481.

343. Eichhorn, J.; Reyes-Lillo, S. E.; Roychoudhury, S.; Sallis, S.; Weis, J.; Larson, D. M.; Cooper, J. K.; Sharp, I. D.; Prendergast, D.; Toma, F. M., Revealing Nanoscale Chemical Heterogeneities in Polycrystalline Mo-$BiVO_4$ Thin Films. *Small* **2020,** *16* (35), e2001600.

344. Eichhorn, J.; Jiang, C.-M.; Cooper, J. K.; Sharp, I. D.; Toma, F. M., Nanoscale Heterogeneities and Composition–Reactivity Relationships in Copper Vanadate Photoanodes. *ACS Applied Materials & Interfaces* **2021,** *13* (20), 23575–23583.

345. Kusoglu, A.; Modestino, M. A.; Hexemer, A.; Segalman, R. A.; Weber, A. Z., Subsecond Morphological Changes in Nafion during Water Uptake Detected by Small-Angle X-ray Scattering. *Acs Macro Letters* **2012,** *1*, 33–36.

346. Modestino, M. A.; Kusoglu, A.; Hexemer, A.; Weber, A. Z.; Segalman, R. A., Controlling Nafion Structure and Properties via Wetting Interactions. *Macromolecules* **2012,** *45*, 4681–4688.

347. Hoarfrost, M. L.; Tyagi, M. S.; Segalman, R. A.; Reimer, J. A., Effect of Confinement on Proton Transport Mechanisms in Block Copolymer/Ionic Liquid Membranes. *Macromolecules* **2012,** *45* (7), 3112–3120.

348. Berger, A.; Segalman, R. A.; Newman, J., Material requirements for membrane separators in a water-splitting photoelectrochemical cell. *Energy & Environmental Science* **2014,** *7* (4), 1468–1476.

349. Gu, Y.; Lodge, T. P., *Macromolecules* **2011,** *44* (7), 1732–1736.

350. Hoarfrost, M. L.; Segalman, R. A., Ionic Conductivity of Nanostructured Block Copolymer/Ionic Liquid Membranes. *Macromolecules* **2011,** *44* (13), 5281–5288.

351. Hoarfrost, M. L.; Tyagi, M.; Segalman, R. A.; Reimer, J. A., Proton Hopping and Long-Range Transport in the Protic Ionic Liquid [Im][TFSI], Probed by Pulsed-Field Gradient NMR and Quasi-Elastic Neutron Scattering. *Journal of Physical Chemistry B* **2012,** *116*, 8201–8209.

352. Jiang, Y.; Freyer, J. L.; Cotanda, P.; Brucks, S. D.; Killops, K. L.; Bandar, J. S.; Torsitano, C.; Balsara, N. P.; Lambert, T. H.; Campos, L. M., The evolution of cyclopropenium ions into functional polyelectrolytes. *Nat Commun* **2015,** *6*.

353. Sudre, G.; Inceoglu, S.; Cotanda, P.; Balsara, N. P., Influence of Bound Ion on the Morphology and Conductivity of Anion-Conducting Block Copolymers. *Macromolecules* **2013,** *46* (4), 1519–1527.

354. Beckingham, B. S.; Sanoja, G. E.; Lynd, N. A., Simple and Accurate Determination of Reactivity Ratios Using a Nonterminal Model of Chain Copolymerization. *Macromolecules* **2015,** *48* (19), 6922–6930.

355. Berger, A.; Segalman, R. A.; Newman, J., Material requirements for membrane separators in a water-splitting photoelectrochemical cell. *Energy Environ. Sci.* **2014,** *7* (4), 1468–1476.

356. Wijmans, J. G.; Baker, R. W., The Solution-Diffusion Model - a Review. *Journal of Membrane Science* **1995,** *107* (1-2), 1-21.

357. Kamcev, J.; Freeman, B. D., Charged Polymer Membranes for Environmental/Energy Applications. *Annual Review of Chemical and Biomolecular Engineering, Vol 7* **2016,** *7*, 111–133.

358. Reijerkerk, S. R.; Nijmeijer, K.; Ribeiro, C. P.; Freeman, B. D.; Wessling, M., On the effects of plasticization in CO_2/light gas separation using polymeric solubility selective membranes. *Journal of Membrane Science* **2011,** *367* (1–2), 33–44.

359. Soniat, M.; Tesfaye, M.; Brooks, D.; Merinov, B.; Goddard, W. A.; Weber, A. Z.; Houle, F. A., Predictive simulation of non-steady-state transport of gases through rubbery polymer membranes. *Polymer* **2018,** *134*, 125–142.

360. Soniat, M.; Houle, F. A., Swelling and Diffusion during Methanol Sorption into Hydrated Nafion. *The Journal of Physical Chemistry B* **2018,** *122* (34), 8255–8268.

361. Soniat, M.; Tesfaye, M.; Mafi, A.; Brooks, D. J.; Humphrey, N. D.; Weng, L. C.; Merinov, B.; Goddard, W. A.; Weber, A. Z.; Houle, F. A., Permeation of CO_2 and N_2 through glassy poly(dimethyl phenylene) oxide under steady- and presteady-state conditions. *Journal of Polymer Science* **2020,** *58* (9), 1207–1228.

362. Subramanian, S.; Heydweiller, J. C.; Stern, S. A., Dual-Mode Sorption Kinetics of Gases in Glassy-Polymers. *Journal of Polymer Science Part B-Polymer Physics* **1989,** *27* (6), 1209–1220.

363. Carter, B. M.; Dobyns, B. M.; Beckingham, B. S.; Miller, D. J., Multicomponent transport of alcohols in an anion exchange membrane measured by in-situ ATR FTIR spectroscopy. *Polymer* **2017,** *123*, 144–152.

364. Soniat, M.; Dischinger, S. M.; Weng, L.-C.; Martinez Beltran, H.; Weber, A. Z.; Miller, D. J.; Houle, F. A., Toward predictive permeabilities: Experimental measurements and multiscale simulation of methanol transport in Nafion. *Journal of Polymer Science* **2021,** *59* (7), 594–613.

365. Dischinger, S. M.; Gupta, S.; Carter, B. M.; Miller, D. J., Transport of Neutral and Charged Solutes in Imidazolium-Functionalized Poly(phenylene oxide) Membranes for Artificial Photosynthesis. *Industrial & Engineering Chemistry Research* **2020,** *59* (12), 5257–5266.

366. Carter, Blaine M.; Keller, L.; Wessling, M.; Miller, D. J., Preparation and characterization of crosslinked poly(vinylimidazolium) anion exchange membranes for artificial photosynthesis. *Journal of Materials Chemistry A* **2019,** *7* (41), 23818–23829.

367. Beckingham, B. S.; Lynd, N. A.; Miller, D. J., Monitoring multicomponent transport using in situ ATR FTIR spectroscopy. *Journal of Membrane Science* **2018,** *550*, 348–356.

368. Krödel, M.; Carter, B. M.; Rall, D.; Lohaus, J.; Wessling, M.; Miller, D. J., Rational Design of Ion Exchange Membrane Material Properties Limits the Crossover of CO_2 Reduction Products in Artificial Photosynthesis Devices. *ACS Applied Materials & Interfaces* **2020,** *12* (10), 12030–12042.

369. Bolton, J. R.; Strickler, S. J.; Connolly, J. S., Limiting and Realizable Efficiencies of Solar Photolysis of Water. *Nature* **1985,** *316* (6028), 495–500.

370. Parkinson, B., On the Efficiency and Stability of Photoelectrochemical Devices. *Accounts of Chemical Research* **1984,** *17* (12), 431–437.

371. Haussener, S.; Xiang, C. X.; Spurgeon, J. M.; Ardo, S.; Lewis, N. S.; Weber, A. Z., Modeling, simulation, and design criteria for photoelectrochemical water-splitting systems. *Energy & Environmental Science* **2012,** *5* (12), 9922–9935.

372. Haussener, S.; Hu, S.; Xiang, C. X.; Weber, A. Z.; Lewis, N. S., Simulations of the irradiation and temperature dependence of the efficiency of tandem photoelectrochemical water-splitting systems. *Energy & Environmental Science* **2013,** *6* (12), 3605–3618.

373. Chen, Y. K.; Xiang, C. X.; Hu, S.; Lewis, N. S., Modeling the Performance of an Integrated Photoelectrolysis System with 10x Solar Concentrators. *Journal of the Electrochemical Society* **2014,** *161* (10), F1101–F1110.

374. Xiang, C. X.; Chen, Y. K.; Lewis, N. S., Modeling an integrated photoelectrolysis system sustained by water vapor. *Energy & Environmental Science* **2013,** *6* (12), 3713–3721.

375. Fountaine, K. T.; Kendall, C. G.; Atwater, H. A., Near-unity broadband absorption designs for semiconducting nanowire arrays via localized radial mode excitation. *Optics Express* **2014,** *22* (9), A930–A940.

376. Shaner, M. R.; Fountaine, K. T.; Ardo, S.; Coridan, R. H.; Atwater, H. A.; Lewis, N. S., Photoelectrochemistry of core-shell tandem junction n-p(+)-Si/n-WO_3 microwire array photoelectrodes. *Energy & Environmental Science* **2014,** *7* (2), 779–790.

377. Hu, S.; Xiang, C. X.; Haussener, S.; Berger, A. D.; Lewis, N. S., An analysis of the optimal band gaps of light absorbers in integrated tandem photoelectrochemical water-splitting systems. *Energy & Environmental Science* **2013,** *6* (10), 2984–2993.

378. Jin, J.; Walczak, K.; Singh, M. R.; Karp, C.; Lewis, N. S.; Xiang, C. X., An experimental and modeling/simulation-based evaluation of the efficiency and operational performance characteristics of an integrated, membrane-free, neutral pH solar-driven water-splitting system. *Energy & Environmental Science* **2014,** *7* (10), 3371–3380.

379. Singh, M. R.; Xiang, C.; Lewis, N. S., Evaluation of flow schemes for near-neutral pH electrolytes in solar-fuel generators. *Sustainable Energy & Fuels* **2017,** *1* (3), 458–466.

380. Chen, Y. K.; Hu, S.; Xiang, C. X.; Lewis, N. S., A sensitivity analysis to assess the relative importance of improvements in electrocatalysts, light absorbers, and system geometry on the efficiency of solar-fuels generators. *Energy & Environmental Science* **2015,** *8* (3), 876–886.

381. Chen, Y.; Sun, K.; Audesirk, H.; Xiang, C.; Lewis, N., A Quantitative Analysis of the Efficiency of Solar-Driven Water-Splitting Device Designs Based on Tandem Photoabsorbers Patterned with Islands of Metallic Electrocatalysts. *Energy & Environmental Science* **2015,** *8*, 1736–1747.

382. Singh, M. R.; Stevens, J. C.; Weber, A. Z., Design of Membrane-Encapsulated Wireless Photoelectrochemical Cells for Hydrogen Production. *Journal of the Electrochemical Society* **2014,** *161* (8), E3283–E3296.

383. Stevens, J. C. W., A. Z., A Computational Study of Optically Concentrating, Solar-Fuels Generators from Annual Thermal- and Fuel-Production Efficiency Perspectives. *Journal of The Electrochemical Society* **2016,** *163*, H475–H484.

384. Xiang, C.; Weber, A. Z.; Ardo, S.; Berger, A.; Chen, Y.; Coridan, R.; Fountaine, K. T.; Haussener, S.; Hu, S.; Liu, R.; Lewis, N. S.; Modestino, M. A.; Shaner, M. M.; Singh, M. R.; Stevens, J. C.; Sun, K.; Walczak, K., Modeling, Simulation, and Implementation of Solar-Driven Water-Splitting Devices. *Angewandte Chemie International Edition* **2016,** *55* (42), 12974–12988.

385. Lobaccaro, P.; Singh, M. R.; Clark, E. L.; Kwon, Y.; Bell, A. T.; Ager, J. W., Effects of Temperature and Gas–liquid Mass Transfer on the Operation of Small Electrochemical Cells for the Quantitative Evaluation of CO_2 Reduction Electrocatalysts. *Physical Chemistry Chemical Physics* **2016,** *18*, 26777–26785.

386. Zhou, X. H.; Liu, R.; Sun, K.; Chen, Y. K.; Verlage, E.; Francis, S. A.; Lewis, N. S.; Xiang, C. X., Solar-Driven Reduction of 1 atm of CO_2 to Formate at 10% Energy-Conversion Efficiency by Use of a TiO_2-Protected III-V Tandem Photoanode in Conjunction with a Bipolar Membrane and a Pd/C Cathode. *Acs Energy Letters* **2016,** *1* (4), 764–770.

387. Chen, Y. K.; Lewis, N. S.; Xiang, C. X., Modeling and Simulation of the Spatial and Light-Intensity Dependence of Product Distributions in an Integrated Photoelectrochemical CO_2 Reduction System. *Acs Energy Letters* **2016,** *1* (1), 273–280.

388. Hashiba, H.; Weng, L.-C.; Chen, Y.; Sato, H. K.; Yotsuhashi, S.; Xiang, C.; Weber, A. Z., Effects of Electrolyte Buffer Capacity on Surface Reactant Species and the Reaction Rate of CO_2 in Electrochemical CO2 Reduction. *The Journal of Physical Chemistry C* **2018,** *122* (7), 3719–3726.

389. Higgins, D.; Hahn, C.; Xiang, C.; Jaramillo, T. F.; Weber, A. Z., Gas-Diffusion Electrodes for Carbon Dioxide Reduction: A New Paradigm. *ACS Energy Letters* **2019,** *4* (1), 317–324.

390. Singh, M. R.; Clark, E. L.; Bell, A. T., Effects of electrolyte, catalyst, and membrane composition and operating conditions on the performance of solar-driven electrochemical reduction of carbon dioxide. *Physical Chemistry Chemical Physics* **2015,** *17*, 18924–18936.

391. Lin, M.; Han, L.; Singh, M. R.; Xiang, C., An Experimental- and Simulation-Based Evaluation of the CO_2 Utilization Efficiency of Aqueous-Based Electrochemical CO_2 Reduction Reactors with Ion-Selective Membranes. *ACS Applied Energy Materials* **2019,** *2* (8), 5843–5850.

392. Weng, L. C.; Bell, A. T.; Weber, A. Z., Towards membrane-electrode assembly systems for CO_2 reduction: a modeling study. *Energy & Environmental Science* **2019,** *12* (6), 1950–1968.

393. Cheng, W.-H.; Richter, M. H.; May, M. M.; Ohlmann, J.; Lackner, D.; Dimroth, F.; Hannappel, T.; Atwater, H. A.; Lewerenz, H.-J., Monolithic Photoelectrochemical Device for Direct Water Splitting with 19% Efficiency. *ACS Energy Letters* **2018,** *3* (8), 1795–1800.

394. Verlage, E.; Hu, S.; Liu, R.; Jones, R. J. R.; Sun, K.; Xiang, C.; Lewis, N. S.; Atwater, H. A., A monolithically integrated, intrinsically safe, 10% efficient, solar-driven water-splitting system based on active, stable earth-abundant electrocatalysts in conjunction with tandem III–V light absorbers protected by amorphous TiO_2 films. *Energy & Environmental Science* **2015,** *8* (11), 3166–3172.

395. Sun, K.; Liu, R.; Chen, Y.; Verlage, E.; Lewis, N. S.; Xiang, C., A Stabilized, Intrinsically Safe, 10% Efficient, Solar-Driven Water-Splitting Cell Incorporating Earth-Abundant Electrocatalysts with Steady-State pH Gradients and Product Separation Enabled by a Bipolar Membrane. *Advanced Energy Materials* **2016,** *6* (13), 1600379.

396. Walczak, K. A.; Segev, G.; Larson, D. M.; Beeman, J. W.; Houle, F. A.; Sharp, I. D., Hybrid Composite Coatings for Durable and Efficient Solar Hydrogen Generation under Diverse Operating Conditions. *Advanced Energy Materials* **2017,** *7* (13), 1602791.

397. Kistler, T. A.; Agbo, P., Current loss analysis in photoelectrochemical devices. *APL Materials* **2020,** *8* (3), 031107.

398. Kistler, T. A.; Um, M. Y.; Agbo, P., Stable Photoelectrochemical Hydrogen Evolution for 1000 h at 14% Efficiency in a Monolithic Vapor-fed Device. *Journal of The Electrochemical Society* **2020,** *167* (6), 066502.

399. Walczak, K.; Chen, Y. K.; Karp, C.; Beeman, J. W.; Shaner, M.; Spurgeon, J.; Sharp, I. D.; Amashukeli, X.; West, W.; Jin, J.; Lewis, N. S.; Xiang, C. X., Modeling, Simulation, and Fabrication of a Fully Integrated, Acid-stable, Scalable Solar-Driven Water-Splitting System. *Chemsuschem* **2015,** *8* (3), 544–551.

400. Shaner, M. R.; McDowell, M. T.; Pien, A.; Atwater, H. A.; Lewis, N. S., Si/TiO_2 Tandem-Junction Microwire Arrays for Unassisted Solar-Driven Water Splitting. *Journal of the Electrochemical Society* **2016,** *163* (5), H261–H264.

401. Shaner, M. R.; McKone, J. R.; Gray, H. B.; Lewis, N. S., Functional integration of Ni-Mo electrocatalysts with Si microwire array photocathodes to simultaneously achieve high fill factors and light-limited photocurrent densities for solar-driven hydrogen evolution. *Energy & Environmental Science* **2015,** *8* (10), 2977–2984.

402. Kempler, P. A.; Coridan, R. H.; Lewis, N. S., Effects of bubbles on the electrochemical behavior of hydrogen-evolving Si microwire arrays oriented against gravity. *Energy & Environmental Science* **2020,** *13* (6), 1808–1817.

403. Yalamanchili, S.; Emmer, H. S.; Fountaine, K. T.; Chen, C. T.; Lewis, N. S.; Atwater, H. A., Enhanced Absorption and <1% Spectrum-and-Angle-Averaged Reflection in Tapered Microwire Arrays. *ACS Photonics* **2016,** *3* (10), 1854–1861.

404. Modestino, M. A.; Walczak, K. A.; Berger, A.; Evans, C. M.; Haussener, S.; Koval, C.; Newman, J. S.; Ager, J. W.; Segalman, R. A., Robust production of purified H_2 in a stable, self-regulating, and continuously operating solar fuel generator. *Energy & Environmental Science* **2014,** *7* (1), 297–301.

405. Gurudayal; Bullock, J.; Srankó, D. F.; Towle, C. M.; Lum, Y.; Hettick, M.; Scott, M. C.; Javey, A.; Ager, J., Efficient solar-driven electrochemical CO_2 reduction to hydrocarbons and oxygenates. *Energy & Environmental Science* **2017,** *10* (10), 2222–2230.

406. Gurudayal; Beeman, J. W.; Bullock, J.; Wang, H.; Eichhorn, J.; Towle, C.; Javey, A.; Toma, F. M.; Mathews, N.; Ager, J. W., Si photocathode with Ag-supported dendritic Cu catalyst for CO_2 reduction. *Energy & Environmental Science* **2019,** *12* (3), 1068–1077.

407. Gurudayal; Perone, D.; Malani, S.; Lum, Y.; Haussener, S.; Ager, J. W., Sequential Cascade Electrocatalytic Conversion of Carbon Dioxide to C–C Coupled Products. *ACS Applied Energy Materials* **2019,** *2* (6), 4551–4559.

408. Guchhait, A.; Dewi, H. A.; Leow, S. W.; Wang, H.; Han, G.; Suhaimi, F. B.; Mhaisalkar, S.; Wong, L. H.; Mathews, N., Over 20% Efficient CIGS–Perovskite Tandem Solar Cells. *ACS Energy Letters* **2017,** *2* (4), 807–812.

409. Monroe, M. M.; Lobaccaro, P.; Lum, Y.; Ager, J. W., Membraneless laminar flow cell for electrocatalytic CO_2 reduction with liquid product separation. *Journal of Physics D: Applied Physics* **2017,** *50* (15), 154006.

410. Han, L.; Zhou, W.; Xiang, C., High-Rate Electrochemical Reduction of Carbon Monoxide to Ethylene Using Cu-Nanoparticle-Based Gas Diffusion Electrodes. *ACS Energy Letters* **2018,** *3* (4), 855–860.

411. Cheng, W.-H.; Richter, M. H.; Sullivan, I.; Larson, D. M.; Xiang, C.; Brunschwig, B. S.; Atwater, H. A., CO_2 Reduction to CO with 19% Efficiency in a Solar-Driven Gas Diffusion Electrode Flow Cell under Outdoor Solar Illumination. *ACS Energy Letters* **2020,** *5* (2), 470–476.

412. Kistler, T. A.; Um, M. Y.; Cooper, J. K.; Sharp, I. D.; Agbo, P., Monolithic Photoelectrochemical CO_2 Reduction Producing Syngas at 10% Efficiency. *Advanced Energy Materials* **2021,** *11* (21), 2100070.

413. Digdaya, I. A.; Sullivan, I.; Lin, M.; Han, L.; Cheng, W.-H.; Atwater, H. A.; Xiang, C., A direct coupled electrochemical system for capture and conversion of CO_2 from oceanwater. *Nature Communications* **2020,** *11* (1), 4412.

414. Li, R.; Cheng, W.-H.; Richter, M. H.; DuChene, J. S.; Tian, W.; Li, C.; Atwater, H. A., Unassisted Highly Selective Gas-Phase CO_2 Reduction with a Plasmonic Au/p-GaN Photocatalyst Using H_2O as an Electron Donor. *ACS Energy Letters* **2021,** *6* (5), 1849–1856.

Bibliography of JCAP–Supported Publications

A complete list of JCAP publications is available at: http://solarfuelshub.org/publications.

2021

Abdelsamie, M., Li, T., Babbe, F., Xu, J., Han, Q., Blum, V., Sutter-Fella, C. M., Mitzi, D., Toney, M. Mechanism of Additive-Assisted Room-Temperature Processing of Metal Halide Perovskite Thin Films., *ACS Appl. Mater. Interfaces*, **13**, 13212–13225 https://doi.org/10.1021/acsami.0c22630 (2021).

Andriuc, O., Siron, M., Monatoya, J., Horton, M., Persson, K., Automated Adsorption Workflow for Semiconductor Surfaces and the Application to Zinc Telluride., *J. Chem. Inf. Model*, **61**, 3908–3916, DOI: https://doi.org/10.1021/acs.jcim.1c00340 (2021).

Baricuatro, J. H., Kwon, S., Kim, Y.-G., Cummins, K. D., Naserifar, S., Goddard, W. A. Operando Electrochemical Spectroscopy for CO on Cu(100) at pH 1 to 13: Validation of Grand Canonical Potential Predictions. *ACS Catal.*, **11**, 3173–3181, https://doi.org/10.1021/acscatal.0c05564 (2021).

Berger, E., Jamnuch, S., Uzundal, C., Woodhal, C., et al. Extreme Ultraviolet Second Harmonic Generation Spectroscopy in a Polar Metal. *Nano Lett.* **21**, 6095–6101, DOI: https://doi.org/10.1021/acs.nanolett.1c01502 (2021).

Buabthong, P., Evans, J., Rinaldi, K., Kennedy, K., Fu, H., Ifkovits, Z., Kuo, T.-J., Brunschwig, B., Lewis, N. GaAs Microisland Anodes Protected by Amorphous TiO_2 Films Mitigate Corrosion Spreading During Water Oxidation in Alkaline Electrolytes., *ACS Energy Lett.*, **6**, 3709–3714, DOI: https://doi.org/10.1021/acsenergylett.1c01174 (2021).

Buckley, A., Cheng, T., Oh, M., Su, G., Garrison, J., Utan, S., Zhu, C., Toste, D., Goddard, W., Toma, F. Approaching 100% Selectivity at Low Potential on Ag for Electrochemical CO_2 Reduction to CO Using a Surface Additive., *ACS Catal.* **11**, 9034–9042, DOI: https://doi.org/10.1021/acscatal.1c00830 (2021).

Bui, J. C., Kim, C., Weber, A., Bell, A. Dynamic Boundary Layer Simulation of Pulsed CO_2 Electrolysis on a Copper Catalyst. ACS Energy Lett., 6, https://doi.org/10.1021/acsenergylett.1c00364 (2021).

Cooper, J., Zhang, Z., Roychoudhury, S., jjiang, C.-M., Gul, S., Liu, Y.-S., Dhall, R., Ceballos, A., Yano, J., Prendergast, D., Reyes-Lillo, S. E. $CuBi_2O_4$: Electronic Structure, Optical Properties, and Photoelectrochemical Performance Limitations of the Photocathode., *Chem. Mater.*, **33**, 934–945, https://doi.org/10.1021/acs.chemmater.0c03930 (2021).

Corson, E. R., Creel, E., Kostecki, R., Urban, J., McCloskey, B. D. Effect of pressure and temperature on carbon dioxide reduction at a plasmonically active silver cathode. *Electrochimica Acta*, **374**, 137820, https://doi.org/10.1016/j.electacta.2021.137820 (2021).

Desai, D., Zviazhynski, B., Zhou, J., Bernardi, M. Magnetotransport in semiconductors and two-dimensional materials from first principles. *Phys. Pev. B* **103**, L161103, DOI: https://doi.org/10.1103/PhysRevB.103.L161103 (2021).

Eichhorn, J., Jiang, C.-M., Cooper, J., Sharp, I., Toma, F. Nanoscale Heterogeneities and Composition–Reactivity Relationships in Copper Vanadate Photoanodes. *ACS Appl. Mater. Interfaces* **13**, 23575–23583, DOI: https://doi.org/10.1021/acsami.1c01848 (2021).

Finke, C., Leandri, H., Karumb, E. T., Zheng, D., Hoffmann, M., Fromer, N. Economically advantageous pathways for reducing greenhouse gas emissions from industrial hydrogen under common, current economic conditions. *Energy Environ. Sci.* **14**, 1517–1529, https://doi.org/10.1039/D0EE03768K (2021).

Guerrero Vela, P., Polk, J., Richter, M., Lopez Ortega, A. Dynamic thermal behavior of polycrystalline LaB6 hollow cathodes., *J. Appl. Phys.* **130**, 083303, DOI: https://doi.org/10.1063/5.0058607 (2021).

Houle, F., Miles, R., Pollak, C., Reid, J. A purely kinetic description of the evaporation of water droplets., *J. Chem. Phys.*, **154**, 054501, https://doi.org/10.1063/5.0037967 (2021).

Ifkovits, Z., Evans, J., Meier, M., Papadantonakis, K., Lewis, N. Decoupled electrochemical water-splitting systems: a review and perspective. *Energy Environ. Sci.*, **14**, 4740–4759, DOI: DOI https://doi.org/10.1039/D1EE01226F (2021).

Jiang, H., Tao, X., Kammler, M., Ding, F., Wodtke, A., Kandratsenka, A., Miller, T., Bunermann, O. Small Nuclear Quantum Effects in Scattering of H and D from Graphene. *Phys. Chem. Lett.*, **12**, 1991–1996, https://doi.org/10.1021/acs.jpclett.0c02933 (2021).

Jiang, S., Link, A., Canning, D., Fooks, J. et al. Enhancing positron production using front surface target structures., *Applied Physics Letters*, **118**, 094101, https://doi.org/10.1063/5.0038222 (2021).

Kennedy, K. M., Kempler, P. A., Caban-Acevedo, M., Papadantonakis, K., Lewis, N. S. Primary Corrosion Processes for Polymer-Embedded Free-Standing or Substrate-Supported Silicon Microwire Arrays in Aqueous Alkaline Electrolytes. *Nano. Lett.*, **21**, 1056-1061, https://doi.org/10.1021/acs.nanolett.0c04298 (2021).

Kim, C., Cho, K., Park, K., Kim, J., Yun, G., Toma, F., Gereige, I., Jung, H. Cu/Cu_2O Interconnected Porous Aerogel Catalyst for Highly Productive Electrosynthesis of Ethanol from CO_2. *Advanced Functional Materials*, **31**, 2102142, DOI: https://doi.org/10.1002/adfm.202102142 (2021).

Kistler, T., Um, M., Cooper, J., Sharp, I., Agbo, P. Monolithic Photoelectrochemical CO_2 Reduction Producing Syngas at 10% Efficiency. *Adv. Mater.*, **11**, 2100070 DOI: https://doi.org/10.1002/aenm.202100070 (2021).

Koshy, D., Nathan, S., Asundi, A., Abdellah, A., Dull, S., Cullen, D., Higgins, D., Bao, Z., Bent, S., Jaramillo, T. Bridging Thermal Catalysis and Electrocatalysis: Catalyzing CO_2 Conversion with Carbon-Based Materials. *Angew Chem Int Ed Engl* **60**, *17472–17480*, DOI: https://doi.org/10.1002/anie.202101326 (2021).

Kwon, S., Kim, Y.-G., Baricuatro, J., Goddard, W. Dramatic Change in the Step Edges of the Cu(100) Electrocatalyst upon Exposure to CO: *Operando* Observations by Electrochemical STM and Explanation Using Quantum Mechanical Calculations., *ACS Catal*, **11**, 12068–12074, DOI: https://doi.org/10.1021/acscatal.1c02844 (2021).

Landers, A., koshy, D., Lee, S., Drisdell, W., Davis, R., Hahn, C., Mehta, A., Jaramillo, T. A refraction correction for buried interfaces applied to in situ grazing-incidence X-ray diffraction studies on Pd electrodes. *J. Synchrotron Rad.*, **28**, 919–923, DOI: https://doi.org/10.1107/S1600577521001557 (2021).

Landers, A., Peng, H., Koshy, D., Lee, S. H., Feaster, J., Lin, J., Beeman, J., Higgins, D., Yano, J., Drisdell, W., Davis, R., Bajdich, M., Abild-Pedersen, F., Mehta, A., Jaramillo, T., Hahn, C. Dynamics and Hysteresis of Hydrogen Intercalation and Deintercalation in Palladium Electrodes: A Multimodal *In Situ* X-ray Diffraction, Coulometry, and Computational Study. *Chem. Mater.*, **33**, 5872–5884, DOI: https://doi.org/10.1021/acs.chemmater.1c00291 (2021).

Lee, N., Chen, H., Zhou, J., Bernardi, M. Facile *ab initio* approach for self-localized polarons from canonical transformations. *Phys. Rev. Materials* **5**, 063805, DOI: https://doi.org/10.1103/PhysRevMaterials.5.063805 (2021).

Li, R., Cheng, W., Richter, M., DuChene, J., Tian, W., Li, C., Atwater, H. Unassisted Highly Selective Gas-Phase CO_2 Reduction with a Plasmonic Au/p-GaN Photocatalyst Using H_2O as an Electron Donor. *ACS Energy Lett.* **6**, 1849–1856, DOI: https://doi.org/10.1021/acsenergylett.1c00392 (2021).

Li, H., Yu, P., Lei, R., Yang, F., Wen, P., Ma, X., Zeng, G., Guo, J., Toma, F..M., Qiu, Y., Geyer, S..M., Wang, X., Cheng, T. and Drisdell, W. (2021), Facet-selective deposition of ultrathin Al_2O_3 on copper nanocrystals for highly stable CO_2 electroreduction to ethylene. *Angew. Chem. Int. Ed.*, DOI: https://doi.org/10.1002/anie.202109600 (2021).

Lindley, S., An, Q., Goddard, W., Cooper, J. Spatiotemporal Temperature and Pressure in Thermoplasmonic Gold Nanosphere–Water Systems. *ACS Nano*, **15**, 6276–6288 DOI: https://doi.org/10.1021/acsnano.0c09804 (2021).

Liu, G., Lee, M., Kwon, S., Zeng, G., Eichhorn, J., Bucklet, A., Toste, D., Goddard, W., Toma, F. CO_2 reduction on pure Cu produces only H_2 after subsurface O is depleted: Theory and experiment. *PNAS*, **118**, e2012649118, DOI: https://doi.org/10.1073/pnas.2012649118 (2021).

Liu, Y., Qiu, H., Li, J., Guo, L., Ager, J. Tandem Electrocatalytic CO_2 Reduction with Efficient Intermediate Conversion over Pyramid-Textured Cu–Ag Catalysts. *ACS Appl. Mater. Interfaces* **13**, 40513–40521, DOI: https://doi.org/10.1021/acsami.1c08688 (2021).

Molina-Ruiz, M., Rosen, J., Jacks, H. C., Abernathy, M. R., Metcalf, T. H., Liu, X., DuBois, J. L., Hellman, F. Origin of mechanical and dielectric losses from two-level systems in amorphous silicon. *Phys. Rev. Materials*, **5**, 035601, https://doi.org/10.1103/PhysRevMaterials.5.035601 (2021).

Nishimura, Y., Peng, H.-J., Nitopi, S., Bajdich, M., Wang, L., Morales-Guio, G., Abild-Pedersen, F., Jaramillo, T., Hahn, C. Guiding the Catalytic Properties of Copper for Electrochemical CO_2 Reduction by Metal Atom Decoration., *ACS Appl. Mater. Interfaces*, DOI: https://doi.org/10.1021/acsami.1c09128 (2021).

Nunez, P., Caban-Acevedo, M., Yu, W., Richter, M., Kennedy, K., Villarino, A., Brunschwig, B., Lewis, N. Origin of the Electrical Barrier in Electrolessly Deposited Platinum Nanoparticles on p-Si Surfaces. *J. Phys. Chem. C*, **125**, 17660–17670, DOI: https://doi.org/10.1021/acs.jpcc.1c03072 (2021).

Otto, L., Gaulding, A., Chen, C., Kuykendall, T., Hammack, A., Toma, F., Ogletree, F., Aloni, S., Stadler, J., Schwartzberg, A. Methods for tuning plasmonic and photonic optical resonances in high surface area porous electrodes. *Nature Scientific Reports*, **11**, 7656, DOI: https://doi.org/10.1038/s41598-021-86813-y (2021).

Ozden, A., Wang, Y., Li, F., Luo, M., Sisler, J., Thevenon, A., Rosas-Hernandez, A., Burdyny, T., Lum, Y., Yedegari, H., Gapie, T., Peters, J., Sargent, E., Sinton, D. Cascade CO_2 electroreduction enables efficient carbonate-free production of ethylene. *Joule*, **5**, 706–719, https://doi.org/10.1016/j.joule.2021.01.007 (2021).

Peng, H., Tang, M., Liu, X., Lamoureux, F. S., Bajdich, M., Abild-Pedersen, F. The role of atomic carbon in directing electrochemical CO(2) reduction to multicarbon products. *Energy Environ. Sci.*, **14**, 473–482, https://doi.org/10.1039/D0EE02826F (2021).

Richter, M., Cheng, W.-H., Crumlin, E., Drisdell, W., Atwater, H. A., Schmeiser, D., Lewis, N., Brunschwig, B. S. X-ray Photoelectron Spectroscopy and Resonant X-ray Spectroscopy Investigations of Interactions between Thin Metal Catalyst Films and Amorphous Titanium Dioxide Photoelectrode Protection Layers. *Chem. Mater.*, **33**, 1265–1275, https://doi.org/10.1021/acs.chemmater.0c04043 (2021).

Richter, M., Peterson, E., Zhou, L., Shinde, A., Newhouse, P., Yan, Q., Fackler, S., Yano, J., Cooper, J., Persson, K. Band Edge Energy Tuning through Electronic Character Hybridization in Ternary Metal Vanadates., *Chem. Mater.*, **33**, 7242–7253, DOI: https://doi.org/10.1021/acs.chemmater.1c01415 (2021).

Schwartz, G., Raj, S., Jamnuch, S., et al., Angstrom-Resolved Interfacial Structure in Buried Organic-Inorganic Junctions., *Phys. Rev. Lett.*, **12**, 096801, DOI: https://doi.org/10.1103/PhysRevLett.127.096801 (2021).

Shi, Y., Ilic, O., Atwater, H., Greer, J. All-day fresh water harvesting by microstructured hydrogel membranes. *Nature Communications*, **12**, 2797, DOI: https://doi.org/10.1038/s41467-021-23174-0 (2021).

Soniat, M., Dischinger, S., Weng, L.-C., Beltran, H. M., Weber, A. Z., Miller, D. J., Houle, F. A. Toward predictive permeabilities: Experimental measurements and multiscale simulation of methanol transport in Nafion., *J. Polym Sci.*, **59**, 594–613, https://doi.org/10.1002/pol.20200771 (2021).

Thevenon, A., Rosas-Hernandez, A., Herros, A., Agapie, T., Peters, J. Dramatic HER Suppression on Ag Electrodes via Molecular Films for Highly Selective CO_2 to CO Reduction. *ACS Catal.*, **11**, 4530–4537, DOI: https://doi.org/10.1021/acscatal.1c00338 (2021).

Wang, J., Cheng, T., Fenwick, A., Baroud, T., Rosas-Hernandez, A., Ko, J. H., Gan, Q., Goddard, W. A., Grubbs, R. H. Selective CO_2 Electrochemical Reduction Enabled by a Tricomponent Copolymer Modifier on a Copper Surface. *J. Am. Chem. Soc.*, **143**, 2857–2865, https://doi.org/10.1021/jacs.0c12478 (2021).

Wang, L., Peng, H., Lamaison, S., Qi, Z., Koshy, D., Stevens, M., Wakerley, D., Zeledon, J., King, L., Zhou, L., Lai, Y., Fontecave, M., Gregoire, J., Abild-Pedersen, F., Jaramillo, T., Hahn, C. Bimetallic effects on Zn-Cu electrocatalysts enhance activity and selectivity for the conversion of CO_2 to CO. *Chem Catalysis*, **1**, 663–680, DOI: https://doi.org/10.1016/j.checat.2021.05.006 (2021).

Wen, Y., Chen, P., Wang, L., Li, S., Wang, Z., Abed, J., Mao, X., Min, Y., Dinh, C., Luna, P., Huang, R., Zhang, L., Wang, L., Wang, L., Nielsen, R., Li, H. Zhuang, T., Ke, O., Voznyy, O., Hu, Y., Li, Y., Goddard, W., Zhang, B., Peng, H., Sargent, E. Stabilizing Highly Active Ru Sites by Suppressing Lattice Oxygen Participation in Acidic Water Oxidation. *J. Am. Chem. Soc.* **143**, 6482–6490, DOI: https://doi.org/10.1021/jacs.1c00384 (2021).

Yang, L., Haber, J., Amstrong, Z., Yang, S., Kan, K., Zhou, L., Richter, M., Roat, C., Wagner, N., Coram, M., Berndl, M., Riley, P., Gregoire, J. Discovery of complex oxides via automated experiments and data science., *PNAS*, **118**, e2106042118, DOI: https://doi.org/10.1073/pnas.2106042118 (2021).

Ye, Y., Su, H., Lee, K., Larson, D., Valero-Vidal, C., Blum, M. A., Yano, J., Crumlin, E. Carbon Dioxide adsorption and activation on Gallium Phosphide surface monitored by ambient pressure X-ray photoelectron spectroscopy. *J. Phys. D: Applied Physics*,**54**, DOI: http://iopscience.iop.org/article/10.1088/1361-6463/abec0a (2021).

Yu, W., Richter, M., Simonaoff, E., Brunschwig, B., Lewis, N. Investigations of the Stability of GaAs for Photoelectrochemical H2 Evolution in Acidic or Alkaline Aqueous Electrolytes., *J. Mater. Chem.* A, DOI: https://doi.org/10.1039/D1TA04145B (2021).

Zhou, J., Park, J., Lu, I., Maliyov, I., Tong, X., Bernardi, M. Perturbo: A software package for *ab initio* electron–phonon interactions, charge transport and ultrafast dynamics. *Computer Physics Communications*, **264**, 107970, DOI: https://doi.org/10.1016/j.cpc.2021.107970 (2021).

Zhou, Y., Gao, G., Chu, W., Wang, L. Transition-metal single atoms embedded into defective BC3 as efficient electrocatalysts for oxygen evolution and reduction reactions. *Nanoscale*, **13**, 1331–1339, DOI: https://doi.org/10.1039/D0NR07580A (2021).

Zhou, Y. Li, J., Gao, X., Chu, W., Gao, G., Wang, L.-W. Recent advances in single-atom electrocatalysts supported on two-dimensional materials for the oxygen evolution reaction. *J. Mater. Chem.* A, **9**, 9979–9999, DOI: https://doi.org/10.1039/D1TA00154J (2021).

2020

Agbo, P. Transparent Dual-Conductivity Membrane Composites as Current Distributors for Diffuse Electrocatalysts. *ACS Appl. Energy Mater.* **3**, 12284–12290 DOI: 10.1021/acsaem.0c02339 (2020).

Agbo, P. *J–V* Decoupling: Independent Control over Current and Potential in Electrocatalysis. *J. Phys. Chem. C*, **124**, 28387–28394, https://doi.org/10.1021/acs.jpcc.0c08142 (2020).

Babbe, F., Sutter-Fella, C. Optical Absorption-Based In Situ Characterization of Halide Perovskites. *Adv. Mater.*, **10**, 1903587 DOI: 10.1002/aenm.201903587 (2020).

Babbe, F., Masquelier, E., Zheng, Z., Sutter-Fella, C. Multi stage and illumination dependent segregation in $MAPb(I,Br)_3$. *SPIE Organic Photonics + Electronics Proceedings Volume 11474*, DOI: https://doi.org/10.1117/12.2568995 (2020).

Babbe, F., Masquelier, E., Zheng, Z., Sutter-Fella, C., Flash Formation of I-Rich Clusters during Multistage Halide Segregation Studied in $MAPbI_{1.5}Br_{1.5}$. *J. Phys. Chem. C*, **124**, 24608–24615, DOI: 10.1021/acs.jpcc.0c07063 (2020).

Baricuatro, J., Kim, Y.-G., Korzeniewski, C., Soriaga, M. Tracking the prelude of the electroreduction of carbon monoxide via its interaction with Cu(100): Studies by operando scanning tunneling microscopy and infrared spectroscopy. *Catalysis Today*, **358**, 210–214 DOI: https://doi.org/10.1016/j.cattod.2020.01.028 (2020).

Baricuatro, J., Kim, Y., Tsang, C., Javier, A., Cummins, K., Hemminger, J. Selective conversion of CO into ethanol on Cu(511) surface reconstructed from Cu(pc): *Operando* studies by electrochemical scanning tunneling microscopy, mass spectrometry, quartz crystal nanobalance, and infrared spectroscopy. *J. Electroanalytical Chemistry 857, 113704*, DOI: https://doi.org/10.1016/j.jelechem.2019.113704 (2020).

Borgwardt, M., Mahl, J., Roth, F., Wenthaus, L., Brausche, F., Blum, M., Schwarzburg, K., Liu, G., Toma, F., Gerssner, O. Photoinduced Charge Carrier Dynamics and Electron Injection Efficiencies in Au Nanoparticle-Sensitized TiO_2 Determined with Picosecond Time-Resolved X-ray Photoelectron Spectroscopy. *J. Phys. Chem. Lett.*, **11**, 5476, DOI: https://doi.org/10.1021/acs.jpclett.0c00825 (2020).

Buabthong, P., Ifkovits, Z., Kempler, P., Chen, Y., Nunez, P., Brunschwig, B., Papadantonakis, K., Lewis, N. Failure modes of protection layers produced by atomic layer deposition of amorphous TiO_2 on GaAs anodes. *Energy Environ. Sci.* **13**, 4269–4279, https://doi.org/10.1039/D0EE02032J (2020).

Bui, J., Digdaya, I., Xiang, C., Bell, A., Weber, A. Understanding Multi-Ion Transport Mechanisms in Bipolar Membranes. *ACS Appl. Mater. Interfaces*, **12**, 52509–52526, DOI: 10.1021/acsami.0c12686 (2020).

Chapovetsky, A., Liu, J., Welborn, M., Luna, J., Do, T., Haiges, R., Miller, T., Marinescu, S. Electronically Modified Cobalt Aminopyridine Complexes Reveal an Orthogonal Axis for Catalytic Optimization for CO_2 Reduction, *Inorg. Chem.*, **59**, 13709–13718, DOI: 10.1021/acs.inorgchem.0c02086 (2020).

Chen, Y. Bai, Y., Zhao, W., Ament, S., Gregoire, J., Gomes, C. Deep Reasoning Networks for Unsupervised Pattern De-mixing with Constraint Reasoning. *Proceedings of the 37th International Conference on Machine Learning*, **PMLR 119**:1500–1509, http://proceedings.mlr.press/v119/chen20a.html (2020).

Chen, Y., Cheng, T., Goddard, W. Atomistic Explanation of the Dramatically Improved Oxygen Reduction Reaction of Jagged Platinum Nanowires, 50 Times Better than Pt. *J. Am. Chem. Soc.* **142**, 8625–8632, DOI: https://doi.org/10.1021/jacs.9b13218 (2020).

Chen, Y., Xiang, C., Lewis, N. Modeling the Performance of A Flow-Through Gas Diffusion Electrode for Electrochemical Reduction of CO or CO_2. *J. Electrochemical Society* **167**, DOI: http://iopscience.iop.org/10.1149/1945-7111/ab987a (2020).

Cheng, W.-H., Richter, M., Sullivan, I., Larson, D., Xiang, C., Brunschwig, B., Atwater, H. CO_2 Reduction to CO with 19% Efficiency in a Solar-Driven Gas Diffusion Electrode Flow Cell under Outdoor Solar Illumination. *ACS Energy Lett.* **5**, 470–476, DOI: 10.1021/acsenergylett.9b02576 (2020).

Chiu, Y.-H., Lindley, S., Tsao, C.-W., Kuo, M.-Y., Cooper, J., Hsu, Y.-J., Zhang, J. Z., Hollow Au Nanosphere-Cu_2O Core-Shell Nanostructures with Controllable Core Surface Morphology. *J. Phys. Chem. C* **124**, 11333–11339, DOI: https://doi.org/10.1021/acs.jpcc.0c02214 (2020).

Choi, C., Kwon, S., Cheng, T., Xu, M., Tieu, P., Lee, C., Cai, J., Lee, H., Pan, X., Duan, X., Goddard, W., and Huang, Y. Highly active and stable stepped Cu surface for enhanced electrochemical CO_2 reduction to C_2H_4, *Nature Catalysis* **3**, 804–812, DOI: https://doi.org/10.1038/s41929-020-00504-x (2020).

Corson, E., Creel, E., Kostecki, R., McCloskey, B., Urban, J. Important Considerations in Plasmon-Enhanced Electrochemical Conversion at Voltage-Biased Electrodes. *iScience*, **23**, 100911 DOI: 10.1016/j.isci.2020.100911 (2020).

Corson, E., Kas, R., Kostecki, R., Urban, J., Smith, W., McCloskey, B., Kortlever, R. In Situ ATR–SEIRAS of Carbon Dioxide Reduction at a Plasmonic Silver Cathode. *J. Am. Chem. Soc.* **142**, 11750–11762, DOI: https://doi.org/10.1021/jacs.0c01953 (2020).

Corson, E., Subramani, A., Cooper, J., Kostecki, R., Urban, J., McCloskey, B. Reduction of Carbon Dioxide at a Plasmonically Active Copper-Silver Cathode. *Chem. Commun.* **56**, 9970–9973, DOI: https://doi.org/10.1039/D0CC03215H (2020).

Digdaya, I., Sullivan, I., Lin, M., Han, L., Cheng, W.-H., Atwater, H., Xiang, C. A direct coupled electrochemical system for capture and conversion of CO_2 from oceanwater, *Nature Communications*, **11**, 4412, DOI: https://doi.org/10.1038/s41467-020-18232-y (2020).

De Riccardis, A., Lee, M., Kazantsev, R., Garza, A., Zeng, G., Larson, D., Clark, E., Labaccaro, P., Burroughs, P., Bloise, E., Ager, J., Bell, A., Head-Gordon, M., Mele, G., Toma, F. Heterogenized Pyridine-Substituted Cobalt (II) Phthalocyanine Yeilds Reduction of CO_2 by Tuning the Electron Affinity of the Co Center. *ACS Appl. Mater. Interfaces*, **12**, 5251, DOI: https://doi.org/10.1021/acsami.9b18924 (2020).

Diederichsen, K. and McCloskey, B. Electrolyte additives to enable nonaqueous polyelectrolyte solutions for lithium ion batteries. *Molecular Systems Design & Engineering* **5**, 91–96, DOI: 10.1039/C9ME00067D (2020).

DuChene, J., Tagliabue, G., Welch, A., Li, X., Cheng, W.-H., Atwater, H. Optical Excitation of a Nanoparticle Cu/p-NiO Photocathode Improves Reaction Selectivity for CO_2 Reduction in Aqueous Electrolytes. *Nano Lett*. **20**, 2348–2358, DOI: 10.1021/acs.nanolett.9b04895 (2020).

Ebaid, M., Jiang, K., Zhang, Z., Drisdell, W., Bell, A., Cooper, J. Production of C2/C3 Oxygenates from Planar Copper Nitride-Derived Mesoporous Copper via Electrochemical Reduction of CO_2. *Chem. Mater.* **32**, 3304–3311, DOI: 10.1021/acs.chemmater.0c00761 (2020).

Ebaid, M., Larson, D., Bustillo, K., Turner, J., Cooper, J. Saw-Tooth Heat-Cycling Nitridation of Metallic Cu Yields First Photoactive p-Cu_3N for PEC Applications. *ACS Appl. Energy Mater*. **3**, 10714–10721, DOI: 10.1021/acsaem.0c01754 (2020).

Eichhorn, J., Reyes-Lillo, S., Roychoudhury, S., Sallis, S., Weis, J., Larson, D., Cooper, J., Sharp, I., Prendergast, D., Toma, F. Revealing Nanoscale Chemical Heterogeneities in Polycrystalline Mo-$BiVO_4$ Thin Films. *Small*, **16**, e2001600, DOI: https://doi.org/10.1002/smll.202001600 (2020).

Ferrah, D., Tieu, P. Controllable Growth of Copper on TiO2 Nanoparticles by Photodeposition Based on Coupled Effects of Solution Viscosity and Photoreduction Rate for Catalysis-Related Applications. *ACS Appl.Nano Mater*., **3**, 5855, DOI: https://doi.org/10.1021/acsanm.0c01015 (2020).

Flores Espinosa, M., Cheng, T., Xu, M., Abatemarco, L., Choi, C., Pan, X., Goddard, W., Zhao, Z., Huang, Y. Compressed Intermetallic PdCu for Enhanced Electrocatalysis. *ACS Energy Lett*. **5**, 3672–3680, DOI: 10.1021/acsenergylett.0c01959 (2020).

Fu, J.-H., Lu, A.-Y., Madden, N., Wu, C., Chen, Y.-C., Chiu, M.-H., Hattar, K., Krogstad, J., Chou, S., Li, L.-J., Kong, J., Tung, V. Additive manufacturing assisted van der Waals integration of 3D/3D hierarchically functional nanostructures. *Comm. Materials*, **1**, 42 DOI: https://doi.org/10.1038/s43246-020-0041-2 (2020).

Fu, J.-H., Moreno-Hernandez, I., Buabthong, P., Papadantonakis, K., Brunschwig, B., Lewis, N. Enhanced Stability of Silicon for Photoelectrochemical Water Oxidation Through Self-Healing Enabled by an Alkaline Protective Electrolyte. *Energy.Environ. Sci*. **13**, 4132–4141, https://doi.org/10.1039/D0EE02250K (2020).

Gai, Y., Tang, G., Gao, G., Wang, L.-W. Thermodynamic Full Landscape Searching Scheme for Identifying the Mechanism of Electrochemical Reaction: A Case Study of Oxygen Evolution on Fe- and Co-Doped Graphene–Nitrogen Sites. *J. Phys. Chem. A*, **124**, 5444–5455DOI: https://doi.org/10.1021/acs.jpca.0c02449 (2020).

Garg, S., Li, M., Weber, A., Ge, L., Li, L., Rudolph, V., Wang, G., Rufford, T. Advances and challenges in electrochemical CO_2 reduction processes: an engineering and design perspective looking beyond new catalyst materials. *J. Mater. Chem.* A, **8**, 1511–1544, DOI: https://doi.org/10.1039/C9TA13298H (2020).

Gauthier, J., Chen., L., Bajdich, M., Chan, K. Implications of the fractional charge of hydroxide at the electrochemical interface. *Phys. Chem. Chem. Phys*. **22**, 6964–6969, DOI: 10.1039/C9CP05952K (2020).

Ge, L., Yuan, H., Min, Y., Li, L., Chen, S., Xu, L., Goddard, W. Predicted Optimal Bifunctional Electrocatalysts for Both HER and OER Using Chalcogenide Heterostructures Based on Machine Learning Analysis of In Silico Quantum Mechanics Based High Throughput Screening. *J. Phys. Chem. Lett*. **11**, 869–876, DOI: 10.1021/acs.jpclett.9b03875 (2020).

Goddard, W. New Quantum Mechanics Based Methods for Multiscale Simulations with Applications to Reaction Mechanisms for Electrocatalysis. *Top Catal*. **63**, 1658–1666, https://doi.org/10.1007/s11244-020-01369-x (2020).

Hahn, C., and Jaramillo, T. Using Microenvironments to Control Reactivity in CO_2 Electrocatalysis. *Joule*, **4**, 292–294, DOI: 10.1016/j.joule.2020.01.017 (2020).

Heenen, H., Gauthier, J., Kristoffersen, H., T. Ludwig, T., Chan, K. Solvation at metal/water interfaces: An *ab initio* molecular dynamics benchmark of common computational approaches. *J. Chem. Phys*. **152**, 144703, DOI: https://doi.org/10.1063/1.5144912 (2020).

Hossain, M. D., Huang, Y., Yu, T., Goddard, W., Luo, Z. Reaction mechanism and kinetics for CO_2 reduction on nickel single atom catalysts from quantum mechanics. *Nature Commun*. **11**, 2256, DOI: https://doi.org/10.1038/s41467-020-16119-6 (2020).

Jeong, H., Kwon, Y., Won, J. H., Lum, Y., Cheng, M.-J., Kim, K., Head-Gordon, M., Kang, J. Atomic-Scale Spacing between Copper Facets for the Electrochemical Reduction of Carbon Dioxide. *Adv. Energy Mater. 10, 1903423*, DOI: https://doi.org/10.1002/aenm.201903423 (2020).

Ji, W., Allen, T., Yang, X., Zeng, G., De Wolf, S., Javey, A. Polymeric Electron-Selective Contact for Crystalline Silicon Solar Cells with an Efficiency Exceeding 19%. *ACS Energy Lett.* **5**, 897-902, DOI: 10.1021/acsenergylett.0c00110 (2020).

Jiang, K., Huang, Y., Zeng, G., Toma, F., Goddard, W., Bell, A. Effects of Surface Roughness on the Electrochemical Reduction of CO_2 over Cu. *ACS Energy Lett.*, **5**, 1206–1214, DOI: 10.1021/acsenergylett.0c00482 (2020).

Kempler, P., Coridan, R., Lewis, N. Effects of Bubbles on the Electrochemical Behavior of Hydrogen-Evolving Si Microwire Arrays Oriented Against Gravity. *Energy Environ. Sci.* **13**, 1808–1817, DOI: https://doi.org/10.1039/D0EE00356E (2020).

Kempler, P., Richter, M., Cheng, W.-H., Brunschwig, B., Lewis, N. Si Microwire-Array Photocathodes Decorated with Cu Allow CO_2 Reduction with Minimal Parasitic Absorption of Sunlight. *ACS Energy Lett.*, **5**, 2528, DOI: https://doi.org/10.1021/acsenergylett.0c01334 (2020).

Kempler, P., Ifkovits, Z., Yu, W., Carim, A., Lewis, N. Optical and electrochemical effects of H_2 and O_2 bubbles at upward-facing Si photoelectrodes. *Energy Environ. Sci.* **14**, 414–423, DOI: 10.1039/D0EE02796K (2020).

Kim, C., Weng, L.-C., Bell, A. Impact of Pulsed Electrochemical Reduction of CO_2 on the Formation of C_{2+} Products over Cu. *ACS Catal.* **10**, 12403–12413, https://doi.org/10.1021/acscatal.0c02915 (2020).

Kim, D., Yu, S., Zheng, F., Roh, I., Li, Y., Louisia, S., Qi, Z., Somorjai, G., Frei, H., Wang, L.-W., Yang, P. Selective CO_2 electrocatalysis at the pseudocapacitive nanoparticle/ordered-ligand interlayer. *Nature Energy*, **5**, 1032–1042, https://doi.org/10.1038/s41560-020-00730-4 (2020).

Kistler, T., Agbo, P. Current loss analysis in photoelectrochemical devices. *APL Materials*, **STF2020**, 031107, DOI: 10.1063/1.5142561@apm.2020.STF2020.issue-1 (2020).

Kistler, T., Um, M., Agbo, P. Stable Photoelectrochemical Hydrogen Evolution for 1000 h at 14% Efficiency in a Monolithic Vapor-fed Device. *J. Electro. Soc.* **167**, 066502, DOI: https://doi.org/10.1149/1945-7111/ab7d93 (2020).

Koshy, D., Chen, S., Lee, D., Stevens, M., Abdellah, A., Dull, S., Chen, G., Norlund, D., Gallo, A., Hahn, C., Higgins, D., Bao, Z., Jaramillo, T. Understanding the Origin of Highly Selective CO_2 Electroreduction to CO on Ni, N-doped Carbon Catalysts. *Angew Chem Int Ed Engl* **59**, 4043–4050, DOI:10.1002/ange.201912857 (2020).

Koshy, D. M., Landers, A. T., Cullen, D. A., Ievlev, A. V., Meyer, H. M., Hahn, C., Bao, Z., Jaramillo, T. F., Direct Characterization of Atomically Dispersed Catalysts: Nitrogen-Coordinated Ni Sites in Carbon-Based Materials for CO_2 Electroreduction. *Adv. Energy Mater.* **10**, 2001836. https://doi.org/10.1002/aenm.202001836 (2020).

Lee, M., De Riccardis, A., Kazantsev, R., Cooper, J., Buckley, A., Burroughs, P., Larson, D., Mele, G., Toma, F. Aluminum Metal Organic Framework Triggers Carbon Dioxide Reduction Activity. *ACS Appl. Energy Mater.*, **3**, 1286–1291, DOI: https://doi.org/10.1021/acsaem.9b02210 (2020).

Lee, S. H., Sullivan, I., Larson, D., Liu, G., Toma, F., Xiang, C., Drisdell, W. Correlating Oxidation State and Surface Area to Activity from *Operando* Studies of Copper CO Electroreduction Catalysts in a Gas-Fed Device. *ACS Catal.* **10**, 8000, DOI: https://doi.org/10.1021/acscatal.0c01670 (2020).

Lin, Y.-R., Cheng, W.-H., Richter, M., DuChene, J., Peterson, E., Went, C. Balushi, Z., Jariwala, D., Neaton, J., Chen, L.-C., Atwater, H. Band Edge Tailoring in Few-layer Two-dimensional Molybdenum Sulfides/Selenides Alloys. *J. Phys. Chem. C* **124**, 22893–22902, DOI: 10.1021/acs.jpcc.0c04719 (2020).

Loipersberger, M., Zee, D., Panetier, J., Chang, C., Long, J., Head-Gordon, M. Computational Study of an Iron(II) Polypyridine Electrocatalyst for CO_2 Reduction: Key Roles for Intramolecular Interactions in CO2 Binding and Proton Transfer. *Inorg. Chem.* **59**, 8146–8160, DOI: https://doi.org/10.1021/acs.inorgchem.0c00454 (2020).

Ludwig, T., Gauthier, J., Dickens, C., Brown, K., Ringe, S., Chan, K., Norskov, J. Atomistic Insight into Cation Effects on Binding Energies in Cu-Catalyzed Carbon Dioxide Reduction. *J. Phys. Chem. C*, **124**, 24765–24775, DOI: 10.1021/acs.jpcc.0c07004 (2020).

Morena-Hernandez, I., Yalamanchili, S., Fu, H., Atwater, H., Brunschwig, B., Lewis, N. Conformal SnO_x heterojunction coatings for stabilized photoelectrochemical water oxidation using arrays of silicon microcones. *J. Mater. Chem. A* **8**, 9292, DOI: https://doi.org/10.1039/D0TA01144D (2020).

Naserifar, S., Chen, Y., Kwon, S., Xiao, H., Goddard, W. Artificial Intelligence and QM/MM with a Polarizable Reactive Force Field for Next-Generation Electrocatalysts. *Matter*, **4**, 195–216, DOI: https://doi.org/10.1016/j.matt.2020.11.010 (2020).

Newhouse, P., Gueverra, D., Zhou, L., Wang, Y., Umehara, M., Boyd, D., Gregoire, J., Haber, J. Enhanced Bulk Transport in Copper Vanadate Photoanodes Identified by Combinatorial Alloying. *Matter* **3**, 1601–1613, https://doi.org/10.1016/j.matt.2020.08.032 (2020).

Newhouse, P., Zhou, L., Umehara, M., Boyd, D., Soedarmadji, E., Haber, J., Gregoire, J. Bi Alloying into Rare Earth Double Perovskites Enhances Synthesizability and Visible Light Absorption. *ACS Comb. Sci.* 22, 895–901, DOI: 10.1021/acscombsci.0c00177 (2020).

Oh, S., Bisbey, R., Gul, S., Yano, J., Fisher, G., Surendranath, Y. N-Heterocyclic Linkages are Produced from Condensation of Amidines onto Graphitic Carbon, *Chem. Mater.*, 32, 8512–8521, https://doi.org/10.1021/acs.chemmater.0c02664 (2020).

Ozden, A., Li, F., de Arquer, P., Rosas-Hernandez, A., Thevenon, A., Wang, Y., Hung, S.-F., Wang, X., Chen, B., Li, J., Wicks, J., Luo, M., Wang, Z., Agapie, T., Peters, J., Sargent, E., Sinton, D. High-Rate and Efficient Ethylene Electrosynthesis Using a Catalyst/Promoter/Transport Layer. *ACS Energy Lett.*, **5**, 2811–2818, DOI: https://doi.org/10.1021/acsenergylett.0c01266 (2020).

Resasco, J.; Bell, A. Electrocatalytic CO_2 Reduction to Fuels: Progress and Opportunities. T*rends in Chemistry*, 2, 825–836, DOI: https://doi.org/10.1016/j.trechm.2020.06.007 (2020).

Ribson, R., Choi, G., Hadt, R., Agapie, T. Controlling Singlet Fission with Coordination Chemistry-Induced Assembly of Dipyridyl Pyrrole Bipentacenes. *ACS Cent. Sci.*, **6**, 2088–2096, DOI: 10.1021/acscentsci.0c01044 (2020).

Richter, M., Lublow, M., Papadantonakis, K., Lewis, N., Lewerenz, H.-J. Genesis and Propagation of Fractal Structures During Photoelectrochemical Etching of n-Silicon. *ACS Appl. Mater. Interfaces*, **12**, 17018–17028, DOI:10.1021/acsami.9b22900 (2020).

Ringe, S., Morales-Guio, C.G., Chen, L.D. *et al.* Double layer charging driven carbon dioxide adsorption limits the rate of electrochemical carbon dioxide reduction on Gold. *Nat. Commun.* **11**, 33, DOI:10.1038/s41467-019-13777-z (2020).

Rohr, B., Stain, H., Guevarra, D., Wang, Y., Haber, J., Aykol, M., Suram, S., Gregoire, J. Benchmarking the acceleration of materials discovery by sequential learning. *Chem. Sci.* **11**, 2696–2706, DOI: 10.1039/C9SC05999G (2020).

Sato, S., McNicholas, B., Grubbs, R. Aqueous electrocatalytic CO_2 reduction using metal complexes dispersed in polymer ion gels. *Chem. Commun.* **56**, 4440, DOI: https://doi.org/10.1039/D0CC00791A (2020).

Shen, X., Yao, M., Sun, K., Zhao, T., He, Y., Chi, C.-Y., Zhou, C., Dapkus, P., Lewis, N., Hu, S. Defect-Tolerant TiO_2-Coated and Discretized Photoanodes for >600 h of Stable Photoelectrochemical Water Oxidation. *ACS Energy Lett.*, **6**, 193–200, https://doi.org/10.1021/acsenergylett.0c02521 (2020).

Song, T.-B., Yuan, Z., Babbe, F., Nenon, D., Aydin, E., De Wolf, S., Sutter-Fella, C. Dynamics of Antisolvent Processed Hybrid Metal Halide Perovskites Studied by *In Situ* Photoluminescence and Its Influence on Optoelectronic Properties. *ACS Appl. Energy Mater.* **3**, 2386–2393, DOI: 10.1021/acsaem.9b02052 (2020).

Song, T.-B., Yan, Z., Mori, M., Motiwala, F., Segev, G., Masquelier, E., Stan, C., Slack, J., Tamura, N., Sutter-Fella, C. Revealing the Dynamics of Hybrid Metal Halide Perovskite Formation via Multimodal In Situ Probes. *Adv. Funct. Mater.* **30**, 1908337, DOI: https://doi.org/10.1002/adfm.201908337 (2020).

Soniat, M., Tesfaye, M., Mafi, A., Brooks, D., Hamphrey, N., Weng, L.-C., Merionov, B., Goddard, W., Weber, A., Houle, F., Permeation of CO_2 and N_2 through glassy poly(dimethyl phenylene) oxide under steady- and presteady-state conditions. *J. Polym. Sci*., **58**, 1207–1228, DOI: 10.1002/pol.20200053 (2020).

Suram, S., Rohr, B., Stein, H., Guevarra, D., Wang, Y., Haber, J., Aykol, M., Gregoire, J. Benchmarking the acceleration of materials discovery by sequential learning. *Chem. Sci*. **11**, 2696–2706, DOI: https://doi.org/10.1039/C9SC05999G (2020).

Tagliabue, G., DuChene, J. S., Abdellah, J. S., Habib, A., Gosztola, D., Hattori, Y., Cheng, W.-H., Zheng, K., Canton, S., Sundararaman, R., Sa, J., Atwater, H. Ultrafast hot-hole injection modifies hot-electron dynamics in Au/p-GaN heterostructures. *Nature Materials* **19**, 1312–1318, DOI: https://doi.org/10.1038/s41563-020-0737-1 (2020).

Tagliabue, G., DuChene, J., Habib, A., Sundarararman, R., Atwater, H. Hot-Hole *versus* Hot-Electron Transport at Cu/GaN Heterojunction Interfaces. *ACS Nano* **14**, 5788–5797, DOI: https://doi.org/10.1021/acsnano.0c00713 (2020).

Tang, M. Peng, H., Lamoureux, P., Bajdich, M., Abild-Pedersen, F. From electricity to fuels: Descriptors for C1 selectivity in electrochemical CO_2 reduction. *Applied Catalysis B: Environmental*, **279**, 119384, DOI: https://doi.org/10.1016/j.apcatb.2020.119384 (2020).

Tang, M., Liu, X., Ji, Y., Norskov, J., Chan, K. Modeling Hydrogen Evolution Reaction Kinetics through Explicit Water–Metal Interfaces. *J. Phys. Chem. C*, **124**), 28083–28092, https://doi.org/10.1021/acs.jpcc.0c08310 (2020)

Torrisi, S., Singh, A., Montoya, J., Biswas, T., Persson, K. Two-dimensional forms of robust CO_2 reduction photocatalysts. *npj 2D Mater. Appl*., **4**, 24, DOI: https://doi.org/10.1038/s41699-020-0154-y (2020).

Umehara, M., Zhou, L., Haber, J., Guevarra, D., Kan, K. Newhouse, P., Gregoire, J. Combinatorial synthesis of oxysulfides in the lanthanum-bismuth-copper system. *ACS Comb. Sci*. 22, 319–326, DOI: https://doi.org/10.1021/acscombsci.0c00015 (2020).

Wang, H., Tzeng, Y.-K., Ji, Y., Li, Y., Li, J., Zheng, X., Yang, A., Liu, Y., Gong, Y., Cai, L., Li, Y., Zhang, X., Chen, W., Liu, B., Lu, H., Melosh, N., Shen, Z.-X., Chan, K., Tan, T., Chu, S., Cui, Y. Synergistic enhancement of electrocatalytic CO_2 reduction to C_2 oxygenates at nitrogen-doped nanodiamonds/Cu interface. *Nat. Nanotechnol*. **15**, 131–137, DOI: 10.1038/s41565-019-0603-y (2020).

Wang, L., Higgins, D., Ji, Y., Morales-Guio, C., Chan, K., Hahn, C., Jaramillo, T. Selective reduction of CO to acetaldehyde with CuAg electrocatalysts. *PNAS* **117**, 201821683, DOI: https://doi.org/10.1073/pnas.1821683117 (2020).

Wang, Z., Yuan, Q., Shan, J., Jiang, Z., Xu, P., Hu, Y., Zhou, J., Wu, L., Niu, Z., Sun, J., Cheng, T., Goddard, W. Highly Selective Electrocatalytic Reduction of CO_2 into Methane on Cu–Bi Nanoalloys. *J. Phys. Chem. Lett*. **11**, 7261–7266, DOI: https://doi.org/10.1021/acs.jpclett.0c01261 (2020).

Weng, L.-C., Bell, A., Weber, A. A systematic analysis of Cu-based membrane-electrode assemblies for CO_2 reduction through multiphysics simulation, *Energy Environ. Sci.* **13**, 3592-3606, https://doi.org/10.1039/D0EE01604G (2020).

Xi, C., Zheng, F., Gao, G., Ye, M., Dong, C., Du, X.-W., Wang, L.-W. Distribution of alkali cations near the Cu(111) surface in aqueous solution. *J. Mater. Chem. A*, **8**, 24428–24437, DOI: 10.1039/D0TA08965F (2020).

Yalamanchili, S., Verlage, E., Cheng, W.-H., Fountaine, K., Jahelka, P., Kempler, P., Saive, R., Lewis, N., Atwater, H. High Broadband Light Transmission for Solar Fuels Production Using Dielectric Optical Waveguides in TiO_2 Nanocone Arrays. *Nano Letters* **20**, 502–508, DOI: https://doi.org/10.1021/acs.nanolett.9b04225 (2020).

Yang, F., Zhou, X., Plymale, N., Sun, K., Lewis, N. Evaluation of sputtered nickel oxide, cobalt oxide and nickel–cobalt oxide on n-type silicon photoanodes for solar-driven O_2(g) evolution from water. *J. Mater. Chem. A*, **8**, 13955, DOI: https://doi.org/10.1039/D0TA03725G (2020).

Yao, Y., Huang, Z., Li, T., Wang, H., Liu, Y., Stein, H., Mao, Y., Gao, J., Jiao, M., Dong, Q., Dai, J., Xie, P., Xie, H., Lacey, S., Takeuchi, I., Gregoire, J., Jiang, R., Wang, C., Taylor, A., Shahbazian-Yassar, R., Hu, L. High-throughput, combinatorial synthesis of multimetallic nanoclusters. *PNAS* **117**, *201903721*, DOI: 10.1073/pnas.1903721117 (2020).

Ye, Y., Qian, J., Yang, H., Su, H., Lee, K.-J., Etxebarria, A., Cheng, T., Xiao, H., Yano, J., Goddrad, W., Crumlin, E. Synergy between Silver-Copper Surface Alloy Composition and Carbon Dioxide Adsorption and Activation. *ACS Appl. Mater. Interfaces* **12**, 25374–25382, DOI: https://doi.org/10.1021/acsami.0c02057 (2020).

Yu, W., Buabthong, P., Read, C., Dalleska, N., Lewis, N., Lewerenz, H.-J., Gray, H., Brinket, K. Cathodic NH_4^+ leaching of nitrogen impurities in CoMo thin-film electrodes in aqueous acidic solutions. *Sustainable Energy Fuels* **4**, 5080–5087, DOI: https://doi.org/10.1039/D0SE00674B (2020).

Yu, W., Lewis, N., Gray, H., Dalleska, N. Isotopically Selective Quantification by UPLC-MS of Aqueous Ammonia at Submicromolar Concentrations Using Dansyl Chloride Derivatization. *ACS Energy Lett*. **5**, 1532–1536, DOI: https://doi.org/10.1021/acsenergylett.0c00496 (2020).

Yu, W., Fu, H., Mueller, T., Brunschwig, B., Lewis, N. Atomic force microscopy: Emerging illuminated and *operando* techniques for solar fuel research. *J. Chem. Phys.* **153**, 020902, DOI: https://doi.org/10.1063/5.0009858 (2020).

Zee, D., Nippe, M., King, A., Chang, C., Long, J. Tuning Second Coordination Sphere Interactions in Polypyridyl–Iron Complexes to Achieve Selective Electrocatalytic Reduction of Carbon Dioxide to Carbon Monoxide. *Inorg. Chem.*, **59**, 5206, DOI:10.1021/acs.inorgchem.0c00455 (2020).

Zhang, Z., Lindley, S., Guevarra, D., Kan, K., Shinde, A., Gregoire, J., Han, W., Xie, E., Haber, J., Cooper, J. Fermi Level Engineering of Passivation and Electron Transport Materials for p-Type $CuBi_2O_4$ Employing a High-Throughput Methodology. *Adv. Funct. Mater*. **30**, 2000948, DOI: https://doi.org/10.1002/adfm.202000948 (2020).

Zheng, F., Wang, L.-W. Exploring non-adiabaticity to CO reduction reaction through ab initio molecular dynamics simulation. *APL Mater* **8**, 041115, DOI: https://doi.org/10.1063/5.0002318 (2020).

Zhou, L., Shinde, A., Guevarra, D., Richter, M., Stein, H., Wang, Y., Newhouse, P., Persson, K., Gregoire, J. Combinatorial screening yields discovery of 29 metal oxide photoanodes for solar fuel generation. *J. Mater. Chem. A* **8**, 4239–4243, DOI: https://doi.org/10.1039/C9TA13829C (2020).

Zhou, L., Shinde, A., Guevarra, D., Haber, J., Persson, K., Neaton, J., Gregoire, J. Successes and opportunities for discovery of metal oxide photoanodes for solar fuels generators. *ACS Energy Lett*. **5**, 1413–1421, DOI: 10.1021/acsenergylett.0c00067 (2020).

Zhou, L., Shinde, A., Newhouse, P., Gueverra, Wang, Y., Lai, Y., Kan, K., Suram, S., Haber, J., Gregiore, J. Quaternary Oxide Photoanode Discovery Improves the Spectral Response and Photovoltage of Copper Vanadates. *Matter* **3**, 1614–1630, DOI: https://doi.org/10.1016/j.matt.2020.08.031 (2020).

Zhou, Y., Gao, G., Chu, W., Wang, L.-W. Computational screening of transition metal-doped phthalocyanine monolayers for oxygen evolution and reduction. *Nanoscale Adv*. **2**, 710–716, DOI: 10.1039/C9NA00648F (2020).

2019

Abbott, L., Buss, H., Thelen, J., McCloskey, B., Lawson, J. Polyanion Electrolytes with Well-Ordered Ionic Layers in Simulations and Experiment. *Macromolecules* **52**, 5518–5528, DOI: https://doi.org/10.1021/acs.macromol.9b00416 (2019).

Agbo, P., Danilovic, N., An Algorithm for the Extraction of Tafel Slopes, *J. Phys. Chem.* **123**, 30252–30264, DOI: https://doi.org/10.1021/acs.jpcc.9b06820 (2019).

Ali-Loytty, H., Hannula, M., Valden, M., Eilert, A., Ogasawara, H., Nilsson, A. Chemical Dissolution of Pt(111) during Potential Cycling under Negative pH Conditions Studied by Operando X-ray Photoelectron Spectroscopy. *J. Phys. Chem. C*, **123**, 25128–25134, DOI: https://doi.org/10.1021/acs.jpcc.9b05201 (2019).

Ament, S., Stain, H., Guevarra, D., Zhou, L., Haber, J., Boyd, D., Umehara, M., Gregoire, J., Gomes, C., Multi-component background learning automates signal detection for spectroscopic data. *npj Computational Materials*, 5, 77, DOI: https://doi.org/10.1038/s41524-019-0213-0 (2019).

Bao, W., Liu, X., Xue, F., Zheng, F., Tao, R., Wang, S., Xia, Y., Zhao, M., Kim, J., Yang, S., Li, Q., Wang, Y., Wang, Y., Wang, L.-W., MacDonald, A., Zhang, X. Observation of Rydberg exciton polaritons and their condensate in a perovskite cavity. *PNAS* **116**, 201909948, DOI: https://doi.org/10.1073/pnas.1909948116 (2019).

Borgwardt, M., Omelchenko, S., Favaro, M., Plate, P., Hohn, C., Abou-Ras, D., Schwarzburg, K., van de Krol, R., Atwater, H., Lewis, N., Eichberger, R., Friedrich, D. Femtosecond time-resolved two-photon photoemission studies of ultrafast carrier relaxation in Cu_2O photoelectrodes. *Nature Comm.*, **10**, 2106, DOI: https://doi.org/10.1038/s41467-019-10143-x (2019).

Buckley, A., Lee, M., Cheng, T., Kazantsev, R., Larson, D., Goddard, W., Toste, D., Toma, F. Electrocatalysis at Organic-Metal Interfaces: Identification of Structure-Reactivity Relationships for CO_2 Reduction at Modified Cu Surfaces. *J. Am. Chem. Soc.* **141**, 7355–7364, DOI: 10.1021/jacs.8b13655 (2019).

Bullock, J., Wan, Y., Hettick, M., Zhaoran, X., Phang, S. P., Yan, D., Wang, H., Ji, W., Samundsett, C., Hameiri, Z., McDonald, D., Cuevas, A., Javey, A. Dopant-Free Partial Rear Contacts Enabling 23% Silicon Solar Cells. *Adv. Mater. 9*, 1803367, DOI: https://doi.org/10.1002/aenm.201803367 (2019).

Cai, I., Ziegler, M., Bunting, P., Nicolay, A., Levine, D., Kalendra, V., Smith, P., Lakshmi, K., Tilley, T. D. Monomeric, Divalent Vanadium Bis(arylamido) Complexes: Linkage Isomerism and Reactivity. *Organometallics* **38**, 1648–1663, DOI: 10.1021/acs.organomet.9b00134 (2019).

Carter, B. Keller, L., Wessling, M., Miller, D. Preparation and characterization of crosslinked poly(vinylimidazolium) anion exchange membranes for artificial photosynthesis. *J. Mater. Chem. A.* 7, 23818–23829, DOI: 10.1039/C9TA00498J (2019).

Chen, C., Pedrini, J., Gaulding, A., Kastl, C., Calafiore, G., Dhuey, S., Kuykendall, T., Cabrini, S., Toma, F., Aloni, S., Schwartzberg, A. Very High Refractive Index Transition Metal Dichalcogenide Photonic Conformal Coatings by Conversion of ALD Metal Oxides. *Scientific Reports 9*, 2768, DOI: https://doi.org/10.1038/s41598-019-39115-3 (2019).

Chen, Y., Huang, Y., Cheng, T., Goddard, W., Identifying Active Sites for CO_2 Reduction on Dealloyed Gold Surfaces by Combining Machine Learning with Multiscale Simulations. *J. Am. Chem. Soc.* **141**, 11651–11657, https://doi.org/10.1021/jacs.9b04956 (2019).

Cheng, T., Fortunelli, A., Goddard, W. Reaction intermediates during operando electrocatalysis identified from full solvent quantum mechanics molecular dynamics. *PNAS* **116**, 201821709, https://doi.org/10.1073/pnas.1821709116 (2019).

Cheng, T., Jaramillo-Botero, A., An, Q., Ilyin, D., Naserifar, S., Goddard, W. First principles-based multiscale atomistic methods for input into first principles nonequilibrium transport across interfaces. *PNAS* **116**, 18193, DOI: https://doi.org/10.1073/pnas.1800035115 (2019).

Choi, C., Cheng, T., Espinosa, M., Fei, H., Duan, X., Goddard, W., Huang, Y. A Highly Active Star Decahedron Cu Nanocatalyst for Hydrocarbon Production at Low Overpotentials. *Adv. Mater.* **31**, 1805405., DOI: https://doi.org/10.1002/adma.201805405 (2019).

Clark, E., Ringe, S., Tang, M., Walton, A., Hahn, Jaramillo, T., Chan, K., Bell, A. Influence of Atomic Surface Structure on the Activity of Ag for the Electrochemical Reduction of CO_2 to CO. *ACS Catalysis* **9**, 4006–4014, DOI: 10.1021/acscatal.9b00260 (2019).

Clark, E., Wong, J., Garza, A., Lin, Z., Head-Gordon, M., Bell, A. Explaining the Incorporation of Oxygen Derived from Solvent Water into the Oxygenated Products of CO Reduction over Cu. *J. Am. Chem. Soc.* **141**, 4191–4193, DOI: 10.1021/jacs.8b13201 (2019).

Cole, W., Wei, H., Nguyen, S., Harris, C., Miller, D., Saykally, R. Dynamics of Micropollutant Adsorption to Polystyrene Surfaces Probed by Angle-Resolved Second Harmonic Scattering. *J. Phys. Chem. C*, **123**, 14362–14369, DOI: https://doi.org/10.1021/acs.jpcc.9b01146 (2019).

Creel, E., Corson, E., Eichhorn, J., Kostecki, R., Urban, J., McCloskey, B. Directing Selectivity of Electrochemical Carbon Dioxide Reduction Using Plasmonics. *ACS Energy Letters* **4**, 1098–1105, DOI: 10.1021/acsenergylett.9b00515 (2019).

De Luna, P., Hahn, C., Higgins, D., Jaffer, S., Jaramillo, T., Sargent, E. What would it take for renewably powered electrosynthesis to displace petrochemical processes? *Science*, **364** (6438), DOI: 10.1126/science.aav3506 (2019).

Diederichsen, K., Terrell, R., McCloskey, B. Counterion Transport and Transference Number in Aqueous and Nonaqueous Short Chain Polyelectrolyte Solutions. *J. Phys. Chem. B* **123**, 10858–10867, DOI: https://doi.org/10.1021/acs.jpcb.9b09517 (2019).

Farmand, M., Landers, A., Lin, J., Feaster, J., Beeman, J., Ye, Y., Clark, E., Higgins, D., Yano, J., Davis, R., Mehta, A., Jaramillo, T., Hahn, C., Drisdell, W. Electrochemical flow cell enabling *operando* probing of electrocatalyst surfaces by X-ray spectroscopy and diffraction. *Phys. Chem. Chem. Phys.***21**, 5402–5408, DOI: 10.1039/C8CP07423B (2019).

Finke, C., Omelchenko, S., Jasper, J., Lichterman, M., Read, C., Lewis, N., Hoffmann, M. Enhancing the activity of oxygen-evolution and chlorine-evolution electrocatalysts by atomic layer deposition of TiO_2. *Energy. Environ. Sci* **12**, *358-365*, DOI: 10.1039/C8EE02351D (2019).

Ferrah, D., Haines, A., Galhehage, R., Bruce, J., Babore, A., Hunt, A., Waluyo, I., Hemminger, J. Wet Chemical Growth and Thermocatalytic Activity of Cu-Based Nanoparticles Supported on TiO_2 Nanoparticles/HOPG: In Situ Ambient Pressure XPS Study of the CO_2 Hydrogenation Reaction. *ACS Catalysis* **9**, 6783–6802, DOI: https://doi.org/10.1021/acscatal.9b01419 (2019).

Gauthier, J., Fields, M., Bajdich, M., Chen, L., Sandberg, R., Chan, K., Norskov, J. Facile Electron Transfer to CO_2 during Adsorption at the Metal|Solution Interface. *J. Phys. Chem. C.* **123**, 29278–29283 DOI: https://doi.org/10.1021/acs.jpcc.9b10205 (2019).

Gomes, C., Selman, B., Gregoire, J., Artificial intelligence for materials discovery. *MRS Bulletin*, **44**, 538–544. doi:10.1557/mrs.2019.158 (2019).

Gomes, C. P.; Bai, J.; Xue, Y.; Björck, J.; Rappazzo, B.; Ament, S.; Bernstein, R.; Kong, S.; Suram, S. K.; van Dover, R. B.; Gregoire, J. M., CRYSTAL: a multi-agent AI system for automated mapping of materials' crystal structures. *MRS Communications* **9**, 600–608, DOI: 10.1557/mrc.2019.50 (2019).

Gregoire, J. Unexpected Transitions Yield Interesting Science and High-Performance Materials. *Matter* **1**, 790–791, DOI: https://doi.org/10.1016/j.matt.2019.09.006 (2019).

Gregoire, J., Stein, H. Progress and prospects for accelerating materials science with automated and autonomous workflows. *Chemical Science* **10**, 9640–9649., DOI: 10.1039/C9SC03766G (2019).

Gurudayal, G., Beeman, J., Bullock, J., Wang, H., Eichhorn, Towle, C., Javey, A., Toma, F., Mathews, N., Ager, J. Si Photocathode with Ag-Supported Dendritic Cu Catalyst for CO_2 Reduction. *Energy Environ. Sci.* **12**, 1068–1077, DOI: 10.1039/C8EE03547D (2019).

Gurudayal, G., Perone, D., Malani, S., Lum, Y., Haussener, S., Ager, J. Sequential Cascade Electrocatalytic Conversion of Carbon Dioxide to C-C Coupled Products. *ACS Appl. Energy Materials*, **2**, 4551–4559, DOI: https://doi.org/10.1021/acsaem.9b00791 (2019).

Ho, A., Zhou, X., Han, L., Sullivan, I., Karp, C., Lewis, N., Xiang, C. Decoupling H_2(g) and O_2(g) Production in Water Splitting by a Solar-Driven $V^{3+/2+}$(aq,H_2SO_4)|KOH(aq) Cell. *ACS Energy Letters* **4**, 968–976, DOI: 10.1021/acsenergylett.9b00278 (2019).

Huang, Y., Kang, J., Goddard, W., Wang, L.-W. Density functional theory based neural network force fields from energy decompositions. *Phys. Rev. B* **99**, 064103, DOI: https://doi.org/10.1103/PhysRevB.99.064103 (2019).

Hull, C., Raj, S., Lam, R., Katayama, T., Pascal,T., Drisdell, W.s., Saykally, R., Schwartz, C. Early time dynamics of laser-ablated silicon using ultrafast grazing incidence X-ray scattering. *Chem Phys. Letters* **736**, 136811, DOI: https://doi.org/10.1016/j.cplett.2019.136811 (2019).

Jermyn, A., Tagliabue, G., Atwater, H., Goddard, W., Narang, P., Sundararaman, R. Transport of hot carriers in plasmonic nanostructures. *Phys. Rev. Materials*, **3**, 075201, DOI: https://doi.org/10.1103/PhysRevMaterials.3.075201 (2019).

Jiang, C.-M., Reyes-Lillo, S., Liang, Y., Liu, Y.-S., Liu, G., Toma, F., Prendergast, D., Sharp, I., Cooper, J. The Electronic Structure and Performance Bottlenecks of $CuFeO_2$ Photocathodes. *Chem. Mater.***31**, 2524–2534, DOI: 10.1021/acs.chemmater.9b00009 (2019).

Jiang, H., Kammel, M., Ding, F., Dorenkamp, Y., Manby, F., Wodtke, A., Miller, T., Kandratsenka, A., Bunermann, O. Imaging covalent bond formation by H atom scattering from graphene. *Science*, **364 (6438)**, 379–382, DOI: 10.1126/science.aaw6378 (2019).

Jouny, M., Lv, J.-J., Cheng, T., Ko, B., Zhu, J.-J., Goddard, W., Jiao, F. Formation of carbon–nitrogen bonds in carbon monoxide electrolysis. *Nature Chemistry*, **11**, 846–851, DOI: https://doi.org/10.1038/s41557-019-0312-z (2019).

Kempler, P., Fu, H., Ifkovits, Z., Papadantonakis, K., Leiws, N. Spontaneous Formation of >90% Optically Transmissive, Electrochemically Active CoP Films for Photoelectrochemical Hydrogen Evolution. *J. Phys. Chem. Lett.*, **11**, 14–20, DOI: https://doi.org/10.1021/acs.jpclett.9b02926 (2019).

Kistler, T., Danilovic, N., Agbo, P. Editors' Choice—A Monolithic Photoelectrochemical Device Evolving Hydrogen in Pure Water. *J. Electrochem. Soc.*, **166**, H656–H661, DOI: 10.1149/2.1151913jes (2019).

Kistler, T., Larson, D., Walczack, K., Agbo, P., Sharp, I., Weber, A., Danilovic, N. Integrated Membrane-Electrode-Assembly Photoelectrochemical Cell under Various Feed Conditions for Solar Water Splitting. *J. Electrochem. Soc*. **166**, H3020–H3028, DOI: 10.1149/2.0041905jes (2019).

Kudrawiec, R., Janicki, L., Linhart, W. M., Mayer, M. A., Sharp, I. D., Choi, S., Bierwagen, O., Speck, J. S., Walukiewicz, W. Photoreflectance and photoinduced microwave reflectance studies of surface band bending in Mg-doped InN. *Journal of Applied Physics* **126**, 045712, DOI: https://doi.org/10.1063/1.5096528 (2019).

Kusoglu, A., Vezzu, K., Hedge, G., Nawn, G., Motz, A., Sadore, H., Haugen, G., Yang, Y., Seifert, S., Yandrasits, M., Hamrock, S., Maupin, M., Weber, A., Di Noto, V., Herring, A. Transport and Morphology of a Proton Exchange Membrane Based on a Doubly Functionalized Perfluorosulfonic Imide Side Chain Perflourinated Polymer. *Chem. Mater.* 32, 38–59, DOI: https://doi.org/10.1021/acs.chemmater.8b05012 (2019).

Lai, Y., Jones, R., Wang, Y., Zhou, L., Gregoire. Scanning Electrochemical Flow Cell with Online Mass Spectroscopy for Accelerated Screening of Carbon Dioxide Reduction Electrocatalysts. *ACS Comb. Sci.* **21**, 692–704, DOI: https://doi.org/10.1021/acscombsci.9b00130 (2019).

Li, F., Thevenon, A., Rosas-Hernandez, A., Wang, Z., li, Y., Gabardo, C., Ozden, A., Dinh, C., Li, Y., Wang, Y., Edwards, J., Xu, Y., McCallum, C., Tao, L., Liang, Z., Luo, M., Wang, Z., Li, H., O-Brien, C., Tan, C., Nam, D., Quintero-Bermudez, R., Zhuang, T., Li, Y., Han, Z., Britt, D., Sinton, D., Agapie, T., Peters, J., Sargent, E. Molecular tuning of CO_2-to-ethylene conversion. *Nature* 577, 509–513, DOI: https://doi.org/10.1038/s41586-019-1782-2 (2019).

Li, L., Yang, J., Ali-Loytty, H., Weng, T.-C., Toma, F., Sokaras, D., Sharp, I., Nilsson, A. Operando observation of chemical transformations of iridium oxide during photoelectrochemical water oxidation. *ACS Appl Energy Mater* **2**, 1371–1379, DOI: 10.1021/acsaem.8b01945 (2019).

Li, M., Duanmi, K., Wan, C., Cheng, T., Zhang, L., Dai, S., Chen, W., Zhiao, Z., Li, P., Fei, H., Zhu, Y., Yu, R., Luo, J., Zang, K., Lin, Z., Ding, M., Huang, J., Sun, H., Guo, J., Pan, X., Goddard, W., Sautet, P., Huang, Y., Duan, X. Single-atom tailoring of platinum nanocatalysts for high-performance multifunctional electrocatalysis. *Nature Catalysis* 2, 495–503, DOI: https://doi.org/10.1038/s41929-019-0279-6 (2019).

Lin, M., Han, L., Singh, M., Xiang, C., An Experimental- and Simulation-Based Evaluation of the CO_2 Utilization Efficiency of Aqueous-Based Electrochemical CO_2 Reduction Reactors with Ion-Selective Membranes. *ACs Appl. Energy Mater*. **2**, 5843–5850, https://doi.org/10.1021/acsaem.9b00986 (2019).

Liu, X., Schlexer, P., Xiao, J., Ji, Y., Wang, L., Sandberg, R., Tang, M., Brown, K., Peng, H., Ringe, S., Hahn, C., Jaramillo, T., Norskov, J., Chan, K. pH effects on the electrochemical reduction of CO(2) towards C_2 products on stepped copper. *Nature Comm.*, **10**, 32, DOI: 10.1038/s41467-018-07970-9 (2019).

Liu, Y.-Y., Zheng, F., Jiang, X., Luo, J.-W., Li, S.-S., Wang, L-W. *Ab Initio* Investigation of Charge Trapping Across the Crystalline-Si–Amorphous-SiO_2 Interface. *Phys. Rev. Applied* **11**, 044058, DOI: 10.1103/PhysRevApplied.11.044058 (2019).

Liu, Y.-Y., Liu, F., Wang, R., Luo, J.-W., Jiang, X., hung, R., Li, S.-S., Wang, L.-W. Characterizing the Charge Trapping across Crystalline and Amorphous Si/SiO_2/HfO_2 Stacks from First-Principle Calculations. *Phys. Rev. Applied*, **12**, 064012, DOI: https://doi.org/10.1103/PhysRevApplied.12.064012 (2019).

Moreno-Hernandez, I., Brunschwig, B., Lewis, N. Crystalline nickel, cobalt, and manganese antimonates as electrocatalysts for the chlorine evolution reaction. *Energy Environ. Sci.* **12**, 1241–1248, DOI: 10.1039/C8EE03676D (2019).

Naserifar, S. and Goddard, W. A. Liquid water is a dynamic polydisperse branched polymer. *PNAS* **116**, 201817383, DOI: https://doi.org/10.1073/pnas.1817383116 (2019).

Naserifar, S. and Goddard, W. A. Anomalies in Supercooled Water at ~230 K Arise from a 1D Polymer to 2D Network Topological Transformation. *J. Phys. Chem. Lett.* **10**, 6267–6273, DOI: https://doi.org/10.1021/acs.jpclett.9b02443 (2019).

Naserifar, S., Oppenheim, J., Yang, H., Zhou, T., Zybin, S., Rizk, M., Goddard, W. Accurate non-bonded potentials based on periodic quantum mechanics calculations for use in molecular simulations of materials and systems. *J. Chem. Phys.* **151**, 154111, DOI: https://doi.org/10.1063/1.5113811 (2019).

Nguyen, A. I., Van Allsburg, K., Terban, M., Bajdich, M., Oktawiec, J., Amtawong, J., Ziegler, M., Dombrowski, J., Lakshmi, K., Drisdell, W., Yano, J., Billinge, S., and Tilley, D. Stabilization of reactive Co_4O_4 cubane oxygen-evolution catalysts within porous frameworks. *PNAS* **116**, 201815013, DOI: https://doi.org/10.1073/pnas.1815013116 (2019).

Nitopi, S., Bertheussen, E., Scott, S., Liu, X., Engstfeld, A., Horch, S., Seger, B., Stephens, I., Chan, K., Hahn, C., Norskov, J., Jaramillo, T., Chorkendorff, I. Progress and Perspectives of Electrochemical CO_2 Reduction on Copper in Aqueous Electrolyte. *Chem. Rev.* **119**, 7610–7672, DOI: https://doi.org/10.1021/acs.chemrev.8b00705 (2019).

Noh, J., Kim, S., Gu, G. H., Shinde, A., Zhou, L., Gregoire, J., Jung, Y. Unveiling new stable Manganese based photoanode materials via theoretical high-throughput screening and experiments. *Chem. Comm.* **55**, 13418–13421, DOI: 10.1039/C9CC06736A (2019).

Noh, J., Kim, J., Stein, H., Sanchez-Lengeling, B., Gregoire, J., Aspuru-Guzik, A., Jung, Y. Inverse Design of Solid-State Materials via a Continuous Representation. *Matter* **1**, 1370–1384, DOI: https://doi.org/10.1016/j.matt.2019.08.017 (2019).

Nunez, P., Richter, M., Piercy, B., Roske, C., Caban-Acevedo, M., Losego, M., Konezny, S., Fermin, D., Hu, S., Brunschwig, B., Lewis, N. Characterization of Electronic Transport through Amorphous TiO_2 Produced by Atomic-Layer Deposition. *J. Phys. Chem. C* **123**, 20116–20129, DOI: https://doi.org/10.1021/acs.jpcc.9b04434 (2019).

Ostericher, A., Porter, T., Reineke, M., Kubiak, C. Thermodynamic Targeting of Electrocatalytic CO_2 Reduction: Advantages, Limitations, and Insights for Catalyst Design. *Dalton Trans.* **48**, 15841–15848, DOI: 10.1039/C9DT03255J (2019).

Qian, J., Ye, Y., Yang, H., Yano, J., Crumlin, E., Goddard, W. Initial steps in forming the electrode electrolyte interface: H_2O adsorption and complex formation on the Ag(111) surface from combining Quantum Mechanics calculations and X-ray Photoelectron Spectroscopy. *J. Am. Chem. Soc.* **141**, 6946–6954, DOI: 10.1021/jacs.8b13672 (2019).

Ringe, S., Clark, E., Resasco, J., Walton, A., Seger, B., Bell, A., Chan, K. Understanding cation effects in electrochemical CO_2 reduction. *Energy Environ. Sci.* **12**, 3001–3014, DOI: 10.1039/C9EE01341E (2019).

Scott, S., Hogg, T., Landers, A., Maagaard, T., Bertheussen, E., Lin, J., Davis, R., Beeman, J., Higgins, D., drisdell, W., Hahn, C., Mehta, A., Seger, B., Jaramillo, T., Chorkendorff, I. Absence of Oxidized Phases in Cu Under CO Reduction Conditions. *ACS Energy Letters* **4**, 803–804, DOI: 10.1021/acsenergylett.9b00172 (2019).

Shen, S., Zhang, X., Mubeen, S., Soriaga, M., Stickney, J. Optimization of the nucleation-site density for the electrodeposition of cadmium sulfide on indium-tin-oxide. *Electrochimica Acta* **316**, 105–112, DOI: https://doi.org/10.1016/j.electacta.2019.05.120 (2019).

Singh, A., Montoya, J., Gregoire, J., Persson, K. Robust and synthesizable photocatalysts for CO_2 reduction: a data-driven materials discovery. *Nature Communications*, **10**, 443, DOI: https://doi.org/10.1038/s41467-019-08356-1 (2019).

Soedarmadji, E., Stein, H., Suram, S., Guevarra, D., Gregoire, J. Tracking materials science data lineage to manage millions of materials experiments and analyses. *npj Computational Materials* **5**, 79, DOI: https://doi.org/10.1038/s41524-019-0216-x (2019).

Stein, H., Guevarra, D., Newhouse, P., Soedarmadji, E., Gregoire, J. Machine learning of optical properties of materials – predicting spectra from images and images from spectra. *Chemical Science* **10**, 47–55, DOI: 10.1039/C8SC03077D (2019).

Stein, H., Guevarra, D., Shinde, A., Jones, R., Gregoire, J., Haber, J. Functional mapping reveals mechanistic clusters for OER catalysis across (Cu–Mn–Ta–Co–Sn–Fe)O_x composition and pH space. *Materials Horizons* **6**, 1251–1258, DOI: 10.1039/C8MH01641K (2019).

Stein, H., Soedarmadji, E., Newhouse, P., Guevarra, D., Gregoire, J. Synthesis, optical imaging, and absorption spectroscopy data for 179072 metal oxides. *Scientific Data* **6**, 9, DOI: https://doi.org/10.1038/s41597-019-0019-4 (2019).

Subramanian, S., Oppenhaim, J., Kim, D., Nguyen, T., Silo, W., Kim, B., Goddard, W., Yavuz, C. Catalytic Non-redox Carbon Dioxide Fixation in Cyclic Carbonates. *Chem* **5**, 3232–3242, DOI: https://doi.org/10.1016/j.chempr.2019.10.009 (2019).

Sullivan, I., Han, L., Lee, S. H., Lin, M., Larson, D., Drisdell, W., Xiang, C. A Hybrid Catalyst-Bonded Membrane Device for Electrochemical Carbon Monoxide Reduction at Different Relative Humidities. *ACS Sustainable Chem. Eng.* **7**, 16964–16970, DOI: https://doi.org/10.1021/acssuschemeng.9b04959 (2019).

Tesfaye, M., Kushner, D., Kusoglu, A. Interplay between Swelling Kinetics and Nanostructure in Perfluorosulfonic Acid Thin-Films: Role of Hygrothermal Aging. *ACS Applied Polymer Materials* **1**, 631–635, DOI: 10.1021/acsapm.9b00005 (2019).

Thevenon, A., Rosas-Hernandez, A., Peters, J., Agapie, T. In-situ Nanostructuring and Stabilization of Polycrystalline Copper by an Organic Salt Additive Promotes Electrocatalytic CO_2 Reduction to Ethylene. *Angew Chem Int Ed Engl* **58**, 16952–16958, DOI: 10.1002/anie.201907935 (2019).

Umehara, M., Stein, H., Guevarra, D., Newhouse, P., Boyd, D., Gregoire, J. Analyzing machine learning models to accelerate generation of fundamental materials insights. *npj Computational Materials* **5**, 34, DOI: https://doi.org/10.1038/s41524-019-0172-5 (2019).

Wang, H., Liang, Z., Tang, M., Chen, G., Li, Y., Chen, W., Lin, D., Zhang, Z., Zhou, G., Li, J., Lu, Z., Chan, K., Tan, T., Cui, Y. Self-Selective Catalyst Synthesis for CO_2 Reduction. *Joule* **3**, 1927–1936, https://doi.org/10.1016/j.joule.2019.05.023 (2019).

Wang, L., Nitopi, S., Wong, A., Snider, J., Nielander, A., Morales-Guio, C., Orazov, M., Higgins, D., Hahn, C., Jaramillo, T. Electrochemically converting carbon monoxide to liquid fuels by directing selectivity with electrode surface area. *Nature Catalysis* **2**, 702–708, DOI: https://doi.org/10.1038/s41929-019-0301-z (2019).

Weng, L.-C., Bell, A., Weber, A. Towards membrane-electrode assembly systems for CO_2 reduction: a modeling study. *Energy Environ. Sci.* **12**, 1950–1968, DOI: 10.1039/C9EE00909D (2019).

Yalamanchili, S., Kempler, P., Papadantonakis, K., Atwater, H., Lewis, N. Integration of electrocatalysts with silicon microcone arrays for minimization of optical and overpotential losses during sunlight-driven hydrogen evolution. *Sust. Energy & Fuels* **3**, 2227–2236, DOI: 10.1039/C9SE00294D (2019).

Yao, Y., Shushkov, P., Miller, T., Giapis, K. Direct dioxygen evolution in collisions of carbon dioxide with surfaces. *Nature Communications* **10**, 2294, DOI: https://doi.org/10.1038/s41467-019-10342-6 (2019).

Ye, Y., Yang, H., Qian, J., Su, H., Lee, K.-J., Cheng, T., Xiao, H., Yano, J., Goddard, W., Crumlin, E. Dramatic differences in carbon dioxide adsorption and initial steps of reduction between silver and copper. *Nature Communications* **10**, 1875, DOI: 10.1038/s41467-019-09846-y (2019).

Zhang, Z., Lindley, S., Dhall, R., Bustillo, K., Han, W., Xie, E., Cooper, J. Beneficial CuO Phase Segregation in the Ternary p-Type Oxide Photocathode $CuBi_2O_4$. *ACS Appl Energy Mater* 2, 4111–4117, DOI: https://doi.org/10.1021/acsaem.9b00297 (2019).

Zhang, H., Chang, X., Chen, J., Goddard, W., Xu, B., Cheng, M.-J., Lu, Q. Computational and experimental demonstrations of one-pot tandem catalysis for electrochemical carbon dioxide reduction to methane. *Nature Communications* **10**, 3340, DOI: https://doi.org/10.1038/s41467-019-11292-9 (2019).

Zheng, F, Wang, L.-W. Large polaron formation and its effect on electron transport in hybrid perovskites. *Energy Environ. Sci.* **12**, 1219–1230, DOI: 10.1039/C8EE03369B (2019).

Zheng, F., Wang L.-W. Ultrafast Hot Carrier Injection in Au/GaN: The Role of Band Bending and the Interface Band Structure. *J. Phys. Chem. Lett.* **10**, 6174–6183, DOI: https://doi.org/10.1021/acs.jpclett.9b02402 (2019).

Zhou, J.-J. and Bernardi, M. Predicting charge transport in the presence of polarons: The beyond-quasiparticle regime in SrTiO3. *Physical Review Research*, **1**, 033138, DOI: https://doi.org/10.1103/PhysRevResearch.1.033138 (2019).

2018

Ager, J., Lapkin, A., Chemical storage of renewable energy. *Science*, **360 (6390)**, 707–708, DOI: 10.1126/science.aat7918 (2018).

Ager, J. W. Chapter 6 Heterojunction Approaches for Stable and Efficient Photoelectrodes. Book Section in Integrated Solar Fuel Generators, The Royal Society of Chemistry, 183–213, DOI: 10.1039/9781788010313-00183 (2018).

Ardo, S., et al. Pathways to Electrochemical Solar-Hydrogen Technologies. *Energy Environ. Sci.*, **11**, 2768–2783, DOI: 10.1039/C7EE03639F (2018).

Bai, J. *et al.* Phase-Mapper: Accelerating Materials Discovery with AI. *AI Magazine* **39**, 15–26, DOI: https://doi.org/10.1609/aimag.v39i1.2785 (2018).

Baricuatro, J. H., Kim, Y.-G., Korzeniewski, C. L., Soriaga, M. P. *Seriatim* ECSTM-ECPMIRS of the adsorption of carbon monoxide on Cu(100) in alkaline solution at CO2-reduction potentials. *Electrochemistry Communications* **91**, 1–4, DOI: https://doi.org/10.1016/j.elecom.2018.04.016 (2018).

Bariya, M., Shahpar, Z., Park, H., Sun, J., Jung, Y., Gao, W., Nyein, H., Liaw, T., Tai, L.-C., Ngo, Q., Chao, M., Zhao, Y., Hettick, M., Cho, G., Javey, A. Roll-to-Roll Gravure Printed Electrochemical Sensors for Wearable and Medical Devices. *ACS Nano* **12**, 6978–6987, DOI: 10.1021/acsnano.8b02505 (2018).

Bell, A. T. Chapter 3 Understanding the Effects of Composition and Structure on the Oxygen Evolution Reaction (OER) Occurring on $NiFeO_x$ Catalysts, Book Section in Integrated Solar Fuel Generators, The Royal Society of Chemistry, 79–116, DOI: 10.1039/9781788010313-00079 (2018).

Brinkert, K., Richter, M., Akay, O., Fountaine, K., Lewerenz, H.-J. Advancing semiconductor–electrocatalyst systems: application of surface transformation films and nanosphere lithography. *Faraday Discuss* **208**, 523–535, DOI: 10.1039/C8FD00003D (2018).

Bullock, J., Wan, Y., Xu, Z., Essig, S., Hettick, M., Wang, H., Ji, W., Boccard, M., Cuevas, A., Ballif, C., Javey, A. Stable Dopant-free Asymmetric Heterocontact Silicon Solar Cells with Efficiencies Above 20%. *ACS Energy Letters* **3**, 508–513, DOI: 10.1021/acsenergylett.7b01279 (2018).

Cave, E. R., Shi, C., Kuhl, K. P., Hatsukade, T., Abram, D. N., Hahn, C., Chan, K., Jaramillo, T. Trends in the Catalytic Activity of Hydrogen Evolution during CO_2 Electroreduction on Transition Metals, *ACS Catalysis*, **8**, 3035–3040, DOI: 10.1021/acscatal.7b03807 (2018).

Chapovetsky, A., Welborn, M., Luna, J. M., Haiges, R., Miller, T., Marinescu, S. C. Pendant Hydrogen-Bond Donors in Cobalt Catalysts Independently Enhance CO_2 Reduction. *ACS Central Science* **4**, 397–404, DOI: 10.1021/acscentsci.7b00607 (2018).

Cheng, T., Jaramillo-Botero, A., An, Q., Ilyin, D., Naserifar, S., Goddard, W. First principles-based multiscale atomistic methods for input into first principles nonequilibrium transport across interfaces. PNAS, DOI: https://doi.org/10.1073/pnas.1800035115(2018).

Cheng, T., Wang, L., Merinov, B., Goddard, W. A. Explanation of Dramatic pH-Dependence of Hydrogen Binding on Noble Metal Electrode: Greatly Weakened Water Adsorption at High pH. *J. Am. Chem. Soc.* **140**, 7787–7790, DOI: 10.1021/jacs.8b04006 (2018).

Cheng, W.-H., Richter, M., May, M., Ohlmann, J., Lackner, D., Dimroth, F., Hannappel, T., Atwater, H., Lewerenz, H.-J. Monolithic Photoelectrochemical Device for Direct Water Splitting with 19% Efficiency. *ACS Energy Letters* **3**, 1795–1800, DOI: 10.1021/acsenergylett.8b00920 (2018).

Clark, E. and Bell, A. Direct Observation of the Local Reaction Environment during the Electrochemical Reduction of CO_2. *J. Am. Chem. Soc.* **140**, 7012–7020, DOI: 10.1021/jacs.8b04058 (2018).

Clark, E., Resasca, J., Landers, A., Lin, A., Chng, L.-T., Walton, A., Hahn, C., Jaramillo, T., Bell, A. Data Acquisition Protocols and Reporting Standards for Studies of the Electrochemical Reduction of Carbon Dioxide. *ACS Catalysis* **8**, 6560–6570, DOI: 10.1021/acscatal.8b01340 (2018).

Cooper, J. K., Reyes-Lillo, S., Hess, L., Jiang, C.-M., Neaton, J., Sharp, I. Physical Origins of the Transient Absorption Spectra and Dynamics in Thin-Film Semiconductors: The Case of $BiVO_4$. *J. Phys. Chem. C* **122**, 20642–20652 DOI: 10.1021/acs.jpcc.8b06645 (2018).

Cornejo, J., Sheng, H., Edri, E., Ajo-Franklin, C., Frei, H. Nanoscale membranes that chemically isolate and electronically wire up the abiotic/biotic interface. *Nature Comm.*, **9**, 2263, DOI: 10.1038/s41467-018-04707-6 (2018).

Corson, E., Creel, E., Kim, Y., Urban, J., Kostecki, R., McCloskey, B. A temperature-controlled photoelectrochemical cell for quantitative product analysis. *Rev Sci Instr* **89**, 055112, DOI: https://doi.org/10.1063/1.5024802 (2018).

DuChene, J., Tagliabue, G., Welch A. J., Cheng, W.-H., and Atwater, H. A. Hot Hole Collection and Photoelectrochemical CO_2 Reduction with Plasmonic Au/p-GaN Photocathodes., *Nano Letters* **18**, 2545–2550, DOI: 10.1021/acs.nanolett.8b00241 (2018).

Edri, E., Aloni, S., Frei, H. Fabrication of Core–Shell Nanotube Array for Artificial Photosynthesis Featuring an Ultrathin Composite Separation Membrane. *ACS Nano* **12**, 533–541, DOI: 10.1021/acsnano.7b07125 (2018).

Eichhorn, J., Liu, G., Toma, F. M. Chapter 8 Degradation of Semiconductor Electrodes in Photoelectrochemical Devices: Principles and Case Studies. Book Section in Integrated Solar Fuels Generators, The Royal Society of Chemistry, 281–303, DOI: 10.1039/9781788010313-00281 (2018).

Fields, M., Hong, X., Norskov, J., Chan, K. Role of Subsurface Oxygen on Cu Surfaces for CO_2 Electrochemical Reduction. *J. Phys. Chem C*, **122**, 16209–16215, DOI: 10.1021/acs.jpcc.8b04983 (2018).

Francis, S., Velazquez, J., Ferrer, I., Torelli, D., Guevarra, D., McDowell, M., Sun, K., Zhou, X., Saadi, F., John, J., Richter, M., Hyler, F., Papadantonakis, K., Brunschwig, B., Lewis, N. Reduction of aqueous CO_2 to 1-Propanol at MoS_2 electrodes. *Chem. Mater.* **30**, 4902–4908, DOI: 10.1021/acs.chemmater.7b04428 (2018).

Friebel, D. Chapter 4 Surface Science, X-ray and Electron Spectroscopy Studies of Electrocatalysis, Book Section in Integrated Solar Fuel Generators, The Royal Society of Chemistry, 117–153, DOI: 10.1039/9781788010313-00117 (2018).

Garza, A. J., Bell, A. T., Head-Gordon, M. Is Subsurface Oxygen Necessary for the Electrochemical Reduction of CO_2 on Copper? *J. Phys. Chem. Lett.* **9**, 601–606, DOI: 10.1021/acs.jpclett.7b03180 (2018).

Garza, A. J., Bell, A. T., Head-Gordon, M. Mechanism of CO_2 Reduction at Copper Surfaces: Pathways to C_2 Products. *Acs Catalysis* **8**, 1490–1499, DOI: 10.1021/acscatal.7b03477 (2018).

Garza, A., Bell, A., Head-Gordon, M. Nonempirical Meta-Generalized Gradient Approximations for Modeling Chemisorption at Metal Surfaces. *J. Chem. Theory Comput*. **14**, 3083–3090, DOI: 10.1021/acs.jctc.8b00288 (2018).

Greenblatt, J. B. Chapter 2 Photo-electrochemical Hydrogen Plants at Scale: A Life-cycle Net Energy Assessment, Book Section in Integrated Solar Fuel Generators, The Royal Society of Chemistry, 43–78, DOI: 10.1039/9781788010313-00043 (2018).

Greenblatt, J. B., Miller, D. J., Ager, J. W., Houle, F. A., Sharp, I. D. The Technical and Energetic Challenges of Separating (Photo)Electrochemical Carbon Dioxide Reduction Products. *Joule* 2, 381–420, https://doi.org/10.1016/j.joule.2018.01.014 (2018).

Gregoire, J. M., Boyd, D. A., Guevarra, D., Haber, J. A., Jones, R., Kan, K., Marcin, M., Newhouse, P. F., Shinde, A., Soedarmadji, E., Suram, S. K., Zhou, L. Chapter 9 High Throughput Experimentation for the Discovery of Water Splitting Materials. Book Section in Integrated Solar Fuel Generators, The Royal Society of Chemistry, 305–340, DOI: 10.1039/9781788010313-00305 (2018).

Han, L., Zhou, W., Xiang, C. High Rate Electrochemical Reduction of Carbon Monoxide to Ethylene using Cu-Nanoparticle-Based Gas Diffusion Electrodes. *ACS Energy Letters* **3**, 855–860, DOI: 10.1021/acsenergylett.8b00164 (2018)

Hashiba, H., Weng, L.-C., Chen, Y., Sate, H. K., Yotsuhashi, S., Xiang, C., Weber, A. Effects of Electrolyte Buffer Capacity on Surface Reactant Species and the Reaction Rate of CO_2 in Electrochemical CO_2 Reduction. *J. Phys. Chem. C* **122**, 3719–3726 DOI: 10.1021/acs.jpcc.7b11316 (2018).

Higgins, D., Landers, A., Ji, S., Nitopi, S., Morales-Guio, C., Wang, L., Chan, K., Hahn, C., Jaramillo, T. Guiding Electrochemical Carbon Dioxide Reduction toward Carbonyls Using Copper Silver Thin Films with Interphase Miscibility. *ACS Energy Letters* **3**, 2947–2955, DOI: 10.1021/acsenergylett.8b01736 (2018).

Higgins, D., Hahn, C., Xiang, C., Jaramillo, T., Weber, A. Gas-Diffusion Electrodes for Carbon Dioxide Reduction: A New Paradigm. *ACS Energy Letters* **4**, 317–324, DOI: 10.1021/acsenergylett.8b02035 (2018).

Huang, Y., Chen, Y., Cheng, T., Wang, L.-W., Goddard, W. Identification of the Selective Sites for Electrochemical Reduction of CO to C_{2+} Products on Copper Nanoparticles by Combining Reactive Force Fields, Density Functional Theory, and Machine Learning. *ACS Energy Letters* **3**, 2983–2988, DOI: 10.1021/acsenergylett.8b01933 (2018).

Huang, Y., Nielsen, R., Goddard, W. Reaction Mechanism for the Hydrogen Evolution Reaction on the Basal Plane Sulfur Vacancy Site of MoS_2 Using Grand Canonical Potential Kinetics. *J. Am. Chem. Soc.* **140**, 16773–16782, DOI: 10.1021/jacs.8b10016 (2018).

Jiang, C.-M., Segev, G., Hess, L. H., Liu, G., Zaborski, G., Toma, F. M., Cooper, J. K., Sharp, I. D. Composition-Dependent Functionality of Copper Vanadate Photoanodes. *ACS Appl. Mater. Interfaces* **10**, 10627-10633, DOI: 10.1021/acsami.8b02977 (2018).

Jiang, K., Sandberg, R. B., Akey, A. J., Liu, X., Bell, D. C., Norskov, J. K., Chan, K., Wang, H. Metal ion cycling of Cu foil for selective C–C coupling in electrochemical CO_2 reduction. *Nature Catalysis* **1**, 111–119, DOI: 10.1038/s41929-017-0009-x (2018).

Jones, R., Wang, Y., Lai, Y., Shinde, A., Gregoire, J. Reactor design and integration with product detection to accelerate screening of electrocatalysts for carbon dioxide reduction. *Review of Scientific Instruments* **89**, 124102, DOI: https://doi.org/10.1063/1.5049704 (2018).

Kempler, P. A., Gonzales, M. A., Papadantonakis, K., Lewis, N. Hydrogen Evolution with Minimal Parasitic Light Absorption by Dense Co–P Catalyst Films on Structured p-Si Photocathodes. *ACS Energy Letters* **3**, 612–617, DOI: 10.1021/acsenergylett.8b00034 (2018).

Kim, Y.-G., Baricuatro, J. H., Soriaga, M. P. Surface Reconstruction of Polycrystalline Cu Electrodes in Aqueous $KHCO_3$ Electrolyte at Potentials in the Early Stages of CO_2 Reduction. *Electrocatalysis* **9**, 526–530, DOI: https://doi.org/10.1007/s12678-018-0469-z (2018).

Kim, Y., Creel, E., Corson, E., McCloskey, B., Urban, J., Kostecki, R. Surface-Plasmon-Assisted Photoelectrochemical Reduction of CO_2 and NO_3^- on Nanostructured Silver Electrodes. *Adv. Mater.* **8**, 1800363, DOI: https://doi.org/10.1002/aenm.201800363 (2018).

Lam, R. K., Raj, S. L., Pascal, T. A., Pemmaraju, C. D., Foglia, L., Simoncig, A., Fabris, N., Miotti, P., Hull, C. J., Rizzuto, A. M., Smith, J. W., Mincigrucci, R., Masciovecchio, C., Gessini, A., Allaria, E., De Ninno, G., Diviacco, B., Roussel, E., Spampinati, S., Penco, G., Di Mitri, S., Trovò, M., Danailov, M., Christensen, S. T., Sokaras, D., Weng, T. C., Coreno, M., Poletto, L., Drisdell, W. S., Prendergast, D., Giannessi, L., Principi, E., Nordlund, D., Saykally, R. J., Schwartz, C. P. Soft X-Ray Second Harmonic Generation as an Interfacial Probe. *Physical Review Letters* **120**, 023901, DOI: https://doi.org/10.1103/PhysRevLett.120.023901 (2018).

Lam, R. K., et al. Two-photon absorption of soft X-ray free electron laser radiation by graphite near the carbon K-absorption edge. *Chemical Physics Letters* **703**, 112–116, DOI: https://doi.org/10.1016/j.cplett.2018.05.021 (2018).

Landers, A., Fields, M., Torelli, D., Xia, J., Hellstern, T., Francis, S., Tsai, C., Kibsgaard, J., Lewis, N., Chan, K., Hahn, C., Jaramillo, T. The Predominance of Hydrogen Evolution on Transition Metal Sulfides and Phosphides under CO_2 Reduction Conditions: An Experimental and Theoretical Study. *ACS Energy Letters* **3**, 1450–1457, DOI: 10.1021/acsenergylett.8b00237 (2018).

Lee, N.-E., Zhou, J.-J., Agapito, L. A., Bernardi, M. Charge transport in organic molecular semiconductors from first principles: The bandlike hole mobility in a naphthalene crystal. *Physical Review B* **97**, 115203, DOI: https://doi.org/10.1103/PhysRevB.97.115203 (2018).

Lewerenz, H. J., Sharp, I. D., Chapter 1 Concepts of Photoelectrochemical Energy Conversion and Fuel Generation, Book Section in Integrated Solar Fuel Generators, The Royal Society of Chemistry, 1–42, DOI: 10.1039/9781788010313-00001 (2018).

Lindley, S. A., Cooper, J. K., Rojas-Andrade, M. D., Fung, V., Leahy, C. J., Chen, S., Zhang, J. Z. Highly Tunable Hollow Gold Nanospheres: Gaining Size Control and Uniform Galvanic Exchange of Sacrificial Cobalt Boride Scaffolds. *ACS Appl. Mater. Interfaces* **10**, 12992–13001, DOI: 10.1021/acsami.8b00726 (2018).

Liu, G., Eichhorn, J., Jiang, C.-M., Scott, M., Hess, L., Gregoire, J., Haber, J., Sharp, I., Toma, F. Interface engineering for light-driven water oxidation: Unravelling the passivating and catalytic mechanism in $BiVO_4$ overlayers. *Sustainable Energy & Fuels* **3**, 127–135, DOI: 10.1039/C8SE00473K (2018).

Lu, Z., Chen, G., Siahrostami, S., Chen, Z., Liu, K., Xie, J., Liao, L., Wu, T., Lin, D., Liu, Y., Jaramillo, T., Norskov, J., Cui, Y. High-efficiency oxygen reduction to hydrogen peroxide catalysed by oxidized carbon materials. *Nature Catalysis* **1**, 156–162, DOI: 10.1038/s41929-017-0017-x (2018).

Lum, Y., Ager, J. W. Stability of residual oxides in oxide-derived Cu catalysts for electrochemical CO_2 reduction investigated with ^{18}O labeling. *Angew. Chem. Int. Ed.* **57**, 551, DOI: 10.1002/anie.201710590 (2018).

Lum, Y and Ager, J. Sequential catalysis controls selectivity in electrochemical CO_2 reduction on Cu. *Energy Environ. Sci.* **11**, 2935-2944, DOI: 10.1039/C8EE01501E (2018).

Lum, Y. and Ager, J., Evidence for product-specific active sites on oxide-derived Cu catalysts for electrochemical CO_2 reduction. *Nature Catalysis* 2, 86–93, DOI: 10.1038/s41929-018-0201-7 (2018).

Lum, Y, Cheng, T., Goddard, W., Ager, J. Electrochemical CO reduction builds solvent water into oxygenate products. *J. Am. Chem. Soc.* **140**, 9337–9340, DOI: 10.1021/jacs.8b03986 (2018).

McCrory, C. C. L., Suho, J., Jeremy, K. Chapter 5 Evaluating Electrocatalysts for Solar Water-splitting Reactions. Book Section in Integrated Solar Fuel Generators, The Royal Society of Chemistry, 154–181, DOI: 10.1039/9781788010313-00154 (2018).

Miller, D., Houle, F. Chapter 10 Membranes for Solar Fuels Devices. Book Section in Integrated Solar Fuel Generators, The Royal Society of Chemistry, 341–385, DOI: 10.1039/9781788010313-00341 (2018).

Morales-Guio, C., Cave, E., Nitopi, S., Feaster, J., Wang, L., Kuhl, K., Johnson, N., Abram, D., Hatsukade, T., Hahn, C., Jaramillo, T. Improved CO_2 reduction activity towards C_{2+} alcohols on a tandem gold on copper electrocatalyst. *Nat. Catal.*, **1**, 764–771, DOI: 10.1038/s41929-018-0139-9 (2018).

Moreno-Hernandez, I., Brunschwig, B., Lewis, N. Tin Oxide as a Protective Heterojunction with Silicon for Efficient Photoelectrochemical Water Oxidation in Strongly Acidic or Alkaline Electrolytes. *Adv. Mater.* **8**, 1801155, DOI: https://doi.org/10.1002/aenm.201801155 (2018).

Newhouse, P., Guevarra, D., Umehara, M., Reyes-Lillo, S., Zhou, L., Boyd, D., Suram, S., Cooper, J., Haber, J., Neaton, J., Gregoire, J. Combinatorial alloying improves bismuth vanadate photoanodes *via* reduced monoclinic distortion. *Energy Environ. Sci.*, **11**, 2444–2457, DOI: 10.1039/C8EE00179K (2018).

Newhouse, P. Guevarra, D., Umehara, M., Boyd, D., Zhou, L., Cooper, J., Haber, J., Gregoire, J. Multi-modal optimization of bismuth vanadate photoanodes via combinatorial alloying and hydrogen processing. *Chem. Comm.* **55**, 489–492, DOI: 10.1039/C8CC07156J (2018).

Osowiecki, W., Ye, X., Satish, P., Bustillo, K., Clark, E., Alivasatos, P. Tailoring Morphology of Cu–Ag Nanocrescents and Core–Shell Nanocrystals Guided by a Thermodynamic Model. *J. Am. Chem. Soc.* **140**, 8569–8577, DOI: 10.1021/jacs.8b04558 (2018).

Ostericher, A., Waldie, K., Kubiak, C. Utilization of thermodynamic scaling relationships in hydricity to develop nickel HER electrocatalysts with weak acids and low overpotentials. *ACS Catalysis* **8**, 9596–9603, DOI: 10.1021/acscatal.8b02922 (2018).

Palmer, C.; Saadi, F.; McFarland, E. Technoeconomics of Commodity Chemical Production Using Sunlight. *ACS Sustainable Chem. Eng.*, **6**, 7003–7009, DOI: 10.1021/acssuschemeng.8b00830 (2018).

Resasco, J., Lum, Y., Clark, E., Zeledon, J., Bell, A. T. Effects of anion identity and concentration on electrochemical reduction of CO2. *ChemElectroChem* **5**, 1064–1072, DOI: 10.1002/celc.201701316 (2018).

Saadi, F. H., Lewis, N. S., McFarland, E. W. Relative costs of transporting electrical and chemical energy. *Energy Environ. Sci.* **11**, 469–475, DOI: 10.1039/C7EE01987D (2018).

Segev, G., Dotan, H., Ellis, D. S., Piekner, Y., Klotz, D., Beeman, J. W., Cooper, J. K., Grave, D. A., Sharp, I. D., Rothschild, A. The Spatial Collection Efficiency of Charge Carriers in Photovoltaic and Photoelectrochemical Cells. J *Joule* 2, 210–224, https://doi.org/10.1016/j.joule.2017.12.007 (2018).

Segev, G., Jiang, C.-M., Cooper, J. K., Eichorn, J., Toma, F., Sharp, I. D. Quantification of the loss mechanisms in emerging water splitting photoanodes through empirical extraction of the spatial charge collection efficiency. *Energy Environ. Sci.* **11**, 904–913, DOI: 10.1039/C7EE03486E (2018).

Segev, G., Beeman, J., Greenblatt, J., Sharp, I. Hybrid photoelectrochemical and photovoltaic cells for simultaneous production of chemical fuels and electrical power. *Nature Materials* **17**, 1115–1121, DOI: https://doi.org/10.1038/s41563-018-0198-y (2018).

Shen, H., Omelchenko, S., Jacobs, D., Yalamanchili, S., Wan, Y., Yan, D., Phang, P., Duong, T., Wu, Y., Samundsett, C., Peng, J., Wu, N., White, T., Andersson, G., Lewis, N., Catchpole, K. In situ recombination junction between p-Si and TiO_2 enables high-efficiency monolithic perovskite/Si tandem cells. *Science Advances* **4**, eaau9711, DOI: 10.1126/sciadv.aau9711 (2018).

Shin, H., Xioa, H., Goddard, W. A. In Silico Discovery of New Dopants for Fe-Doped Ni Oxyhydroxide ($Ni_{1-x}Fe_xOOH$) Catalysts for Oxygen Evolution Reaction. *J. Am. Chem. Soc.* **140**, 6745–6748, DOI: 10.1021/jacs.8b02225 (2018).

Singh, M. R., Haussener, S., Weber, A., Chapter 13 Continuum-scale Modeling of Solar Water-splitting Devices. Book Section in Integrated Solar Fuel Generators, The Royal Society of Chemistry, 500–536, DOI: 10.1039/9781788010313-00500 (2019).

Soniat, M. and Houle, F. Swelling and Diffusion during Methanol Sorption into Hydrated Nafion. *J. Phys. Chem. B* **122**, 8255–8268, DOI: 10.1021/acs.jpcb.8b03169 (2018).

Soniat, M., Tasfaye, M., Brooks, D., Merinov, B., Goddard, W. A., Weber, A. Z., Houle, F. A. Predictive simulation of non-steady-state transport of gases through rubbery polymer membranes. *Polymer* **134**, 125–142, https://doi.org/10.1016/j.polymer.2017.11.055 (2018).

Stoerzinger, K., Favaro, M., Ross, P., Hussain, Z., Liu, Z., Yano, J., Crumlin, E. Stabilizing the Meniscus for Operando Characterization of Platinum During the Electrolyte-Consuming Alkaline Oxygen Evolution Reaction. *Topics in Catalysis* **61**, 2152–2160, DOI: https://doi.org/10.1007/s11244-018-1063-6 (2018).

Sun, K., Ritzert, N. L., John, J., Tan, H., Hale, W., Joang, J., Moreno-Hernandez, I. A., Papadantonakis, K., Moffat, T., Brunschwig, B., Lewis, N. Performance and Failure Modes of Si Anodes Patterned with Thin-Film Ni Catalyst Islands for Water Oxidation. *Sustainable Energy & Fuels* 2, 983–998, DOI: 10.1039/C7SE00583K (2018).

Suram, S. K., Zhou, L., Shinde, A., Yan, Q., Yu, Y., Umehara, M., Stein, H. S., Neaton, J., and Gregoire, J. Discovery of alkaline-stable nickel manganese oxides with visible photoresponse for solar fuels photoanodes. *Chemical Communications* **54**, 4625–4628, DOI: 10.1039/C7CC08002F (2018).

Sutter-Fella, C., Ngo, Q. P., Cefarin, N., Gardner, K. L., Tamura, N., Stan, C., Drisdell, W., Javey, A., Toma, F., Sharp, I. D. Cation-Dependent Light-Induced Halide Demixing in Hybrid Organic–Inorganic Perovskites. *Nano Letters* **18**, 3473–3480, DOI: 10.1021/acs.nanolett.8b00541 (2018).

Swierk, J. R. and Tilley, T. D. Electrocatalytic Water Oxidation by Single Site and Small Nuclearity Clusters of Cobalt. *J. Electrochem. Soc.*, **165**, H3028–H3033, DOI: 10.1149/2.0041804jes (2018).

Tagliabue, G., Jermyn, A., Sundararaman, R., Welch, A., DeChene, J., Pala, R., Dovoyan, A., Narang, P., Atwater, H. Quantifying the role of surface plasmon excitation and hot carrier transport in plasmonic devices. *Nature Comm.*, **9**, 3394, DOI: https://doi.org/10.1038/s41467-018-05968-x (2018).

Tang, M., Ulissi, Z., Chan, K. Theoretical Investigations of Transition Metal Surface Energies under Lattice Strain and CO Environment. *J. Phys. Chem. C* **122**, 14481–14487, DOI: 10.1021/acs.jpcc.8b02094 (2018).

Tesfaye, M., Kushner, D., McCloskey, B., Weber, A., Kusoglu, A. Thermal Transitions in Perfluorosulfonated Ionomer Thin-Films. *ACS Macro Letters* **7**, 1237–1242, DOI: 10.1021/acsmacrolett.8b00628 (2018).

Tsang, C., Javier, A., Kim, Y.-G., Baricuatro, J., Cummins, K., Kim, J., Jerkiewicz, G., Hemminger, J., Soriaga, J. Potential-Dependent Adsorption of CO and Its Low-Overpotential Reduction to CH_3CH_2OH on Cu(511) Surface Reconstructed from Cu(pc): Operando Studies by Seriatim STM-EQCN-DEMS. *J. Electrochem. Soc.* **165**, J3350–J3354, DOI: 10.1149/2.0451815jes (2018).

Waldie, K., Ostericher, A. L., Reineke, M. H., Sasayama, A. F., Kubiak, C. P. Hydricity of Transition-Metal Hydrides: Thermodynamic Considerations for CO_2 Reduction. *ACS Catalysis* **8**, 1313–1324, DOI: 10.1021/acscatal.7b03396 (2018).

Waldie, K., Brunner, F. M., Kubiak, C. P., Transition Metal Hydride Catalysts for Sustainable Interconversion of CO_2 and Formate: Thermodynamic and Mechanistic Considerations. *ACS Sustainable Chemistry & Engineering* **6**, 6841–6848, DOI: 10.1021/acssuschemeng.8b00628 (2018).

Wan, Y., Bullock, J., Xu, Z., Yan, D., Peng, J., Javey, A., Cuevas, A. Zirconium oxide surface passivation of crystalline silicon. *Appl. Phys. Lett.*, **112**, 201604, DOI: https://doi.org/10.1063/1.5032226 (2018).

Wan, Y., Bullock, J., Hettick, M., Xu, Z., Samundsett, C., Yan, D., Peng, J., Ye, J., Javey, A., Cuevas, A. Temperature and Humidity Stable Alkali/Alkaline-Earth Metal Carbonates as Electron Heterocontacts for Silicon Photovoltaics. *Adv. Energy Mater.* **8**, 1800743, DOI: https://doi.org/10.1002/aenm.201800743 (2018).

Wang, L., Goddard, W., Cheng, T., Xiao, H., Li, Y. In Silico Optimization of Organic-Inorganic Hybrid Perovskites for Photocatalytic Hydrogen Evolution Reaction in Acidic Solution. *J. Phys. Chem. C* **122**, 20918–20922, DOI: 10.1021/acs.jpcc.8b07380 (2018).

Wang, L., Xiao, H., Cheng, T., Li, Y., Goddard, W. A. Pb-Activated Amine-Assisted Photocatalytic Hydrogen Evolution Reaction on Organic–Inorganic Perovskites. *J. Am. Chem. Soc.* **140**, 1994–1997, DOI: 10.1021/jacs.7b12028 (2018).

Wang, L., Nitopi, S., Bertheussen, E., Orazov, M., Morales-Guio, C., Liu, X., Higgins, D., Cahn, K., Norskov, J., Hahn, C., Jaramillo, T. Electrochemical Carbon Monoxide Reduction on Polycrystalline Copper: Effects of Potential, Pressure, and pH on Selectivity toward Multicarbon and Oxygenated Products. *ACS Catalysis* **8**, 7445–7454, DOI: *DOI: 10.1021/acscatal.8b01200* (2018).

Wang, Z., Wu, L., Sun, K., Jiang, Z., Cheng, T., Goddard, W. Surface Ligand Promotion of Carbon Dioxide Reduction through Stabilizing Chemisorbed Reactive Intermediates. *J. Phys. Chem. Lett.*, **9**, 3057–3061, DOI: 10.1021/acs.jpclett.8b00959 (2018).

Welborn, M., Manby, F., Miller, T. Even-handed subsystem selection in projection-based embedding. *The Journal of Chemical Physics* **149**, 144101, DOI: https://doi.org/10.1063/1.5050533 (2018).

Welch, A., DuChene, J., Tagliabue, G., Danoyan, A., Cheng, W.-H., Atwater, H. Nanoporous Gold as a Highly Selective and Active Carbon Dioxide Reduction Catalyst. *ACS Applied Energy Materials* **2**, 164–170, DOI: 10.1021/acsaem.8b01570 (2018).

Weng, L.-C., Bell, A., Weber, A. Modeling gas-diffusion electrodes for CO_2 reduction. *Phys. Chem. Chem. Phys.* **20**, 16973–16984, DOI: 10.1039/C8CP01319E (2018).

Xaing, C., Walczak, K., Haber, J., Jones, R., Beeman, J., Guevarra, D., Karp, C., Liu, R., Shaner, M., Sun, K., West, W., Zhou, L. Chapter 11 Prototyping Development of Integrated Solar-driven Water-splitting Cells. Book Section in Integrated Solar Fuel Generators, The Royal Society of Chemistry, 387–453, DOI: 10.1039/9781788010313-00387 (2018).

Xiao, H., Shin, H., Goddard, W. Synergy between Fe and Ni in the optimal performance of (Ni,Fe) OOH catalysts for the oxygen evolution reaction. *PNAS* **115**, 5872–5877, DOI: https://doi.org/10.1073/pnas.1722034115(2018).

Zhang, H., Goddard, W. A., Lu, Q., Cheng, M.-J. The importance of grand-canonical quantum mechanical methods to describe the effect of electrode potential on the stability of intermediates involved in both electrochemical CO_2 reduction and hydrogen evolution. *Phys. Chem. Chem. Phys*, **20**, 2549–2557, DOI: 10.1039/C7CP08153G (2018).

Zheng, X., Ji, Y., Tang, J., Wang, J., Liu, B., Steinruck, H.-G., Lim, K., Li, Y., Toney, M., Chan, K., Cui, Y. Theory-guided Sn/Cu alloying for efficient CO_2 electroreduction at low overpotentials. *Nature Catalysis* 2, 55–61, DOI: 10.1038/s41929-018-0200-8 (2018).

Zhou, J.-J., Hellman, O., Bernardi, M. Electron-Phonon Scattering in the Presence of Soft Modes and Electron Mobility in $SrTiO_3$ Perovskite from First Principles. *Phys. Rev. Lett.* **121**, 226603, https://doi.org/10.1103/PhysRevLett.121.226603 (2018).

Zhou, L., Shinde, A., Guevarra, D., Toma, F., Stein, H., Gregoire, J., Haber, J. Balancing Surface Passivation and Catalysis with Integrated $BiVO_4$/(Fe-Ce)O_x Photoanodes in pH 9 Borate Electrolyte. *ACS Applied Energy Materials*, DOI: 10.1021/acsaem.8b01377 (2018).

Zhou, L., Shinde, A., Suram, S., Stein, H., Bauers, S., Zakutayev, A., DuChene, J., Liu, G., Peterson, E., Neaton, J., Gregoire, J. Bi-containing n-$FeWO_4$ Thin Films Provide the Largest Photovoltage and Highest Stability for a sub-2 eV Band Gap Photoanode. *ACS Energy Letters* **3**, 1892–1897, DOI: 10.1021/acsenergylett.8b01514 (2018).

Zhou, L., Shinde, A., Montoya, J., Singh, A., Gul, S., Yano, J., Ye, Y., Crumlin, E., Richter, M., Cooper, J., Stein, H., Haber, J., Persson, K., Gregoire, J. Rutile alloys in the Mn-Sb-O system stabilize Mn^{+3} to enable oxygen evolution in strong acid. *ACS Catalysis* **8**, 10938–10948, DOI: 10.1021/acscatal.8b02689 (2018).

Zhou, X. and Xiang, C. Comparative Analysis of Solar-to-Fuel Conversion Efficiency: A Direct, One-Step Electrochemical CO2 Reduction Reactor versus a Two-Step, Cascade Electrochemical CO_2 Reduction Reactor. *ACS Energy Letters* **3**, 1892–1897, DOI: *10.1021/acsenergylett.8b01077* (2018).

2017

Bai, J., Bjorck, J., Xue, Y., Suram, S. K., Gregoire, J., Gomes, C. Relaxation Methods for Constrained Matrix Factorization Problems: Solving the Phase Mapping Problem in Materials Discovery. in Integration of AI and OR Techniques in Constraint Programming, Springer, ISBN: 978–3–319–59776–8 (2017).

Beckingham, B. S., Lynd, N. A., Miller, D. J. Monitoring Multicomponent Transport using *In Situ* ATR FTIR Spectroscopy. *Journal of Membrane Science* **550**, 348–356, DOI: https://doi.org/10.1016/j.memsci.2017.12.072 (2017).

Bouabadi, B., et al. Enhanced plasmon-mediated photo-assisted hydrogen evolution on silicon by interfacial modification. *J. Appl. Electrochem.* **47**, 457–466, DOI: 10.1007/s10800-017-1055-4 (2017).

Brown, A. M. et al. Experimental and *Ab Initio* Ultrafast Carrier Dynamics in Plasmonic Nanoparticles. *Physical Review Letters* **118**, 087401, DOI: 10.1103/PhysRevLett.118.087401 (2017).

Buabthong, P., Stasiewicz, N., Mitrovic, S., Lewis, N. S. Vanadium, niobium and tantalum by XPS. *Surface Science Spectra* 24, 024001, DOI: http://dx.doi.org/10.1116/1.4998018 (2017).

Bukowsky, C. R. et al. Photon and carrier management design for nonplanar thin-film copper indium gallium selenide photovoltaics. *Solar Energy Materials and Solar Cells* **161**, 149–156, DOI: http://dx.doi.org/10.1016/j.solmat.2016.11.008 (2017).

Buss, H. G., Chan, S. Y., Lynd, N. A., and McCloskey, B. D. Nonaqueous Polyelectrolyte Solutions as Liquid Electrolytes with High Lithium Ion Transference Number and Conductivity. *ACS Energy Letters* 2, 481–487, DOI: 10.1021/acsenergylett.6b00724 (2017).

Carter, B. M., Dobyns, B. M., Beckingham, B. S., Miller, D. J. Multicomponent transport of alcohols in an anion exchange membrane measured by *in-situ* ATR FTIR spectroscopy. *Polymer* **123**, 144–152, DOI: 10.1016/j.polymer.2017.06.070 (2017).

Chen, Y.-C., lu, A.-Y., Lu, P., Yang, X., Jiang, C.-M., Mariano, M., Kaehr, B., Lin, O., Taylor, A., Sharp, I. D., Li, L.-J., Chou, S. S., Tung, V. Structurally Deformed MoS2 for Electrochemically Stable, Thermally Resistant, and Highly Efficient Hydrogen Evolution Reaction. *Adv. Mater.* **29**, 1703863, DOI: 10.1002/adma.201703863 (2017).

Cheng, T., Xiao, H, and Goddard, W. A. Full atomistic reaction mechanism with kinetics for CO reduction on Cu(100) from ab initio molecular dynamics free-energy calculations at 298 K. *PNAS* **114**, 1795–1800, DOI: 10.1073/pnas.1612106114 (2017).

Cheng, T., Hung, Y., Xiao, H., and Goddard, W. A. Predicted Structures of the Active Sites Responsible for the Improved Reduction of Carbon Dioxide by Gold Nanoparticles. *J. Phys. Chem. Lett.*, **8**, 3317–3320, DOI: 10.1021/acs.jpclett.7b01335 (2017).

Cheng, T., Xiao, H., Goddard, W. A. Nature of the Active Sites for CO Reduction on Copper Nanoparticles; Suggestions for Optimizing Performance. *J. Am. Chem. Soc.* **139**, 11642–11645, DOI: 10.1021/jacs.7b03300 (2017).

Clark, E. L., Hahn, C., Jaramillo, T. F., Bell, A. B. Electrochemical CO_2 Reduction over Compressively Strained CuAg Surface Alloys with Enhanced Multi-Carbon Oxygenate Selectivity. *J. Am. Chem. Soc.* **139**, 15848–15857, DOI: 10.1021/jacs.7b08607 (2017).

Contanda, P., Petzetakis, N., Jiang, X., Stone, G., and Balsara, N. P. Hydroxide-ion transport and stability of diblock copolymers with a polydiallyldimethyl ammonium hydroxide block. *Polymer Chemistry* **55**, 2243–2248, DOI: 10.1002/pola.28611 (2017).

Ding, F., Manby, F. R., and Miller, T. F. Embedded Mean-Field Theory with Block-Orthogonalized Partitioning. *J. Chem. Theory Comput.* **13**, 1605–1615, DOI: 10.1021/acs.jctc.6b01065 (2017).

Ding, F., Tsuchiya, T., Manby, F. R., and Miller, T. F. Linear-response time-dependent embedded mean-field theory. *J. Chem. Theory Comput.* **13**, 4216–4227, DOI: 10.1021/acs.jctc.7b00666 (2017).

Drisdell, W. S., Leppert, L., Sutter-Fella, C. M., Lang, Y., Li, Y., Ngo, Q., Wan, L., Gul, S., Kroll, T., Sokaras, D., Javey, A., Yano, J., Neaton, J., Toma, F., Prendergast, D., and Sharp, I. Determining Atomic-scale Structure and Composition of Organo-lead Halide Perovskites by Combining High-resolution X-ray Absorption Spectroscopy and First-principles Calculations. *ACS Energy Letters* **2**, 1183–1189, DOI: 10.1021/acsenergylett.7b00182 (2017).

Edri, E., Cooper, J. K., Sharp, I. D., Culdi, D. M., and Frei, H. Ultrafast Charge Transfer Between Light Absorber and Co_3O_4 Water Oxidation Catalyst Across Molecular Wires Embedded in Silica Membrane. *J. Am. Chem. Soc.* **139**, 5458–5466, DOI: 10.1021/jacs.7b01070 (2017).

Eilert, A. et al. Subsurface Oxygen in Oxide-Derived Copper Electrocatalysts for Carbon Dioxide Reduction. *J. Phys. Chem. Lett.* **8**, 285–290, DOI: 10.1021/acs.jpclett.6b02273 (2017).

Fan, Z., Xiao, H., Wang, Y., Zhao, Z., Lin, Z., Cheng, H.-C., Lee, S.-J., Wang, G., Feng, Z., Goddard, W., Hung, Y., Duan, X. Layer-by-Layer Degradation of Methylammonium Lead Tri-iodide Perovskite Microplates. *Joule* **1**, 548–562, https://doi.org/10.1016/j.joule.2017.08.005 (2017).

Favaro, M. et al. An *Operando* Investigation of (Ni-Fe-Co-Ce)O_x System as Highly Efficient Electrocatalyst for Oxygen Evolution Reaction. *ACS Catalysis* **7**, 1248–1258, DOI: 10.1021/acscatal.6b03126 (2017).

Favaro, M., Valero-Vidal, C., Eichhorn, J., Toma, F. M., Rosse, P. N., Yano, J., Liu, Z., and Crumplin, E. J. Elucidating the alkaline oxygen evolution reaction mechanism on platinum. *J. Mater. Chem. A* **5**, 11634–11643, DOI: 10.1039/C7TA00409E (2017).

Favaro, M., Xiao, H., Cheng, T., Goddard, W. A., Yano, J., and Crumlin, E. J. Subsurface oxide plays a critical role in CO_2 activation by Cu(111) surfaces to form chemisorbed CO_2, the first step in reduction of CO_2. *PNAS* **114**, 6706–6711, DOI: 10.1073/pnas.1701405114 (2017).

Favaro, M., Yang, J., Nappini, S., Magnano, E., Toma, F. M., Crumlin, E. J., Yano, J., and Sharp, I. D. Understanding the oxygen evolution reaction mechanism on CoO_x using operando ambient pressure X-ray photoelectron spectroscopy. *J. Am. Chem. Soc.* **139**, 8960–8970, DOI: 10.1021/jacs.7b03211 (2017).

Feaster, J. T., Jongerius, A. L., liu, X., Urushihara, M., Nitopi, S. A., Hahn, C., Chan, K., Norskov, J. K., and Jaramillo, T. F. Understanding the Influence of [EMIM]Cl on the Suppression of the Hydrogen Evolution Reaction on Transition Metal Electrodes. *Langmuir* **33**, 9464–9471, DOI: 10.1021/acs.langmuir.7b01170 (2017).

Gaulding, E. A., Liu, G., Chen, C. T., Lobbert, L., Li, A., Segev, G., Eichhorn, J., Aloni, S., Schwartzberg, A., Sharp, I. D., and Toma, F. Fabrication and optical characterization of polystyrene opal templates for the synthesis of scalable, nanoporous (photo)electrocatalytic materials by electrodeposition. *J. Mater. Chem. A* **5**, 11601–11614, DOI:10.1039/C7TA00512A (2017).

Green, M. L., Choi, C. L., Hattrick-Simpers, J. R., Joshi, A. M., Takeuchi, I., Barron, S. C., Campo, E., Chiang, T., Empadocles, S., Gregoire, J. M., Kusne, A. G., Martin, J., Mehta, A., Persson, K., Trautt, Z., Van Duren, J., and Zakutayev, A. Fulfilling the promise of the materials genome initiative with high-throughput experimental methodologies. *Applied Physics Reviews* **4**, 011105, DOI: 10.1063/1.4977487 (2017).

Gurudayal, G., Bullock, J., Sranko, D. F., Towle, C. M., Lum, Y., Hettick, M., Scott, M. C., Javey, A., Ager, J. W. Efficient solar-driven electrochemical CO_2 reduction to hydrocarbons and oxygenates. *Energy Environ. Sci.* **10**, 2222–2230, DOI: 10.1039/C7EE01764B (2017).

Hahn, C., Hatsukade, T., Kim, Y.-G., Vailionis, A., Baricuatro, J. H., Higgins, D. C., Nitopi, S. A., Soriaga, M. P., and Jaramillo, T. F. Engineering Cu surfaces for the electrocatalytic conversion of CO_2: Controlling selectivity toward oxygenates and hydrocarbons. *PNAS* **114**, 5918–5923, DOI: 10.1073/pnas.1618935114 (2017).

Han, Z., Kortlever, R., Chen H.-Y., Peters, J. C., and Agapie, T. CO_2 Reduction Selective for C≥2 Products on Polycrystalline Copper with N-Substituted Pyridinium Additives. *ACS Central Science* **3**, 853–859, DOI: 10.1021/acscentsci.7b00180 (2017).

Hess, L. H. et al. Probing interfacial energetics and charge transfer kinetics in semiconductor nanocomposites: New insights into heterostructured TiO_2/$BiVO_4$ photoanodes. *Nano Energy* **34**, 375–384, DOI: 10.1016/j.nanoen.2017.02.051 (2017).

Javier, A. et al. Electrocatalytic Reduction of CO_2 on Cu and Au/W Electrode Surfaces: Empirical (DEMS) Confirmation of Computational (DFT) Predictions. *ECS Transactions* **75**, 1–17, DOI:10.1149/07548.0001ecst (2017).

Jhalani, V. A., Zhou, J.-J., and Bernardi, M. Ultrafast Hot Carrier Dynamics in GaN and Its Impact on the Efficiency Droop. *Nano Lett*, **17**, 5012–5019, DOI: 10.1021/acs.nanolett.7b02212 (2017).

Jiang, C.-M., Farmand, M., Wu, C., Liu, Y.-S., Guo, J., Drisdell, W.S., Cooper, J. K., and Sharp, I. D. Electronic Structure, Optoelectronic Properties, and Photoelectrochemical Characteristics of γ-$Cu_3V_2O_8$ Thin Films. *Chem. Mater.***29**, 3334–3345, DOI: 10.1021/acs.chemmater.7b00807 (2017).

Jiang, J., Huang, Z., Xiang, C., Poddar, R., Lewerenz, H.-J., Papadantonakis, K. M., Lewis, N. S., and Brunschwig, B. Nanoelectrical and Nanoelectrochemical Imaging of Pt/p-Si and Pt/p+-Si Electrodes. *ChemSusChem* **10**, 4657–4663, DOI: 10.1002/cssc.201700893 (2017).

Jiang, K., Siahrostami, S., Akey, A. J., Li, Y., Lu, Z., Lattimer, J., Hu, Y., Stikes, C., Gangishetty, M., Chen, G., Zhou, Y., Hill, W., Cai, W.-B., Bell, D., Chan, K., Norskov, J. K., Cui, Y., Wang, H. Transition-Metal Single Atoms in a Graphene Shell as Active Centers for Highly Efficient Artificial Photosynthesis. *Chem* **3**, 950–960, DOI: https://doi.org/10.1016/j.chempr.2017.09.014 (2017)

Jung, S. et al. Gastight Hydrodynamic Electrochemistry: Design for a Hermetically Sealed Rotating Disk Electrode Cell. *Analytical Chemistry* **89**, 581–585, DOI: 10.1021/acs.analchem.6b04228 (2017).

Kim, Y.-G. et al. Tuning the CO-Reduction Product Distribution by Structural Modification of the Cu Electrode Surface. *ECS Transactions* **75**, 87–97, DOI: 10.1149/07550.0087ecst (2017).

Kim, Y.-G., Javier, A., Baricuatro, J. H., Torelli, D., Cummins, K. D., Tsang, C. F., Hemminger, J. C., and Soriaga, M. P. Surface reconstruction of pure-Cu single-crystal electrodes under CO-reduction potentials in alkaline solutions: A study by seriatim ECSTM-DEMS. *Journal of Electroanalytical Chemistry* **793**, 113–118, DOI 10.1016/j.jelechem.2017.04.037 (2017).

Kirk, C., Chen, L. D., Siahrostami, S., Karamad, M., Badjich, M., Voss, J., Norskov, J., Chan, K. Theoretical Investigations of the Electrochemical Reduction of CO on Single Metal Atoms Embedded in Graphene. *ACS Central Science* **3**, 1286–1293, DOI: 10.1021/acscentsci.7b00442 (2017).

Ledina, M. A., Bui, N., Liang, X., Kim, Y.-G., Jung, J., Perdue, B., Tsang, C., Drnec, J., Cerla, F., Soriaga, M. P., Reber, T. J., Steckey, J. L. Electrochemical Formation of Germanene: pH 4.5. *J. Electrochem. Soc.* **164**, D469–477, DOI: 10.1149/2.1221707jes (2017).

Lee, S. J. R., Miyamoto, K., Ding, F., Manby, F. R., and Miller, T. F. Density-based errors in mixed-basis mean-field electronic structure, with implications for embedding and QM/MM methods. *Chemical Physics Letters* **683**, 375–382, DOI: 10.1016/j.cplett.2017.04.059 (2017).

Liang, Y., Vinson, J., Pemmaraju, S., Drisdell, W. S., Shirley, E. L. and Prendergast, D. Accurate X-Ray Spectral Predictions: An Advanced Self-Consistent-Field Approach Inspired by Many-Body Perturbation Theory. *Phys. Rev. Lett.* **118**, 096402, DOI: 10.1103/PhysRevLett.118.096402 (2017).

Lichterman, M. F., Richter, M. H., Brunschwig, B. S., Lewis, N. S., and Lewerenz, H. J. Operando X-ray Photoelectron Spectroscopic Investigations of the Electrochemical Double Layer at Ir/KOH(aq) Interfaces. *Journal of Electron Spectroscopy and Related Phenomena* **221**, 99–105, DOI: 10.1016/j.elspec.2017.03.011 (2017).

Liu, X., Xiao, J., Peng, H., Hong, X., Chan, K., and Norskov, J. K. Understanding trends in electrochemical carbon dioxide reduction rates. *Nat Commun* **8**, 15438, DOI: 10.1038/ncomms15438 (2017).

Lum, Y., Yue, B., Lobaccaro, P., Bell, A. T., and Ager, J. W. Optimizing C-C Coupling on Oxide-Derived Copper Catalysts for Electrochemical CO_2 Reduction. *J. Phys. Chem. C.* **121**, 14191–14203, DOI: 10.1021/acs.jpcc.7b03673 (2017).

Ma, J. and Wang, L.-W. The Nature of Electron Mobility in Hybrid Perovskite $CH_3NH_3PbI_3$. *Nano Letters* **17**, 3646–3654, DOI: 10.1021/acs.nanolett.7b00832 (2017).

Maurya, S. K., Liu, Y., Das, C., Xu, X., Woods-Robinson, R., Ager, J. W., Kavaipatti, B. High figure-of-merit p-type transparent conductor, Cu alloyed ZnS via radio frequency magnetron sputtering. *Journal of Physics D: Applied Physics* **50**, https://doi.org/10.1088/1361-6463/aa95b3 (2017).

Monroe, M. M., Lobaccaro, P., Lum, Y. and Ager, J. W. Membraneless laminar flow cell for electrocatalytic CO_2 reduction with liquid product separation. *J. Phys. D: Appl. Phys.* **50**, 154006, DOI: 10.1088/1361-6463/aa6359 (2017).

Montoya, J. H., Seitz, L. C., Chakthranont, P., Vojvodic, A., Jaramillo, T. F., and Norskov, J. K. Materials for solar fuels and chemicals. *Nature Mater* **16**, 70–81, DOI: 10.1038/nmat4778 (2017).

Moreno-Hernandez, I. A., MacFarland, C. A., Read, C. G., Brunschwig, B. S., Papadantonakis, K. M., and Lewis, N. Crystalline Nickel Manganese Antimonate as a Stable Water-Oxidation Catalyst in Aqueous 1.0 M H_2SO_4. *Energy Environ Sci* **10**, 2103–2108, DOI: 10.1039/C7EE01486D (2017).

Naserifar, S., Brooks, D. J., Goddard, W. A., and Cvicek, V. Polarizable charge equilibration model for predicting accurate electrostatic interactions in molecules and solids. *J Chem Phys* **146**, 124117, DOI: 10.1063/1.4978891 (2017).

Nellist, M. R. et al. Atomic force microscopy with nanoelectrode tips for high resolution electrochemical, nanoadhesion and nanoelectrical imaging. *Nanotechnology* 28, 095711, DOI: https://doi.org/10.1088/1361-6528/aa5839 (2017).

Newhouse, P. F., Reyes-Lillo, S. E., Li, G., Zhou, L., Shinde, A., Guevarra, D., Suram, S. K., Soedarmadji, E., Richetr, M. H., Qu, X., Persson, K., Neaton, J. B., Gregoire, J. M. Discovery and Characterization of a Pourbaix Stable, 1.8 eV Direct Gap Bismuth Manganate Photoanode. *Chem. Mater* 29, 10027–10036, DOI: 10.1021/acs.chemmater.7b03591 (2017).

Omelchenko, S. T. et al. Excitonic Effects in Emerging Photovoltaic Materials: A Case Study in Cu_2O. *ACS Energy Letters* 2, 431–437, DOI: 10.1021/acsenergylett.6b00704 (2017).

Resasco, J., Chen, L. D., Clark, E., Tsai, C., Hahn, C., Jaramillo, T. F., Chan, K., and Bell, A. T. Promoter Effects of Alkali Metal Cations on the Electrochemical Reduction of Carbon Dioxide. *J. Am. Chem. Soc.* **139**, 11277–11287, DOI: 10.1021/jacs.7b06765 (2017).

Saadi, F. H., Carim, A. I., Drisdell, W. S., Gul, S., Baricuatro, J. H., Yano, J., Soriaga, M. P., Lewis, N. S. *Operando* Spectroscopic Analysis of CoP Films Electrocatalyzing the Hydrogen-Evolution Reaction. *J. Am. Chem. Soc.* **139**, 12927–12930, DOI: 10.1021/jacs.7b07606 (2017).

Sharp, I. D. et al. Bismuth Vanadate as a Platform for Accelerating Discovery and Development of Complex Transition Metal Oxide Photoanodes. *ACS Energy Letters*, 2, 139–150, DOI: 10.1021/acsenergylett.6b00586 (2017).

Shinde, A., Suram, S. K., Yan, Q., Zhou, Q., Zhou, L., Singh, A. K., Persson, K. A., Neaton, J. B., Gregoire, J. M. Discovery of Manganese-Based Solar Fuel Photoanodes via Integration of Electronic Structure Calculations, Pourbaix Stability Modeling, and High-Throughput Experiments. *ACS Energy Letters*, 2, 2307–2312, DOI: 10.1021/acsenergylett.7b00607 (2017).

Siahrostami, S., Jiang, K., Karamad, M., Chan, K., Wang, H., Norskov, J. Theoretical Investigations into Defected Graphene for Electrochemical Reduction of CO_2. *ACS Sustainable Chemistry & Engineering* **5**, 11080–11085, DOI: 10.1021/acssuschemeng.7b03031 (2017).

Singh, M. R., Xiang, C., and Lewis, N. Evaluation of Flow Schemes for Near-Neutral Electrolytes in Solar-Fuels Generators. *Sustainable Energy & Fuels* **1**, 458–466, DOI: 10.1039/C7SE00062F (2017).

Singh, M. R., Goodpaster, J. D., Weber, A. Z., Head-Gordon, M., Bell, A. T. Mechanistic insights into electrochemical reduction of CO_2 over Ag using density functional theory and transport models. *PNAS* **114**, E8812–E8821, DOI: 10.1073/pnas.1713164114 (2017).

Singh, A. K., Zhou, L., Shinde, A., Suram, S. K., Montoya, J. H., Winston, D., Gregoire, J. M., Persson, K. A. Electrochemical Stability of Metastable Materials. *Chem. Mater.***29**, 10159–10167, DOI: 10.1021/acs.chemmater.7b03980 (2017).

Soriaga, M. P., Baricuatro, J. H., Javier, A., A., Kim, Y.-G., Cummins, K. D., Tsang, C. F. Electrochemical Surface Science of CO_2 Reduction at Well-Defined Cu Electrodes: Surface Characterization by Emersion, Ex Situ, In Situ, and Operando Methods. Reference Module in Chemistry, Molecular Sciences and Chemical Engineering, DOI: https://doi.org/10.1016/B978-0-12-409547-2.13643-1 (2017).

Stoerzinger, K., Favaro, M., Ross, P. N., Yano, J., Liu, Z., Hussain, Z., Crumlin, E. Probing the Surface of Platinum During the Hydrogen Evolution Reaction in Alkaline Electrolyte. *J. Phys. Chem. B* **122**, 864–870, DOI: 10.1021/acs.jpcb.7b06953 (2017).

Sun, K., Moreno-Hernandez, I. A., Schmidt, W. C., Zhou, X., Crompton, J. C., Liu, R., Saadi, F. H., Chen, Y., Papadantonakis, K. M., and Lewis, N. A Comparison of the Chemical, Optical and Electrocatalytic Properties of Water-Oxidation Catalysts for Use in Integrated Solar-Fuels Generators. *Energy Environ. Sci.* **10**, 987–1002, DOI: 10.1039/C6EE03563A (2017).

Sun, K., Cheng, T., Wu, L., Hu, Y., Zhou, J., Maclennan, A., Jiang, Z., Gao, Y., Goddard, W. A., Wang, Z. Ultrahigh Mass Activity for Carbon Dioxide Reduction Enabled by Gold–Iron Core–Shell Nanoparticles. *J. Am. Chem. Soc.* **139**, 15608–15611, DOI: 10.1021/jacs.7b09251 (2017).

Sundararaman, R., Goddard, W. A. and Aries, T. A. Grand canonical electronic density-functional theory: Algorithms and applications to electrochemistry. *The Journal of Chemical Physics* **146**, 114104, DOI: 10.1063/1.4978411 (2017).

Sundararaman, R., Letchworth-Weaver, K., Schwarz, K. A., Gunceler, D., Ozhabes, Y., Arias, T. A. JDFTx: Software for joint density-functional theory. *SoftwareX* **6**, 278–284, https://doi.org/10.1016/j.softx.2017.10.006 (2017).

Suram, S. K., Fackler, S. W., Zhou, L., N'Diaye, A. T., Drisdell, W. S., Yano, J., Gregoire, J. M. Combinatorial Discovery of Lanthanum–Tantalum Oxynitride Solar Light Absorbers with Dilute Nitrogen for Solar Fuel Applications. *ACS Combinatorial Science* **20**, 26–34, DOI: 10.1021/acscombsci.7b00143 (2017).

Sutter-Fella, C. M., Li, Y., Cefarin, N., Buckley, A., Ngo, Q. P., Javey, A., Sharp, I. D., Toma, F. M. Low Pressure Vapor-assisted Solution Process for Tunable Band Gap Pinhole-free Methylammonium Lead Halide Perovskite Films. J. Vis. Exp. (127), e55404, DOI:10.3791/55404 (2017).

Taheri, P., Fahad, H. M., Tosun, M., Hettick, M., Kiriya, D., Chen, K., and Javey, A. Nanoscale Junction Formation by Gas-Phase Monolayer Doping. *ACS Appl. Mater. Interfaces* **9**, 20648–20655, DOI: 10.1021/acsami.7b03974 (2017).

Tolstova, Y. et al. Polycrystalline Cu2O photovoltaic devices incorporating Zn(O,S) window layers. *Solar Energy Materials and Solar Cells* **160**, 340–345, DOI: 10.1016/j.solmat.2016.10.049 (2017).

Ulissi, Z. W., Tang, M. T., Xiao, J., Liu, X., Torelli, D. A., Karamad, M., Cummins, K., Hahn, C., Lewis, N. S., Jaramillo, T. F., Chan, K., Norskov, J. K. Machine-Learning Methods Enable Exhaustive Searches for Active Bimetallic Facets and Reveal Active Site Motifs for CO_2 Reduction. *ACS Catalysis* 7, 6600–6608, DOI: 10.1021/acscatal.7b01648 (2017).

Walczak, K. A., Segev, G., Larson, D. M., Beeman, J. W., Houle, F. A., and Sharp, I. D. Hybrid Composite Coatings for Durable and Efficient Solar Hydrogen Generation under Diverse Operating Conditions. *Adv. Mater.* 7, 1602791, DOI: 10.1002/aenm.201602791 (2017).

Wan, Y., Karuturi, S. K., Samundsett, C., Bullock, J., Hettick, M., Yan, D., Peng, J., Narangari, P. R., Mokkapati, S., Tan, H. H., Jagadish, C., Javey, A., Cuevas, A. Tantalum Oxide Electron-Selective Heterocontacts for Silicon Photovoltaics and Photoelectrochemical Water Reduction. *ACS Energy Letters* **3**, 125–131, DOI: 10.1021/acsenergylett.7b01153 (2017).

Wan, Y., Samundsett, C., Bullock, J., Hettick, M., Allen, T., Yan, D., Peng, J., Wu, Y., Cui, J., Javey, A., Cuevas, A. Conductive and Stable Magnesium Oxide Electron-Selective Contacts for Efficient Silicon Solar Cells. *Adv. Energy Mater.* 7, 1601863., DOI: 10.1002/aenm.201601863 (2017).

Wiensch, J. D., John, J., Valazquez, J. M., Torelli, D. A., Pieterick, A. P., McDowell, M. T., Sun, K., Zhao, X., Brunschwig, B. S., Lewis, N. S. Comparative Study in Acidic and Alkaline Media of the Effects of pH and Crystallinity on the Hydrogen-Evolution Reaction on MoS_2 and $MoSe_2$. *ACS Energy Letters* 2, 2234–2238, DOI: 10.1021/acsenergylett.7b00700 (2017).

Xiao, H., Goddard, W. A., Cheng, T., and Liu, Y. Cu metal embedded in oxidized matrix catalyst to promote CO_2 activation and CO dimerization for electrochemical reduction of CO2. *PNAS* **114**, 6685–6688, DOI: 10.1073/pnas.1702405114 (2017).

Xue, Y., Bai, J., Le Bras, R., Rappazzo, B., Berstein, R., Bjorck, J., Longpre, L., Suram, S. K., van Dover, R. B., Gregoire, J., Gomes, C. P. Phase-Mapper: An AI Platform to Accelerate High Throughput Materials Discovery. Proceedings of the Twenty-Ninth AAAI Conference on Innovative Applications (IAAI-17)) (2017).

Yan, Q. et al. Solar fuels photoanode materials discovery by integrating high-throughput theory and experiment. . *PNAS* **114**, 3040–3043, DOI: 10.1073/pnas.1619940114 (2017).

Yang, J., Cooper, J. K., Toma, F. M., Walczak, K. A., Favaro, M., Beeman, J. W., Hess, L. H., Wang, C., Zhu, C., Gul, S., Yano, J., Kisielowski, C., Schwartzberg, A., Sharp, I. D. A multifunctional biphasic water splitting catalyst tailored for integration with high-performance semiconductor photoanodes. *Nat Mater* **16**, 335–341, DOI: 10.1038/nmat4794 (2017).

Ye, Q., Ziegler, M. S., Lakshmi, K. V., and Tilley, T. D. Titanium Imido Complexes by Displacement of $-SiMe_3$ and C–H Bond Activation in a TiIII Amido Complex, Promoted by a Cyclic (Alkyl)(Amino) Carbene (cAAC). *European Journal of Inorganic Chemistry* **2017**, 2484–2487, DOI: 10.1002/ejic.201700295 (2017).

Zheng, F., Pham, H. H., Wang, L.-W. The effects of c-Si/a-SiO_2 interface atomic structure on its band alignment: an *ab initio* study. *Phys. Chem. Chem. Phys.***19**, 32617–32625, DOI: 10.1039/C7CP05879A (2017).

Zhou, X., Liu, R., Chen, Y., Verlage, E., Francis, S. A., Lewis, N. S., Xiang, C. Solar-Driven Reduction of 1 atm CO_2 to Formate at 10% Energy-Conversion Efficiency by Use of a TiO_2-Protected III-V Tandem Photoanode in Conjunction with a Bipolar Membrane and a Pd/C Cathode Electrocatalyst. *ECS Transactions* 77, 31–41, DOI: 10.1149/07704.0031ecst (2017).

Ziegler, M. S., Lakshmi, K. V., and Tilley, T. D. Dicopper Cu(I)Cu(I) and Cu(I)Cu(II) Complexes in Copper-Catalyzed Azide–Alkyne Cycloaddition. *J. Am. Chem. Soc.* **139**, 5378–5386, DOI: 10.1021/jacs.6b13261 (2017).

2016

Ager III, J. W. Photoelectrochemical Approach for Water Splitting. in Solar to Chemical Energy Conversion, Volume 32, 249–260 (2016).

Agnoli, S. and Favaro, M. Doping graphene with boron: a review of synthesis methods, physicochemical characterization, and emerging applications. *J. Mater. Chem. A* **4**, 5002–5025, DOI: 10.1039/C5TA10599D (2016).

Ali-Löytty, H. et al. Ambient-Pressure XPS Study of a Ni–Fe Electrocatalyst for the Oxygen Evolution Reaction. *J. Phys. Chem. C* **120**, 2247–2253, DOI: 10.1021/acs.jpcc.5b10931 (2016).

Amani, M. et al. High Luminescence Efficiency in MoS_2 Grown by Chemical Vapor Deposition. *ACS Nano* **10**, 6535–6541, DOI: 10.1021/acsnano.6b03443 (2016).

Azarpira, A. et al. Sustained Water Oxidation by Direct Electrosynthesis of Ultrathin Organic Protection Films on Silicon. *Adv. Mater.* **6**, DOI: 10.1002/aenm.201502314 (2016).

Baricuatro, J. H. et al. Influence of Redox-Inactive Cations on the Structure and Electrochemical Reactivity of Synthetic Birnessite, a Heterogeneous Analog for the Oxygen–Evolving Complex. The . *Phys. Chem. C*, **120**, 15618–15631, DOI: 10.1021/acs.jpcc.5b07028 (2016).

Bernardi, M. & Grossman, J. C. Computer Calculations across Time and Length Scales in Photovoltaic Solar Cells. *Energy Environ. Sci.* **9**, 2197–2218, DOI: 10.1039/C6EE01010E (2016).

Brown, A. M., Sundararaman, R., Narang, P., Goddard, W. A., Atwater, H. A. Nonradiative Plasmon Decay and Hot Carrier Dynamics: Effects of Phonons, Surfaces, and Geometry. *ACS Nano* **10**, 957–966, DOI: 10.1021/acsnano.5b06199 (2016)

Brown, A. M. et al. *Ab initio* phonon coupling and optical response of hot electrons in plasmonic metals. *Physical Review B* **94**, 075120, DOI: http://dx.doi.org/10.1103/PhysRevB.94.075120 (2016).

Bullock, J. et al. Efficient silicon solar cells with dopant-free asymmetric heterocontacts. *Nature Energy* **1**, 15031, DOI: 10.1038/nenergy.2015.31 (2016).

Buonsanti, R. Colloidal Chemistry to Advance Studies in Artificial Photosynthesis. *CHIMIA International Journal for Chemistry* **70**, 780–786, DOI: https://doi.org/10.2533/chimia.2016.780 (2016).

Chan, K. & Norskov, J. K. Potential Dependence of Electrochemical Barriers from ab Initio Calculations. *J Phys Chem Lett* **7**, 1686–1690, DOI: 10.1021/acs.jpclett.6b00382 (2016).

Chen, L. D., Urushihara, M., Chan, K. & Norskov, J. K. Electric Field Effects in Electrochemical CO_2 Reduction. *ACS Catalysis* **6**, 7133–7139, DOI: 10.1021/acscatal.6b02299 (2016).

Chen, Y., Lewis, N. S. & Xiang, C. Modeling and Simulation of the Spatial and Light-Intensity Dependence of Product Distributions in an Integrated Photoelectrochemical CO_2 Reduction System. *ACS Energy Letters* **1**, 273-280, DOI: 10.1021/acsenergylett.6b00134 (2016).

Cheng, C. et al. Influence of Constitution and Charge on Radical Pairing Interactions in Trisradical Tricationic Complexes. *J Am Chem Soc* **138**, 8288-8300, DOI: 10.1021/jacs.6b04343 (2016).

Cheng, M.-J. et al. Quantum Mechanical Screening of Single-Atom Bimetallic Alloys for the Selective Reduction of CO_2 to C_1 Hydrocarbons. *ACS Catalysis* **6**, 7769-7777, DOI: 10.1021/acscatal.6b01393 (2016).

Cheng, T., Xiao, H. & Goddard, W. A. Reaction Mechanisms for the Electrochemical Reduction of CO_2 to CO and Formate on the Cu(100) Surface at 298 K from Quantum Mechanics Free Energy Calculations with Explicit Water. *J Am Chem Soc* **138**, 13802-13805, DOI: 10.1021/jacs.6b08534 (2016).

Cooper, J. K. et al. Role of Hydrogen in Defining the n-Type Character of $BiVO_4$ Photoanodes. *Chem. Mater.***28**, 5761-5771, DOI: 10.1021/acs.chemmater.6b01994 (2016).

Crowley, J. M., Tahir-Kheli, J. & Goddard III, W. A. Resolution of the Band Gap Prediction Problem for Materials Design. *J. Phys. Chem. Letters* 7, 1198-1203, DOI: 10.1021/acs.jpclett.5b02870 (2016).

Desai, S. B. et al. Gold-Mediated Exfoliation of Ultralarge Optoelectronically-Perfect Monolayers. *Adv. Mater.* 28, DOI: 10.1002/adma.201506171 (2016).

Eaton, S. W. et al. Lasing in robust cesium lead halide perovskite nanowires. *PNAS* **113**, 1993-1998, DOI: 10.1073/pnas.1600789113 (2016).

Favaro, M. et al. Unravelling the electrochemical double layer by direct probing of the solid/liquid interface. *Nat Commun* 7, 12695, DOI: 10.1038/ncomms12695 (2016).

Fountaine, K. T., Cheng, W.-H., Bukowsky, C. R. & Atwater, H. A. Near-Unity Unselective Absorption in Sparse InP Nanowire Arrays. *ACS Photonics* 3, 1826-1832, DOI: 10.1021/acsphotonics.6b00341 (2016).

Fountaine, K. T., Lewerenz, H. J. & Atwater, H. A. Efficiency limits for photoelectrochemical water-splitting. *Nature Communications* 7, 13706, DOI: 10.1038/ncomms13706 (2016).

Goodpaster, J. D., Bell, A. T. & Head-Gordon, M. Identification of Possible Pathways for C–C Bond Formation during Electrochemical Reduction of CO_2: New Theoretical Insights from an Improved Electrochemical Model. *J. Phys. Chem. Letters* 7, 1471-1477, DOI: 10.1021/acs.jpclett.6b00358 (2016).

Hansen, H. A. et al. Bifunctional alloys for the electroreduction of CO_2 and CO. *Phys. Chem. Chem. Phys.***18**, 9194-9201, DOI: 10.1039/C5CP07717F (2016).

Hattrick-Simpers, J. R., Gregoire, J. M & Kusne, G. Perspective: Composition–structure–property mapping in high-throughput experiments: Turning data into knowledge. *APL Mater.* **4**, 053211, http://dx.doi.org/10.1063/1.4950995 (2016).

Hong, X. et al. How Doped MoS2 Breaks Transition-Metal Scaling Relations for CO_2 Electrochemical Reduction. *ACS Catalysis* **6**, 4428-4437, DOI: 10.1021/acscatal.6b00619 (2016).

Hu, S. et al. Electrical, Photoelectrochemical, and Photoelectron Spectroscopic Investigation of the Interfacial Transport and Energetics of Amorphous TiO_2/Si Heterojunctions. *J. Phys. Chem. C* **120**, 3117-3129, DOI: 10.1021/acs.jpcc.5b09121 (2016).

Huang, Z. et al. PeakForce Scanning Electrochemical Microscopy with Nanoelectrode Probes. *Microscopy Today* **24**, 18-25, DOI: 10.1017/18 S1551929516000882 (2016).

Jiang, S. et al. Pressure-Dependent Polymorphism and Band-Gap Tuning of Methylammonium Lead Iodide Perovskite. *Angew Chem Int Ed Engl* 55, 6540-6544, DOI: 10.1002/anie.201601788 (2016).

Johnson, S. I, Nielsen, R. J. & Goddard, W. A. Selectivity for HCO_2^- over H_2 in the Electrochemical Catalytic Reduction of CO_2 by (POCOP)IrH_2. *ACS Catalysis* **6**, 6362-6371, DOI: 10.1021/acscatal.6b01755 (2016).

Jung, S. et al. Benchmarking nanoparticulate metal oxide electrocatalysts for the alkaline water oxidation reaction. *J. Mater. Chem. A* **4**, 3068-3076, DOI: 10.1039/C5TA07586F (2016).

Kim, Y.-G. et al. Regulating the Product Distribution of CO Reduction by the Atomic-Level Structural Modification of the Cu Electrode Surface. *Electrocatalysis* 7, 1-9, DOI: 10.1007/s12678-016-0314-1 (2016).

Kim, Y.-G. et al. Surface reconstruction of pure-Cu single-crystal electrodes under Co-reduction potentials in alkaline solutions: A study by seriatim ECSTM-DEMS. *Journal of Electroanalytical Chemistry* **780**, 290–295, http://dx.doi.org/10.1016/j.jelechem.2016.09.029 (2016).

Kiriya, D. et al. General Thermal Texturization Process of MoS_2 for Efficient Electrocatalytic Hydrogen Evolution Reaction. *Nano Letters* **16**, 4047–4053, DOI: 10.1021/acs.nanolett.6b00569 (2016).

Kisielowski, C. et al. Detecting structural variances of Co_3O_4 catalysts by controlling beam-induced sample alterations in the vacuum of a transmission electron microscope. *Advanced Structural and Chemical Imaging* 2, 13, DOI: 10.1186/s40679-016-0027-9 (2016).

Kwon, Y. et al. CO_2 electroreduction with high ethylene selectivity via nanostructuring of polycrystalline copper. *ChemElectroChem* **3**, 1012–1019, DOI: 10.1002/celc.201600068 (2016).

Leblebici, S. Y. et al. Facet-dependent photovoltaic efficiency variations in single grains of hybrid halide perovskite. *Nature Energy* **1**, 16093, DOI: 10.1038/nenergy.2016.93 (2016).

Lewerenz, H.-J. et al. *Operando* Analyses of Solar Fuels Light Absorbers and Catalysts. *Electrochimica Acta* **211**, 711–719, DOI: 10.1016/j.electacta.2016.06.006 (2016).

Lewis, N. S. Research opportunities to advance solar energy utilization. *Science*, **351** (6271), DOI: 10.1126/science.aad1920 (2016).

Li, Y. et al. Defective TiO_2 with high photoconductive gain for efficient and stable planar heterojunction perovskite solar cells. *Nat Commun* **7**, 12446, DOI: 10.1038/ncomms12446 (2016).

Liberman-Martin, A. L. et al. Biaryl Reductive Elimination Is Dramatically Accelerated by Remote Lewis Acid Binding to a 2,2′-Bipyrimidyl–Platinum Complex: Evidence for a Bidentate Ligand Dissociation Mechanism. *Organometallics* **35**, 1064–1069, DOI: 10.1021/acs.organomet.5b01003 (2016).

Lichterman, M. F. et al. An Electrochemical, Microtopographical and Ambient Pressure X-Ray Photoelectron Spectroscopic Investigation of Si/TiO_2/Ni/Electrolyte Interfaces. *J. Electrochem. Soc.* **163**, H139–H146, DOI: 10.1149/2.0861602jes (2016).

Lichterman, M. F. et al. Protection of inorganic semiconductors for sustained, efficient photoelectrochemical water oxidation. *Catalysis Today* **262**, 11–23, DOI: 10.1016/j.cattod.2015.08.017 (2016)

Liu, Y., Xiao, H. & Goddard, W. A. Two-Dimensional Halide Perovskites: Tuning Electronic Activities of Defects. *Nano Letters* **16**, 3335–3340, DOI: 10.1021/acs.nanolett.6b00964 (2016).

Liu, Y., et al. Undoped and Ni-Doped CoO_x Surface Modification of Porous $BiVO_4$ Photoelectrodes for Water Oxidation. *J. Phys. Chem. C* **120**, 23449–23457, DOI: 10.1021/acs.jpcc.6b08654 (2016).

Lobaccaro, P. et al. Effects of Temperature and Gas-Liquid Mass Transfer on the Operation of Small Electrochemical Cells for the Quantitative Evaluation of CO_2 Reduction Electrocatalysts. *Phys. Chem. Chem. Phys.***18**, 26777–26785, DOI: 10.1039/C6CP05287H (2016).

Loiudice, A. et al. Tailoring Copper Nanocrystals towards C2 Products in Electrochemical CO_2 Reduction. *Angewandte Chemie Int. Ed.* **55**, DOI: 10.1002/anie.201601582 (2016).

Lum, Y. et al. Trace Levels of Copper in Carbon Materials Show Significant Electrochemical CO_2 Reduction Activity. *ACS Catal.* **6**, 202–209, DOI: 10.1021/acscatal.5b02399 (2016)

Luz, I. et al. Understanding the Formation Mechanism of Metal Nanocrystal@MOF-74 Hybrids. *Chem. Mater.***28**, 3839–3849, DOI: 10.1021/acs.chemmater.6b00880 (2016).

Meng, X. et al. Discovery of Fe_2P-Type $Ti(Zr/Hf)_2O_6$ Photocatalysts toward Water Splitting. *Chem. Mater.***28**, 1335–1342, DOI: 10.1021/acs.chemmater.5b04256 (2016).

Mori, R. A. et al. Towards Characterization of Photo-Excited Electron Transfer and Catalysis in Natural and Artificial Systems Using XFELs. *Faraday Discussions* **194**, 621–638, DOI: 10.1039/C6FD00084C (2016).

Narang, P., Sundararaman, R. & Atwater, H. A. Plasmonic hot carrier dynamics in solid-state and chemical systems for energy conversion. *Nanophotonics*, DOI: 10.1515/nanoph-2016-0007 (2016).

Narang, P. et al. Cubic Nonlinearity Driven Up-Conversion in High-Field Plasmonic Hot Carrier Systems. *J. Phys. Chem. C* **120**, 21056–21062, DOI: 10.1021/acs.jpcc.6b03463 (2016).

Newhouse, P. et al. Solar Fuels Photoanodes Prepared by Inkjet Printing of Copper Vanadates. *J. Mater. Chem. A* **4**, 7483–7494, DOI: 10.1039/C6TA01252C (2016).

Ogasawara, H., Kaya, S. &Nilsson, A. *Operando* X-Ray Photoelectron Spectroscopy Studies of Aqueous Electrocatalytic Systems. *Topics in Catalysis* **59**, 439–447, DOI: 10.1007/s11244-015-0525-3 (2016).

Panetier, J. A., Letko, C. S., Tilley, T. D. & Head-Gordon, M. Computational Characterization of Redox Non-Innocence in Cobalt-Bis(Diaryldithiolene)-Catalyzed Proton Reduction. *J. Chem. Theory Comput.* **12**, 223–230, DOI: https://doi.org/10.1021/acs.jctc.5b00968 (2016).

Pham, H. H., Cheng, M.-J., Frei, H. & Wang, L.-W. Surface Proton Hopping and Fast-Kinetics Pathway of Water Oxidation on Co_3O_4 (001) Surface. *ACS Catalysis* **6**, 5610–5617, DOI: 10.1021/acscatal.6b00713 (2016).

Ping, Y., Nielsen, R. J., and Goddard, W. A. The Reaction Mechanism with Free Energy Barriers at Constant Potentials for the Oxygen Evolution Reaction at the IrO_2 (110) Surface. *J Am Chem Soc* **139**, 149–155, DOI: 10.1021/jacs.6b07557 (2016).

Ristova, M. M. et al. Electrochemical modification of the optical and electrical properties of Cd-rich $Ni_xCd_{1-x}O$ alloys. *Solar Energy Materials and Solar Cells* **147**, 127–133, DOI:10.1016/j.solmat.2015.12.008 (2016).

Roy, T. et al. 2D-2D tunneling field-effect transistors using $WSe_2/SnSe_2$ heterostructures. *Applied Physics Letters* **108**, 083111, http://dx.doi.org/10.1063/1.4942647 (2016).

Sachsenhauser, M. et al. Suppression of Photoanodic Surface Oxidation of N-type 6H-SiC Electrodes in Aqueous Electrolytes. *Langmuir* **32**, 1637–1644, DOI: 10.1021/acs.langmuir.5b04376 (2016).

Sachsenhauser, M., Sharp, I. D., Stutzmann, M. & Garrido, J. A. A. Surface State Mediated Electron Transfer Across the N-type SiC/Electrolyte Interface. *J. Phys. Chem. C* **120**, 6524–6533, DOI: 10.1021/acs.jpcc.5b11569 (2016).

Sandberg, R. B., Montoya, J. H, Chan, K. & Norskov, J. K. CO-CO coupling on Cu facets: Coverage, strain and field effects. *Surface Science* **654**, 56–62, DOI: http://dx.doi.org/10.1016/j.susc.2016.08.006 (2016).

Sanoja, G. E., et al. Structure–Conductivity Relationships of Block Copolymer Membranes Based on Hydrated Protic Polymerized Ionic Liquids: Effect of Domain Spacing, *Macromolecules* **49**, 2216–2223, DOI: 10.1021/acs.macromol.5b02614 (2016).

Sathre, R. et al. Opportunities to improve the net energy performance of photoelectrochemical water-splitting technology. *Energy Environ. Sci.* **9**, 803–819, DOI: 10.1039/C5EE03040D (2016).

Schwarz, K. et al. Partial oxidation of step-bound water leads to anomalous pH effects on metal electrode step-edges. *Phys. Chem. Chem. Phys.***18**, 16216–16223, DOI: 10.1039/C6CP01652A (2016).

Shaner, M. R. et al. Si/TiO_2 Tandem-Junction Microwire Arrays for Unassisted Solar-DrivenWater Splitting. *J. Electrochem. Soc.* **163**, H261–H264, DOI: 10.1149/2.0141605jes (2016).

Shaner, M. R. et al. A comparative technoeconomic analysis of renewable hydrogen production using solar energy. *Energy Environ. Sci.* **9**, 2354–2371, DOI: 10.1039/C5EE02573G (2016).

Sheng, H. & Frei, H. Direct Observation by Rapid-Scan FT-IR Spectroscopy of Two-Electron-Reduced Intermediate of Tetraaza Catalyst $[CoIIN_4H(MeCN)]^{2+}$ Converting CO_2 to CO. *J Am Chem Soc* **138**, 9959–9967, DOI: 10.1021/jacs.6b05248 (2016).

Shi, C., Chan, K., Yoo, J. S. & Norskov, J. K. Barriers of Electrochemical CO_2 Reduction on Transition Metals. *Org. Process Res. Dev.* **20**, 1424–1430, DOI: 10.1021/acs.oprd.6b00103 (2016).

Shinde, A. et al. Discovery of Fe–Ce Oxide/$BiVO_4$ Photoanodes through Combinatorial Exploration of Ni–Fe–Co–Ce Oxide Coatings. ACS *Appl. Mater. Interfaces* **8**, 23696–23705, DOI: 10.1021/acsami.6b06714 (2016).

Shinde, A. et al. The role of the $CeO_2/BiVO_4$ interface in optimized Fe–Ce oxide coatings for solar fuels photoanodes. *J. Mater. Chem. A* **4**, 14356–14363, DOI: 10.1039/C6TA04746G (2016).

Sieh, D. & Kubiak, C. P. A Series of Diamagnetic Pyridine Monoimine Rhenium Complexes with Different Degrees of Metal-to-Ligand Charge Transfer: Correlating ^{13}C NMR Chemical Shifts with Bond Lengths in Redox-Active Ligands. *Chemistry – A European Journal* 22, 10638–10650, DOI: 10.1002/chem.201600679 (2016).

Singh, M. R. & Bell, A. T. Design of an artificial photosynthetic system for production of alcohols in high concentration from CO_2. *Energy Environ. Sci.* **9**, 193–199, DOI: 10.1039/C5EE02783G (2016).

Singh, M. R. et al. Hydrolysis of Electrolyte Cations Enhances the Electrochemical Reduction of CO_2 over Ag and Cu. *J Am Chem Soc* **138**, 13006–13012, DOI: 10.1021/jacs.6b07612 (2016).

Stevens, J. C. & Weber, A. Z. A Computational Study of Optically Concentrating, Solar-Fuels Generators from Annual Thermal- and Fuel-Production Efficiency Perspectives. *J. Electrochem. Soc.* **163**, H475–H484, DOI: 10.1149/2.0121607jes (2016).

Sun, K. et al. A Stabilized, Intrinsically Safe, 10% Efficient, Solar-Driven Water-Splitting Cell Incorporating Earth-Abundant Electrocatalysts with Steady-State pH Gradients and Product Separation Enabled by a Bipolar Membrane. *Adv. Mater.* **6**, 1600379, DOI: 10.1002/aenm.201600379 (2016).

Suram, S. K., Newhouse, P. F. and Gregoire, J. M. High Throughput Light Absorber Discovery, Part 1: An Algorithm for Automated Tauc Analysis. *ACS Combinatorial Science* **18**, 673–681, DOI: 10.1021/acscombsci.6b00053 (2016)

Suram, S. K. et al. High Throughput Light Absorber Discovery, Part 2: Establishing Structure-Band Gap Energy Relationships. *ACS Combinatorial Science* **18**, 682–688, DOI: 10.1021/acscombsci.6b00054 (2016).

Suram, S. K. et al. Automated Phase Mapping with AgileFD and its Application to Light Absorber Discovery in the V-Mn-Nb Oxide System. *ACS Combinatorial Science*, **19**, 37–46 DOI: 10.1021/acscombsci.6b00153 (2016).

Tolstova, Y., Omelchenko, S. T., Shing, A. M. & Atwater, H. A. Heteroepitaxial growth of Pt and Au thin films on MgO single crystals by bias-assisted sputtering. *Scientific Reports* **6**, 23232, DOI: 10.1038/srep23232 (2016).

Toma, et al. Mechanistic insights into chemical and photochemical transformations of bismuth vanadate photoanodes. *Nat Commun* **7**, 12012, DOI: 10.1038/ncomms12012 (2016).

Torelli, D. A. et al. Nickel–Gallium-Catalyzed Electrochemical Reduction of CO_2 to Highly Reduced Products at Low Overpotentials. *ACS Catalysis* **6**, 2100–2104, DOI: 10.1021/acscatal.5b02888 (2016).

Ugeda, M. M. et al. Covalent Functionalization of GaP(110) Surfaces via a Staudinger-Type Reaction with Perfluorophenyl Azide. *J. Phys. Chem. C*, **120**, 26448–26452, DOI: 10.1021/acs.jpcc.6b10691 (2016).

Velazquez, J. M. et al. A Scanning Probe Investigation of the Role of Surface Motifs in the Behavior of p-WSe_2 Photocathodes. *Energy Environ. Sci.* **9**, 164–175, DOI: 10.1039/C5EE02530C (2016).

Wan, Y. et al. Magnesium Fluoride Electron-Selective Contacts for Crystalline Silicon Solar Cells. *ACS Appl. Mater. Interfaces* **8**, 14671–14677, DOI: 10.1021/acsami.6b03599 (2016).

Wang, Q. et al. Scalable water splitting on particulate photocatalyst sheets with a solar-to-hydrogen energy conversion efficiency exceeding 1%. *Nat Mater* **15**, 611–615, DOI: 10.1038/nmat4589 (2016).

Wang, R. et al. Solar-Driven H_2O_2 Generation From H_2O and O_2 Using Earth-Abundant Mixed-Metal Oxide@Carbon Nitride Photocatalysts. *ChemSusChem* **9**, 2470–2479, DOI: 10.1002/cssc.201600705 (2016).

Woods-Robinson, R. et al. P-Type Transparent Cu–Alloyed ZnS Deposited at Room Temperature. *Advanced Electronic Materials* 2, DOI: 10.1002/aelm.201500396 (2016)

Xiang, C., Papadantonakis, K. M. & Lewis, N. Principles and Implementations of Electrolysis Systems for Water Splitting. *Materials Horizons* **3**, 169–173, DOI: 10.1039/C6MH00016A (2016).

Xiang, C. et al. Modeling, Simulation, and Implementation of Solar-Driven Water-Splitting Devices. *Angew Chem Int Ed Engl* **55**, 12974–12988, DOI: 10.1002/anie.201510463 (2016).

Xiao, H., Cheng, T. and Goddard, W. A. Atomistic Mechanisms Underlying Selectivities in C1 and C2 Products from Electrochemical Reduction of CO on Cu(111). *J Am Chem Soc* **139**, 130–136, DOI: 10.1021/jacs.6b06846 (2016).

Xu, X. et al. Chemical Bath Deposition of p-Type Transparent, Highly Conducting $(CuS)_x$:$(ZnS)_{1-x}$ Nanocomposite Thin Films and Fabrication of Si Heterojunction Solar Cells. *Nano Letters* **16**, 1925–1932, DOI: 10.1021/acs.nanolett.5b05124 (2016).

Yalamanchili, S., et al. Enhanced Absorption and <1% Spectrum-and-Angle-Averaged Reflection in Tapered Microwire Arrays. *ACS Photonics* **3**, 1854–1861, DOI: 10.1021/acsphotonics.6b00370 (2016).

Yang, X. et al. Dual Influence of Reduction Annealing on Diffused Hematite/FTO Junction for Enhanced Photoelectrochemical Water Oxidation. *ACS Appl. Mater. Interfaces* **8**, 16476–16485, DOI: 10.1021/acsami.6b04213 (2016).

Zhou, H. et al. Efficient hydrogen evolution by ternary molybdenum sulfoselenide particles on self-standing porous nickel diselenide foam. *Nature Communications* **7**, 12765, DOI:10.1038/ncomms12765 (2016).

Zhou, J. -J. and Bernardi, M. *Ab initio* electron mobility and polar phonon scattering in GaAs. *Physical Review B* **94**, 201201, DOI: https://doi.org/10.1103/PhysRevB.94.201201 (2016).

Zhou, L. et al. Stability and Self-passivation of Copper Vanadate Photoanodes under Chemical, Electrochemical, and Photoelectrochemical Operation. *Phys. Chem. Chem. Phys.***18**, 9349–9352, DOI: 10.1039/C6CP00473C (2016).

Zhou, X. et al. 570 mV Photovoltage, Stabilized n-Si/CoO_x Heterojunction Photoanodes Fabricated Using Atomic Layer Deposition. *Energy Environ. Sci.* **9**, 892–897, DOI: 10.1039/C5EE03655K (2016).

Zhou X. et al. Solar-Driven Reduction of 1 atm CO_2 to Formate at 10% Energy-Conversion Efficiency by Use of a TiO_2-Protected III-V Tandem Photoanode in Conjunction with Bipolar Membrane and a Pd/C Cathode Electrocatalyst. *ACS Energy Letters* **1**, 764–770, DOI: 10.1021/acsenergylett.6b00317 (2016).

Zhu, Y. et al. Location of Co and Ni Promoter Atoms in Multi-layer MoS_2 Nanocrystals for Hydrotreating Catalysis. *Catalysis Today* **261**, 75–81, DOI: 10.1016/j.cattod.2015.08.053 (2016).

Ziegler, M. S. et al. Aryl Group Transfer from Tetraarylborato Anions to an Electrophilic Dicopper(I) Center and Mixed-Valence μ-Aryl Dicopper(I,II) Complexes. *J Am Chem Soc* , **138**, 6484–6491, DOI: 10.1021/jacs.6b00802 (2016).

2015

Ager III, J. W. et al. Experimental Demonstrations of Spontaneous, Solar-Driven Photoelectrochemical Water Splitting. *Energy Environ. Sci.* **8**, 2811–2824, DOI: 10.1039/C5EE00457H (2015).

Ardo, S. et al. Unassisted solar-driven photoelectrosynthetic HI splitting using membrane-embedded Si microwire arrays. *Energy Environ. Sci.* **8**, 1484–1492, DOI: 10.1039/C5EE00227C4 (2015).

Beckingham, B. S., Sanoja, G. E. & Lynd, N. A. Simple and Accurate Determination of Reactivity Ratios Using a Nonterminal Model of Chain Copolymerization. *Macromolecules* **48**, 6922–6930, DOI: 10.1021/acs.macromol.5b01631 (2015).

Berweger, S. et al. Microwave Near-Field Imaging of Two-Dimensional Semiconductors. *Nano Letters* **15**, 1122–1127, DOI: 10.1021/nl504960u (2015).

Chen, L. et al. Mo-Doped $BiVO_4$ Photoanodes Synthesized by Reactive Sputtering. C *Chemsuschem* **8**, 1066–1071, DOI: 10.1002/cssc.201402984 (2015).

Chen, L. et al. P-type Transparent Conducting Oxide / n-type Semiconductor Heterojunctions for Efficient and Stable Solar Water Oxidation. *J Am Chem Soc* **137**, 9595–9603, DOI: 10.1021/jacs.5b03536 (2015).

Chen, Y., Hu, S., Xiang, C. & Lewis, N. A Sensitivity Analysis to Assess the Relative Importance of Improvements in Electrocatalysts, Light Absorbers, and System Geometry on the Efficiency of Solar-Fuels Generators. *Energy Environ. Sci.* **8**, 876–886, DOI: 10.1039/C4EE02314E (2015).

Chen, Y. et al. A Quantitative Analysis of the Efficiency of Solar-Driven Water-Splitting Device Designs Based on Tandem Photoabsorbers Patterned with Islands of Metallic Electrocatalysts. *Energy Environ. Sci.* **8**, 1736–1747, DOI: 10.1039/C5EE00311C (2015).

Chen, Y., Lewis, N. S., & Xiang, C. Operational Constraints and Strategies for Systems to Effect the Sustainable, Solar-Driven Reduction of Atmospheric CO2. *Energy Environ. Sci.* **8**, 3663–3674, DOI: 10.1039/C5EE02908B (2015).

Cheng, M.-J., Kwon, Y., Head-Gordon, M., & Bell, A. T. Tailoring Metal-Porphyrin-Like Active Sites on Graphene to Improve the Efficiency and Selectivity of Electrochemical CO_2 Reduction. *J. Phys. Chem. C* **119**, 21345–21352, DOI: 10.1021/acs.jpcc.5b05518 (2015).

Cheng, T., Xiao, H. & Goddard, W. A. Free-Energy Barriers and Reaction Mechanisms for the Electrochemical Reduction of CO on the Cu(100) Surface, Including Multiple Layers of Explicit Solvent at pH 0. *J. Phys. Chem. Letters* **6**, 4767–4773, DOI: 10.1021/acs.jpclett.5b02247(2015).

Cho, E. S. et al. Enhanced Water Vapor Blocking in Transparent Hybrid Polymer-Nanocrystal Films. *Acs Macro Letters* **4**, 70–74, DOI: 10.1021/mz500765y (2015).

Clark, E. L., Singh, M. R., Kwon, Y. & Bell, A. T. Differential Electrochemical Mass Spectrometer Cell Design for Online Quantification of Products Produced during Electrochemical Reduction of CO_2. *Analytical Chemistry* **87**, 8013–8020, DOI: 10.1021/acs.analchem.5b02080 (2015).

Cooper, J. K. et al. Indirect Bandgap and Optical Properties of Monoclinic Bismuth Vanadate. *J. Phys. Chem. C* **119**, 2969–2974, DOI: 10.1021/jp512169w (2015).

Coridan, R. H. et al. Methods for Comparing the Performance of Energy-Conversion Systems for Use in Solar Fuels and Solar Electricity Generation. *Energy Environ. Sci.* **8**, 2886–2901, DOI: 10.1039/C5EE00777A (2015).

Edri, E. & Frei, H. Charge Transport through Organic Molecular Wires Embedded in Ultrathin Insulating Inorganic Layer. *J. Phys. Chem. C* **119**, 28326–28334, DOI: 10.1021/acs.jpcc.5b09994 (2015).

Esposito, D. V. et al. Methods of photoelectrode characterization with high spatial and temporal resolution. *Energy Environ. Sci.* **8**, 2863–2885, DOI: 10.1039/C5EE00835B (2015).

Evans, C. M., Singh, M. R., Lynd, N. A. & Segalman, R. A. Improving the Gas Barrier Properties of Nafion via Thermal Annealing: Evidence for Diffusion through Hydrophilic Channels and Matrix. *Macromolecules* **48**, 3303–3309, DOI: 10.1021/acs.macromol.5b00579 (2015).

Fabian, D. M. et al. Particle Suspension Reactors and Materials for Solar–Driven Water Splitting. *Energy Environ. Sci.* **8**, 2825–2850, DOI: 10.1039/C5EE01434D (2015).

Faludi, J., Bayley, C., Bhogal, S. & Iribarne, M. Comparing environmental impacts of additive manufacturing vs traditional machining via life-cycle assessment. *Rapid Prototyping Journal* **21**, 14–33, DOI: 10.1108/rpj-07-2013-0067 (2015).

Fenwick, A. Q. & Luca, O. R. The Formation of CO by Thermal Decomposition of Formic Acid under Electrochemical Conditions of CO2 Reduction. *Journal of Photochemistry and Photobiology B: Biology* **152A**, 43–46, DOI: 10.1016/j.jphotobiol.2015.04.003 (2015).

Friebel, D. et al. Identification of highly active Fe sites in (Ni,Fe)OOH for electrocatalytic water splitting. *J Am Chem Soc* **137**, 1305–1313, DOI: 10.1021/ja511559d (2015).

Fukushima, T., Drisdell, W., Yano, J. & Surendranath, Y. Graphite-Conjugated Pyrazines as Molecularly Tunable Heterogeneous Electrocatalysts. *J Am Chem Soc* **137**, 10926–10929, DOI: 10.1021/jacs.5b06737 (2015).

Guevarra, D. et al. Development of solar fuels photoanodes through combinatorial integration of Ni–La–Co–Ce oxide catalysts on $BiVO_4$. *Energy Environ. Sci.* **9**, 565–580, DOI: 10.1039/C5EE03488D (2015).

Gul, S. et al. Simultaneous detection of electronic structure changes from two elements of a bifunctional catalyst using wavelength-dispersive X-ray emission spectroscopy and in situ electrochemistry. *Phys. Chem. Chem. Phys.***17**, 8901–8912, DOI: 10.1039/C5CP01023C (2015).

Haber, J. A., Anzenburg, E., Yano, J., Kisielowski, C. & Gregoire, J. M. Multiphase Nanostructure of a Quinary Metal Oxide Electrocatalyst Reveals a New Direction for OER Electrocatalyst Design. *Adv. Mater.* **5**, DOI: 10.1002/aenm.201402307 (2015).

Han, L. H. et al. Gradient dopant profiling and spectral utilization of monolithic thin-film silicon photoelectrochemical tandem devices for solar water splitting. *J. Mater. Chem. A* **3**, 4155–4162, DOI: 10.1039/c4ta05523c (2015).

Helms, B. A. et al. Colloidal Nanocrystal Frameworks. *Adv. Mater.* **27**, 5820–5829, DOI: 10.1002/adma.201500127 (2015).

Helveg, S. et al. Observing gas-catalyst dynamics at atomic resolution and single-atom sensitivity. *Micron* **68**, 176–185, DOI: 10.1016/j.micron.2014.07.009 (2015).

Hettick, M. et al. Nonepitaxial Thin-Film InP for Scalable and Efficient Photocathodes. *J. Phys. Chem. Letters* **6**, 2177–2182, DOI: 10.1021/acs.jpclett.5b00744 (2015).

Hu, S. et al. Thin-Film Materials for the Protection of Semiconducting Photoelectrodes in Solar-Fuel Generators. *J. Phys. Chem. C* **119**, 24201–24228, DOI: 10.1021/acs.jpcc.5b05976 (2015).

Huang, Y., Nielsen, R. J., Goddard, W. A. & Soriaga, M. P. The Reaction Mechanism with Free Energy Barriers for Electrochemical Dihydrogen Evolution on MoS_2. *J Am Chem Soc* **137**, 6692–6698, DOI: 10.1021/jacs.5b03329 (2015).

Huang, Z. et al. Atomic Force Microscopy for Solar Fuels Research: An Introductory Review. *Energy and Environmental Focus* **4**, 260–277, DOI: 10.1166/eef.2015.1180 (2015).

Javier, A. et al. A DEMS Study of the Reduction of CO_2, CO, and HCHO Pre-Adsorbed on Cu Electrodes: Empirical Inferences on the CO_2RR Mechanism. *Electrocatalysis* **6**, 127–131, DOI: 10.1007/s12678-015-0246-1 (2015).

Javier, A. et al. Overlayer Au-on-W Near-Surface Alloy for the Selective Electrochemical Reduction of CO_2 to Methanol: Empirical (DEMS) Corroboration of a Computational (DFT) Prediction. *Electrocatalysis* **6**, 493–497, DOI: 10.1007/s12678-015-0276-8 (2015).

Jiang, Y. et al. The evolution of cyclopropenium ions into functional polyelectrolytes. *Nat Commun* **6**, 5950, DOI: 10.1038/ncomms6950 (2015).

Jones, R. J. R. et al. Parallel Electrochemical Treatment System and Application for Identifying Acid-Stable Oxygen Evolution Electrocatalysts. *ACS Combinatorial Science* **17**, 71–75, DOI: 10.1021/co500148p (2015).

Jurss, J. W. et al. Bioinspired design of redox-active ligands for multielectron catalysis: effects of positioning pyrazine reservoirs on cobalt for electro- and photocatalytic generation of hydrogen from water. *Chemical Science* **6**, 4954–4972, DOI: 10.1039/C5SC01414J (2015).

Kisielowski, C. et al. Instrumental requirements for the detection of electron beam-induced object excitations at the single atom level in high-resolution transmission electron microscopy. *Micron* **68**, 186–193, DOI: 10.1016/j.micron.2014.07.010 (2015).

Klaus, S. et al. Experimental and Computational Evidence of Highly-Active Fe Impurity Sites on the Surface of Oxidized Au for the Electrocatalytic Oxidation of Water in Basic Media. *ChemElectroChem* **3**, 66–73, DOI: 10.1002/celc.201500364 (2015).

Klaus, S., Cai, Y., Louie, M. W., Trotochaud, L. & Bell, A. T. Effects of Fe Electrolyte Impurities on $Ni(OH)_2$/NiOOH Structure and Oxygen Evolution Activity. *J. Phys. Chem. C* **119**, 7243–7254, DOI: 10.1021/acs.jpcc.5b00105 (2015).

Klaus, S., Louie, M. W., Trotochaud, L. & Bell, A. T. Role of Catalyst Preparation on the Electrocatalytic Activity of $Ni_{1-x}Fe_xOOH$ for the Oxygen Evolution Reaction. *J. Phys. Chem. C* **119**, 18303–18316, DOI: 10.1021/acs.jpcc.5b04776 (2015).

Kuang, Y. et al. Enhancement of the performance of GaP solar cells by embedded In(N)P quantum dots. *Nano Energy* **15**, 782–788, DOI: 10.1016/j.nanoen.2015.06.003 (2015).

Lam, Y. C., Nielsen, R. J., Gray, H. B. & Goddard, W. A. A Mn Bipyrimidine Catalyst Predicted To Reduce CO_2 at Lower Overpotential. *ACS Catalysis* **5**, 2521–2528, DOI: 10.1021/cs501963v (2015).

Li, Y. et al. Fabrication of Planar Heterojunction Perovskite Solar Cells by Controlled Low-Pressure Vapor Annealing. *J. Phys. Chem. Letters* **6**, 493–499, DOI: 10.1021/jz502720a (2015).

Li, Y. P. et al. Engineering the Composition and Crystallinity of Molybdenum Sulfide for High-Performance Electrocatalytic Hydrogen Evolution. *ACS Catalysis* **5**, 448–455, DOI: 10.1021/cs501635v (2015).

Lichterman, M. F. et al. Direct Observation of the Energetics at a Semiconductor/Liquid Junction by Operando X-ray Photoelectron Spectroscopy. *Energy Environ. Sci.* **8**, 2409–2416, DOI: 10.1039/C5EE01014D(2015).

Lilio, A. M. et al. Incorporation of pendant bases into Rh(diphosphine)2 complexes: Synthesis, thermodynamic studies, and catalytic CO_2 hydrogenation activity of $[Rh(P_2N_2)_2]^+$ complexes. *J Am Chem Soc* **137**, 8251–8260, DOI: 10.1021/jacs.5b04291 (2015).

Lin, Y. et al. Role of TiO_2 Surface Passivation on Improving the Performance of p-InP Photocathodes. *J. Phys. Chem. C* **119**, 2308–2313, DOI: 10.1021/jp5107313 (2015).

Liu, R. et al. Tuning redox potentials of CO_2 reduction catalysts for carbon photofixation by Si nanowires. *Sci. China Mater.* **58**, 515–520, DOI: 10.1007/s40843-015-0068-8 (2015).

Liu, R. A. et al. Low Temperature Synthesis of Electrochemical Active Pt Nanoparticles and Thin Films by Atomic Layer Deposition on Si(111) and Glassy Carbon Surfaces. *Thin Solid Films* **586**, 28–34, DOI: 10.1016/j.tsf.2015.04.018 (2015).

Liu, W. & Tilley, T. D. Sterically Controlled Functionalization of Carbon Surfaces with -C6H4CH2X (X = OSO2Me or N3) Groups for Surface Attachment of Redox-Active Molecules. *Langmuir* **31**, 1189–1195, DOI: 10.1021/la503796z (2015).

Loiudice, A. et al. Assembly and Photocarrier Dynamics of Heterostructured Nanocomposite Photoanodes from Multicomponent Colloidal Nanocrystals. *Nano Letters* **15**, 7347–7354, DOI: 10.1021/acs.nanolett.5b03871(2015).

Loiudice, A. et al. Bandgap Tunability in Sb-Alloyed $BiVO_4$ Quaternary Oxides as Visible Light Absorbers for Solar Fuel Applications. *Adv Mater* **27**, 6733–6740, DOI: 10.1002/adma.201502361 (2015).

Luca, O. R. et al. Catalysis by electrons and holes: formal potential scales and preparative organic electrochemistry. *Organic Chemistry Frontiers* 2, 823–848, DOI: 10.1039/C5QO00075K (2015).

Luca, O. R. & Fenwick, A. Q. Organic reactions for the electrochemical and photochemical production of chemical fuels from CO_2 – The reduction chemistry of carboxylic acids and derivatives as bent CO2surrogates. *Journal of Photochemistry and Photobiology B: Biology* **152A**, 26–42, DOI: 10.1016/j.jphotobiol.2015.04.015 (2015).

Luca, O. R., McCrory, C. C. L., Dalleska, N. F. & Koval, C. A. The Selective Electrochemical Conversion of Preactivated CO_2 to Methane. *J. Electrochem. Soc.* **162**, H473–H476, DOI: 10.1149/2.0371507jes (2015).

Lucht, K. P. & Mendoza-Cortes, J. L. Birnessite: A Layered Manganese Oxide To Capture Sunlight for Water-Splitting Catalysis. *J. Phys. Chem. C* **119**, 22838–22846, DOI: 10.1021/acs.jpcc.5b07860 (2015).

Lynch, J. et al. Substitutional or Interstitial Site-Selective Nitrogen Doping in TiO_2 Nanostructures. *J. Phys. Chem. C* **119**, 7443–7452, DOI: 10.1021/jp512775s (2015).

Ma, J., Wang, Z. & Wang, L.-W. Interplay between plasmon and single-particle excitations in a metal nanocluster. *Nat Commun* **6**, 10107, DOI: 10.1038/ncomms10107 (2015).

Ma, J. & Wang, L. W. Nanoscale Charge Localization Induced by Random Orientations of Organic Molecules in Hybrid Perovskite $CH_3NH_3PbI_3$. *Nano Letters* **15**, 248–253, DOI: 10.1021/nl503494y (2015).

Malacrida, P. et al. Direct observation of the dealloying process of a platinum–yttrium nanoparticle fuel cell cathode and its oxygenated species during the oxygen reduction reaction. *Phys. Chem. Chem. Phys.* **17**, 28121–28128, DOI: 10.1039/C5CP00283D (2015).

May, M. M. et al. Efficient direct solar-to-hydrogen conversion by in situ interface transformation of a tandem structure. *Nat Commun* **6**, 8286, DOI: 10.1038/ncomms9286 (2015).

McCrory, C. C. L. et al. Benchmarking HER and OER Electrocatalysts for Solar Water Splitting Devices. *J Am Chem Soc* **137**, 4347–4357, DOI: 10.1021/ja510442p (2015).

McDowell, M. T. et al. The Influence of Structure and Processing on the Behavior of TiO_2 Protective Layers for Stabilization of n-Si/TiO_2/Ni Photoanodes for Water Oxidation. *ACS Appl. Mater. Interfaces* 7, 15189–15199, DOI: 10.1021/acsami.5b00379 (2015).

Mitrovic, S. et al. Colorimetric Screening for High-Throughput Discovery of Light Absorbers. *ACS Combinatorial Science* **17**, 176–181, DOI: 10.1021/co500151u (2015).

Mitrovic, S. et al. High-throughput on-the-fly scanning ultraviolet-visible dual-sphere spectrometer. *Review of Scientific Instruments* **86**, 5, DOI: 10.1063/1.4905365 (2015).

Nielander, A. C., Shaner, M., Papadantonakis, K. M., Francis, S. A. & Lewis, N. A Taxonomy for Solar Fuels Generators. *Energy Environ. Sci.* **8**, 16–25, DOI: 10.1039/C4EE02251C (2015).

Niu, K.-Y. et al. Tuning Complex Transition Metal Hydroxide Nanostructures as Active Catalysts for Water Oxidation by a Laser–Chemical Route. *Nano Letters* **15**, 2498–2503, DOI: 10.1021/acs.nanolett.5b00026 (2015).

Petzetakis, N. et al. Membranes with artificial free-volume for biofuel production. *Nature Communications* **6**, 7529, DOI: 10.1038/ncomms8529 (2015).

Pham, H. H. & Wang, L. W. Electronic structures and current conductivities of B, C, N and F defects in amorphous titanium dioxide. *Phys. Chem. Chem. Phys.***17**, 11908–11913, DOI: 10.1039/c5cp00890e (2015).

Pham, H. H. & Wang, L. W. Oxygen vacancy and hole conduction in amorphous TiO_2. *Phys. Chem. Chem. Phys.***17**, 541–550, DOI: 10.1039/c4cp04209c (2015).

Pham, H. H., Barkema, G. T. & Wang, L.-W. DFT+U studies of Cu doping and p-type compensation in crystalline and amorphous ZnS, *Phys. Chem. Chem. Phys.***17**, 26270–26276, DOI: 10.1039/C5CP04623H (2015).

Ping, Y., Galli, G. & Goddard, W. A. Electronic Structure of IrO_2: The Role of the Metal d Orbitals. *J. Phys. Chem. C* **119**, 11570–11577, DOI: 10.1021/acs.jpcc.5b00861 (2015).

Ping, Y., Goddard, W. A. & Galli, G. A. Energetics and solvation effects at the photoanode-catalyst interface: Ohmic contact versus Schottky barrier. *J Am Chem Soc* **137**, 5264–5267, DOI: 10.1021/jacs.5b00798 (2015).

Ping, Y., Sundararaman, R. & Goddard, W. A. Solvation effects on the band edge positions of photocatalysts from first principles. *Phys. Chem. Chem. Phys.***17**, 30499–30509, DOI: 10.1039/C5CP05740J(2015).

Plymale, N. T., Kim, Y.-G., Soriaga, M. P., Brunschwig, B. S. & Lewis, N. S. Synthesis, Characterization, and Reactivity of Ethynyl- and Propynyl-Terminated Si(111) Surfaces. *J. Phys. Chem. C* **119**, 19847–19862, DOI: 10.1021/acs.jpcc.5b05028 (2015).

Popczun, E. et al. Highly Branched Cobalt Phosphide Nanostructures for Hydrogen-Evolution Electrocatalysis. *J. Mater. Chem. A* **3**, 5420-5425, DOI: 10.1039/C4TA06642A (2015).

Schwarz, K. A. et al. Formic acid oxidation on platinum: a simple mechanistic study. *Phys. Chem. Chem. Phys.***17**, 20805-20813, DOI: 10.1039/C5CP03045E (2015).

Shaner, M. R., Hu, S., Sun, K. & Lewis, N. S. Stabilization of Si microwire arrays for solar-driven H_2O oxidation to O_2(g) in 1.0 M KOH(aq) using conformal coatings of amorphous TiO_2. *Energy Environ. Sci.* **8**, 203-207, DOI: 10.1039/c4ee03012e (2015).

Shaner, M. R., McKone, J. R., Gray, H. B. & Lewis, N. S. Functional integration of Ni–Mo electrocatalysts with Si microwire array photocathodes to simultaneously achieve high fill factors and light-limited photocurrent densities for solar-driven hydrogen evolution. *Energy Environ. Sci.* **8**, 2977-2984, DOI: 10.1039/C5EE01076D (2015).

Shinde, A. et al. High-Throughput Screening for Acid-Stable Oxygen Evolution Electrocatalysts in the (Mn–Co–Ta–Sb)O_x Composition Space. *Electrocatalysis* **6**, 229-236, DOI: 10.1007/s12678-014-0237-7 (2015).

Shinde, A., Guevarra, D., Haber, J. A., Jin, J. & Gregoire, J. M. Identification of optimal solar fuel electrocatalysts via high throughput in situ optical measurements. *Journal of Materials Research* **30**, 442-450, DOI: 10.1557/jmr.2014.296 (2015).

Sieh, D., Lacy, D. C., Peters, J. C. & Kubiak, C. P. Reduction of CO_2 by Pyridine Monoimine Molybdenum Carbonyl Complexes: Cooperative Metal–Ligand Binding of CO_2. *Chemistry – A European Journal* **21**, 8497-8503, DOI: 10.1002/chem.201500463 (2015).

Singh, M. R., Clark, E. L. & Bell, A. T. Effects of electrolyte, catalyst, and membrane composition and operating conditions on the performance of solar-driven electrochemical reduction of carbon dioxide. *Phys. Chem. Chem. Phys.***17**, 18924-18936, DOI: 10.1039/C5CP03283K (2015).

Singh, M. R., Clark, E. L. & Bell, A. T. Thermodynamic and achievable efficiencies for solar-driven electrochemical reduction of carbon dioxide to transportation fuels. *PNAS* **112**, E6111-E6118, DOI: 10.1073/pnas.1519212112 (2015).

Singh, M. R., Papadantonakis, K. M., Xiang, C. & Lewis, N. S. An Electrochemical Engineering Assessment of the Operational Conditions and Constraints for Solar-Driven Water-Splitting Systems at Near-Neutral pH. *Energy Environ. Sci.* **8**, 2760-2767, DOI: 10.1039/C5EE01721A (2015).

Smith, W. A. et al. Interfacial Band-Edge Energetics for Solar Fuels Production. *Energy Environ. Sci.* **8**, 2851-2862, DOI: 10.1039/C5EE01822F (2015).

Soriaga, M. P. et al. Electrochemical surface science twenty years later: Expeditions into the electrocatalysis of reactions at the core of artificial photosynthesis. *Surface Science* **631**, 285-294, DOI: 10.1016/j.susc.2014.06.028 (2015).

Sun, J. et al. Low-Temperature Solution-Phase Growth of Silicon and Silicon-Containing Alloy Nanowires. *J. Phys. Chem. C* **120**, 20525-20529, DOI: 10.1021/acs.jpcc.5b08289 (2015).

Sun, K. et al. Sputtered NiO_x Films for Stabilization of p^+n-InP Photoanodes for Solar-Driven Water Oxidation. *Adv. Mater.* **5**, DOI: 10.1002/aenm.201402276 (2015).

Sun, K. et al. Stable solar-driven oxidation of water by semiconducting photoanodes protected by transparent catalytic nickel oxide films. *PNAS* **112**, 3612-3617, DOI: 10.1073/pnas.1423034112(2015).

Sun, K. et al. Stable Solar-Driven Water Oxidation to O_2(g) by Ni-Oxide-Coated Silicon Photoanodes. *J. Phys. Chem. Letters* **6**, 592-598, DOI: 10.1021/jz5026195 (2015).

Sundararaman, R. & Goddard, W. A. The charge-asymmetric nonlocally determined local-electric (CANDLE) solvation model. *Journal of Chemical Physics* **142**, 064107, DOI: 10.1063/1.4907731(2015).

Suram, S. K. et al. Combinatorial thin film composition mapping using three dimensional deposition profiles. *Review of Scientific Instruments* **86**, 033904-1–6, DOI: 10.1063/1.4914466 (2015).

Suram, S. K., Haber, J. A., Jin, J. & Gregoire, J. M. Generating Information Rich High-Throughput Experimental Materials Genomes using Functional Clustering via Multi-Tree Genetic Programming and Information Theory. *ACS Combinatorial Science* **17**, 224-233, DOI: 10.1021/co5001579 (2015).

Suseno, S. et al. Molecular Mixed-Metal Manganese Oxido Cubanes as Precursors to Heterogeneous Oxygen Evolution Catalysts. *Chemistry – A European Journal* **21**, 13420-13430, DOI: 10.1002/chem.201501104 (2015).

Sutter-Fella, C. M. et al. High Photoluminescence Quantum Yield in Band Gap Tunable Bromide Containing Mixed Halide Perovskites. *Nano Letters* **16**, 800-806, DOI: 10.1021/acs.nanolett.5b04884 (2015).

Swierk, J. R. et al. An Electrochemical Study of the Energetics of the Oxygen Evolution Reaction at Nickel Iron (oxy)hydroxide Catalysts. *J. Phys. Chem. C* **119**, 19022-19029, DOI: 10.1021/acs.jpcc.5b05861 (2015).

Van Allsburg, K., Anzenberg, E., Drisdell, W., Yano, J. & Tilley, T. D. Oxygen-Atom Transfer Chemistry and Thermolytic Properties of a Di-tert-butylphosphate-Ligated Mn_4O_4 Cubane. *Chemistry-a European Journal* **21**, 4646-4654, DOI: 10.1002/chem.201406114 (2015).

Van Dyck, D., Lobato, I., Chen, F. R. & Kisielowski, C. Do you believe that atoms stay in place when you observe them in HREM? *Micron* **68**, 158-163, DOI: 10.1016/j.micron.2014.09.003 (2015).

Verlage, E. et al. A Monolithically Integrated, Intrinsically Safe, 10% Efficient, Solar-Driven Water-Splitting System Based on Active, Stable Earth-Abundant Electrocatalysts in Conjunction with Tandem III-V Light Absorbers Protected by Amorphous TiO_2 Films. *Energy Environ. Sci.* **8**, 3166-3172, DOI: 10.1039/C5EE01786F (2015).

Walczak, K. et al. Modeling, Simulation, and Fabrication of a Fully Integrated, Acid-stable, Scalable Solar-Driven Water-Splitting System. *Chemsuschem* **8**, 544-551, DOI: 10.1002/cssc.201402896 (2015).

Wong, K. T. et al. Synthesis and Characterization of Atomically Flat Methyl-Terminated Ge(111) Surfaces. *J Am Chem Soc* **137**, 9006-9014, DOI: 10.1021/jacs.5b03339 (2015).

Xiao, H. et al. Mechanistic Explanation of the pH Dependence and Onset Potentials for Hydrocarbon Products from Electrochemical Reduction of CO on Cu (111). *J Am Chem Soc* **138**, 483-486, DOI: 10.1021/jacs.5b11390 (2015).

Yan, Q. et al. Mn2V2O7: An Earth Abundant Light Absorber for Solar Water Splitting. *Adv. Mater.* **5**, 6, DOI: 10.1002/aenm.201401840 (2015).

Yang, X. G. et al. Enabling practical electrocatalyst-assisted photoelectron-chemical water splitting with earth abundant materials. *Nano Research* **8**, 56-81, DOI: 10.1007/s12274-014-0645-2 (2015).

You, B. et al. Bimetal-Organic Framework Self-Adjusted Synthesis of Support-Free Nonprecious Electrocatalysts for Efficient Oxygen Reduction. *ACS Catalysis* **5**, 7068–7076, DOI: 10.1021/acscatal.5b02325 (2015).

Yu, J. et al. First-principles study of electronic structure and photocatalytic properties of $MnNiO_3$ as an alkaline oxygen-evolution photocatalyst. *Chemical Communications* **51**, 2867–2870, DOI: 10.1039/C4CC08111K (2015).

Zee, D. Z. et al. Metal–Polypyridyl Catalysts for Electro- and Photochemical Reduction of Water to Hydrogen. *Accounts of Chemical Research* **48**, 2027–2036, DOI: 10.1021/acs.accounts.5b00082(2015).

Zhang, M. et al. Visible Light Sensitized CO_2 Activation by the Tetraaza $[CoIIN_4H(MeCN)]^{2+}$ Complex Investigated by FT-IR Spectroscopy and DFT Calculations. *J. Phys. Chem. C* **119**, 4645–4654, DOI: 10.1021/jp5127738 (2015).

Zhou, L. et al. Combining reactive sputtering and rapid thermal processing for synthesis and discovery of metal oxynitrides. *J. Mater. Res.* **30**, 2928–2933, DOI: 10.1557/jmr.2015.140 (2015).

Zhou, L. et al. High Throughput Discovery of Solar Fuels Photoanodes in the CuO-V_2O_5 System. *Adv. Mater.* **5**, 1500968, DOI: 10.1002/aenm.201500968 (2015).

Zhou, X. et al. Interface Engineering of the Photoelectrochemical Performance of Ni-Oxide-Coated n-Si Photoanodes by Atomic-Layer Deposition of Ultrathin Films of Cobalt Oxide. *Energy Environ. Sci.* **8**, 2644–2649, DOI: 10.1039/C5EE01687H (2015).

2014

Alarcon-Llado, E. et al. $BiVO_4$ thin film photoanodes grown by chemical vapor deposition. *Phys. Chem. Chem. Phys.***16**, 1651–1657, DOI: 10.1039/c3cp53904k (2014).

Antunez, P. D. et al. Low Temperature Solution-Phase Deposition of SnS Thin Films. *Chem. Mater.***26**, 5444–5446, DOI: 10.1021/cm503124u (2014).

Baricuatro, J. et al. Heterogenization of a Water-Insoluble Molecular Complex for Catalysis of the Proton-Reduction Reaction in Highly Acidic Aqueous Solutions *Electrocatalysis* **5**, 1–3, DOI: 10.1007/s12678-014-0200-7 (2014).

Baricuatro, J. H. et al. Structure and composition of Cu(hkl) surfaces exposed to O_2 and emersed from alkaline solutions: Prelude to UHV-EC studies of CO_2 reduction at well-defined copper catalysts. *Journal of Electroanalytical Chemistry* **716**, 101–105, DOI: 10.1016/j.jelechem.2013.10.001 (2014).

Battaglia, C. et al. Hole Selective MoO_x Contact for Silicon Solar Cells. *Nano Letters* **14**, 967–971, DOI: 10.1021/nl404389u (2014).

Berger, A. & Newman, J. An Integrated 1-Dimensional Model of a Photoelectrochemical Cell for Water Splitting. *J. Electrochem. Soc.* **161**, E3328–E3340, DOI: 10.1149/2.035408jes (2014).

Berger, A., Segalman, R. A. & Newman, J. Material requirements for membrane separators in a water-splitting photoelectrochemical cell. *Energy Environ. Sci.* **7**, 1468–1476, DOI: 10.1039/c3ee43807d (2014).

Bruce, J. P. et al. Measurement of the Electrical Resistance of n-Type Si Microwire/p-Type Conducting Polymer Junctions for Use in Artificial Photosynthesis. *J. Phys. Chem. C* **118**, 27742–27748, DOI: 10.1021/jp509211k (2014).

Cai, S. L. et al. Tunable electrical conductivity in oriented thin films of tetrathiafulvalene-based covalent organic framework. *Chemical Science* **5**, 4693–4700, DOI: 10.1039/c4sc02593h (2014).

Callejas, J. F. et al. Electrocatalytic and Photocatalytic Hydrogen Production from Acidic and Neutral-pH Aqueous Solutions Using Iron Phosphide Nanoparticles. *Acs Nano* **8**, 11101–11107, DOI: 10.1021/nn5048553 (2014).

Carim, A. I., Saadi, F. H., Soriaga, M. P. & Lewis, N. S. Electrocatalysis of the hydrogen-evolution reaction by electrodeposited amorphous cobalt selenide films. *J. Mater. Chem. A* **2**, 13835–13839, DOI: 10.1039/c4ta02611j (2014).

Cedeno, D. et al. Using Molecular Design to Control the Performance of Hydrogen-Producing Polymer-Brush-Modified Photocathodes. *J. Phys. Chem. Letters* **5**, 3222–3226, DOI: 10.1021/jz5016394 (2014).

Chen, S. Y. & Wang, L. W. Double-hole-induced oxygen dimerization in transition metal oxides. *Physical Review B* **89**, 6, DOI: 10.1103/PhysRevB.89.014109 (2014).

Chen, S. Y., Narang, P., Atwater, H. A. & Wang, L. W. Phase Stability and Defect Physics of a Ternary ZnSnN2 Semiconductor: First Principles Insights. *Adv. Mater.* **26**, 311–315, DOI: 10.1002/adma.201302727 (2014).

Chen, Y. K., Xiang, C. X., Hu, S. & Lewis, N. S. Modeling the Performance of an Integrated Photoelectrolysis System with 10 x Solar Concentrators. *J. Electrochem. Soc.* **161**, F1101–F1110, DOI: 10.1149/2.0751410jes (2014).

Cheng, M. J., Head-Gordon, M. & Bell, A. T. How to Chemically Tailor Metal-Porphyrin-Like Active Sites on Carbon Nanotubes and Graphene for Minimal Overpotential in the Electrochemical Oxygen Evolution and Oxygen Reduction Reactions. *J. Phys. Chem. C* **118**, 29482–29491, DOI: 10.1021/jp507638v (2014).

Cooper, J. K. et al. Electronic Structure of Monoclinic $BiVO_4$. *Chem. Mater.***26**, 5365–5373, DOI: 10.1021/cm5025074 (2014).

Cotanda, P., Sudre, G., Modestino, M. A., Chen, X. C. & Balsara, N. P. High Anion Conductivity and Low Water Uptake of Phosphonium Containing Diblock Copolymer Membranes. *Macromolecules* **47**, 7540–7547, DOI: 10.1021/ma501744w (2014).

Fenwick, A. Q., Gregoire, J. M. & Luca, O. R. Electrocatalytic Reduction of Nitrogen and Carbon Dioxide to Chemical Fuels: Challenges and Opportunities for a Solar Fuel Device. *Journal of Photochemistry and Photobiology B: Biology* **152**, 47–57, DOI: 10.1016/j.jphotobiol.2014.12.019 (2014).

Fong, H. & Peters, J. Hydricity of an Fe–H Species and Catalytic CO_2 Hydrogenation. *Inorganic Chemistry* **54**, 5124–5135, DOI: 10.101021/9c502508p (2014).

Fountaine, K. T. & Atwater, H. A. Mesoscale modeling of photoelectrochemical devices: light absorption and carrier collection in monolithic, tandem, Si vertical bar WO_3 microwires. *Optics Express* 22, A1453–A1461, DOI: 10.1364/oe.22.0a1453 (2014).

Fountaine, K. T., Kendall, C. G. & Atwater, H. A. Near-unity broadband absorption designs for semiconducting nanowire arrays via localized radial mode excitation. *Optics Express* 22, A930–A940, DOI: 10.1364/oe.22.00a930 (2014).

Fountaine, K. T., Lewerenz, H. J. & Atwater, H. A. Interplay of light transmission and catalytic exchange current in photoelectrochemical systems. *Applied Physics Letters* **105**, 3, DOI: 10.1063/1.4900612 (2014).

Fountaine, K. T., Whitney, W. S. & Atwater, H. A. Resonant absorption in semiconductor nanowires and nanowire arrays: Relating leaky waveguide modes to Bloch photonic crystal modes. *Journal of Applied Physics* **116**, 6, DOI: 10.1063/1.4898758 (2014).

Grauer, D. C. & Alivisatos, A. P. Ligand Dissociation Mediated Charge Transfer Observed at Colloidal W18O49 Nanoparticle Interfaces. *Langmuir* **30**, 2325–2328, DOI: 10.1021/la404019v (2014).

Gregoire, J. M. et al. High-throughput synchrotron X-ray diffraction for combinatorial phase mapping. *Journal of Synchrotron Radiation* **21**, 1262–1268, DOI: 10.1107/s1600577514016488 (2014).

Haber, J. A. et al. Discovering Ce-rich oxygen evolution catalysts, from high throughput screening to water electrolysis. *Energy Environ. Sci.* 7, 682–688, DOI: 10.1039/c3ee43683g (2014).

Haber, J. A. et al. High-Throughput Mapping of the Electrochemical Properties of (Ni-Fe-Co-Ce)O-x Oxygen-Evolution Catalysts. *Chemelectrochem* **1**, 524–528, DOI: 10.1002/celc.201300229 (2014).

Haber, J. A., Guevarra, D., Jung, S. H., Jin, J. & Gregoire, J. M. Discovery of New Oxygen Evolution Reaction Electrocatalysts by Combinatorial Investigation of the Ni-La-Co-Ce Oxide Composition Space. *Chemelectrochem* **1**, 1613–1617, DOI: 10.1002/celc.201402149 (2014).

Han, L. H. et al. Efficient Water-Splitting Device Based on a Bismuth Vanadate Photoanode and Thin-Film Silicon Solar Cells. *Chemsuschem* 7, 2832–2838, DOI: 10.1002/cssc.201402456 (2014).

Hsieh, C. H. et al. Redox active iron nitrosyl units in proton reduction electrocatalysis. *Nature Communications* **5**, 8, DOI: 10.1038/ncomms4684 (2014).

Hu, S. et al. Amorphous TiO2 coatings stabilize Si, GaAs, and GaP photoanodes for efficient water oxidation. *Science* **344**, 1005–1009, DOI: 10.1126/science.1251428 (2014).

Huang, Z. et al. Comparison between the measured and modeled hydrogen-evolution activity of Ni- or Pt-coated silicon photocathodes. *International Journal of Hydrogen Energy* **39**, 16220–16226, DOI: 10.1016/j.ijhydene.2013.12.162 (2014).

Huang, Z., Xiang, C. & Lewis, N. S. Two 1 stories from the ISACS 12 conference: solarfuel devices and catalyst identification (editorial). *EES* 7, 1207–1211, DOI: 10.1039/c3ee90043f (2014).

Javier, A. et al. C-H activation and metalation at electrode surfaces: 2,3-dimethyl-1,4-dihydroxybenzene on Pd(pc) and Pd(111) studied by TLE, HREELS and DFT. *Dalton Transactions* **43**, 14798–14805, DOI: 10.1039/c4dt02137a (2014).

Jeon, J. et al. Rapid Dye Regeneration Mechanism of Dye-Sensitized Solar Cells. *J. Phys. Chem. Letters* **5**, 4285–4290, DOI: 10.1021/jz502197b (2014).

Jin, J. et al. An experimental and modeling/simulation-based evaluation of the efficiency and operational performance characteristics of an integrated, membrane-free, neutral pH solar-driven water-splitting system. *Energy Environ. Sci.* 7, 3371–3380, DOI: 10.1039/c4ee01824a (2014).

Kim, Y. G. & Soriaga, M. P. Cathodic regeneration of a clean and ordered Cu(100)-(1 x 1) surface from an air-oxidized and disordered electrode: An operando STM study. *Journal of Electroanalytical Chemistry* **734**, 7–9, DOI: 10.1016/j.jelechem.2014.09.010 (2014).

Kim, Y. G., Baricuatro, J. H., Javier, A., Gregoire, J. M. & Soriaga, M. P. The Evolution of the Polycrystalline Copper Surface, First to Cu(111) and Then to Cu(100), at a Fixed CO_2RR Potential: A Study by Operand EC-STM. *Langmuir* **30**, 15053–15056, DOI: 10.1021/la504445g (2014).

Krawicz, A., Cedeno, D. & Moore, G. F. Energetics and efficiency analysis of a cobaloxime-modified semiconductor under simulated air mass 1.5 illumination. *Phys. Chem. Chem. Phys.***16**, 15818–15824, DOI: 10.1039/c4cp00495g (2014).

Lacy, D. C., McCrory, C. C. L. & Peters, J. C. Studies of Cobalt-Mediated Electrocatalytic CO2 Reduction Using a Redox-Active Ligand. *Inorganic Chemistry* **53**, 4980–4988, DOI: 10.1021/ic403122j (2014).

Leenheer, A. J., Narang, P., Lewis, N. S. & Atwater, H. A. Solar energy conversion via hot electron internal photoemission in metallic nanostructures: Efficiency estimates. *Journal of Applied Physics* **115**, 7, DOI: 10.1063/1.4870040 (2014).

Letko, C. S., Panetier, J. A., Head-Gordon, M. & Tilley, T. D. Mechanism of the Electrocatalytic Reduction of Protons with Diaryldithiolene Cobalt Complexes. *J Am Chem Soc* **136**, 9364–9376, DOI: 10.1021/ja5019755 (2014).

Lewerenz, H. J. Semiconductor Surface Transformations for Photoelectrochemical Energy Conversion. *J. Electrochem. Soc.* **161**, H3117–H3129, DOI: 10.1149/2.0211413jes (2014).

Lewerenz, J. H. Self-Organization Phenomena in Photoelectrochemical Energy Conversion: Nanoemitter Solar Cells. *Reviews in Advanced Sciences and Engineering* **4**, 1–11, DOI: 10.1166/rase.2014.1081(2014).

Lichterman, M. F. et al. Stabilization of n-cadmium telluride photoanodes for water oxidation to O_2(g) in aqueous alkaline electrolytes using amorphous TiO_2 films formed by atomic-layer deposition. *Energy Environ. Sci.* 7, 3334–3337, DOI: 10.1039/c4ee01914h (2014).

Lin, T. P. & Peters, J. C. Boryl-Metal Bonds Facilitate Cobalt/Nickel-Catalyzed Olefin Hydrogenation. *J Am Chem Soc* **136**, 13672–13683, DOI: 10.1021/ja504667f (2014).

Liu, R., Zheng, Z., Spurgeon, J. & Yang, X. G. Enhanced photoelectrochemical water-splitting performance of semiconductors by surface passivation layers. *Energy Environ. Sci.* 7, 2504–2517, DOI: 10.1039/c4ee00450g (2014).

Liu, W. J., Sharp, I. D. & Tilley, T. D. Multifunctional Silicon Surfaces: Reaction of Dichlorocarbene Generated from Seyferth Reagent with Hydrogen-Terminated Silicon (111) Surfaces. *Langmuir* **30**, 172–178, DOI: 10.1021/la403789a (2014).

Lobaccaro, P. et al. Electrodeposition of High-Purity Indium Thin Films and Its Application to Indium Phosphide Solar Cells. *J. Electrochem. Soc.* **161**, D794–D800, DOI: 10.1149/2.0821414jes (2014).

Ma, J. & Wang, L. W. The role of the isolated 6s states in $BiVO_4$ on the electronic and atomic structures. *Applied Physics Letters* **105**, 4, DOI: 10.1063/1.4900549 (2014).

May, M. M., Lewerenz, H. J. & Hannappel, T. Optical in Situ Study of InP(100) Surface Chemistry: Dissociative Adsorption of Water and Oxygen. *J. Phys. Chem. C* **118**, 19032–19041, DOI: 10.1021/jp502955m (2014).

McDonald, M. B., Ardo, S., Lewis, N. S. & Freund, M. S. Use of Bipolar Membranes for Maintaining Steady-State pH Gradients in Membrane-Supported, Solar-Driven Water Splitting Michael. *Chemsuschem* **7**, 3021–3027, DOI: 10.1002/cssc.201402288 (2014).

McDowell, M. T. et al. Improved Stability of Polycrystalline Bismuth Vanadate Photoanodes by Use of Dual-Layer Thin TiO_2/Ni Coatings. *J. Phys. Chem. C* **118**, 19618–19624, DOI: 10.1021/jp506133y (2014).

McEnaney, J. M. et al. Amorphous Molybdenum Phosphide Nanoparticles for Electrocatalytic Hydrogen Evolution. *Chem. Mater.***26**, 4826–4831, DOI: 10.1021/cm502035s (2014).

McEnaney, J. M. et al. Electrocatalytic hydrogen evolution using amorphous tungsten phosphide nanoparticles. *Chem Comm* **50**, 11026–11028, DOI: 10.1039/c4cc04709e (2014).

McKone, J. R., Lewis, N. S. & Gray, H. B. Will Solar-Driven Water-Splitting Devices See the Light of Day? *Chem Mater* **26**, 407–414, DOI: 10.1021/cm4021518 (2014).

Modestino, M. A. et al. Robust production of purified H_2 in a stable, self-regulating, and continuously operating solar fuel generator. *Energy Environ. Sci.* **7**, 297–301, DOI: 10.1039/c3ee43214a(2014).

Narang, P. et al. Bandgap Tunability in Zn(Sn,Ge)N-2 Semiconductor Alloys. *Adv Mater* **26**, 1235–1241, DOI: 10.1002/adma.201304473 (2014).

Pala, R. A., Leenheer, A. J., Lichterman, M., Atwater, H. A. & Lewis, N. S. Measurement of minority-carrier diffusion lengths using wedge-shaped semiconductor photoelectrodes. *Energy Environ. Sci.* **7**, 3424–3430, DOI: 10.1039/c4ee01580k (2014).

Pesenson, M. Z., Suram, S. K. & Gregoire, J. M. Statistical Analysis and Interpolation of Compositional Data in Materials Science. *ACS Combinatorial Science* **17**, 130–136, DOI: 10.1021/co5001458 (2014).

Rivest, J. B., Li, G., Sharp, I. D., Neaton, J. B. & Milliron, D. J. Phosphonic Acid Adsorbates Tune the Surface Potential of TiO2 in Gas and Liquid Environments. *J. Phys. Chem. Letters* **5**, 2450–2454, DOI: 10.1021/jz501050f (2014).

Saadi, F. H. et al. CoP as an Acid-Stable Active Electrocatalyst for the Hydrogen-Evolution Reaction: Electrochemical Synthesis, Interfacial Characterization and Performance Evaluation. *J. Phys. Chem. C* **118**, 29294–29300, DOI: 10.1021/jp5054452 (2014).

Saadi, F. H. et al. Operand Synthesis of Macroporous Molybdenum Diselenide Films for Electrocatalysis of the Hydrogen-Evolution Reaction. *ACS Catalysis* **4**, 2866–2873, DOI: 10.1021/cs500412u (2014).

Sanabria-Chinchilla, J. et al. Immobilization-Enabled Proton Reduction Catalysis by a Di-iron Hydrogenase Mimic. *Electrocatalysis* **5**, 5–7, DOI: 10.1007/s12678-013-0157-y (2014).

Sanchez Casalongue, H. G. et al. In Situ Observation of Surface Species on Iridium Oxide Nanoparticles during the Oxygen Evolution Reaction. *Angewandte Chemie-International Edition* **53**, 7169–7172, DOI: 10.1002/anie.201402311 (2014).

Sanchez Casalongue, H. G. et al. Operando Characterization of an Amorphous Molybdenum Sulfide Nanoparticle Catalyst during the Hydrogen Evolution Reaction. *J. Phys. Chem. C* **118**, 29252–29259, DOI: 10.1021/jp505394e (2014).

Sathre, R. et al. Life-cycle net energy assessment of large-scale hydrogen production via photoelectrochemical water splitting. *Energy Environ. Sci.* **7**, 3264–3278, DOI: 10.1039/c4ee01019a (2014).

Shaffer, D. W. et al. Reactivity of a Series of Isostructural Cobalt Pincer Complexes with CO_2, CO, and H+. *Inorganic Chemistry* **53**, 13031–13041, DOI: 10.1021/ic5021725 (2014).

Shaner, M. R. et al. Photoelectrochemistry of core-shell tandem junction n-p(+)-Si/n-WO_3 microwire array photoelectrodes. *Energy Environ. Sci.* **7**, 779–790, DOI: 10.1039/c3ee43048k (2014).

Singh, M. R., Stevens, J. C. & Weber, A. Z. Design of Membrane-Encapsulated Wireless Photoelectrochemical Cells for Hydrogen Production. *J. Electrochem. Soc.* **161**, E3283–E3296, DOI: 10.1149/2.033408jes (2014).

Spurgeon, J. M., Velazquez, J. M. & McDowell, M. T. Improving O-2 production of WO_3 photoanodes with IrO2 in acidic aqueous electrolyte. *Phys. Chem. Chem. Phys.***16**, 3623–3631, DOI: 10.1039/c3cp55527e (2014).

Sundararaman, R., Narang, P., Jermyn, A. S., Goddard, W. A. & Atwater, H. A. Theoretical predictions for hot-carrier generation from surface plasmon decay. *Nature Communications* **5**, 8, DOI: 10.1038/ncomms6788 (2014).

Supplie, O. et al. Materials for light-induced water splitting: In situ controlled surface preparation of GaPN epilayers grown lattice-matched on Si(100). *Journal of Applied Physics* **115**, 18, DOI: 10.1063/1.4869121(2014).

Velazquez, J. M. et al. Synthesis and hydrogen-evolution activity of tungsten selenide thin films deposited on tungsten foils. *Journal of Electroanalytical Chemistry* **716**, 45–48, DOI: 10.1016/j.jelechem.2013.11.030 (2014).

Warren, E. L., Atwater, H. A. & Lewis, N. S. Silicon Microwire Arrays for Solar Energy-Conversion Applications. *J. Phys. Chem. C* **118**, 747–759, DOI: 10.1021/jp406280x (2014).

Williams, T. E. et al. NIR-Selective electrochromic heteromaterial frameworks: a platform to understand mesoscale transport phenomena in solid-state electrochemical devices. *J. Mater. Chem. C* 2, 3328–3335, DOI: 10.1039/c3tc32247e (2014).

Xiang, C. et al. High-Throughput Bubble Screening Method for Combinatorial Discovery of Electrocatalysts for Water Splitting. *ACS Combinatorial Science* **16**, 47–52, DOI: 10.1021/co400151h(2014).

Xiang, C. et al. Mapping Quantum Yield for (Fe–Zn–Sn–Ti)O_x Photoabsorbers Using a High Throughput Photoelectrochemical Screening System. *ACS Combinatorial Science* **16**, 120–127, DOI: 10.1021/co400081w (2014).

Xiao, H. & Goddard, W. A. Predicted roles of defects on band offsets and energetics at CIGS (Cu(In,Ga) Se-2/CdS) solar cell interfaces and implications for improving performance. *Journal of Chemical Physics* **141**, 7, DOI: 10.1063/1.4893985 (2014).

Yang, J. H. et al. Efficient and Sustained Photoelectrochemical Water Oxidation by Cobalt Oxide/Silicon Photoanodes with Nanotextured Interfaces. *J Am Chem Soc* **136**, 6191–6194, DOI: 10.1021/ja501513t (2014).

Zhu, Y. et al. Visualizing the Stoichiometry of Industrial-Style Co-Mo-S Catalysts with Single-Atom Sensitivity. *Angew Chem Int Ed Engl* **53**, 10723–10727, DOI: 10.1002/anie.201405690 (2014).

2013

Alayoglu, S. et al. Pt-Mediated Reversible Reduction and Expansion of CeO_2 in Pt Nanoparticle/Mesoporous CeO_2 Catalyst: In Situ X-ray Spectroscopy and Diffraction Studies under Redox (H-2 and O-2) Atmospheres. *J. Phys. Chem. C* **117**, 26608–26616, DOI: 10.1021/jp407280e (2013).

Bajdich, M., Garcia-Mota, M., Vojvodic, A., Norskov, J. K. & Bell, A. T. Theoretical Investigation of the Activity of Cobalt Oxides for the Electrochemical Oxidation of Water. *J Am Chem Soc* **135**, 13521–13530, DOI: 10.1021/ja405997s (2013).

Baricuatro, J. H., Soto, J. C., Cummins, K. D. & Soriaga, M. P. High-resolution electron energy loss spectroscopy of anions chemisorbed on electrode surfaces: The effect of counter cations. *Electrochem. Commun.* 27, 176–179, DOI: 10.1016/j.elecom.2012.11.005 (2013).

Chen, L. et al. Reactive Sputtering of Bismuth Vanadate Photoanodes for Solar Water Splitting. *J. Phys. Chem. C* **117**, 21635–21642, DOI: 10.1021/jp406019r (2013).

Chi, C. Y. et al. Twin-Free GaAs Nanosheets by Selective Area Growth: Implications for Defect-Free Nanostructures. *Nano Letters* **13**, 2506–2515, DOI: 10.1021/nl400561j (2013).

Chmielowiec, B. et al. Molecular catalysis that transpires only when the complex is heterogenized: studies of a hydrogenase complex surface-tethered on polycrystalline and (111)-faceted gold by EC, PM-FT-IRRAS, HREELS, XPS and STM. *Journal of Electroanalytical Chemistry* **716**, 63–70, DOI: 10.1016/j.jelechem.2013.12.025 (2013).

Coridan, R. H., Shaner, M., Wiggenhorn, C., Brunschwig, B. S. & Lewis, N. S. Electrical and Photoelectrochemical Properties of WO_3/Si Tandem Photoelectrodes. *J. Phys. Chem. C* **117**, 6949–6957, DOI: 10.1021/jp311947x (2013).

Friebel, D. et al. On the chemical state of Co oxide electrocatalysts during alkaline water splitting. *Phys. Chem. Chem. Phys.***15**, 17460–17467, DOI: 10.1039/c3cp52981a (2013).

Gorlin, Y. et al. In Situ X-ray Absorption Spectroscopy Investigation of a Bifunctional Manganese Oxide Catalyst with High Activity for Electrochemical Water Oxidation and Oxygen Reduction. *J Am Chem Soc* **135**, 8525–8534, DOI: 10.1021/ja3104632 (2013).

Gregoire, J. M. et al. Combined Catalysis and Optical Screening for High Throughput Discovery of Solar Fuels Catalysts. *J. Electrochem. Soc.* **160**, F337–F342, DOI: 10.1149/2.035304jes(2013).

Gregoire, J. M., Xiang, C. X., Liu, X. N., Marcin, M. & Jin, J. Scanning droplet cell for high throughput electrochemical and photoelectrochemical measurements. *Review of Scientific Instruments* **84**, 6, DOI: 10.1063/1.4790419 (2013).

Hannappel, T., May, M. M. & Lewerenz, H. J. in "Photoelectrochemical Water Splitting: Materials, Processes and Architectures" (eds H. J. Lewerenz & L. M. Peter) Ch. Chapter 9, (The Royal Society of Chemistry, 2013).

Haussener, S., Hu, S., Xiang, C. X., Weber, A. Z. & Lewis, N. S. Simulations of the irradiation and temperature dependence of the efficiency of tandem photoelectrochemical water-splitting systems. *Energy Environ. Sci.* **6**, 3605–3618, DOI: 10.1039/c3ee41302k (2013).

Hu, S. et al. Optical, electrical, and solar energy-conversion properties of gallium arsenide nanowire-array photoanodes. *Energy Environ. Sci.* **6**, 1879–1890, DOI: 10.1039/c3ee40243f (2013).

Hu, S., Xiang, C. X., Haussener, S., Berger, A. D. & Lewis, N. S. An analysis of the optimal band gaps of light absorbers in integrated tandem photoelectrochemical water-splitting systems. *Energy Environ. Sci.* **6**, 2984–2993, DOI: 10.1039/c3ee40453f (2013).

Kashif, M. K. et al. Stable Dye-Sensitized Solar Cell Electrolytes Based on Cobalt(II)/(III) Complexes of a Hexadentate Pyridyl Ligand. *Angewandte Chemie-International Edition* **52**, 5527–5531, DOI: 10.1002/anie.201300070 (2013).

Kisielowski, C. et al. Real-time sub-Angstrom imaging of reversible and irreversible conformations in rhodium catalysts and graphene. *Physical Review B* **88**, 12, DOI: 10.1103/PhysRevB.88.024305 (2013).

Krawicz, A. et al. Photofunctional Construct That Interfaces Molecular Cobalt-Based Catalysts for H-2 Production to a Visible-Light-Absorbing Semiconductor. *J Am Chem Soc* **135**, 11861–11868, DOI: 10.1021/ja404158r (2013).

Letilly, M., Skorupska, K. & Lewerenz, H. J. Initial Phase of Photoelectrochemical Conditioning of Silicon in Alkaline Media: Surface Chemistry and Topography. *J. Phys. Chem. C* **117**, 16381–16391, DOI: 10.1021/jp401853p (2013).

Lewerenz, H. J. in Encyclopedia of Applied Electrochemistry" (eds R. F. Savinell, K. I. Ota, & G. Kreysa) 1893–1924 (Spinger Heidelberg, 2013).

Lewerenz, H. J. & Peter, L. M. in "Photoelectrochemical Water Splitting: Materials, Processes and Architectures" (eds H. J. Lewerenz & L. M. Peter) Chapter 16, (The Royal Society of Chemistry, 2013).

Lewerenz, H. J. On the Structure of the Helmholtz Layer and its Implications on Electrode Kinetics. *Electrochemical Society Transactions* **50**, 3–20, DOI: 10.1149/05052.0003ecst (2013).

Lewis, N. S. An integrated, systems approach to the development of solar-fuels generators. *The Electrochemical Society, Interface*, 43–49 (2013).

Lichterman, M. F. et al. Enhanced Stability and Activity for Water Oxidation in Alkaline Media with Bismuth Vanadate Photoelectrodes Modified with a Cobalt Oxide Catalytic Layer Produced by Atomic Layer Deposition. *J. Phys. Chem. Letters* **4**, 4188–4191, DOI: 10.1021/jz4022415 (2013).

Lin, T. P. & Peters, J. C. Boryl-Mediated Reversible H-2 Activation at Cobalt: Catalytic Hydrogenation, Dehydrogenation, and Transfer Hydrogenation. J *J Am Chem Soc* **135**, 15310–15313, DOI: 10.1021/ja408397v (2013).

Lin, Y. J. et al. Amorphous Si Thin Film Based Photocathodes with High Photovoltage for Efficient Hydrogen Production. *Nano Letters* **13**, 5615–5618, DOI: 10.1021/nl403265k (2013).

Louie, M. W. & Bell, A. T. An Investigation of Thin-Film Ni-Fe Oxide Catalysts for the Electrochemical Evolution of Oxygen. *J Am Chem Soc* **135**, 12329–12337, DOI: 10.1021/ja405351s (2013).

McCrory, C. C. L., Jung, S. H., Peters, J. C. & Jaramillo, T. F. Benchmarking Heterogeneous Electrocatalysts for the Oxygen Evolution Reaction. *J Am Chem Soc* **135**, 16977–16987, DOI: 10.1021/ja407115p (2013).

McKone, J. R., Grimm, R. L. & Lewis, N. S. in Photoelectrochemical Water Splitting: Materials, Processes and Architecture (eds H. J. Lewerenz & L. M. Peter) Chapter 3, (Royal Society of Chemistry, 2013).

McKone, J. R., Pieterick, A. P., Gray, H. B. & Lewis, N. S. Hydrogen Evolution from Pt/Ru-Coated p-Type WSe2 Photocathodes. *J Am Chem Soc* **135**, 223–231, DOI: 10.1021/ja308581g(2013).

Modestino, M. A. et al. Integrated microfluidic test-bed for energy conversion devices. *Phys. Chem. Chem. Phys.***15**, 7050–7054, DOI: 10.1039/c3cp51302e (2013).

Modestino, M. A. et al. Self-Assembly and Transport Limitations in Confined Nafion Films. *Macromolecules* **46**, 867–873, DOI: 10.1021/ma301999a (2013).

Moore, G. F. & Sharp, I. D. A Noble-Metal-Free Hydrogen Evolution Catalyst Grafted to Visible Light-Absorbing Semiconductors. *J. Phys. Chem. Letters* **4**, 568–572, DOI: 10.1021/jz400028z(2013).

Nippe, M. et al. Catalytic proton reduction with transition metal complexes of the redox-active ligand bpy2PYMe. *Chemical Science* **4**, 3934–3945, DOI: 10.1039/c3sc51660a (2013).

Sampson, M. D. et al. Direct observation of the reduction of carbon dioxide by rhenium bipyridine catalysts. *Energy Environ. Sci.* **6**, 3748–3755, DOI: 10.1039/c3ee42186d (2013).

Sanabria-Chinchilla, J., Chen, X. L., Li, D. & Soriaga, M. P. Chemisorption-Isotherm Measurements at Electrode Surfaces by Quantitative High-Resolution Electron Energy Loss Spectroscopy. *Electrocatalysis* **4**, 101–103, DOI: 10.1007/s12678-013-0125-6 (2013).

Sanchez Casalongue, H. et al. Direct observation of the oxygenated species during oxygen reduction on a platinum fuel cell cathode. *Nature Communications* **4**, 6, DOI: 10.1038/ncomms3817 (2013).

Schneider, Y. et al. Ionic Conduction in Nanostructured Membranes Based on Polymerized Protic Ionic Liquids. *Macromolecules* **46**, 1543–1548, DOI: 10.1021/ma3024624 (2013).

Shaner, M. R., Fountaine, K. T. & Lewerenz, H. J. Current-voltage characteristics of coupled photodiode-electrocatalyst devices. *Applied Physics Letters* **103**, 4, DOI: 10.1063/1.4822179 (2013).

Sudre, G., Inceoglu, S., Cotanda, P. & Balsara, N. P. Influence of Bound Ion on the Morphology and Conductivity of Anion-Conducting Block Copolymers. *Macromolecules* **46**, 1519–1527, DOI: 10.1021/ma302357k (2013).

Thoi, V. S., Sun, Y. J., Long, J. R. & Chang, C. J. Complexes of earth-abundant metals for catalytic electrochemical hydrogen generation under aqueous conditions. *Chem. Soc. Rev.* **42**, 2388–2400, DOI: 10.1039/c2cs35272a (2013).

Ugeda, M. M. et al. Adsorption and Stability of pi-Bonded Ethylene on GaP(110). *J. Phys. Chem. C* **117**, 26091–26096, DOI: 10.1021/jp408539x (2013).

Wang, W. C., Chen, S. Y., Yang, P. X., Duan, C. G. & Wang, L. W. Si:WO_3 heterostructure for Z-scheme water splitting: an ab initio study. *J. Mater. Chem. A* **1**, 1078–1085, DOI: 10.1039/c2ta00441k (2013).

Xiang, C. X., Chen, Y. K. & Lewis, N. S. Modeling an integrated photoelectrolysis system sustained by water vapor. *Energy Environ. Sci.* **6**, 3713–3721, DOI: 10.1039/c3ee42143k (2013).

Yu, M., Doak, P., Tamblyn, I. & Neaton, J. B. Theory of Covalent Adsorbate Frontier Orbital Energies on Functionalized Light-Absorbing Semiconductor Surfaces. *J. Phys. Chem. Letters* **4**, 1701–1706, DOI: 10.1021/jz400601t (2013).

Zhai, P. et al. Net primary energy balance of a solar-driven photoelectrochemical water-splitting device. *Energy Environ. Sci.* **6**, 2380–2389, DOI: 10.1039/c3ee40880a (2013).

2012

Chen, S. Y. & Wang, L. W. Thermodynamic Oxidation and Reduction Potentials of Photocatalytic Semiconductors in Aqueous Solution. *Chem. Mater.***24**, 3659–3666, DOI: 10.1021/cm302533s(2012).

Chen, S. Y., Wang, L. W., Walsh, A., Gong, X. G. & Wei, S. H. Abundance of Cu-Zn + Sn-Zn and 2Cu(Zn) + Sn-Zn defect clusters in kesterite solar cells. *Applied Physics Letters* **101**, 4, DOI: 10.1063/1.4768215(2012).

Diamond, A. M. et al. Copper-alloyed ZnS as a p-type transparent conducting material. *Phys. Status Solidi A-Appl. Mat.* **209**, 2101–2107, DOI: 10.1002/pssa.201228181 (2012).

Garcia-Mota, M. et al. Importance of Correlation in Determining Electrocatalytic Oxygen Evolution Activity on Cobalt Oxides. *J. Phys. Chem. C* **116**, 21077–21082, DOI: 10.1021/jp306303y (2012).

Haussener, S. et al. Modeling, simulation, and design criteria for photoelectrochemical water-splitting systems. *Energy Environ. Sci.* **5**, 9922–9935, DOI: 10.1039/c2ee23187e (2012).

Hoarfrost, M. L. & Segalman, R. A. Conductivity Scaling Relationships for Nanostructured Block Copolymer/Ionic Liquid Membranes. *ACS Macro Letters* **1**, 937–943, DOI: 10.1021/mz300241g (2012).

Hoarfrost, M. L., Tyagi, M., Segalman, R. A. & Reimer, J. A. Proton Hopping and Long-Range Transport in the Protic Ionic Liquid [Im][TFSI], Probed by Pulsed-Field Gradient NMR and Quasi-Elastic Neutron Scattering. *J. Phys. Chem. B* **116**, 8201–8209, DOI: 10.1021/jp3044237 (2012).

Karunadasa, H. I. et al. A Molecular MoS2 Edge Site Mimic for Catalytic Hydrogen Generation. *Science* **335**, 698–702, DOI: 10.1126/science.1215868 (2012).

Kusoglu, A., Modestino, M. A., Hexemer, A., Segalman, R. A. & Weber, A. Z. Subsecond Morphological Changes in Nafion during Water Uptake Detected by Small-Angle X-ray Scattering. *ACS Macro Letters* **1**, 33–36, DOI: 10.1021/mz200015c (2012).

Lee, M. H. et al. p-Type InP Nanopillar Photocathodes for Efficient Solar-Driven Hydrogen Production. *Angewandte Chemie-International Edition* **51**, 10760–10764, DOI: 10.1002/anie.201203174 (2012).

Leenheer, A. J. & Atwater, H. A. Imaging Water-Splitting Electrocatalysts with pH-Sensing Confocal Fluorescence Microscopy. *J. Electrochem. Soc.* **159**, H752–H757, DOI: 10.1149/2.022209jes (2012).

Modestino, M. A., Kusoglu, A., Hexemer, A., Weber, A. Z. & Segalman, R. A. Controlling Nafion Structure and Properties via Wetting Interactions. *Macromolecules* **45**, 4681–4688, DOI: 10.1021/ma300212f (2012).

Yeo, B. S. & Bell, A. T. In Situ Raman Study of Nickel Oxide and Gold-Supported Nickel Oxide Catalysts for the Electrochemical Evolution of Oxygen. *J. Phys. Chem. C* **116**, 8394–8400, DOI: 10.1021/jp3007415 (2012).

2011

Chen, S. Y. & Wang, L. W. Intrinsic defects and electronic conductivity of TaON: First-principles insights. *Applied Physics Letters* **99**, 222103, DOI: 10.1063/1.3664346 (2011).

Spurgeon, J. M. & Lewis, N. S. Proton exchange membrane electrolysis sustained by water vapor. *Energy Environ. Sci.* **4**, 2993–2998, DOI: 10.1039/c1ee01203g (2011).

Sun, J. W., Liu, C. & Yang, P. D. Surfactant-Free, Large-Scale, Solution-Liquid-Solid Growth of Gallium Phosphide Nanowires and Their Use for Visible-Light-Driven Hydrogen Production from Water Reduction. *J Am Chem Soc* **133**, 19306–19309, DOI: 10.1021/ja2083398 (2011).

Sun, Y. J. et al. Molecular Cobalt Pentapyridine Catalysts for Generating Hydrogen from Water. *J Am Chem Soc* **133**, 9212–9215, DOI: 10.1021/ja202743r (2011).

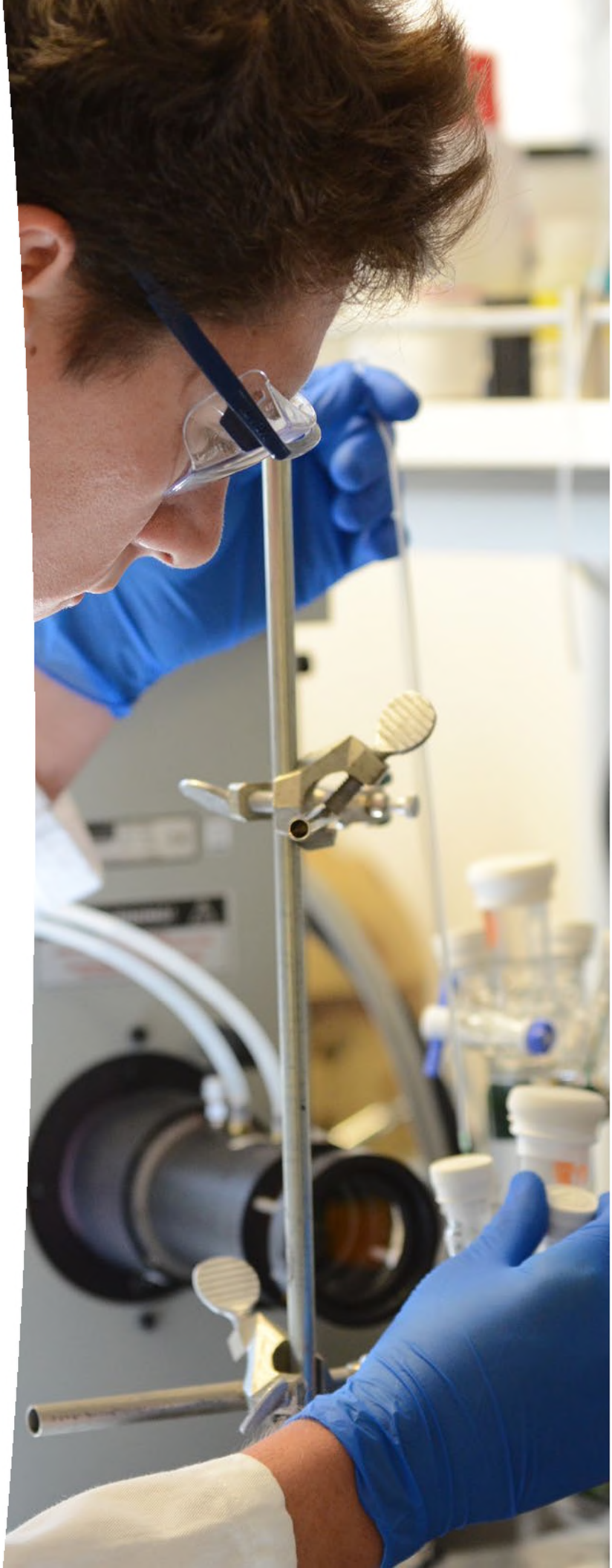

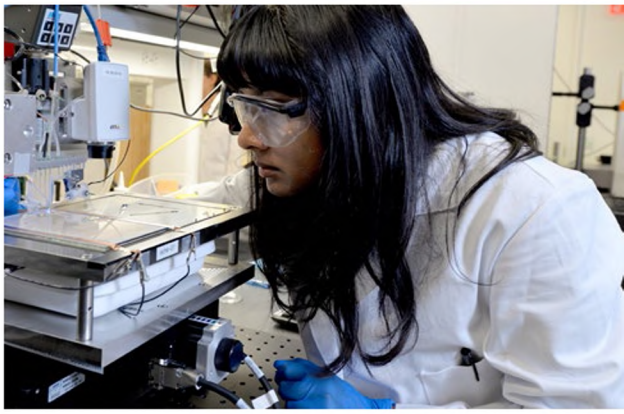

U.S. DEPARTMENT OF ENERGY

Caltech

BERKELEY LAB

SLAC

UC San Diego

UCI

21-ESAO-17009